TREATMENT OPTIMIZATION FOR

METASTATIC PROSTATE CANCER

THROUGH PRECLINICAL MODELS AND SYSTEMS

LISANNE MOUT

Treatment Optimization for Metastatic Prostate Cancer through Preclinical Models and Systems

Lisanne Mout

Colofon

ISBN: 978-94-6423-213-4
Cover design: Wendy Schoneveld
Print: Proefschriftmaken.nl

The printing of this thesis was financially supported by: Stichting Urologisch Wetenschappelijk Onderzoek (SUWO)

Treatment Optimization for
Metastatic Prostate Cancer
through Preclinical Models and Systems

Verbeterde behandeling van
uitgezaaide prostaatkanker
door preklinische studies

Proefschrift

ter verkrijging van de graad van doctor aan de
Erasmus Universiteit Rotterdam
op gezag van de
rector magnificus

Prof.dr. F.A. van der Duijn Schouten

en volgens besluit van het College voor Promoties.
De openbare verdediging zal plaatsvinden op

dinsdag 11 mei 2021 om 10.30 uur

door

Lisanne Mout
geboren op 3 mei 1991
te Rotterdam.

Erasmus University Rotterdam

Erasmus

Promotiecommissie

Promotor	prof. dr. R. de Wit
Overige leden	prof. dr. ir. G.W. Jenster prof. dr. S.M.A. Lens prof. dr. W. Zwart
Copromotoren	dr. ir. W.M. van Weerden dr. M.P.J.K. Lolkema

Table of contents

Chapter I

General Introduction

Prostate cancer

Prostate cancer (PCa) is currently one of the most common types of cancer in men and the incidence is rising. In 2018, 376,000 European men were diagnosed with and 107,000 died of PCa.[1] Consequently one of the major challenges in PCa is defining the best strategy for the individual patient within a vast and heterogeneous patient population. In localized disease, the chance of dying from PCa within 10 years without direct treatment ranges between 8.3 and 25.6%.[2] For these patients, the initial consideration is whether the potential survival benefit from treatment outweighs the impact on the quality of life. Risk stratification in PCa aims to identify those patients with a low risk of dying from their malignancy using tumor grade, stage and serum prostate specific antigen (PSA) levels.[3] For histological grading, prostate (tumor) biopsies are obtained, the tissue is fixed, sectioned, stained and assessed using the Gleason grading system. Initially developed by Donald Gleason in 1966, the Gleason grading system characterizes the PCa tissue based on histological growth patterns and loss of normal glandular structures.[4] The Gleason score is the sum of the two most frequent growth patterns, graded from 1-5 with increasing invasiveness and loss of normal tissue architecture. While a Gleason score ≤6 is defined as clinically irrelevant and ≥8 as aggressive, Gleason 7 encompasses a heterogeneous patient population with variable clinical outcome. Patients with a Gleason 7 PCa can be further stratified by scoring for the presence of cribriform and/or intraductal tumor growth patterns, which correlates with worse disease specific survival.[5] TNM staging is generally applied to solid cancers and describes to which extent **Tumors** have invaded the healthy tissue, disregarded natural organ boundaries, spread to (nearby) lymph **Nodes** and **Metastasized** to distant sites.[6] PSA serves as a biomarker for PCa despite its lack of cancer specificity. In the healthy prostate, luminal epithelial cells express kallikrein 3 (*KLK3*) which encodes for PSA.[7] PSA is a serine protease that is excreted by prostate cells and collected in the urethra, where it cleaves several matrix proteins and contributes to semen motility.[8] In healthy individuals, only very low levels of PSA are detected in the bloodstream compared to the seminal fluid. Several conditions affecting the prostate, both benign and malignant, can give rise to serum PSA levels. It is commonly thought that PCa growth patterns, including loss of the basal cell layer and disruption of the basement membrane, leads to increased PSA levels in the bloodstream.[9] If the Gleason grade, TNM stage and serum PSA levels together indicate (very) low-risk PCa, an active surveillance program is usually recommended.[3] Active surveillance includes regular prostate examinations, PSA monitoring and repeated tumor sampling to initiate active treatment only when signs of disease progression arise.[6] For patients with intermediate or high risk localized PCa there are two major treatment options that aim to cure; surgery and radiotherapy. Surgical removal of the prostate aims to eradicate the PCa while retaining continence, potency and can be performed using modern laparoscopic or robot-assisted

techniques. This decreases hospital stay and blood loss compared to more invasive open surgery procedures.[3] Radiotherapy is particularly effective when combined with neoadjuvant androgen deprivation therapy. *In vitro* studies have shown that hormonal manipulation act as a radiosensitizer, by interfering with radiation induced DNA damage repair.[10,11] Overall local treatment with curative intent is highly effective, as the onset of metastatic disease is about 2.4-3 per 1000 person-years.[12] However in subsets of patients, such as those with a cribriform and/or intraductal carcinoma positive tumor, the disease specific survival can drop from 97-99% to 65-69% during 15 years of follow-up.[5]

The role of androgens in prostate cancer

The work of Charles Huggins in the 1940s established PCa as an endocrine related disease. First Huggins showed that androgens were vital for normal prostate physiology, as surgical castration decreased prostate size and function in dogs, which could be reversed by testosterone.[13] Huggins together with Hodges, then aimed to define serum phosphatases as biomarkers for PCa and studied the impact of androgens on alkaline and acid phosphatase levels.[14] They observed that acid phosphatase levels were increased in patients with metastatic PCa (mPCa), decreased by bilateral orchiectomy and increased again after testosterone injections.[15] Huggins was awarded the Nobel prize in 1966 and his work transformed the field of PCa. Since then, testosterone has been validated as a vital component in prostate organogenesis, tissue homeostasis and neoplastic development.[16] Cycles of gonadotropin-releasing hormone (GnRH) production in the hypothalamus, stimulates luteinizing hormone (LH) release from the pituitary, which in turn activates testosterone production by the Leydig cells in the testes. The secondary source of testosterone production are the adrenal glands, which account for 5% of the total production.[17] Removing the testes by bilateral orchiectomy thus depletes patients of the vast majority of their circulating testosterone. Nowadays, androgen deprivation therapy (ADT) is the most commonly used method to infer testosterone depletion and is the first line of defense in mPCa.[18] Continuous stimulation with GnRH agonists or antagonists block the release of LH, resulting in testosterone levels to drop with acceptable testosterone levels being below ≤50ng/dl.[19,20] Testosterone, and its more potent derivative dihydrotestosterone (DHT), stimulate neoplastic behavior in PCa through the transcriptional activity of the androgen receptor (AR). The AR is part of the nuclear receptor family, and bears strong resemblance to family members such as the progesterone and glucocorticoid receptor.[21] These paralogs share a common protein structure of an amino(N)-terminal domain (NTD) harboring the transactivation units, a central DNA binding domain (DBD), a flexible hinge region and the carboxyl(C)-terminal ligand binding domain (LBD) which interacts with hormones.[22] Upon binding of testosterone or DHT, the AR dislocates from its chaperones, a complex of heat shock proteins including

HSP90 and initiates a conformational change (Figure 1). This N/C interaction is unique for the AR and locks the ligand in its place to prevent receptor degradation.[23,24] The AR then translocates to the nucleus, although the mechanism underlying AR transport has not yet been fully elucidated. The current hypothesis is that the AR is tethered to tubulins until ligand binding initiates transport across the microtubule structures by the motor-protein dynein.[25] Contrastingly, nuclear import of the AR has been well established and relies on the interaction of the nuclear localization signal (NLS) with nuclear importin proteins.[26] In the nucleus, the AR interacts as a homodimer with palindromic DNA sequences, known as androgen response elements (AREs), which are located in the promotor/enhancer region of AR regulated genes. The AR relies on co-factors to initiate chromatin relaxation, recruit the preinitiation complex and initiate transcription.

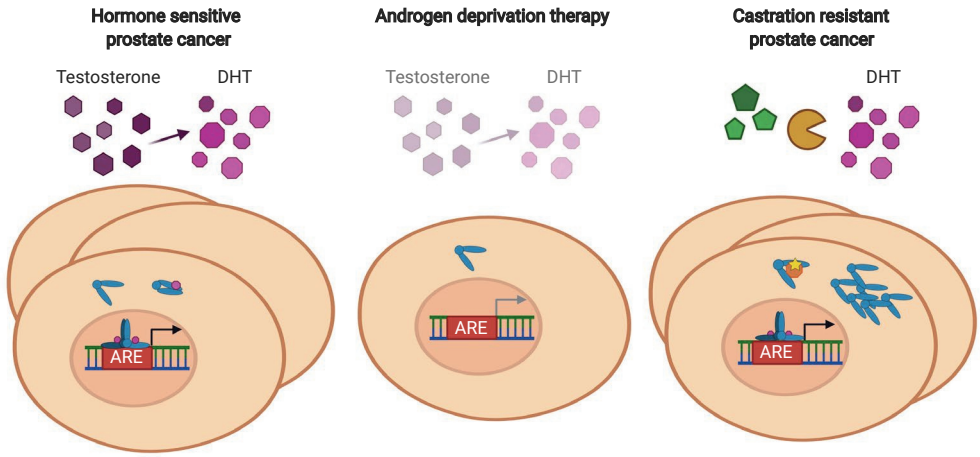

Figure 1: The role of the androgen receptor in the different stages of prostate cancer. During the hormone sensitive stage, testosterone and dihydrotestosterone (DHT) bind and activate the androgen receptor (AR) which then translocates to the nucleus (left). Here it dimerizes and binds androgen response elements (ARE) to initiate gene transcription. Androgen deprivation therapy blocks the vast majority of testosterone productions and results in inativation of the AR pathway (middle). Alterations to the AR gene, including mutations and amplifications, can reactivate the AR pathway and promote castrate resistance (right).

Recently, the crystal structure of a ligand activated AR homodimer interacting with DNA was revealed. This showed that two AR-LBDs and DBDs lie at the center bound to DNA, while two NTDs wrap around and interact with co-factors.[27] Furthermore, AR activation can lead to transcriptional activation and indirect suppression of several hundred genes.[28] ChIP-Seq studies have identified that the AR cistrome diverges between healthy and PCa, showing its differential role in cancer versus normal.[29] Two examples of oncogenes which are differentially expressed in PCa versus normal are *MYC* and *ERG*. In normal prostate epithelial cells, AR activation triggers growth arrest and differentiation, which is in part due to suppression of the transcription factor MYC.[30] Contrastingly, *MYC* is commonly expressed, and amplification of the gene locus on chromosome 8q frequently occurs in advanced PCa.[31,32] The expression of *ERG* is the product of a fusion with the AR regulated *TMPRSS2* gene. The 5' region of *TMPRSS2* is fused to *ERG* caused by a interstitial deletion between the two genes, that allows the *TMPRSS2* promotor to activate *ERG* expression via the AR.[33] The AR has also been shown to interact with different cofactors in PCa, such as FOXA1 and HOXB13. This enables genomic redistribution of the AR and results in differential activation/repression of genes with a FOXA1 and ARE DNA motifs in promotor or enhancer regions.[34] ADT blocks the transcriptional activity of the AR in PCa, thereby stalling proliferation and malignant behavior. Although ADT is initially effective in the vast majority of patients with mPCa, disease progression is inevitable and typically occurs between 6 months and 2 years after initiation of ADT.[35]

Castration resistant prostate cancer

In the early 1990s, several *in vitro* studies aimed to dissect the underlying mechanism(s) of disease progression in PCa patient exposed to ADT. The mechanisms described *in vitro* included bypass of the AR receptor pathway, AR mutations and hypersensitivity for androgens, however clinical validation was lacking. In 1995 Visakorpi et al. showed that AR gene amplifications were frequent in recurrent tumor samples but absent in primary disease.[36] Additionally, AR mutations were found to be associated with a short time to progression in mPCa patients treated with ADT.[37] These studies implied that the AR pathway plays an essential role in disease progression despite castrate levels of serum testosterone. Until then, disease progression under ADT was defined as hormone refractory PCa, but given these developments was redefined as castration resistant PCa (CRPC). Recent whole genome sequencing studies underscore the role of AR in CRPC, as AR amplifications, mutations and promotor site alterations occur in ~80% of CRPC patients but are rare in castration naïve patients.[38] These AR aberrations induce castration resistance by androgen hypersensitivity, due to AR overexpression or amplification and ligand promiscuity caused by AR mutations.[39,40] Additionally, tumor samples from CRPC patients have been shown to harbor testosterone levels similar to benign prostate.[40,41] This

has been linked to overexpression of the steroid enzyme 17β-HSD in CRPC which enables adrenal androgen precursors to be converted to testosterone and DHT.[20]

Targeting androgen receptor signaling in CRPC

The discovery that the AR pathway plays an important role in the development of castration resistant disease sparked the development of several AR (pathway) inhibitors. In the late 1960s, testosterone was already known as a ligand for cytoplasmic receptors, which promoted transcriptional activity and proliferation in prostate cells. Although the exact structure of these "androgen receptors " were then unknown, cyproterone acetate was found to interfere with the receptor-testosterone interaction.[41] Unfortunately, the steroidal cyproterone acetate had limited clinical efficacy and was characterized by several (adverse) effects. The non-steroidal flutamide and bicalutamide were approved for clinical use in 1982 and 1995 resp. due to their increased AR affinity, selectivity and potency to suppress testosterone mediated proliferation.[42] These targeted anti-androgens can be used in conjunction with GnRH analogues to infer complete androgen blockade. This has the added benefit of compensating for the initial surge in testosterone levels after initiating GnRH analogue treatment. Interestingly, in some patients that progressed to the CRPC stage while receiving complete androgen blockade treatment, discontinuation of bicalutamide or flutamide resulted in a PSA drop. The short-term disease regression observed in these patients was termed the "anti-androgen withdrawal phenomenon". It was later identified that AR mutations within the LBD were able to not only confer anti-androgen resistance but could confer ligand promiscuity. Anti-androgens target the hormone binding pocket in the LBD of the AR, alterations within this region such as the T877A and W741C/L mutations impact the AR-LBD interaction with flutamide and bicalutamide respectively, resulting in an agonist-like activation.[43] In 2009 the third-generation anti-androgen enzalutamide was selected from a compound screen as it showed superior antagonistic properties compared to bicalutamide. Moreover, enzalutamide interfered with AR pathway activity in LNCaP cells, which harbors the AR T877A mutation conferring bicalutamide resistance.[44,45]

Enzalutamide was approved for clinical use after the pivotal PREVAIL and AFFIRM trials showed increased survival in chemotherapy-naïve and chemotherapy-resistant CRPC patients respectively.[46,47] Abiraterone was introduced following the COU-AA-302 trial and functions upstream in the AR pathway.[48] Abiraterone interferes with CYP17A1, a crucial enzyme in the production of adrenal androgens. Therefore, abiraterone blocks the remaining source of testosterone production from adrenal precursors in patients receiving ADT. Although enzalutamide and abiraterone show substantial efficacy, overall response is hampered by intrinsic, acquired and cross-resistance between the two

androgen-directed therapies.[49-51] In 2012, Li and colleagues showed that cells expressing AR splice variants were inherently resistant to enzalutamide. These AR splice variants lack the AR-LBD, which allows for ligand independent activation and circumvents antagonist binding.[52] Expression of the AR variant 7 (AR-V7) in PCa patients treated with enzalutamide or abiraterone has been associated with impaired PSA response and inferior treatment outcome.[53] Therefore, detection of AR splice variants can help to stratify patients towards chemotherapy, rather than androgen directed treatment.[54,55]

Taxane chemotherapy in mCRPC

Until 2004, the use of chemotherapy in CRPC was limited to mitoxantrone, which provided palliative support but no survival benefit.[56] The TAX327 trial led to the introduction of docetaxel for metastatic CRPC. This taxane chemotherapeutic, induced a 3-month overall survival benefit compared to mitoxantrone.[57] The first-generation taxane paclitaxel, was discovered in the 1960s as part of a screening program for antitumor agents in the plant kingdom and is derived from the Pacific Yew tree (*Taxus brevifolia*).[58] Because extraction was a time consuming and ineffective process, extensive efforts were initiated to determine the chemical structure of paclitaxel. This eventually led to semi-synthetization and production of analogues including docetaxel. Cabazitaxel is the most recent addition to the taxane chemotherapeutics and has been approved for treatment in docetaxel refractory patients.[59] Taxanes function by targeting the β-tubulin subunit of the tubulin polymer that make up the cytoskeleton structure called microtubules and induce microtubule stabilization.[60] Microtubules are dependent on a cycle of tubulin polymerization and depolymerization to shorten and lengthen filaments and function in key cellular processes such as cell mobility, transport and chromatid separation in mitosis. Taxanes block tubulin depolymerization leading to microtubule stabilization. This disrupts the mitotic spindle formation, that subsequently activates the spindle assembly checkpoint and leads to cell cycle stalling in the G2/M phase.[61] Arrest in mitosis can directly lead to cell death induction, called mitotic catastrophe, or cells can exit mitosis without proper chromosome segregation leading to aneuploidy.[62] Whether cells slip out of cell cycle arrest or die depends on competing signals. Slow degradation of the cell cycle regulator cyclin B1 promotes slippage, while build-up of apoptotic activators promotes cell death.[63] Recent data shows that the STING/cGAS apoptosis pathway may also play a role in determining cell fate after taxane treatment. The STING/cGAS pathway is a natural defense mechanism for foreign extra-nuclear DNA, and triggers immunogenic cell death. Paclitaxel treatment in breast cancer cells has been shown to activate intrinsic apoptosis during mitotic arrest cells via cGAS, but had limited therapeutic efficacy in cells lacking cGAS due to mitotic slippage.[64] However, taxane efficacy is most likely not limited to mitogenic cell death, as illustrated by the lack of clinical efficacy of targeted therapeutics

that block target mitotic spindle formation which mimic the effect of taxanes on mitosis.[61] *In vitro* studies have suggested that part of the taxane efficacy in PCa is due to the block in AR transport which is mediated by microtubule dynamics.[25,65]

Intrinsic and acquired resistance towards taxane treatment often occurs in mPCa, however there is little knowledge about the underlying mechanisms, at least in a clinical setting. Overexpression of *ABCB1* has been frequently described as a multi drug-resistance mechanism in various cancer models. *ABCB1* encodes for the transporter P-glycoprotein 1 (Pgp), which has broad substrate affinity and is able to export a wide range of chemotherapeutics, including taxanes. Cabazitaxel has decreased affinity for Pgp compared to docetaxel, potentiating its activity in docetaxel resistant cells with Pgp overexpression.[66] However, *ABCB1* gene expression is frequently reduced due to hyper-methylation in PCa compared to normal prostate tissue.[67] Overall, genomic alterations or overexpression of *ABCB1* occurs in small subset of cancer patients, implicating a minor role in chemoresistance.[68] Our group has previously described the loss of *SLCO1B3* expression in a docetaxel resistant *in vivo* model of PCa, which could lead to reduced docetaxel uptake, tumor accumulation and target engagement.[69,70] Diminished target engagement can also be a direct consequence of altered expression of tubulin isoforms. *Tubulin-βIII* overexpression has been shown to impair taxane efficacy and is associated with tumor aggressiveness.[71,72] Several other cancer associated pathways have been implicated in taxane resistance including epithelial to mesenchymal transition, which contributes to metastatic potential, and mutations in the DNA repair protein BRCA2.[73-75]

The interaction between androgens and taxane treatment efficacy in mPCa

While taxanes and AR pathway inhibitors were initially approved for the use in CRPC patients, the CHAARTED and STAMPEDE trials have caused a paradigm shift in the field. These clinical studies showed that adding docetaxel to ADT, induced a tremendous overall survival benefit of 10-13 months in metastatic castrate naïve PCa (mCNPC) patients.[76,77] Contrastingly, adjuvant docetaxel monotherapy was found to be ineffective in delaying biochemical recurrence in patients with high risk PCa undergoing radical prostatectomy. These clinical studies show that ADT improves docetaxel treatment efficacy, suggesting an interaction between the AR pathway and taxane induced cell death. The underlying mechanism of increased taxane treatment efficacy in androgen deprived patient is likely multifaceted. It has been shown that docetaxel pharmacokinetics are affected by ADT, with CRPC patients showing a 100% increase in docetaxel clearance and a two-fold decrease in exposure.[78] This is in line with the observations that docetaxel treatment in the castrate naïve setting is associated with an increase in neutropenic fever, most likely

due to increased exposure.[79] Moreover, increased testosterone levels in CRPC patients have been correlated with significantly shorter progression free survival after taxane treatment in two retrospective studies.[80,81] There have also been several preclinical studies that showed an interaction between AR signalling and taxane efficacy. AR activation by DHT was shown to increase cell viability of LAPC4 cells treated with docetaxel.[82] Moreover, combining enzalutamide with cabazitaxel treatment decreased cell viability in VCaP cells as well as inducing a small increase in TUNEL (apoptotic) positive cells in the 22RV1 *in vivo* model.[74] Overall these studies support an interaction between the AR pathway and taxane activity and suggest that suppressing androgen signalling could improve taxane treatment efficacy, leading the way for new combination modalities.

With these recent shifts and several new therapeutics under clinical evaluation, the treatment landscape of metastatic PCa has become increasingly complex. Furthermore, several interactions have been observed, impacting treatment efficacy and sequencing. Impaired response to enzalutamide treatment has been reported for CRPC patients who have progressed on abiraterone and vice versa, implicating cross-resistance.[83,84] Moreover, cabazitaxel was found to be superior as a third-line treatment in patients pretreated with docetaxel and AR pathway inhibitors, compared to the alternative AR pathway inhibitor.[85] A retrospective analysis of the GETUG-AFU trial also implicated that docetaxel rechallenge in mCRPC patients previously treated with ADT and docetaxel has limited efficacy.[86] Overall, with the expanding landscape and treatment interactions observed, there is an unmet need for biomarkers to support treatment selection.

Circulating tumor cells

Circulating tumor cells (CTCs) are neoplastic cells that originate from solid tumors and have entered the peripheral bloodstream or lymphatic system. CTCs can originate from primary or metastatic tumors, but are identified in greater numbers in patients with disseminated disease.[87] CTCs are part of the metastatic cascade in cancer, and hold strong clinical implications, as the majority patients with solid cancers die from metastatic disease.[88] This is in part illustrated by the predictive value of high CTC numbers (≥5 per 7.5 ml peripheral blood) in relation to disease progression and response to therapeutic interventions.[89,90] In order to successfully invade foreign tissue, tumor cells have to overcome several rate limiting steps including extravasation from the primary tumor, survival and escape from the circulation, successfully invading foreign tissue and initiating tumor formation. The metastatic process thus invokes a major bottleneck for cell survival, and the amount of CTCs identified in the circulation far exceeds the successfully disseminated tumor cells.[91] Moreover, the metastatic process is seemingly far from random, as distinct tissue preferences have been identified for metastatic spread of different solid cancers, including

PCa which frequently metastasizes to the bone.[92] Although the metastasizing capacity of a single CTC is low, insights into the underlying mechanisms promoting dissemination have been gained from studying CTCs. Both CTC clusters and CTCs adhering to neutrophils, harbor increased metastatic potential.[93] Interestingly, large scale whole genome analysis of metastatic cancers did not reveal unique genomic alterations compared localized disease, implicating that the metastatic potential could be inherent to cancer.[94]

Sampling CTCs as a liquid biopsy harbors the potential to study disease progression in individual patients as an alternative to using static sources such as tumor biopsy samples. For example, the expression of AR-V7 in CTCs of mCRPC patients has recently been validated as a prognostic marker for response to AR pathway inhibitors in a prospective clinical trial.[95] Advances into CTC enrichment, detection and single cell omics techniques also enable more in-depth studies into genetic and transcriptomic heterogeneity of cancer.[96] mPCa has been shown to harbor extensive intra-patient genomic heterogeneity and complex seeding relationships between primary and metastatic tumor sites.[97] A single-cell RNA sequencing study in mPCa unveiled extensive intra- and inter-patient heterogeneity from CTCs, which shows the potential of CTCs to capture intra-patient heterogeneity.98 However, the authors noted that the study was hampered by the limited number of CTCs analyzed. In-depth omics studies are thus limited by the number of CTCs obtained by standard sampling as the median CTC count in mPCa patients is 2-20 per 7.5 ml peripheral blood.[89] Leukapheresis is a standardized procedure to enrich for mononuclear cells by continuously centrifugation of blood, including CTCs.[99] Leukapheresis thus harbors the potential to maximize the CTC yield thereby providing a platform for in-depth studies into intra-patient heterogeneity. Using leukapheresis, Lambros et al. performed single cell copy number analysis on 185 CTCs from 14 mPCa patients.[100] The CTCs displayed substantial copy number heterogeneity, with divergent clones that were previously unidentified in matching biopsy samples. Besides omics studies, viable CTCs could be expanded *ex vivo* to provide new preclinical models and may be used in drug screening. Overall, sampling CTCs could offer a real-time insights into the genetic, transcriptomic and phenotypic make-up of cancer.

Models of prostate cancer

In vitro and *in vivo* models play a vital role in pre-clinical oncology research and enabled the implementation of numerous new treatment modalities. However, obtaining new models of (metastatic) PCa has shown to be particularly challenging. As PCa is a relatively slow growing neoplasm, *in vitro* expansion of tumor cells has been hampered by the overgrowth of benign basal and stromal cells.[101] The initial repertoire of commonly used PCa cell lines consisted of PC3, DU145 and LNCaP, of which only the latter expresses AR and PSA.[102] The development of patient derived xenograft (PDX) substantially increased the catalogue of PCa models, as the success rate for *in vivo* expansion of PCa cells is considerably higher than *in vitro*. Examples include the Rotterdam panel of 12 unique PDX models developed in the department of Urology at the Erasmus MC, the LuCaP panel from the University of Washington and the large sets from MD-Anderson and the University of Vancouver (characterized by Navone et al.).[103-105] Unfortunately, establishing a PDX is a lengthy procedure and serial transplantation requires numerous laboratory animals to maintain a stable model. *In vitro* expansion of established PDX models harbors several advantages and has been successfully achieved for some models, including the AR and PSA expressing cell lines PC346C, VCaP and 22RV1. Still the clinical disease course of PCa with its inherent heterogeneity is underrepresented. This is in part highlighted by the underrepresentation of TMPRSS2-ERG fusions in PDX models which enables AR regulated ERG expression. While expression of ERG was identified in 28% of the Movember GAP1 PDX panel, while the *TMPRSS2-ERG* fusion was previously detected 38% of the PCa patients with localized non-indolent disease and in 43% of the mCRPC population.[32,38,106] To expand the current set of available models and to mimic the impact of therapeutic interventions, established *in vitro* or *in vivo* models can be subjected to ADT or other commonly applied treatments. The established sublines are used to study resistance mechanisms, such as the previously identified cross-resistance between androgen directed therapies.[65,107] A recent addition to *in vitro* models used are organoids, a three dimensional, self-organizing model that more accurately represents the original tissue organization and composition than standard 2D *in vitro* models. Organoids were first described by Sato and colleagues in 2009, who recreated the crypt-villus structure in colorectal tissue *in vitro*, with inherent cell phenotypes.[108] To obtain colorectal organoids, the cell culture media was composed of epithelial/stem cell factors and cells were mixed with a gel that mimics the tissue extracellular matrix composition. This culture technique has now been adapted and applied to several different healthy tissues and tumor types.[109] In 2016 the first patient derived PCa organoids were established, Gao et al. obtained seven organoid cell lines with an overall success rate of 19%.[110,111] This is a substantial improvement compared to standard culture techniques, although contamination of normal cells still presents as a major limitation. Interestingly, one of the obtained organoid models was derived

from CTCs, thereby circumventing the outgrowth of normal epithelial and stromal cells. However, obtaining sufficient amounts of cells for *ex vivo* culture most likely limits this approach to patients from which we can obtain several hundreds of CTCs. This hurdle could potentially be resolved by obtaining high number of CTCs by leukapheresis as previously mentioned. Overall the organoid models obtained by Gao et al. are a valuable addition to the current set of PCa models, as they maintained common genomic alterations such as a *TMPRSS2-ERG* fusion, *PTEN* loss and *TP53* mutations. The PCa organoids were also used in drug screening, which shows potential for high throughput drug testing in models that better represent tumor tissue organization, bridging the gap between 2D cell lines and PDX models. For example, gastrointestinal cancer organoid models have already been shown to reflect the clinical response of the individual patient, highlighting the potential for personalized cancer therapy.[112] High-throughput drug screening using patient-derived neuroendocrine PCa organoids, for which effective treatment options are limited, revealed potentially effective treatment combinations using inhibitor of the epigenetic modulator EZH2.[113]

Scope of this thesis

This thesis consists of two parts. In **Part I** we aimed to demonstrate that androgen signaling impacts taxane activity and define the mechanisms underlying optimal taxane treatment efficacy in CRPC.

In **Chapter II and III** we set out to demonstrate that AR pathway stimulation by testosterone impacts taxane treatment activity, using *in vivo* and *in vitro* models of AR positive CRPC. We aimed to define mechanisms underlying taxane activity by investigating tumor accumulation, target engagement, cell viability and death. In **Chapter IV** we set out to validate cellular thermal shift assays (CETSA) as a method to infer taxane target engagement and its correlation to taxane tumor accumulation.

Based on the results described in Chapter II and III we hypothesized that targeting AR signaling improves taxane treatment efficacy. We therefore intended to define the combination of cabazitaxel with enzalutamide as a viable treatment strategy for CRPC in **Chapter V**.

In **Part II** we aimed to provide a platform for personalized cancer therapy in mPCa. In **Chapter VI** we enriched CTCs from mPCa patients using diagnostic leukapheresis (DLA) to enable *ex vivo* expansion of PCa organoids. Subsequently, we aimed to show that these CTC derived organoids can reflect treatment response of the individual patient and function as reliable disease models. Lastly, we aimed to show that enriched CTCs capture the inherent intratumor heterogeneity of mPCa.

References

1. Ferlay J, Colombet M, Soerjomataram I, et al. Cancer incidence and mortality patterns in Europe: Estimates for 40 countries and 25 major cancers in 2018. Eur J Cancer. 2018;103:356-387.
2. Lu-Yao GL, Albertsen PC, Moore DF, et al. Outcomes of localized prostate cancer following conservative management. JAMA. 2009;302(11):1202-1209.
3. Sathianathen NJ, Konety BR, Crook J, Saad F, Lawrentschuk N. Landmarks in prostate cancer. Nat Rev Urol. 2018;15(10):627-642.
4. Epstein JI, Allsbrook WC, Jr., Amin MB, Egevad LL, and the IGC. The 2005 International Society of Urological Pathology (ISUP) Consensus Conference on Gleason Grading of Prostatic Carcinoma. The American Journal of Surgical Pathology. 2005;29(9):1228-1242.
5. Kweldam CF, Kummerlin IP, Nieboer D, et al. Disease-specific survival of patients with invasive cribriform and intraductal prostate cancer at diagnostic biopsy. Mod Pathol. 2016;29(6):630-636.
6. S. Gillessen; J. Grummet; A.M. Henry; T.B. Lam; M.D. Mason; T.H. van der Kwast; H.G. van der Poel; O. Rouvière; I.G. Schoots; D. Tilki; T. Wiegel NMCPCV-cRCNvdBEBPRMDSSF. EAU Guidelines. Edn. presented at the EAU Annual Congress Amsterdam 2020 ; Classification and Staging Systems. Arnhem, The Netherlands.: EAU Guidelines Office; 2020.
7. Balk SP, Ko YJ, Bubley GJ. Biology of prostate-specific antigen. J Clin Oncol. 2003;21(2):383-391.
8. Wang TJ, Rittenhouse HG, Wolfert RL, Lynne CM, Brackett NL. PSA Concentrations in Seminal Plasma. Clinical Chemistry. 1998;44(4):895a-896.
9. Lilja H, Ulmert D, Vickers AJ. Prostate-specific antigen and prostate cancer: prediction, detection and monitoring. Nature Reviews Cancer. 2008;8(4):268-278.
10. Denham JW, Steigler A, Lamb DS, et al. Short-term neoadjuvant androgen deprivation and radiotherapy for locally advanced prostate cancer: 10-year data from the TROG 96.01 randomised trial. Lancet Oncol. 2011;12(5):451-459.
11. Tarish FL, Schultz N, Tanoglidi A, et al. Castration radiosensitizes prostate cancer tissue by impairing DNA double-strand break repair. Sci Transl Med. 2015;7(312):312re311.
12. Hamdy FC, Donovan JL, Lane JA, et al. 10-Year Outcomes after Monitoring, Surgery, or Radiotherapy for Localized Prostate Cancer. N Engl J Med. 2016;375(15):1415-1424.
13. Huggins C, Clark PJ. Quantitative Studies of Prostatic Secretion : Ii. The Effect of Castration and of Estrogen Injection on the Normal and on the Hyperplastic Prostate Glands of Dogs. J Exp Med. 1940;72(6):747-762.
14. Huggins C, Hodges CV. Studies on prostatic cancer. I. The effect of castration, of estrogen and androgen injection on serum phosphatases in metastatic carcinoma of the prostate. CA Cancer J Clin. 1972;22(4):232-240.
15. Glina S, Rivero MA, Morales A, Morgentaler A. Studies on prostatic cancer I. The effect of castration, of estrogen and of androgen injection on serum phosphatases in metastatic carcinoma of the prostate by Charles Huggins and Clarence V. Hodges. J Sex Med. 2010;7(2 Pt 1):640-644.
16. Toivanen R, Shen MM. Prostate organogenesis: tissue induction, hormonal regulation and cell type specification. Development. 2017;144(8):1382-1398.
17. Diala El-Maouche; Adrian Dobs. Chapter 60 - Testosterone Replacement Therapy in Men and Women. In: Legato MJ, ed. Principles of Gender-Specific Medicine: Academic Press; 2010:737-760.

18. Sharifi N, Gulley JL, Dahut WL. Androgen Deprivation Therapy for Prostate Cancer. Jama. 2005;294(2):238-244.
19. Morote J, Comas I, Planas J, et al. Serum Testosterone Levels in Prostate Cancer Patients Undergoing Luteinizing Hormone-Releasing Hormone Agonist Therapy. Clin Genitourin Cancer. 2018;16(2):e491-e496.
20. Snaterse G, Visser JA, Arlt W, Hofland J. Circulating steroid hormone variations throughout different stages of prostate cancer. Endocr Relat Cancer. 2017;24(11):R403-R420.
21. Aranda A, Pascual A. Nuclear hormone receptors and gene expression. Physiol Rev. 2001;81(3):1269-1304.
22. Jenster G. The role of the androgen receptor in the development and progression of prostate cancer. Semin Oncol. 1999;26(4):407-421.
23. van de Wijngaart DJ, Dubbink HJ, van Royen ME, Trapman J, Jenster G. Androgen receptor coregulators: recruitment via the coactivator binding groove. Mol Cell Endocrinol. 2012;352(1-2):57-69.
24. Azad AA, Zoubeidi A, Gleave ME, Chi KN. Targeting heat shock proteins in metastatic castration-resistant prostate cancer. Nat Rev Urol. 2015;12(1):26-36.
25. Thadani-Mulero M, Nanus DM, Giannakakou P. Androgen receptor on the move: boarding the microtubule expressway to the nucleus. Cancer Res. 2012;72(18):4611-4615.
26. Clinckemalie L, Vanderschueren D, Boonen S, Claessens F. The hinge region in androgen receptor control. Mol Cell Endocrinol. 2012;358(1):1-8.
27. Yu X, Yi P, Hamilton RA, et al. Structural Insights of Transcriptionally Active, Full-Length Androgen Receptor Coactivator Complexes. Molecular Cell.
28. Poluri RTK, Beauparlant CJ, Droit A, Audet-Walsh E. RNA sequencing data of human prostate cancer cells treated with androgens. Data Brief. 2019;25:104372.
29. Pomerantz MM, Li F, Takeda DY, et al. The androgen receptor cistrome is extensively reprogrammed in human prostate tumorigenesis. Nat Genet. 2015;47(11):1346-1351.
30. Isaacs JT. Resolving the Coffey Paradox: what does the androgen receptor do in normal vs. malignant prostate epithelial cells? Am J Clin Exp Urol. 2018;6(2):55-61.
31. Gurel B, Iwata T, Koh CM, et al. Nuclear MYC protein overexpression is an early alteration in human prostate carcinogenesis. Mod Pathol. 2008;21(9):1156-1167.
32. Robinson D, Van Allen EM, Wu YM, et al. Integrative clinical genomics of advanced prostate cancer. Cell. 2015;161(5):1215-1228.
33. Tomlins SA, Rhodes DR, Perner S, et al. Recurrent fusion of TMPRSS2 and ETS transcription factor genes in prostate cancer. Science. 2005;310(5748):644-648.
34. Stelloo S, Bergman AM, Zwart W. Androgen receptor enhancer usage and the chromatin regulatory landscape in human prostate cancers. Endocr Relat Cancer. 2019;26(5):R267-R285.
35. James ND, Spears MR, Clarke NW, et al. Survival with Newly Diagnosed Metastatic Prostate Cancer in the "Docetaxel Era": Data from 917 Patients in the Control Arm of the STAMPEDE Trial (MRC PR08, CRUK/06/019). Eur Urol. 2015;67(6):1028-1038.
36. Visakorpi T, Hyytinen E, Koivisto P, et al. In vivo amplification of the androgen receptor gene and progression of human prostate cancer. Nat Genet. 1995;9(4):401-406.
37. Tilley WD, Buchanan G, Hickey TE, Bentel JM. Mutations in the androgen receptor gene are associated with progression of human prostate cancer to androgen independence. Clin Cancer Res. 1996;2(2):277-285.
38. van Dessel LF, van Riet J, Smits M, et al. The genomic landscape of metastatic castration-resistant prostate cancers reveals multiple distinct genotypes with potential clinical impact.

Nature Communications. 2019;10(1):5251.
39. Chen CD, Welsbie DS, Tran C, et al. Molecular determinants of resistance to antiandrogen therapy. Nat Med. 2004;10(1):33-39.
40. Taplin ME. Androgen receptor: role and novel therapeutic prospects in prostate cancer. Expert Rev Anticancer Ther. 2008;8(9):1495-1508.
41. Sluyser M, Kassenaar AAH. Mechanism of androgen action at the cellular level. Pharmacology & Therapeutics Part B: General and Systematic Pharmacology. 1975;1(2):179-188.
42. Crawford ED, Schellhammer PF, McLeod DG, et al. Androgen Receptor Targeted Treatments of Prostate Cancer: 35 Years of Progress with Antiandrogens. J Urol. 2018;200(5):956-966.
43. Bohl CE, Miller DD, Chen J, Bell CE, Dalton JT. Structural basis for accommodation of nonsteroidal ligands in the androgen receptor. J Biol Chem. 2005;280(45):37747-37754.
44. Tran C, Ouk S, Clegg NJ, et al. Development of a second-generation antiandrogen for treatment of advanced prostate cancer. Science. 2009;324(5928):787-790.
45. Shore ND, Chowdhury S, Villers A, et al. Efficacy and safety of enzalutamide versus bicalutamide for patients with metastatic prostate cancer (TERRAIN): a randomised, double-blind, phase 2 study. Lancet Oncol. 2016;17(2):153-163.
46. Beer TM, Armstrong AJ, Rathkopf DE, et al. Enzalutamide in metastatic prostate cancer before chemotherapy. N Engl J Med. 2014;371(5):424-433.
47. Scher HI, Fizazi K, Saad F, et al. Increased survival with enzalutamide in prostate cancer after chemotherapy. N Engl J Med. 2012;367(13):1187-1197.
48. Ryan CJ, Smith MR, de Bono JS, et al. Abiraterone in metastatic prostate cancer without previous chemotherapy. N Engl J Med. 2013;368(2):138-148.
49. Loriot Y, Bianchini D, Ileana E, et al. Antitumour activity of abiraterone acetate against metastatic castration-resistant prostate cancer progressing after docetaxel and enzalutamide (MDV3100). Ann Oncol. 2013;24(7):1807-1812.
50. de Wit R, de Bono J, Sternberg CN, et al. Cabazitaxel versus Abiraterone or Enzalutamide in Metastatic Prostate Cancer. N Engl J Med. 2019;381(26):2506-2518.
51. Rathkopf D, Scher HI. Androgen receptor antagonists in castration-resistant prostate cancer. Cancer J. 2013;19(1):43-49.
52. Li Y, Chan SC, Brand LJ, Hwang TH, Silverstein KAT, Dehm SM. Androgen Receptor Splice Variants Mediate Enzalutamide Resistance in Castration-Resistant Prostate Cancer Cell Lines. Cancer Research. 2013;73(2):483-489.
53. Antonarakis ES, Lu C, Wang H, et al. AR-V7 and resistance to enzalutamide and abiraterone in prostate cancer. N Engl J Med. 2014;371(11):1028-1038.
54. Onstenk W, Sieuwerts AM, Kraan J, et al. Efficacy of Cabazitaxel in Castration-resistant Prostate Cancer Is Independent of the Presence of AR-V7 in Circulating Tumor Cells. Eur Urol. 2015;68(6):939-945.
55. Antonarakis ES, Lu C, Luber B, et al. Androgen Receptor Splice Variant 7 and Efficacy of Taxane Chemotherapy in Patients With Metastatic Castration-Resistant Prostate Cancer. JAMA Oncol. 2015;1(5):582-591.
56. Tannock IF, Osoba D, Stockler MR, et al. Chemotherapy with mitoxantrone plus prednisone or prednisone alone for symptomatic hormone-resistant prostate cancer: a Canadian randomized trial with palliative end points. Journal of Clinical Oncology. 1996;14(6):1756-1764.
57. Tannock IF, de Wit R, Berry WR, et al. Docetaxel plus prednisone or mitoxantrone plus prednisone for advanced prostate cancer. N Engl J Med. 2004;351(15):1502-1512.
58. Wall ME, Wani MC. Camptothecin and taxol: discovery to clinic--thirteenth Bruce F. Cain

Memorial Award Lecture. Cancer Res. 1995;55(4):753-760.
59. de Bono JS, Oudard S, Ozguroglu M, et al. Prednisone plus cabazitaxel or mitoxantrone for metastatic castration-resistant prostate cancer progressing after docetaxel treatment: a randomised open-label trial. Lancet. 2010;376(9747):1147-1154.
60. Field JJ, Diaz JF, Miller JH. The binding sites of microtubule-stabilizing agents. Chem Biol. 2013;20(3):301-315.
61. Shi J, Mitchison TJ. Cell death response to anti-mitotic drug treatment in cell culture, mouse tumor model and the clinic. Endocr Relat Cancer. 2017;24(9):T83-T96.
62. Lens SMA, Medema RH. Cytokinesis defects and cancer. Nat Rev Cancer. 2019;19(1):32-45.
63. Haschka M, Karbon G, Fava LL, Villunger A. Perturbing mitosis for anti-cancer therapy: is cell death the only answer? EMBO Rep. 2018;19(3).
64. Zierhut C, Yamaguchi N, Paredes M, Luo J-D, Carroll T, Funabiki H. The Cytoplasmic DNA Sensor cGAS Promotes Mitotic Cell Death. Cell. 2019;178(2):302-315.e323.
65. van Soest RJ, van Royen ME, de Morree ES, et al. Cross-resistance between taxanes and new hormonal agents abiraterone and enzalutamide may affect drug sequence choices in metastatic castration-resistant prostate cancer. Eur J Cancer. 2013;49(18):3821-3830.
66. Vrignaud P, Semiond D, Lejeune P, et al. Preclinical antitumor activity of cabazitaxel, a semisynthetic taxane active in taxane-resistant tumors. Clin Cancer Res. 2013;19(11):2973-2983.
67. Demidenko R, Razanauskas D, Daniunaite K, Lazutka JR, Jankevicius F, Jarmalaite S. Frequent down-regulation of ABC transporter genes in prostate cancer. BMC Cancer. 2015;15:683.
68. Robey RW, Pluchino KM, Hall MD, Fojo AT, Bates SE, Gottesman MM. Revisiting the role of ABC transporters in multidrug-resistant cancer. Nat Rev Cancer. 2018;18(7):452-464.
69. de Morree E, van Soest R, Aghai A, et al. Understanding taxanes in prostate cancer; importance of intratumoral drug accumulation. Prostate. 2016;76(10):927-936.
70. de Morree ES, Bottcher R, van Soest RJ, et al. Loss of SLCO1B3 drives taxane resistance in prostate cancer. Br J Cancer. 2016;115(6):674-681.
71. Ploussard G, Terry S, Maille P, et al. Class III beta-tubulin expression predicts prostate tumor aggressiveness and patient response to docetaxel-based chemotherapy. Cancer Res. 2010;70(22):9253-9264.
72. Kavallaris M. Microtubules and resistance to tubulin-binding agents. Nat Rev Cancer. 2010;10(3):194-204.
73. Nientiedt C, Heller M, Endris V, et al. Mutations in BRCA2 and taxane resistance in prostate cancer. Sci Rep. 2017;7(1):4574.
74. Martin SK, Pu H, Penticuff JC, Cao Z, Horbinski C, Kyprianou N. Multinucleation and Mesenchymal-to-Epithelial Transition Alleviate Resistance to Combined Cabazitaxel and Antiandrogen Therapy in Advanced Prostate Cancer. Cancer Res. 2016;76(4):912-926.
75. Castro E, Romero-Laorden N, Del Pozo A, et al. PROREPAIR-B: A Prospective Cohort Study of the Impact of Germline DNA Repair Mutations on the Outcomes of Patients With Metastatic Castration-Resistant Prostate Cancer. J Clin Oncol. 2019;37(6):490-503.
76. James ND, Sydes MR, Clarke NW, et al. Addition of docetaxel, zoledronic acid, or both to first-line long-term hormone therapy in prostate cancer (STAMPEDE): survival results from an adaptive, multiarm, multistage, platform randomised controlled trial. Lancet. 2016;387(10024):1163-1177.
77. Sweeney CJ, Chen YH, Carducci M, et al. Chemohormonal Therapy in Metastatic Hormone-Sensitive Prostate Cancer. N Engl J Med. 2015;373(8):737-746.

78. Franke RM, Carducci MA, Rudek MA, Baker SD, Sparreboom A. Castration-Dependent Pharmacokinetics of Docetaxel in Patients With Prostate Cancer. Journal of Clinical Oncology. 2010;28(30):4562-4567.
79. van Soest RJ, de Wit R. Irrefutable evidence for the use of docetaxel in newly diagnosed metastatic prostate cancer: results from the STAMPEDE and CHAARTED trials. BMC Med. 2015;13:304.
80. Shiota M, Kashiwagi E, Murakami T, et al. Serum testosterone level as possible predictive marker in androgen receptor axis-targeting agents and taxane chemotherapies for castration-resistant prostate cancer. Urol Oncol. 2019;37(3):180 e119-180 e124.
81. Ando K, Sakamoto S, Takeshita N, et al. Higher serum testosterone levels predict poor prognosis in castration-resistant prostate cancer patients treated with docetaxel. Prostate. 2020;80(3):247-255.
82. Komura K, Jeong SH, Hinohara K, et al. Resistance to docetaxel in prostate cancer is associated with androgen receptor activation and loss of KDM5D expression. Proc Natl Acad Sci U S A. 2016;113(22):6259-6264.
83. de Bono JS, Chowdhury S, Feyerabend S, et al. Antitumour Activity and Safety of Enzalutamide in Patients with Metastatic Castration-resistant Prostate Cancer Previously Treated with Abiraterone Acetate Plus Prednisone for =24 weeks in Europe. European Urology. 2018;74(1):37-45.
84. Loriot Y, Bianchini D, Ileana E, et al. Antitumour activity of abiraterone acetate against metastatic castration-resistant prostate cancer progressing after docetaxel and enzalutamide (MDV3100). Annals of Oncology. 2013;24(7):1807-1812.
85. de Wit R, de Bono J, Sternberg CN, et al. Cabazitaxel versus Abiraterone or Enzalutamide in Metastatic Prostate Cancer. New England Journal of Medicine. 2019;381(26):2506-2518.
86. Lavaud P, Gravis G, Foulon S, et al. Anticancer Activity and Tolerance of Treatments Received Beyond Progression in Men Treated Upfront with Androgen Deprivation Therapy With or Without Docetaxel for Metastatic Castration-naïve Prostate Cancer in the GETUG-AFU 15 Phase 3 Trial. European Urology. 2018;73(5):696-703.
87. Alix-Panabières C, Pantel K. Clinical Applications of Circulating Tumor Cells and Circulating Tumor DNA as Liquid Biopsy. Cancer Discovery. 2016;6(5):479-491.
88. Dillekås H, Rogers MS, Straume O. Are 90% of deaths from cancer caused by metastases? Cancer Med. 2019;8(12):5574-5576.
89. Heller G, McCormack R, Kheoh T, et al. Circulating Tumor Cell Number as a Response Measure of Prolonged Survival for Metastatic Castration-Resistant Prostate Cancer: A Comparison With Prostate-Specific Antigen Across Five Randomized Phase III Clinical Trials. J Clin Oncol. 2018;36(6):572-580.
90. de Bono JS, Scher HI, Montgomery RB, et al. Circulating tumor cells predict survival benefit from treatment in metastatic castration-resistant prostate cancer. Clin Cancer Res. 2008;14(19):6302-6309.
91. Massague J, Obenauf AC. Metastatic colonization by circulating tumour cells. Nature. 2016;529(7586):298-306.
92. Nguyen DX, Bos PD, Massagué J. Metastasis: from dissemination to organ-specific colonization. Nat Rev Cancer. 2009;9(4):274-284.
93. Aceto N. Bring along your friends: Homotypic and heterotypic circulating tumor cell clustering to accelerate metastasis. Biomed J. 2020;43(1):18-23.
94. Priestley P, Baber J, Lolkema MP, et al. Pan-cancer whole-genome analyses of metastatic solid

tumours. Nature. 2019;575(7781):210-216.
95. Andrew JA, Susan H, Jun L, et al. Prospective Multicenter Validation of Androgen Receptor Splice Variant 7 and Hormone Therapy Resistance in High-Risk Castration-Resistant Prostate Cancer: The PROPHECY Study. Journal of Clinical Oncology. 2019;37(13):1120-1129.
96. Keller L, Pantel K. Unravelling tumour heterogeneity by single-cell profiling of circulating tumour cells. Nat Rev Cancer. 2019;19(10):553-567.
97. Gundem G, Van Loo P, Kremeyer B, et al. The evolutionary history of lethal metastatic prostate cancer. Nature. 2015;520(7547):353-357.
98. Miyamoto DT, Zheng Y, Wittner BS, et al. RNA-Seq of single prostate CTCs implicates noncanonical Wnt signaling in antiandrogen resistance. Science. 2015;349(6254):1351-1356.
99. Fischer JC, Niederacher D, Topp SA, et al. Diagnostic leukapheresis enables reliable detection of circulating tumor cells of nonmetastatic cancer patients. Proc Natl Acad Sci U S A. 2013;110(41):16580-16585.
100. Lambros MB, Seed G, Sumanasuriya S, et al. Single-Cell Analyses of Prostate Cancer Liquid Biopsies Acquired by Apheresis. Clin Cancer Res. 2018;24(22):5635-5644.
101. Risbridger GP, Toivanen R, Taylor RA. Preclinical Models of Prostate Cancer: Patient-Derived Xenografts, Organoids, and Other Explant Models. Cold Spring Harb Perspect Med. 2018;8(8).
102. Sobel RE, Sadar MD. Cell lines used in prostate cancer research: a compendium of old and new lines--part 1. J Urol. 2005;173(2):342-359.
103. Nguyen HM, Vessella RL, Morrissey C, et al. LuCaP Prostate Cancer Patient-Derived Xenografts Reflect the Molecular Heterogeneity of Advanced Disease an--d Serve as Models for Evaluating Cancer Therapeutics. Prostate. 2017;77(6):654-671.
104. Marques RB, van Weerden WM, Erkens-Schulze S, et al. The human PC346 xenograft and cell line panel: a model system for prostate cancer progression. Eur Urol. 2006;49(2):245-257.
105. Navone NM, van Weerden WM, Vessella RL, et al. Movember GAP1 PDX project: An international collection of serially transplantable prostate cancer patient-derived xenograft (PDX) models. Prostate. 2018;78(16):1262-1282.
106. Fraser M, Sabelnykova VY, Yamaguchi TN, et al. Genomic hallmarks of localized, non-indolent prostate cancer. Nature. 2017;541(7637):359-364.
107. van Soest RJ, de Morree ES, Kweldam CF, et al. Targeting the Androgen Receptor Confers In Vivo Cross-resistance Between Enzalutamide and Docetaxel, But Not Cabazitaxel, in Castration-resistant Prostate Cancer. Eur Urol. 2015;67(6):981-985.
108. Sato T, Vries RG, Snippert HJ, et al. Single Lgr5 stem cells build crypt-villus structures in vitro without a mesenchymal niche. Nature. 2009;459(7244):262-265.
109. Drost J, Clevers H. Organoids in cancer research. Nat Rev Cancer. 2018;18(7):407-418.
110. Gao D, Vela I, Sboner A, et al. Organoid cultures derived from patients with advanced prostate cancer. Cell. 2014;159(1):176-187.
111. Van Hemelryk A, van Weerden WM. Novel patient-derived 3D culture models to guide clinical decision-making in prostate cancer. Current Opinion in Endocrine and Metabolic Research. 2020;10:7-15.
112. Vlachogiannis G, Hedayat S, Vatsiou A, et al. Patient-derived organoids model treatment response of metastatic gastrointestinal cancers. Science. 2018;359(6378):920-926.
113. Puca L, Bareja R, Prandi D, et al. Patient derived organoids to model rare prostate cancer phenotypes. Nat Commun. 2018;9(1):2404.

Part I

Androgens and Taxanes

Chapter II

Testosterone Diminishes Cabazitaxel Efficacy and Intratumoral Accumulation in a Prostate Cancer Xenograft Model

Lisanne Mout, Ronald de Wit, Debra Stuurman, Esther Verhoef, Ron Mathijssen, Corrina de Ridder, Martijn Lolkema and Wytske van Weerden.

EBioMedicine. 2018 Jan;27:182-186.

Abstract

Inactivation of the androgen receptor (AR) pathway by androgen deprivation therapy (ADT) is the mainstay of (metastatic) prostate cancer therapy. Ultimately, the AR pathway will be re-activated despite castrate levels of circulating androgens. Thereby, maintaining its role even in castration resistant prostate cancer (CRPC). The recent STAMPEDE and CHAARTED trials showed that docetaxel in combination with ADT increased survival in hormone sensitive prostate cancer patients, suggesting cross-talk between AR signaling and chemotherapy efficacy. We hypothesized that a similar interaction may also apply for CRPC that is treated with cabazitaxel. We studied the impact of androgen status on the efficacy, pharmacodynamics and -kinetics of cabazitaxel in a unique and clinically relevant patient derived xenograft model of castration resistant disease. We found that cabazitaxel is highly effective in a castrate setting with strongly reduced AR activation, while tumor growth inhibition by cabazitaxel was completely abolished in the presence of high AR pathway activity. Moreover, additional experiments showed that intratumoral cabazitaxel levels were 3.5 times higher in tumors from castrated mice as compared to tumors from androgen-supplemented animals. We confirmed that cabazitaxel pharmacokinetics were not affected by testosterone, suggesting that androgen status might influence cabazitaxel tumor uptake directly. This study reveals the impact of androgen status on cabazitaxel efficacy and supports the potential of combination of taxane chemotherapeutics with AR axis targeting agents.

Introduction

The treatment landscape of metastatic castration resistant prostate cancer (mCRPC) has expanded with the introduction of taxanes (docetaxel and cabazitaxel), second generation androgen receptor (AR) antagonists and the CYP17A inhibitor abiraterone. Despite substantial clinical impact, the absolute survival benefit in mCRPC remains limited, additionally cross-resistance between drugs may affect treatment efficacy.[1] As a result, attention has been directed towards defining the optimal treatment sequence. Recent clinical trial results have shown that combining therapies rather than treatment sequence, may provide the most optimal approach for metastatic prostate cancer patients. The CHAARTED and STAMPEDE trials have shown robust overall survival benefits by combining androgen deprivation therapy (ADT) with docetaxel.[2,3] Of note, preliminary results have shown that docetaxel without ADT is ineffective in castrate-naive patients (SPCG12, trial NCT00376792)4. This might suggest that reducing circulating androgen levels and androgen receptor activity affects taxane efficacy. Cabazitaxel is the second-line taxane, which is effective in patients with disease progression during or after docetaxel.[5] We hypothesized that, similarly to docetaxel, cabazitaxel efficacy could be affected by androgen-induced AR activation. To test our hypothesis, we evaluated the efficacy of cabazitaxel in a preclinical model of CRPC in the presence or absence of androgens. Since previous work from our group has shown that reduced intratumoral taxane concentrations affect treatment activity,[6] we also studied the effect of hormone manipulation on cabazitaxel pharmacokinetics and intratumoral cabazitaxel concentrations.

Material and Methods

Cell culture

The human prostate CRPC cell line PC346C-DCC-K was established from the PC346C cell line by long-term culturing in the absence of androgens 7,8. The AR expressing PC346C-DCC-K cell line can grow in the absence of androgens, but the AR pathway remains active, as indicated by prostate specific antigen (PSA) expression (supplementary figure 1a). Cell line authenticity was confirmed by short tandem repeat analysis with the Promega PowerPlex 16 kit. Cells were regularly tested for mycoplasma infection, and kept into culture for a maximum of 25 passages after initiating the castrate resistance phenotype.

Animal welfare

All animal experiments were approved by the Animal experiment committee under the Dutch experiments on Animal Act. The current study is in compliance with the Arrive guidelines.

Effect of testosterone on cabazitaxel efficacy

Twenty-four athymic male NMRI nude mice (NMRI-Foxn1nu; Taconic, Ry, Denmark) were subcutaneously inoculated with 5 million PC346C-DCC-K cells, while being anesthetized with isoflurane/O2. Tumor volume (TV) was monitored twice weekly by digital calipers, animals were randomized based on TV at start to ensure homogeneous groups. Mice were surgical castrated once tumors surpassed a volume of 150 mm^3, during the surgical castration mice were anesthetized with Ketamine/Medetomidine (75 mg/kg and 1 mg/kg) and analgesia was provided by Carprofen (5 mg/kg). Six to ten days after castration, mice were randomized to receive either a silastic implant (Freudenberg Medical) containing testosterone (40 mg), or an empty implant as a control. During implantation of the silastic pellets mice were anesthetized with isoflurane/O2. The next day, mice were randomized to receive either one intraperitoneal injection of cabazitaxel (33mg/kg, Sanofi) or placebo (saline). Blood for PSA analysis was sampled (submandibular vein) at tumor formation and biweekly during the experiment until sacrifice. Plasma was isolated from whole blood samples by centrifugation at 8000 rpm for 10 minutes, and PSA was analyzed by an electrochemiluminescence immunoassay. Mice were kept on a 12h dark/light cycle, food and water were provided ad libitum. Mice were sacrificed once the tumors surpassed a volume of 1500 mm^3, or at 90 days after cabazitaxel. Statistical analysis was performed using either SPSS (IBM, version 21) or Graphpad prism (Graphpad software, version 5.01), sample size was calculated using G*power (Kiel University, version 3.1.9.2) and based on

an *in vivo* pilot study (power of 90%, α = 0.01 and effect size of 0.85). Statistical analyses of tumor growth was performed using SPSS and Graphpad prism.
Tumor tissues were formalin fixed and paraffin embedded for immunohistochemistry (IHC) analysis of the AR and cell cycle marker Ki67. In short, 4 µm tissue sections were incubated with primary anti-AR (1:300, SP107 Cell Marque) or anti-Ki67 (1:100, MIB-1 Dako) and visualized with DAB/H2O2 (Dako EnVision kit). IHC staining's were blinded for treatment and scored by two readers, AR staining was scored by multiplying the percentage positive tumor cells with the staining intensity score (0-3). Ki67 staining was scored for percentage positive in the tumor cells.

Cabazitaxel uptake

The experimental set-up and group size was similar to the cabazitaxel efficacy experiment, with the following exception; tumors were isolated 7 days after cabazitaxel injection. Tumors were snap frozen and stored in -80°C. Intratumoral cabazitaxel concentration was determined by a five times dilution of tissue in blank human lithium heparinized plasma (w/v), and homogenized by using a tissue homogenizer. Cabazitaxel concentrations were determined by a validated UPLC-MS/MS method and based on the method as described previously[6,9], and corrected for tumor weight. The lower limit of quantitation (LLOQ) was established at 1.00 ng/mL for cabazitaxel in human lithium heparinized plasma. Peak area ratios of cabazitaxel versus the Internal Standard in human lithium heparinized plasma was a linear function of the concentration from 1.00 to 500 ng/mL. The within- and between-run precision at four tested concentrations, including the LLQ, were ≤10.1 and ≤10.9%, respectively, while the average accuracy ranged from 97.5 to 110%.

Cabazitaxel PK

Fourteen non-tumor baring athymic male nude mice were castrated, and seven days later, randomized to receive either a silastic implant containing testosterone or an empty pellet as a control. Two days later mice received one bolus injection of cabazitaxel (33 mg/kg), and blood was sampled from the submandibular vein at the following time points: 30, 60, 120 and 180 minutes. Plasma was isolated from whole blood samples by centrifugation at 6800 g for 10 minutes. Cabazitaxel concentrations were determined by UPLC-MS/MS.[6,9] Sample size was calculated using Gpower and based on a previous study (power of 80%, α = 0.05 and effect size of 0.4).[6]

Results

We subcutaneously implanted male immune-deficient mice with the AR wt and PSA secreting CRPC cell line PC346C-DCC-K (Figure 1a). [7] The PC346C-DCC-K model does not express AR variants (supplementary figure 1a) and shows reduced *in vitro* response to the anti-androgen enzalutamide compared to the parental model (supplementary figure 1b).[10] We confirmed the CRPC phenotype of this model *in vivo*, as tumors continued to grow after surgical castration of the mice (Figure 1b, c). Subsequent treatment with cabazitaxel induced a near-complete tumor response with none of the castrate mice reaching the end-point (TV 1500 mm^3) (Figure 2a). In contrast, tumors in castrate mice that received testosterone supplementation failed to show a response to cabazitaxel treatment, with time till TV 1500 mm^3 not significantly different from placebo-treated mice (log-rank P=0.199). Testosterone supplemented mice had, even after correcting for tumor volume, increased levels of PSA compared to castrate mice, indicating an active AR pathway in these tumors (Figure 2b).[11] IHC analysis of cabazitaxel-treated tumors in testosterone-supplemented mice showed high levels of AR positive cells with strong nuclear staining (Figure 2c). Moreover, in tumors from cabazitaxel-treated castrate mice, fewer AR positive cells with less intense nuclear staining were observed, as well as reduced Ki67 staining (Figure 2d). To determine a potential mechanism of interaction we measured intratumoral cabazitaxel levels; drug concentrations were 3.5 times higher in tumors from castrate mice compared to testosterone supplemented mice (Figure 3a; 1.36 ng cabazitaxel/mg tumor tissue vs. 0.39 ng cabazitaxel/mg tumor tissue, respectively). Pharmacokinetic analysis of cabazitaxel serum levels showed that the systemic exposure to cabazitaxel was not affected by testosterone supplementation (Figure 3b).

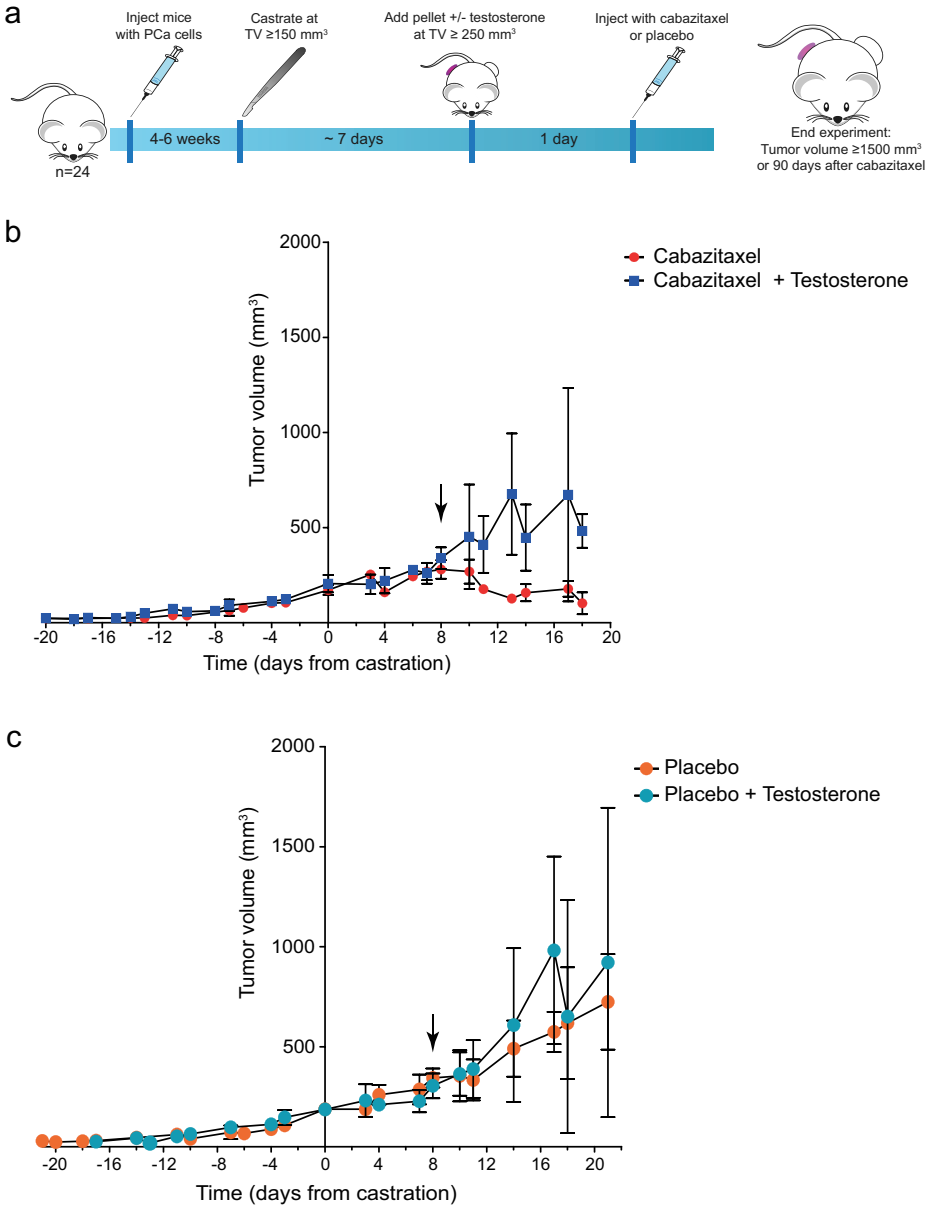

Figure 1: Tumor growth dynamics of the PC346-DCC-K tumor model, confirms CRPC phenotype. **(a)** Schematic overview of the experimental set-up; mice were inoculated with PC346-DCC-K cells and castrated at TV>150 mm³. The next week, mice were randomized to receive either a testosterone pellet or treatment control, and either cabazitaxel or placebo. **(b, c)** Average tumor growth of the cabazitaxel **(b)** and placebo **(c)** treated tumors (± SEM). The PC346-DCC-K tumors (n=5-6) continued to grow after surgical castration of the mice (day 0), underlining the CRPC phenotype of this model. Arrow indicates time of cabazitaxel treatment (b) or placebo control (c).

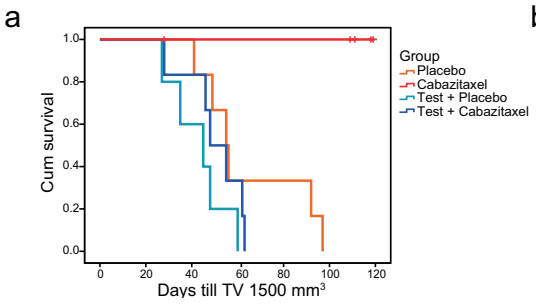

Statistical comparison	P-value log-rank test
Placebo vs. Cabazitaxel	0.01
Test + Placebo vs Test + Cabazitaxel	0.199

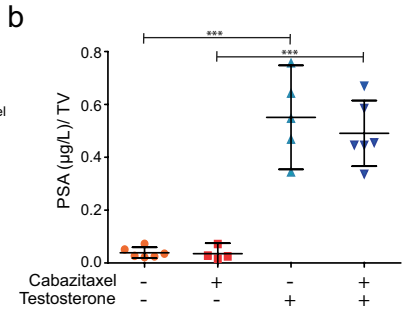

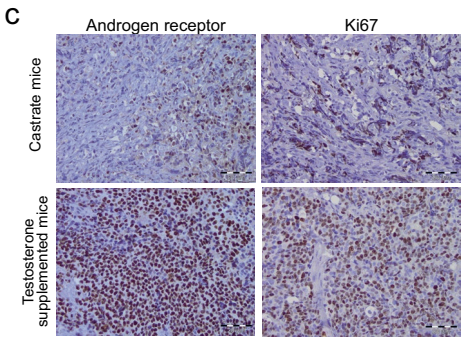

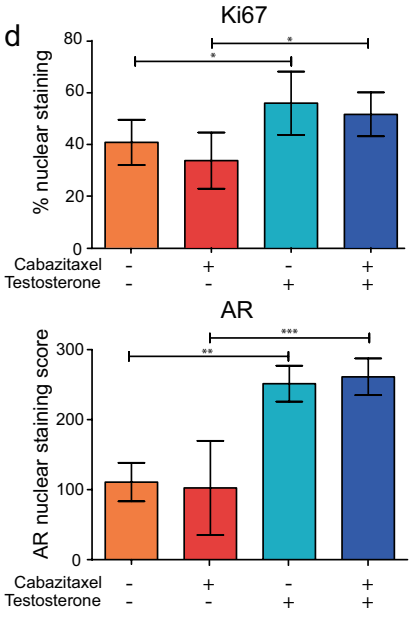

Figure 2. The efficacy of cabazitaxel is abolished by testosterone supplementation while remaining high in castrate mice. (a) Kaplan Meier survival curve showing the time till TV 1500 mm^3 for the four treatment groups (n=5-6), survival was compared by a log-rank test. One mice in the cabazitaxel group was excluded due to weight loss. **(b)** Normalized PSA (µg/L) levels ± SD. PSA was measured in plasma collected at the end of the experiment and normalized for TV. One cabazitaxel treated castrate mice had undetectable PSA levels (<0.1 µg/L). PSA values were compared by a one-way Anova with a Bonferroni post-test, *** indicates a p-value <0.001. **(c)** Representative images of the IHC staining of the AR and Ki67 in PC346C-DCC-K tumors from cabazitaxel treated castrate or testosterone supplemented mice. **(d)** Scoring of IHC staining; the percentage positive Ki67 cells ± SEM and the AR nuclear staining score ± SEM. The percentage Ki67 positive cells was compared by a one-way Anova with a Bonferroni post-test, * indicates a P-value <0.05. The AR nuclear staining score was compared by a Kruskal-Wallis test with a Dunn's post-test, ** indicates a P-value of <0.01 and *** indicate a P value of <0.001.

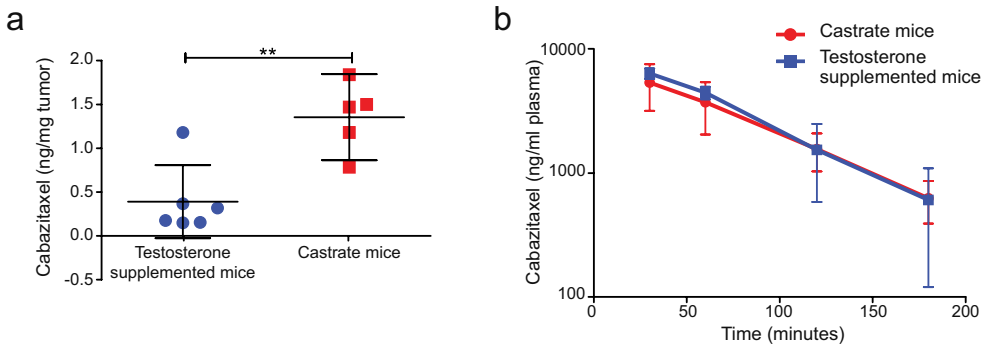

	AUC cabazitaxel mg*h/L
Castrate mice	9.68 (7.02 - 12.34)
Testosterone supplemented mice	11.28 (9.01 - 13.55)

Figure 3: Testosterone supplementation decreases the intratumoral cabazitaxel concentration, but does not alter the cabazitaxel pharmacokinetics. (a) Intratumoral cabazitaxel concentrations were measured in PC346-DCC-K tumors from castrate and testosterone supplemented mice, tumors were excised seven days after cabazitaxel treatment (33 mg/kg). Mean intratumoral cabazitaxel concentrations (ng/mg tumor) ± SD are plotted, t-test was used to compare the concentrations, ** indicates a P-value of 0.0031. **(b)** Castrate or testosterone supplemented mice received one bolus injection of cabazitaxel, blood samples were drawn at four time-points (30, 60, 120 and 180 minutes). Cabazitaxel concentrations were measured in plasma fraction, mean cabazitaxel concentrations ± 95% CI (n=7) are shown.

Discussion

In conclusion, this preclinical study supports recent clinical data of improved taxane efficacy when combined with ADT. Additionally it provides a potential mechanism of action by greater intratumoral accumulation of taxanes during ADT. This preclinical study emphasizes the permanent role of the AR pathway in CRPC and demonstrate its impact on the antitumor activity of cabazitaxel. We show that response to cabazitaxel in an AR-positive CRPC model can be successfully prolonged and resistance delayed by concomitant androgen depletion, thereby reducing AR-activation. As reduced cabazitaxel accumulation seems not to be a consequence of a testosterone-induced change in cabazitaxel exposure, alternatively, testosterone may have an impact on cabazitaxel accumulation. We have previously shown that docetaxel and cabazitaxel uptake is reduced by knockdown of SLCO1B3.[12] Interestingly, OATP drug transporters (encoded by the SLCO family) are also known to function as steroid transporters.[13] Further studies are underway to unravel the molecular mechanisms that link the testosterone to the cellular cytotoxic effect of cabazitaxel. The current study was performed in a unique CRPC tumor models that retained its AR expression upon castration (or testosterone-free culture conditions), which allows us to study the role of the AR in cabazitaxel efficacy. Most hormone sensitive prostate cancer cell lines cultured in the absence of androgens lose their AR expression, and are therefore unfit to examine the interplay between the AR and taxane efficacy. Our data provides a rationale for the combined treatment of cabazitaxel with novel antiandrogen treatments in CRPC patients with an active AR pathway, in order to maximize efficacy of the taxane treatment.[14] Additional studies are warranted to test whether novel antiandrogen treatment, such as abiraterone and enzalutamide, indeed increase taxane efficacy. Such studies may provide guidance to define the optimal window of opportunity for clinical use of combined treatment of taxanes and antiandrogen agents not only in castrate-naïve, but also in metastatic CRPC patients.

References

1. Mezynski J, Pezaro C, Bianchini D, et al. Antitumour activity of docetaxel following treatment with the CYP17A1 inhibitor abiraterone: clinical evidence for cross-resistance? Ann Oncol. 2012;23(11):2943-2947.
2. James ND, Sydes MR, Clarke NW, et al. Addition of docetaxel, zoledronic acid, or both to first-line long-term hormone therapy in prostate cancer (STAMPEDE): survival results from an adaptive, multiarm, multistage, platform randomised controlled trial. Lancet. 2016;387(10024):1163-1177.
3. Sweeney CJ, Chen YH, Carducci M, et al. Chemohormonal Therapy in Metastatic Hormone-Sensitive Prostate Cancer. N Engl J Med. 2015;373(8):737-746.
4. Ahlgren G, Flodgren P, Tammela TLJ, et al. A randomized phase III trial between adjuvant docetaxel and surveillance after radical prostatectomy for high risk prostate cancer: Results of SPCG12. ASCO; 2016.
5. de Bono JS, Oudard S, Ozguroglu M, et al. Prednisone plus cabazitaxel or mitoxantrone for metastatic castration-resistant prostate cancer progressing after docetaxel treatment: a randomised open-label trial. Lancet. 2010;376(9747):1147-1154.
6. de Morree E, van Soest R, Aghai A, et al. Understanding taxanes in prostate cancer; importance of intratumoral drug accumulation. Prostate. 2016;76(10):927-936.
7. Marques RB, van Weerden WM, Erkens-Schulze S, et al. The human PC346 xenograft and cell line panel: a model system for prostate cancer progression. Eur Urol. 2006;49(2):245-257.
8. Marques RB, Erkens-Schulze S, de Ridder CM, et al. Androgen receptor modifications in prostate cancer cells upon long-termandrogen ablation and antiandrogen treatment. Int J Cancer. 2005;117(2):221-229.
9. de Bruijn P, de Graan AJ, Nieuweboer A, et al. Quantification of cabazitaxel in human plasma by liquid chromatography/triple-quadrupole mass spectrometry: a practical solution for non-specific binding. J Pharm Biomed Anal. 2012;59:117-122.
10. van Soest RJ, van Royen ME, de Morree ES, et al. Cross-resistance between taxanes and new hormonal agents abiraterone and enzalutamide may affect drug sequence choices in metastatic castration-resistant prostate cancer. European journal of cancer. 2013;49(18):3821-3830.
11. Marques RB, Dits NF, Erkens-Schulze S, van Weerden WM, Jenster G. Bypass mechanisms of the androgen receptor pathway in therapy-resistant prostate cancer cell models. PLoS One. 2010;5(10):e13500.
12. de Morree ES, Bottcher R, van Soest RJ, et al. Loss of SLCO1B3 drives taxane resistance in prostate cancer. Br J Cancer. 2016;115(6):674-681.
13. Green SM, Kaipainen A, Bullock K, et al. Role of OATP transporters in steroid uptake by prostate cancer cells in vivo. Prostate Cancer Prostatic Dis. 2017;20(1):20-27.
14. Sternberg CN. Improving Survival for Metastatic Castrate-resistant Prostate Cancer: Will Combination Therapy Help Us To Move Forward? Eur Urol. 2016;70(5):722-723.

Supplementary data

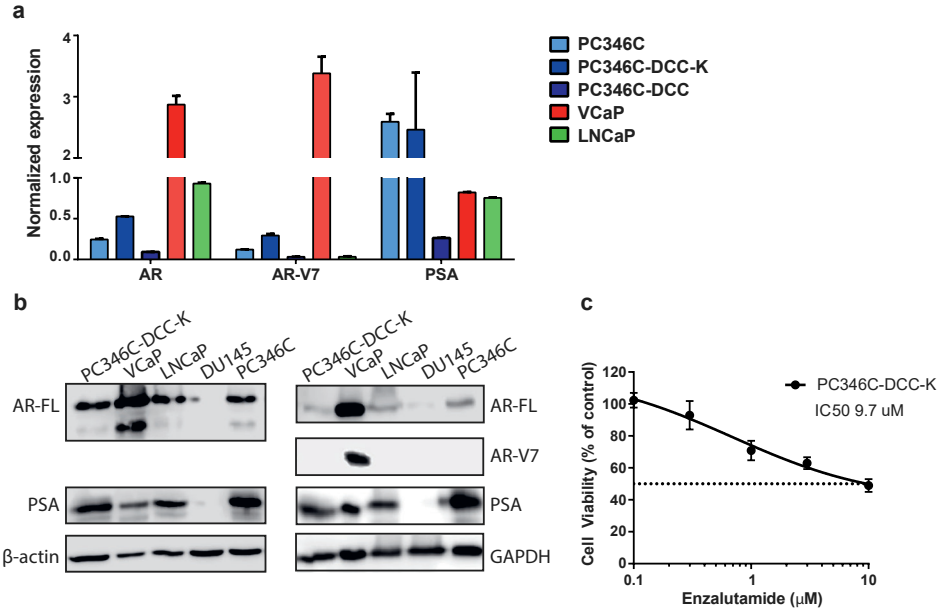

Supplementary figure 1: Androgen receptor characterization of the PC346C-DCC-K model. (a) Normalized gene expression of the AR, AR-V7 and PSA in PC346C-DCC-K and a panel of well-established prostate cancer cell lines. Gene expression was normalized using three housekeeping genes (HPRT1, PBGD and GAPDH). Data is expressed as mean ±SEM (n=2-4). **(b)** Western blot showing the expression of the full length AR (AR-FL, SP107 Cell Marque) and PSA (ER-PR8 Dako Agilent, left panel) in PC346C-DCC-K and AR-V7 (Abcam, ab198394) in comparison to well established prostate cancer cell lines. **(c)** Cell survival assay (MTT) showing the response of the PC346C-DCC-K to the anti-androgen enzalutamide. Data shown is average of three experiments, mean ± SD is plotted on logarithmic scale. IC50 value was calculated using Graphpad.

Supplementary Table 1 – Primers and probes for AR-V7 and HPRT1

Gene	Primer/probe/assay ID	Assay	Supplier
AR-V7	Forward: 5'-CTG TGC GCC AGC AGA AAT-3' Reverse: 5'-TCA GGG TCT GGT CAT TTT GA-3' Probe: 5'-TGTCCATCTTGTCGTCTTCG-3'	Taqman	Sigma-Aldrich, IBA-Lifesciences
HPRT1	5'-TTC CTT GGT CAG GCA GTA TAA TCC-3' 5'-GGT CCT TTT CAC CAG CAA GCT-3'	SYBR green	Sigma-Aldrich

Supplementary methods

mRNA expression of the AR pathway using real-time PCR

Total RNA of the cell lines was isolated using RNA-Bee (Amsbio). For characterization of the AR and AR-V7 in the PC346C-DCC-K model we included the following cell lines: the parental AR/PSA positive PC346C, an AR negative PC346C derived CRPC clone (PC346C-DCC)[1], the AR-V7 positive VCaP and the AR-V7 negative cell line LnCaP.[2] Real-time polymerase chain reaction (RT-PCR) was performed in a 7500 Fast Real-Time PCR System (Applied Biosystems, Thermo Fisher Scientific Inc.), as described previously.[3] In short, AR, AR-V7, PSA, and glyceraldehyde-3-phosphate dehydrogenase (GAPDH) were measured by TaqMan assay (ABsolute QPCR ROX Mix, Thermo Scientific) while Porphobilinogen Deaminase (PBGD) and hypoxanthineguanine phosphoribosyltransferase 1 (HPRT1) were measured by SYBER Green assay (Absolute SYBER Green ROX Mix; Thermo Fisher Scientific). Primers and probes for AR, PSA, GAPDH and PBGD have previously been described.[4] The primer probe sequences for AR-V7 and HPRT1 are shown in supplementary table 1. Gene expression was normalized, using the standard curve method, against the geometric mean of three housekeeping genes HPRT, PBGD and GAPDH.

Western Blot

Western blotting was performed as described previously.[5] In short cell were lysed used RIPA buffer (10 mM TRIS-HCl (pH 7.4), 50 mM NaCl, 5 mM EDTA, 1% Triton X-100, 1% desoxycholate, 0.1% SDS) with a protease inhibitor cocktail (Sigma). Fifteen µg total protein lysates were loaded on a 10% polyacrylamide gel and were blotted on a nitrocellulose membrane. Blots were incubated with AR (1:2000, Sp107 Cell Marque), AR-V7 (1:1000, Abcam EPR15656) or PSA (1:2000, Dako Agilent ER-PR8) and either beta-actin or GAPDH as a loading control (1:10.000 Sigma A1978 and 1:5000 Santa Cruz SC47724, resp.) and imaged using chemiluminescence.

Cell viability assay PC346C-DCC-K

The cell viability assay based on the enzymatic reduction of MTT (3-(4, 5-dimethylthiazolyl-2)-2, 5-diphenyltetrazolium bromide, Sigma) was performed as described previously,[5] with the following modifications. Cells were seeded at a density of 5.000 cells per well in a 96-wells plate. The following day cells were exposed to enzalutamide (ranging from 0.1 to 10 uM, Axon Medchem) in the presence of 0.1 nM R1881, and cells were incubated for 10 days. Three replicates per condition were use, data presented is the average of three individual experiments (mean ±SD). IC50 values were calculated with Graphpad prism (Graphpad software, version 6.07).

References

1. Marques RB, van Weerden WM, Erkens-Schulze S, et al. The human PC346 xenograft and cell line panel: a model system for prostate cancer progression. Eur Urol. 2006;49(2):245-257.
2. Watson PA, Chen YF, Balbas MD, et al. Constitutively active androgen receptor splice variants expressed in castration-resistant prostate cancer require full-length androgen receptor. Proceedings of the National Academy of Sciences of the United States of America. 2010;107(39):16759-16765.
3. Marques RB, Dits NF, Erkens-Schulze S, van Ijcken WF, van Weerden WM, Jenster G. Modulation of androgen receptor signaling in hormonal therapy-resistant prostate cancer cell lines. PLoS One. 2011;6(8):e23144.
4. Marques RB, Aghai A, de Ridder CMA, et al. High Efficacy of Combination Therapy Using PI3K/AKT Inhibitors with Androgen Deprivation in Prostate Cancer Preclinical Models. Eur Urol. 2015;67(6):1177-1185.
5. Marques RB, Erkens-Schulze S, de Ridder CM, et al. Androgen receptor modifications in prostate cancer cells upon long-termandrogen ablation and antiandrogen treatment. Int J Cancer. 2005;117(2):221-229.

Chapter III

Androgen Receptor Signaling Impairs Docetaxel Efficacy in Castration Resistant Prostate Cancer

Lisanne Mout, Matthijs Moll, Mingqing Chen, Eleonora S. de Morrée, Corrina M.A. de Ridder, Alice Gibson, Debra Stuurman, Ashraf Aghai, Sigrun Erkens-Schulze, Ron H.J. Mathijssen, Alex Sparreboom, Ronald de Wit, Martijn P. Lolkema and Wytske M. van Weerden

Br J Cancer. 2020 Dec;123(12):1715-1719

Abstract

Androgen receptor (AR) signaling drives neoplastic growth and therapy resistance in prostate cancer. Recent clinical data show that docetaxel combined with androgen deprivation therapy improves outcome in hormone sensitive disease. We studied whether testosterone and AR signaling interferes with docetaxel treatment efficacy in castration resistant prostate cancer (CRPC). We found that testosterone supplementation significantly impaired docetaxel tumor accumulation in a CRPC model, resulting in decreased tubulin stabilization and anti-tumor activity. Furthermore, testosterone competed with docetaxel for uptake by the drug transporter OATP1B3. Irrespective of docetaxel-induced tubulin stabilization, AR signaling by testosterone counteracted docetaxel efficacy. AR pathway activation could also reverse long-term tumor regression by docetaxel treatment *in vivo*. These results indicate that to optimize docetaxel efficacy, androgen levels and AR signaling need to be suppressed. This study lends evidence for continued maximum suppression of AR signaling by combining targeted therapeutics with docetaxel in castrate-resistant prostate cancer.

Background

The treatment of advanced or metastatic prostate cancer is focused around androgen deprivation therapy (ADT), as testosterone and dihydrotestosterone (DHT) promote neoplastic behavior of prostate cancer cells through androgen receptor (AR) signaling. While ADT almost invariably induces disease regression, the majority of prostate tumors will at some point become resistant due to AR pathway aberrations.[1-3] For patients who progress while receiving ADT, also referred to castration resistant prostate cancer (CRPC), docetaxel is the standard first-line chemotherapy. Recently, the combination of ADT with docetaxel, has been introduced also in the metastatic castrate-naïve setting as this combination significantly increased overall survival.[4,5] Conversely, docetaxel without ADT after radical prostatectomy did not delay disease recurrence.[6] These clinical trials suggest that the anti-tumor efficacy of docetaxel in castrate-naïve prostate cancer is improved by inhibition of AR pathway signaling. In this study we explore the impact of sustained (adrenal) androgen levels and/or AR pathway signaling on docetaxel efficacy in CRPC. Moreover, we studied the underlying mechanisms of AR-pathway activation on docetaxel treatment efficacy by examining docetaxel tumor accumulation, target engagement and cell death induction.

Methods

The AR-positive CRPC patient-derived cell line models, PC346C-DCC-K and VCaP-DCC-E, were derived from the hormone sensitive prostate cancer cell lines, PC346C and VCaP resp. through long-term propagation in castrate conditions.[7] Both PC346C-DCC-K and the parental cell line PC346C do not express AR variants (supplementary figure 1)[8], while VCaP-DCC-E shows increased expression of AR-V7 compared to VCaP. Furthermore, these cell lines do not express *ABCB1* (P-glycoprotein) which has been shown to induce multi-drug resistance.[9] For *in vivo* experiments, NMRI nu/nu male mice were subcutaneously inoculated with PC346C-DCC-K cells and surgically castrated once tumors established (supplementary methods). After one week, mice received a testosterone pellet or treatment control. One injection of docetaxel (33 mg/kg) or NaCl was given the following day. Tumor volume was monitored weekly by calipers and mice were euthanized before the humane endpoint was reached by cervical dislocation (details in supplementary methods).[10] For *in vivo* accumulation studies, tumors were obtained three days after docetaxel treatment. Tumor samples were used to determine docetaxel accumulation by LC-MS/MS[11,12], α-tubulin acetylation by western blot and cell-death by TUNEL staining. Uptake of docetaxel by OATP1B3 was studied in Hek293T cells transiently expressing *SLCO1B3*, uptake of C^{14}-docetaxel was measured in the presence or absence of testosterone. To assess the impact of AR pathway stimulation on docetaxel sensitivity, cell viability assays were conducted. We exposed PC346C-DCC-K and VCaP-DCC-E cells *in vitro* to a dose range of docetaxel with or without androgens.

Results

We first investigated the effect of androgen signaling on the anti-tumor efficacy of docetaxel in the AR positive CRPC model PC346C-DCC-K (Supplementary figure 1). In all castrate mice, docetaxel treatment resulted in long-term and complete tumor regression (Figure 1A). While in testosterone supplemented mice, docetaxel treatment only induced a short-term tumor response, after which all tumors rapidly progressed. The partial response to docetaxel in these mice, shows that testosterone interfered with docetaxel treatment efficacy. We therefore examined docetaxel tumor accumulation in the presence of testosterone, as we previously identified that impaired uptake of taxane chemotherapeutics correlates with treatment resistance.[11] Indeed, testosterone supplemented mice displayed a 40% reduction of docetaxel tumor levels: median of 2.8 ng/mg tumor from testosterone supplemented mice versus 4.4 ng/mg in androgen deprived animals (P-value <0.001, Figure 1B). Moreover, testosterone supplementation resulted in strong AR pathway activation in PC346C-DCC-K tumors as exemplified by increased PSA production, AR nuclear localization, AR target gene expression and tumor cell proliferation (Supplementary figure 2).

To study the underlying mechanism of impaired docetaxel tumor accumulation, we examined the impact of testosterone on docetaxel uptake by the influx drug transporter OATP1B3 (encoded by *SLCO1B3*). *SLCO1B3* is frequently overexpressed in prostate cancer, and docetaxel and testosterone are both OATP1B3 substrates (Supplementary figure 3).[13-16] We found that in Hek293T cells expressing *SLCO1B3*, pre/co-incubation with testosterone, decreased docetaxel uptake by 17% (P-value =0.004, Figure 1C). This implicates that testosterone competes with docetaxel for OATP1B3 mediated uptake, resulting in reduced docetaxel tumor accumulation. As testosterone supplementation interferes with docetaxel accumulation, this will likely affect tubulin target engagement and subsequent stabilization.

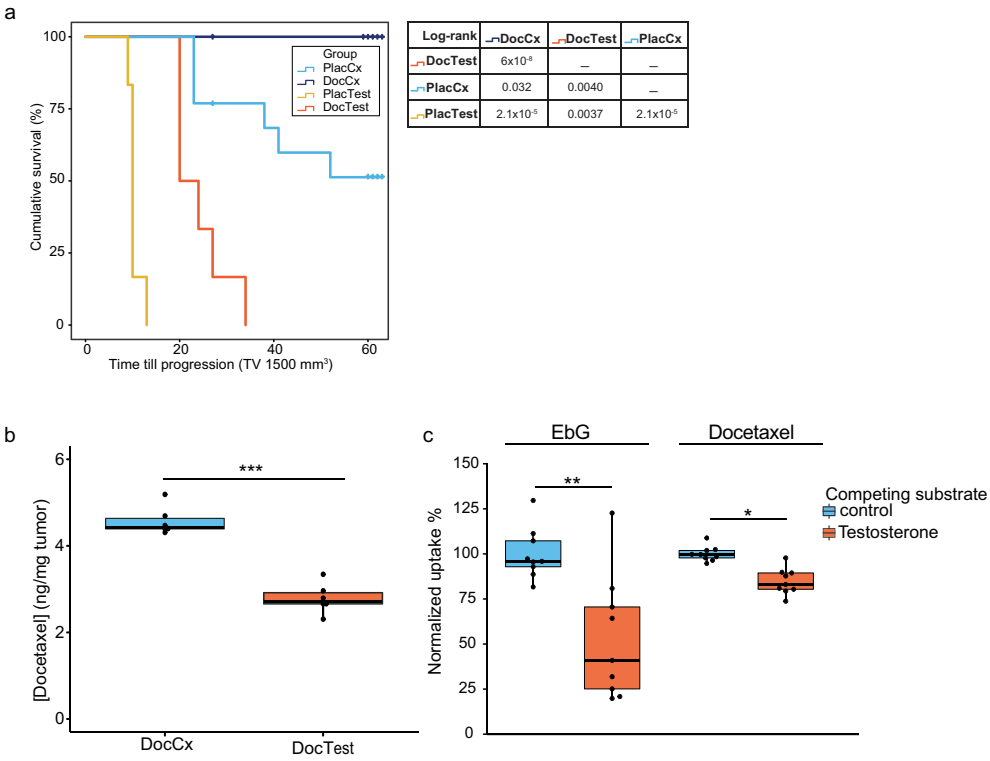

Log-rank	DocCx	DocTest	PlacCx
DocTest	$6x10^{-8}$	_	_
PlacCx	0.032	0.0040	_
PlacTest	$2.1x10^{-5}$	0.0037	$2.1x10^{-5}$

Figure 1: Testosterone supplementation strongly impairs docetaxel efficacy and accumulation. **A)** Impact of testosterone supplementation on docetaxel treatment in tumor bearing mice (PC346C-DCC-K). Kaplan-Meier curve depicting the cumulative survival in the four treatment groups; Docetaxel (once 33 mg/kg i.v.) or placebo in castrate (DocCx n=13 and PlacCx n=13 resp.) or testosterone supplemented mice (PlacTest n=6 and DocTest n=6 resp.). Time till progression was calculated from the day of docetaxel treatment until tumors exceeded a volume of 1500 mm^3. Mice were censored when tumors did not reach 1500 mm^3 in size during the maximum follow-up of 60 days. One mouse in the DocCx treatment group was euthanized due to continued weight loss after treatment. Results from the pair-wise comparison using the log-rank test are shown in the table. **B)** Docetaxel accumulation in PC346C-DCC-K tumors obtained three days after treatment in castrate or testosterone supplemented mice (DocCx n=6 and DocTest n=6 resp.). *** indicates $P < 0.0001$. **C)** Normalized uptake of ^{3}H-estradiol-17β-D-glucuronide (EbG) and C^{14}-docetaxel in Hek293T cells transiently expressing *SLCO1B3*, pre/co-incubated with 200 μM testosterone or vehicle control. Uptake of EbG and docetaxel was normalized to uptake in *SLCO1B3* expressing cells in the absence of testosterone, EbG was used as a positive control for OATP1B3 mediated uptake. Shown are the individual normalized uptake values (n=9) obtained from three experiments. ** indicate $P<0.01$ and * is $P<0.05$ resp.

We therefore investigated acetylation of a-tubulin, which is a result of taxane-mediated tubulin stabilization.[17] Indeed, α-tubulin acetylation was significantly correlated with docetaxel tumor accumulation levels (supplementary figure 4A and B). Moreover, we observed a trend towards decreased tubulin stabilization in PC346C-DCC-K tumors from short-term docetaxel-treated mice supplemented with testosterone (19% decrease, P=0.17, Figure 2A and Supplementary figure 4C). Overall, these data confirm that testosterone reduces docetaxel target engagement as a result of impaired tumor accumulation. To further assess docetaxel activity, we quantified docetaxel-induced cell-death by TUNEL. Testosterone interfered with docetaxel induced cell-death, as shown by the strong reduction in TUNEL staining compared to docetaxel treated castrate mice (P=<0.001, Figure 2B and Supplementary figure 5). Moreover, TUNEL staining in tumors from docetaxel-treated mice supplemented with testosterone was not significantly different to untreated controls (P-value=0.36). Therefore, tubulin stabilization by docetaxel treatment in testosterone supplemented mice, albeit reduced, did not translate into cell-death induction.

We thus hypothesized that AR pathway activation by testosterone further abrogates docetaxel efficacy. Indeed, a small but consistent survival advantage was achieved by R1881 under effective docetaxel concentrations in AR positive CRPC cell lines (Figure 2C, >0.3 nM docetaxel with P=0.032 and P=0.073 for PC346C-DCC-K and VCaP-DCC-E resp). R1881 did not impact docetaxel response in AR negative PCa cells (Supplementary figure 6). This indicates that androgen stimulation can protect AR positive CRPC cells from docetaxel-induced cell death. The increased cell viability under docetaxel treatment led us to investigate whether AR-pathway stimulation alone could re-induce proliferation *in vivo*. We therefore repeated the docetaxel treatment in castrate mice as depicted in Figure 1A and investigated the impact of AR-pathway activation. Testosterone-induced strong AR pathway stimulation, as shown by AR nuclear localization and target gene expression, which led to rapid outgrowth in five out of seven PC346C-DCC-K tumors (Figure 2D, supplementary figure 7). Overall, AR pathway activation was able to overcome long-term tumor regression induced by docetaxel treatment.

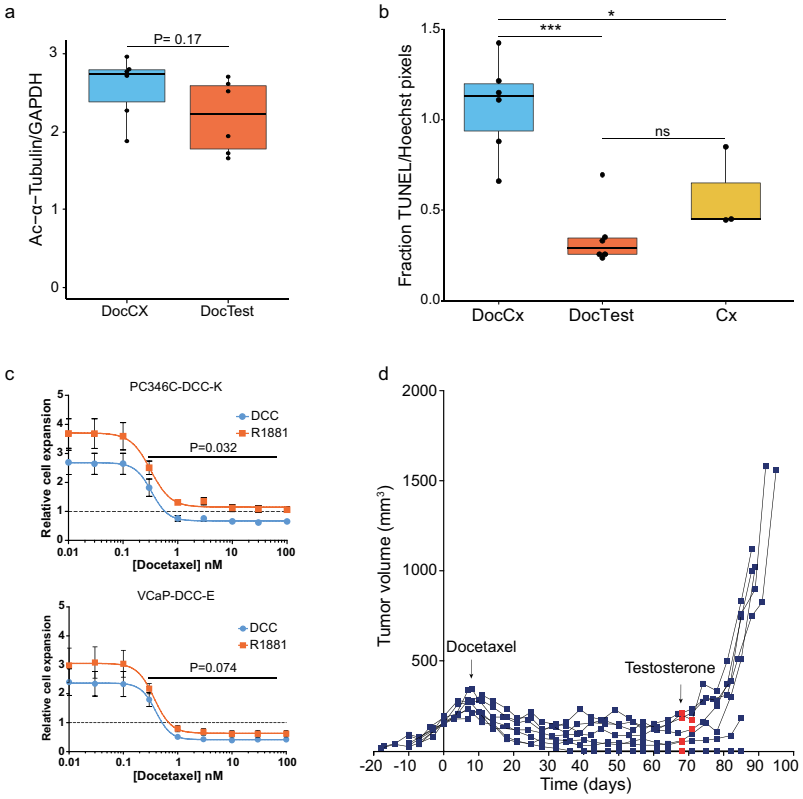

Figure 2: Testosterone and AR pathway activity interfere with docetaxel induced target engagement and cell death. A) Acetylated-α-tubulin as a measurement for tubulin stabilization in PC346C-DCC-K tumors obtained 3 days after docetaxel treatment, in castrate and testosterone supplemented mice (DocCx n=6 and DocTest n=6 resp.). Acetylated-α-tubulin signal intensity was obtained by immunoblotting individual tumor samples and normalized to GAPDH loading control. Statistical comparison was performed by a two-sided T-test. **B)** Quantification of TUNEL stainings in short-term docetaxel treated PC346C-DCC-K tumors from castrate and testosterone supplemented mice (DocCx n=6 and DocTest n=6 resp.). TUNEL signal was compared to three tumors obtained from castrate mice (Cx) with no/low docetaxel accumulation (≤0.1 ng/mg tumor) after short-term treatment. Fraction of TUNEL positive pixels was normalized to Hoechst signal, data plotted is the median TUNEL positive pixels of the individual tumor samples. *** indicate P<0.001 and * is P<0.05. **C)** Impact of androgen supplementation (R1881; orange data points) on docetaxel response as compared to androgen deprived culture conditions (DCC; blue data points). Docetaxel sensitivity was assessed in the AR positive CRPC cell lines PC346C-DCC-K (top panel) and VCaP-DCC-E (lower panel) (both n=3). Docetaxel response was normalized to cell density at start of docetaxel treatment (dashed line) and plotted as relative cell expansion. Data was fitted using a non-linear curve fit to compare the two culture conditions, P-values are displayed. **D)** Individual tumor-growth curves of docetaxel treated PC346C-DCC-K tumors under castrate conditions (from day 0, n=7). Sixty days after docetaxel treatment, mice were supplemented with a testosterone implant (red data-points) and tumor growth was monitored until tumors exceeded 1000 mm^3, or a maximum follow-up of 21 days.

Discussion

In this study we investigated the impact of testosterone and AR-pathway stimulation on the anti-tumor efficacy of docetaxel in CRPC xenografts and cell lines. Testosterone impaired docetaxel anti-tumor activity through two different modes of action; interference with docetaxel tumor accumulation thereby reducing tubulin stabilization and AR-pathway activation protecting cells from docetaxel induced cell-death (Figure 1B). Reduced levels of docetaxel tumor accumulating by testosterone is, at least partially, mediated through competition for OATP1B3 uptake (Figure 1C). OATP1B3 is an influx transporter of particular interest, because it is frequently overexpressed in CNPC and mCRPC compared to normal adjacent prostate.[18-20] Moreover, OATP1B3 seems to have a dual character in PCa, while *SLCO1B3* overexpression has been linked to testosterone uptake, downregulation was correlated with docetaxel resistance *in vivo*.[13,21] We previously showed that cabazitaxel efficacy and tumor accumulation are also impaired by testosterone, indicating that testosterone impacts taxane efficacy in general.[8]

The current study explored the impact of reduced taxane tumor accumulation on tubulin target engagement. The absence of acetylated α-tubulin has previously been described as a biomarker of paclitaxel resistance, and was shown to be restored upon re-sensitization.[17] Here, we found that docetaxel accumulation strongly correlated with acetylated α-tubulin signal in short-term docetaxel treated tumors. Moreover, tubulin acetylation tended to be decreased in mice receiving docetaxel together with testosterone (Figure 2A). Although CRPC xenografts from testosterone-supplemented docetaxel-treated mice still displayed substantial tubulin stabilization, this did not translate into increased cell-death induction (Figure 2B). These results led us to conclude that testosterone-activation of the AR pathway, compromised the anti-tumor activity of docetaxel. This was in part demonstrated by the impact of R1881 supplementation on docetaxel sensitivity *in vitro* in two AR expressing CRPC cell lines. Of note, the VCaP-DCC-E cell line is positive for AR-V7 while PC346C-DCC-K does not express AR-variants (supplementary figure 1)[8] this implicates that regardless of variant expression, AR pathway activity interferes with taxane efficacy. Additionally, AR pathway activation by testosterone stimulated regrowth of docetaxel-treated dormant tumors (Figure 2D). Recent clinical findings, albeit retrospective analyses, also suggest an interaction between taxane efficacy and testosterone. These studies showed that CRPC patients with suboptimal testosterone serum levels had significantly shorter progression free survival following docetaxel treatment.[22,23]

Our data strongly suggests that taxane efficacy can be optimized by maintaining suppression of testosterone levels in order to minimize interference with docetaxel tumor accumulation and block AR-driven pro-survival signaling. Several phase II/III trials are currently combining (novel) AR targeted therapies with taxanes in mCRPC.[24] Our findings lend support to investigate such potential benefit of combining docetaxel with additional blocking of AR signaling in mCRPC.

Acknowledgements

The authors would like to thank Sanofi for providing the radio-labelled taxanes for use in uptake experiments and Zoran Culig for providing the *ABCB1* expression DU145-docetaxel resistant cell line. The authors would also like to thank Sigrun Erkens-Schulze and Esther Verhoef for their expertise and support in assessing the immunohistochemical stainings.

References

1. Mohler JL, Gregory CW, Ford OH, 3rd, et al. The androgen axis in recurrent prostate cancer. Clin Cancer Res. 2004;10(2):440-448.
2. Titus MA, Schell MJ, Lih FB, Tomer KB, Mohler JL. Testosterone and dihydrotestosterone tissue levels in recurrent prostate cancer. Clin Cancer Res. 2005;11(13):4653-4657.
3. van Dessel LF, van Riet J, Smits M, et al. The genomic landscape of metastatic castration-resistant prostate cancers reveals multiple distinct genotypes with potential clinical impact. Nature Communications. 2019;10(1):5251.
4. James ND, Sydes MR, Clarke NW, et al. Addition of docetaxel, zoledronic acid, or both to first-line long-term hormone therapy in prostate cancer (STAMPEDE): survival results from an adaptive, multiarm, multistage, platform randomised controlled trial. Lancet. 2016;387(10024):1163-1177.
5. Sweeney CJ, Chen YH, Carducci M, et al. Chemohormonal Therapy in Metastatic Hormone-Sensitive Prostate Cancer. N Engl J Med. 2015;373(8):737-746.
6. Ahlgren GM, Flodgren P, Tammela TLJ, et al. Docetaxel Versus Surveillance After Radical Prostatectomy for High-risk Prostate Cancer: Results from the Prospective Randomised, Open-label Phase 3 Scandinavian Prostate Cancer Group 12 Trial. Eur Urol. 2018;73(6):870-876.
7. Marques RB, van Weerden WM, Erkens-Schulze S, et al. The human PC346 xenograft and cell line panel: a model system for prostate cancer progression. Eur Urol. 2006;49(2):245-257.
8. Mout L, de Wit R, Stuurman D, et al. Testosterone Diminishes Cabazitaxel Efficacy and Intratumoral Accumulation in a Prostate Cancer Xenograft Model. EBioMedicine. 2018;27:182-186.
9. O'Neill AJ, Prencipe M, Dowling C, et al. Characterisation and manipulation of docetaxel resistant prostate cancer cell lines. Mol Cancer. 2011;10:126.
10. Workman P, Aboagye EO, Balkwill F, et al. Guidelines for the welfare and use of animals in cancer research. Brit J Cancer. 2010;102(11):1555-1577.
11. de Morree E, van Soest R, Aghai A, et al. Understanding taxanes in prostate cancer; importance of intratumoral drug accumulation. Prostate. 2016;76(10):927-936.
12. Engels FK, Mathot RA, Loos WJ, van Schaik RH, Verweij J. Influence of high-dose ketoconazole on the pharmacokinetics of docetaxel. Cancer Biol Ther. 2006;5(7):833-839.
13. Green SM, Kaipainen A, Bullock K, et al. Role of OATP transporters in steroid uptake by prostate cancer cells *in vivo*. Prostate Cancer Prostatic Dis. 2017;20(1):20-27.
14. Sissung TM, Ley AM, Strope JD, et al. Differential Expression of OATP1B3 Mediates Unconjugated Testosterone Influx. Mol Cancer Res. 2017;15(8):1096-1105.
15. Smith NF, Acharya MR, Desai N, Figg WD, Sparreboom A. Identification of OATP1B3 as a high-affinity hepatocellular transporter of paclitaxel. Cancer Biol Ther. 2005;4(8):815-818.
16. de Graan AJ, Lancaster CS, Obaidat A, et al. Influence of polymorphic OATP1B-type carriers on the disposition of docetaxel. Clin Cancer Res. 2012;18(16):4433-4440.
17. Marcus AI, O'Brate AM, Buey RM, et al. Farnesyltransferase inhibitors reverse taxane resistance. Cancer Res. 2006;66(17):8838-8846.
18. Alsinnawi M, Zhang A, Bianchi-Frias D, et al. Association of prostate cancer SLCO gene expression with Gleason grade and alterations following androgen deprivation therapy. Prostate Cancer Prostatic Dis. 2019.
19. Pressler H, Sissung TM, Venzon D, Price DK, Figg WD. Expression of OATP family members in hormone-related cancers: potential markers of progression. PLoS One. 2011;6(5):e20372.

20. Wright JL, Kwon EM, Ostrander EA, et al. Expression of SLCO transport genes in castration-resistant prostate cancer and impact of genetic variation in SLCO1B3 and SLCO2B1 on prostate cancer outcomes. Cancer Epidemiol Biomarkers Prev. 2011;20(4):619-627.
21. de Morree ES, Bottcher R, van Soest RJ, et al. Loss of SLCO1B3 drives taxane resistance in prostate cancer. Br J Cancer. 2016;115(6):674-681.
22. Shiota M, Kashiwagi E, Murakami T, et al. Serum testosterone level as possible predictive marker in androgen receptor axis-targeting agents and taxane chemotherapies for castration-resistant prostate cancer. Urol Oncol. 2019;37(3):180 e119-180 e124.
23. Ando K, Sakamoto S, Takeshita N, et al. Higher serum testosterone levels predict poor prognosis in castration-resistant prostate cancer patients treated with docetaxel. Prostate. 2020;80(3):247-255.
24. Corn PG, Agarwal N, Araujo JC, Sonpavde G. Taxane-based Combination Therapies for Metastatic Prostate Cancer. Eur Urol Focus. 2019;5(3):369-380.

Supplementary figure 1

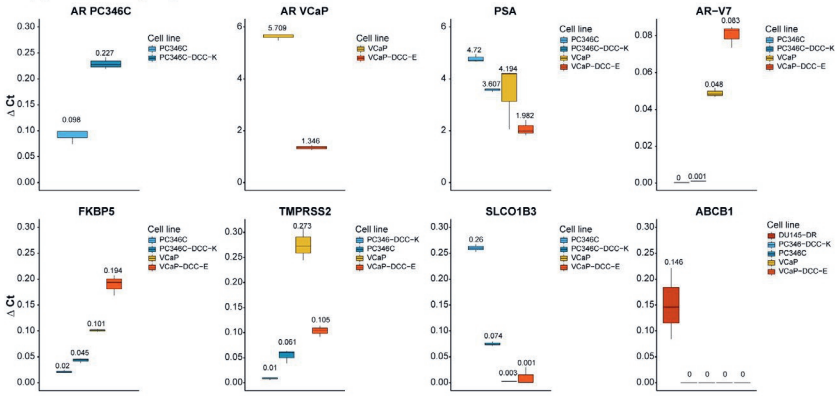

Supplementary figure 2

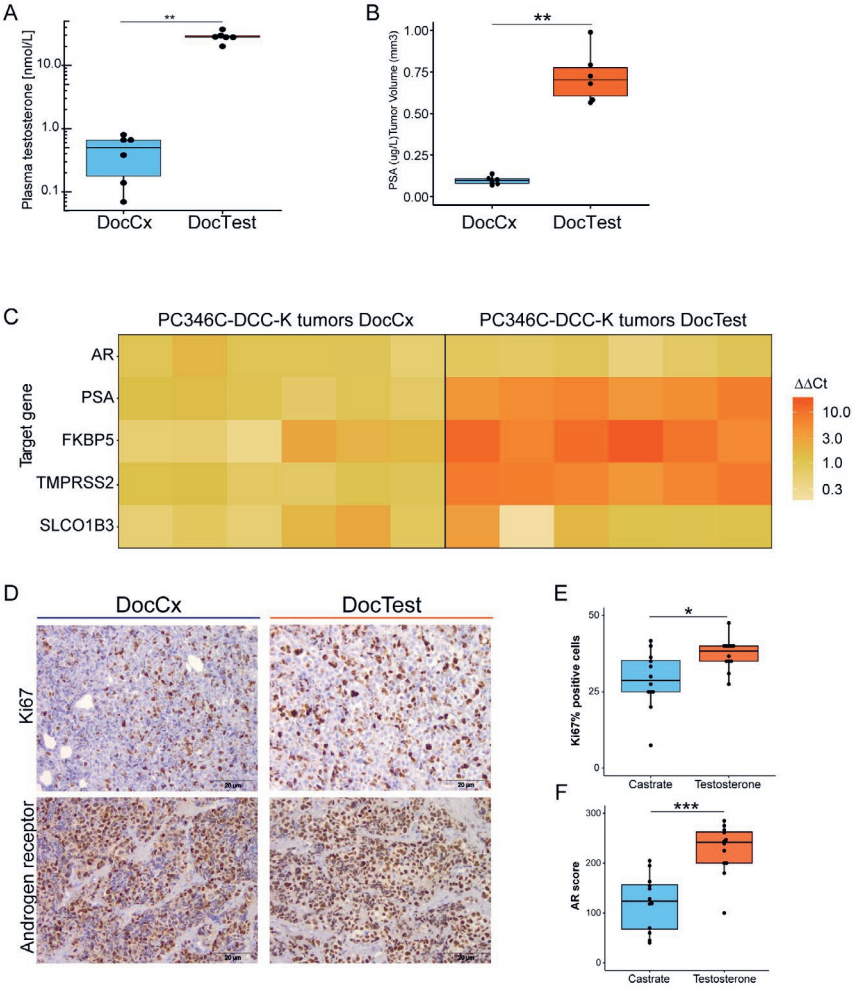

Supplementary figure 1: Expression of relevant genes in prostate cancer cell line models used. Gene expression of the AR, AR-target genes and *SLCO1B3* in PC346C-DCC-K, VCaP-DCC-E and the corresponding parental cell lines as assessed by qRT-PCR. Additionally the expression of the drug transporter *ABCB1* was assessed, for which a positive control (DU145-DR) was included. The hinges of the boxplots represent the 25th and 75th percentile with the median and the whiskers represent 1.5x the interquartile range (IQR). For each gene three technical replicates were included and expression was normalized to two household genes using the $2^{-\Delta Ct}$ method.

Supplementary figure 2: Testosterone supplementation in mice leads to increased plasma testosterone, prostate specific antigen levels, AR target gene expression and cancer cell proliferation. A) Testosterone plasma levels in short-term docetaxel treated castrate and testosterone supplemented tumor bearing mice (DocCx n=6 and DocTest n=6 resp.). Plasma samples were collected four days after mice received silastics implants containing testosterone or empty controls. The hinges of the boxplots represent the 25th and 75th percentile with the median and the whiskers represent 1.5x the interquartile range (IQR), ** indicates P<0.01. **B)** Normalized PSA plasma levels in short-term docetaxel treated castrate and testosterone supplemented tumor bearing mice (DocCx n=6 and DocTest n=6 resp.). Plasma samples were collected four days after mice received silastics implants containing testosterone or empty controls. PSA values were normalized to tumor volumes. The hinges of the boxplots represent the 25th and 75th percentile with the median and the whiskers represent 1.5x the IQR, ** indicates P<0.01. **C)** Gene expression of the AR and AR-target genes expressed in PC346C-DCC-K tumors after short-term docetaxel treatment in castrate and testosterone supplemented mice (both n=6). Heatmap depicts gene expression as assessed by qRT-PCR of the individual genes, with each row being one tumor sample. Plotted is the geomean of three technical replicates, normalized to two household genes and gene expression in tumors from castrate mice, using the $2^{-\Delta\Delta Ct}$ method. **D)** Representative immunohistochemistry images of PC346C-DCC-K tumors, obtained three days after docetaxel treatment in castrate or testosterone supplemented mice (DocCx and DocTest resp.). Tumor sections were stained for the AR and cell cycle marker Ki67, scale-bars represent 20 µm and 10 µm for the enlarged images. Images were scored by two independent viewers for Ki67 **(E)** percentage positive cells and AR **(F)** percentage positive cells which was multiplied by the AR staining intensity (scale 0-3).

Supplementary figure 3

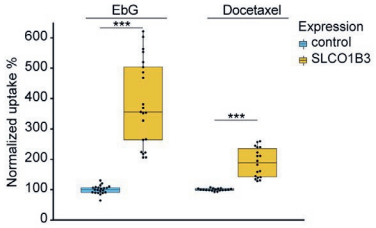

Supplementary figure 4

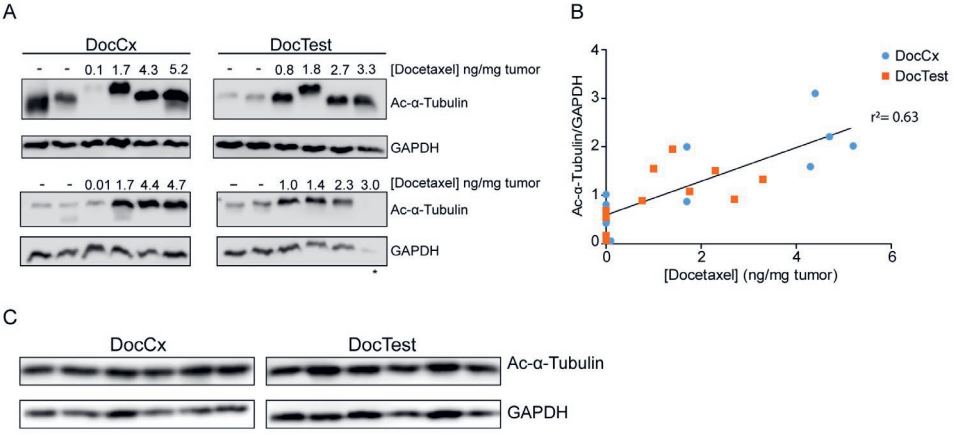

Supplementary figure 5

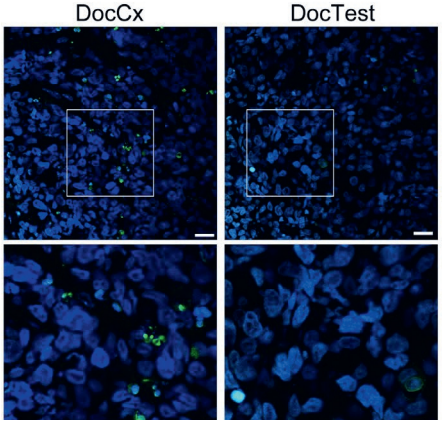

Supplementary figure 3: Docetaxel is a substrate for OATP1B3 mediated uptake. Uptake of C^{14}-Docetaxel and ^{3}H-estradiol-17β-D-glucuronide (^{3}H-EbG) in Hek293T cells transiently expressing SLCO1B3 and normalized to cells expressing the vector backbone. ^{3}H-EbG uptake was used as a positive control for OATP1B3 uptake. Shown are the individual normalized uptake levels (Docetaxel n=18 and EbG n=21) obtained from six or seven individual experiments. The hinges of the boxplots represent the 25th and 75th percentile with the median and the whiskers represent 1.5x the interquartile range (IQR), *** indicates P<0.001.

Supplementary figure 4: Docetaxel tumor accumulation levels correlate with α-tubulin acetylation. A) Immunoblots stained for acetylated α-tubulin in short-term docetaxel treated tumors. Shown are six biological replicates of PC346C-DCC-K tumors with varying levels of docetaxel tumor accumulation. Individual docetaxel concentrations are indicated above each lane. Lane marked by * was excluded from analysis due to low GAPDH signal. **B)** Correlation between signal intensity of acetylated-α-tubulin, and docetaxel tumor accumulation in PC346C-DCC-K. Samples correspond to immunoblots depicted in Supplementary figure 4A, correlation was assessed by linear regression analysis. **C)** Immunoblots corresponding to Figure 2A, in which the impact of testosterone supplementation on α-tubulin acetylation was examined. Shown are the biological replicates of short-term docetaxel treated PC346C-DCC-K tumors obtained from castrate and testosterone supplemented mice.

Supplementary figure 5: Docetaxel induced cell death is impaired by testosterone. Representative confocal images of TUNEL staining in short-term docetaxel treated tumors obtained from castrate or testosterone supplemented mice (DocCx and DocTest resp.). Blue nuclear staining is Hoechst and green is TUNEL, scale bars represent 20 µm. The lower panels show an enlarged view.

Supplementary figure 6

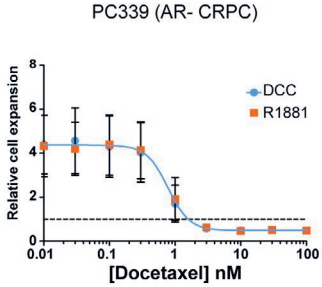

Supplementary figure 7

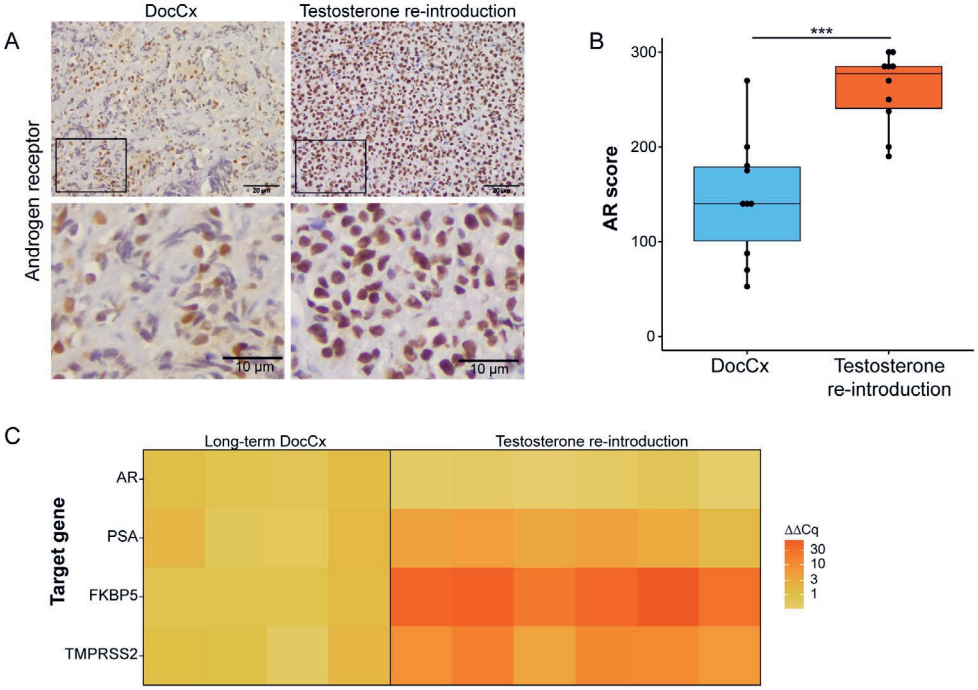

Supplementary figure 6: AR stimulation does not affect docetaxel response in an AR negative prostate cancer cell line. Impact of androgen supplementation (0.1 nM R1881) on docetaxel response as compared to androgen deprived culture conditions (DCC) in the AR-negative PCa cell line PC339C (n=3). Docetaxel response was normalized to cell density at start of docetaxel treatment (dashed line) and plotted as relative cell expansion. Data was fitted using a non-linear curve fit, represented by the solid line.

Supplementary figure 7: Testosterone mediated AR-pathway activation overcomes docetaxel induced long-term tumor regression *in vivo*. A) Representative immunohistochemical stainings of the AR in tumors obtained after testosterone re-introduction, compared to docetaxel treated tumors in castrate mice (left panels). Scale bars represent 20 µm and 10 µm for the enlarged images (lower panels). Images were scored by two independent viewers for AR **(B)** percentage positive cells which was multiplied by the AR staining intensity (scale 0-3). **C)** Gene expression of the AR and AR-target genes expressed in PC346C-DCC-K dormant tumors after docetaxel treatment in castrate (n=4) and after testosterone re-introduction (both n=6). Heatmap depicts gene expression as assessed by qRT-PCR of the individual genes, with each row being one tumor sample. Plotted is the geomean of three technical replicates, normalized to two household genes and gene expression in tumors from castrate mice, using the $2^{-\Delta\Delta Ct}$ method.

Supplementary Material and Methods

Cell culture

The human AR-positive CRPC cell line PC346C-DCC-K was derived from the human prostate cancer cell line PC346C, through long-term propagation in prostate growth medium (PGM) with 2% steroid stripped fetal calf serum (FCS) and in the absence of R1881.[1,2] The human AR-positive CRPC cell line VCaP-DCC-E was derived from the VCaP cell line through long-term propagation in RPMI with 10% steroid stripped FCS. DU145 docetaxel resistant cells (DU145-DR) were kindly provided by Zoran Culig and maintained as previously described.[3] Cell lines were characterized for the expression of prostate (cancer) transcripts (Supplementary figure 1), in short total RNA was isolated using RNA-Bee (Tel-Test, Friendwood, Texas, USA) according to the manufacturer's protocol. qRT-PCR was performed as described previously[2], and gene-expression of the following targets was assessed; *AR*, *AR-V7*, *KLK3* (PSA) (using custom assays)[2], *SLCO1B3*, *ABCB1*, *TMPRSS2* and *FKBP5* and normalized to household genes *GAPDH* and *HMBS* (ThermoFisher Scientific, Hs00251986, Hs00184500, Hs01120965, Hs01561006, Hs99999905 and Hs00609296 resp.). Gene expression was normalized using the $2^{-\Delta Ct}$ method, DU145-DR was used as a positive control for *ABCB1* expression. Mycoplasma testing was performed every 6 months, cell line authentication was performed by short tandem repeat analysis by the Promega PowerPlex 16 kit. PC346C-DCC-K cells were kept into culture for a maximum of 25 passages after initiating the castrate resistance phenotype, while the VCaP-DCC-E clone was kept in culture for 50 passages.

Docetaxel uptake in SLCO1B3 expressing cells

For Docetaxel uptake assays we used Hek293T to over-express *SLCO1B3*. Hek293T cells were maintained in DMEM with 5% FCS. For drug uptake experiments, $1*10^5$ cells were plated in a 24-wells plate in phenol-red free medium (DMEM, ref # 31053-028, ThermoFisher Scientific, Waltham, Massachusetts, USA). After overnight incubation, cells were transfected with 0.5 µg of SLCO1B3 plasmid DNA (GenScript, New Jersey, USA) or control vector (pCMV6-AC-IRES-GFP) using Lipofectamin 3000 (1 µl/µg DNA, ref # L3000015, ThermoFisher Scientific). Transfection efficiency was monitored visually by GFP expression, and uptake experiments were performed 24-48h after transfection. For competition assays, cells were incubated with phenol-red/FCS free media containing 200 µM testosterone or vehicle control for 15 minutes. Media was removed and cells were incubated with C^{14}-Docetaxel (1 µM, 56.27 µCi/mM) or ^{3}H-estradiol-17β-D-glucuronide (EbG; 0.2 µM) with or without testosterone for 10 minutes. After drug uptake, cells were washed three times with ice-cold PBS and lysed using 1 M NaOH at 4°C overnight. Cell lysates were neutralized using 2 M HCl and

radioactivity measured using a scintillation counter (LS 6500 Counter, Beckman Coulter, Brea, California, USA). Radioactivity was corrected for protein concentration and activity of the drug solutions used. Uptake levels were normalized to vector control, or uptake in the absence of testosterone (vehicle control).

Animal Welfare

All animal experiments were approved by the Animal experiment committee under the Dutch experiments on Animal Act, with the reference number AVD101002017867. The current study is in compliance with the Arrive guidelines. Group size and experimental set-up was based on a previous study.[2] All operations (tumor inoculation, castration, blood sampling) are conducted under adequate anesthesia to minimize animal discomfort. Subcutaneously growing tumors only cause mild discomfort.

Docetaxel activity in vivo

Forty, six weeks old, NMRI nu/nu male mice (Janvier, Le Genest Saint Isle, France) were subcutaneously inoculated with $5*10^6$ PC346C-DCC-K cells, while being anesthetized with isoflurane/O2. Tumor growth was observed after 2-4 weeks in ~95% of the mice. Once tumors reached a volume of 150 mm^3, mice were surgically castrated. Anaesthesia was provided by with Ketamine/Medetomidine (75 mg/kg and 1 mg/kg) and analgesia by Carprofen (5 mg/kg). After one week, mice were split into in two groups (based on tumor volume), to receive either a silastic implant with 40 mg of testosterone (ref #A0671, AppliChem, Darmstadt, Germany) or an empty implant to serve as control. During implantation of the silastic pellets, mice received anesthesia by isoflurane/O2. The following day, mice were given an intravenous administration of docetaxel (33 mg/kg; 10% ETOH, 10% Tween-80 and 80% glucose solution, Sanofi, Paris, France) or NaCl as treatment control (inclusion was based on tumor volume). Overall we had four treatment groups with six mice each, docetaxel treatment or placebo control in castrate or testosterone supplemented mice. The experiment was repeated in 16 castrate mice, comparing docetaxel efficacy to placebo controls. Tumor volume was measured twice weekly by calipers and mice were followed until tumors exceeded a volume of 1500 mm^3, or a maximum follow up of 60 days after docetaxel treatment. At tumor volume 1500 mm^3 no tumor-related discomfort is observed, mice were euthanized by cervical dislocation. Other reasons for euthanizing the mice included continued weight loss, >15% loss in bodyweight in two days or >20% compared to start, and abnormal behavior. Mice were maintained in an individually ventilated cage at 2-4 mice per cage, on a 12h dark/light cycle and cage enrichment was provided. Treatments or surgical procedures were initiated in the morning and food and water were provided ad libitum. Blood was sampled

for prostate specific antigen (PSA) and testosterone analysis at tumor take, one week after testosterone (or empty control) supplementation and at end of the study. Blood plasma was isolated by centrifugation at 6800 RCF for 10 min and PSA was analysed by an electrochemiluminescence immunoassay (Cobas 8000, Roche, Basel, Switzerland). Plasma testosterone levels were analyzed using a ChemiLuminescent Enzyme Immunoassay (Lumipulse G1200, Fujirebio, Gent, Belgium).

Docetaxel accumulation in vivo

Sixteen NMRI nu/nu male mice were inoculated subcutaneously with $5*10^6$ PC346C-DCC-K cells. When tumors reached a volume of 150 mm^3, mice were surgically castrated and after one week supplemented with testosterone-containing or empty silastic implant (based on tumor volume). Three days after intravenous administration of docetaxel (33 mg/kg), mice were sacrificed to determine docetaxel tumor accumulation. At least 40 mg of tumor sample was snap-frozen and used to determine docetaxel accumulation, which has been described previously.[4,5]

Immunohistochemistry

Tumor tissue was formalin fixed paraffin embedded (FFPE) and 4 µm sections were stained for presence of the AR (1:200, SP107, Cell Marque, Rocklin, California, USA) and the cell cycle marker Ki67 (1:100, MIB-1, Agilent, Santa Clara, USA) using validated antibodies.[6,7] The secondary antibodies used were Goat anti-Rabbit and Goat anti-Rabbit/Mouse for the AR and Ki67 resp. (#P0448 and #K5007, Envision Dako Santa Clara, USA). Expression was visualized with DAB/H2O2 (EnVision kit, #K5007 Dako) and sections were counterstained with haematoxylin. For all tissue sections stained we included one sample with the secondary antibody (goat anti-Rabbit/Mouse) only, to visualize potential a-specific staining. Images were obtained using the Olympus BX41 microscope equipped with 2x, 10x, 20x and 40x UPlanFL N objectives, a ColorView III camera and CellB imaging software (version 3.4, Olympus, Shinjuku, Tokyo, Japan). All IHC stainings were blinded for treatment and quantified by two independent persons based on two or three representative images. Ki67 was scored based on percentage positive tumor cells only while AR score was calculated by multiplying percentage positive tumor cells with the staining intensity score (0-3).

TUNEL staining

Cell-death was assessed using TdT-mediated dUTP-X nick end labelling (TUNEL). Four µm FFPE sections were stained according to manufacturer's protocol (ref #11684795910, Merck, Darmstadt, Germany), and counterstained with Hoechst (ref # H3570, ThermoFisher Scientific). Tumor sections were blinded to treatment group and imaged using a Leica fluorescent microscope (DM4000b, Nussloch, Germany). Ten fields per tumor sample were imaged at a 400x magnification and quantification was performed as described previously.[8] Representative images were obtained using the SP5 Leica confocal microscope at a 630x magnification (HCX PL APO CS objective with Photo Multiplier Tube detector and LAS X imaging software).

AR-pathway expression upon testosterone stimulation in vivo

Tumor tissue was lysed and homogenized in QIAzol (ref #79306, Qiagen, Hilden, Germany) using an Ultra-Turrax T25 (Janke & Kunkel, Staufen, Germany). Total RNA was isolated using the miRNA-easy mini kit (ref # 217004, Qiagen), and RNA quality was measured using the Bioanalyzer RNA 6000 Nano assay (ref #5067, Agilent, Santa Clara, California, USA). All RNA samples had a RIN value ≥7. qRT-PCR was performed as described previously, gene-expression was normalized to household genes (*GAPDH* and *HMBS*) and gene expression in castrate tumors using the $2^{-\Delta\Delta Ct}$ method.

Tubulin stabilization by docetaxel treatment in vivo

Tumors tissue was lysed and homogenized in RIPA buffer (0.01 M Tris-HCl, 0.05 M NaCl, 0.05% deoxycholate, 0.1% sodiumdodecyl sulfate (SDS), 5 mM ethylenediaminetetraacetic acid (EDTA) and 1% Triton x-100) supplemented with protease and phosphatase inhibitors (ref #78429, HaltTM Protease Inhibitor Cocktail and ref# 78420 HaltTM Phosphatase Inhibitor Cocktail both ThermoFisher Scientific), using an Ultra-Turrax T25. Protein homogenates were separated from the nucleic acids by centrifugation (4°C, 15 min at 20.000 g). Protein concentration was measured by the Pierce BCA protein assay (ref #23227, ThermoFisher Scientific), and 10 µg of protein lysate was used for immuno-blotting. Tubulin stabilization was visualized by staining for acetylated-α-tubulin (1:1000, ref #6-11B-1, Santa Cruz, Dallas, USA) and imaged using chemiluminescence (ref #11500694001, Merck). Staining intensity was assessed by the Odyssey Li-COR (C-Digit model 3600, Lincoln, Nebraska, USA) imaging system and normalized to GAPDH (1:10.000, ref #SC-47724, Santa Cruz) signal intensity.

Cell viability assay

For cell viability assays PC346C-DCC-K and VCaP-DCC-E cells were plated at a cell density of $5*10^3$ cells per well in a 96-wells plate. VCaP-DCC-E cells were maintained in RMPI containing 10% DCC serum, while PC346C-DCC-K cells were maintained in PGM-basic medium.[9] After overnight incubation, cells were exposed to a dose-range of docetaxel (0-100 nM, Sanofi) with or without the addition of 0.1 nM R1881, using six replicates per condition. After 10 days cell viability was measured by MTT assay, as described previously[9], and normalized to values of six untreated wells at day one. The docetaxel sensitivity of the non-adherent, AR and SLCO1B3 negative cell line PC339C was examined using the PrestoBlue assay (ref #A13261, ThermoFisher Scientific).[10] The experimental set-up was similar to the MTT assay described above, with the following alteration, cells were plated at a cell density of $2.5*10^3$ and docetaxel response was measured after 7 days.

Statistical analysis

Kaplan-Meier plots and log-rank survival analysis as depicted in Figure 1A, were performed using the survival package version 3.1-6 in Rstudio Version 1.1.463.[11,12] A pairwise comparison with Bonferroni correction was used to compare survival in the independent groups. The boxplot graphs shown throughout the manuscript were produced using ggplot2 version 3.2.1 in Rstudio[13], the hinges of the boxplots represent the 25th and 75th percentile with the median and the whiskers represent 1.5x the interquartile range, individual data points were plotted on the boxplots using ggbeeswarm.[14] Statistical analysis of uptake and subsequent competition assays was performed using an one-way Anova with Dunn's post-test for multiple comparisons using Rstudio[15]. The frequency of TUNEL positive cells after treatment (Figure 2B) was analyzed using an one-way Anova with Tukey post-test for multiple comparisons using Rstudio. The relation between acetylated-α-tubulin staining intensity as obtained by immunoblotting and docetaxel tumor accumulation was analyzed using linear regression analysis in GraphPad Prism (version 5.01, GraphPad Software, San Diego, California, USA). The cell viability data was analyzed using non-linear fit in GraphPad, we used a log(inhibitor) versus response and variable slope to compare EC50 and maximum effect in castrate and androgen supplemented conditions. The impact of testosterone supplementation on plasma PSA, testosterone levels, docetaxel tumor accumulation and AR nuclear localization or Ki67 expression was assessed using a two-sided T-test in Rstudio.

References

1. Marques, R. B., van Weerden, W. M., Erkens-Schulze, S., de Ridder, C. M., Bangma, C. H., Trapman, J. et al. The human PC346 xenograft and cell line panel: a model system for prostate cancer progression. Eur Urol 49, 245-257 (2006).
2. Mout, L., de Wit, R., Stuurman, D., Verhoef, E., Mathijssen, R., de Ridder, C. et al. Testosterone Diminishes Cabazitaxel Efficacy and Intratumoral Accumulation in a Prostate Cancer Xenograft Model. EBioMedicine 27, 182-186 (2018).
3. O'Neill, A. J., Prencipe, M., Dowling, C., Fan, Y., Mulrane, L., Gallagher, W. M. et al. Characterisation and manipulation of docetaxel resistant prostate cancer cell lines. Mol Cancer 10, 126 (2011).
4. de Morree, E., van Soest, R., Aghai, A., de Ridder, C., de Bruijn, P., Ghobadi Moghaddam-Helmantel, I. et al. Understanding taxanes in prostate cancer; importance of intratumoral drug accumulation. Prostate 76, 927-936 (2016).
5. Engels, F. K., Mathot, R. A., Loos, W. J., van Schaik, R. H. & Verweij, J. Influence of high-dose ketoconazole on the pharmacokinetics of docetaxel. Cancer Biol Ther 5, 833-839 (2006).
6. Varun, K., Jianjun, Y., Vernon, P., Iulia Cristina, T., Amy, P. & Hirdesh, U. Androgen Receptor Immunohistochemistry as a Companion Diagnostic Approach to Predict Clinical Response to Enzalutamide in Triple-Negative Breast Cancer. JCO Precision Oncology 10.1200/po.17.00075, 1-19 (2017).
7. Lindboe, C. F. & Torp, S. H. Comparison of Ki-67 equivalent antibodies. J Clin Pathol 55, 467-471 (2002).
8. Zhang, W., van Weerden, W. M., de Ridder, C. M. A., Erkens-Schulze, S., Schonfeld, E., Meijer, T. G. et al. Ex vivo treatment of prostate tumor tissue recapitulates in vivo therapy response. Prostate 79, 390-402 (2019).
9. Marques, R. B., Erkens-Schulze, S., de Ridder, C. M., Hermans, K. G., Waltering, K., Visakorpi, T. et al. Androgen receptor modifications in prostate cancer cells upon long-termandrogen ablation and antiandrogen treatment. Int J Cancer 117, 221-229 (2005).
10. de Morree, E. S., Bottcher, R., van Soest, R. J., Aghai, A., de Ridder, C. M., Gibson, A. A. et al. Loss of SLCO1B3 drives taxane resistance in prostate cancer. Br J Cancer 115, 674-681 (2016).
11. R: A Language and Environment for Statistical Computing v. Version 1.1.463 (R Foundation for Statistical Computing, Vienna, Austria, 2019).
12. A Package for Survival Analysis in S v. version 2.38 (2015).
13. Ginestet, C. ggplot2: Elegant Graphics for Data Analysis. J R Stat Soc a Stat 174, 245-245 (2011).
14. ggbeeswarm: Categorical Scatter (Violin Point) Plots v. R package version 0.6.0.
15. dunn.test: Dunn's Test of Multiple Comparisons Using Rank Sums. v. R package version 1.3.5. (2017).

Chapter IV

CETSA-Based Target Engagement of Taxanes as Biomarkers for Efficacy and Resistance

Anette Langebäck[1], Smaranda Bacanu[1], Henriette Laursen[1], Lisanne Mout[1], Takahiro Seki, Sigrun erkens-Schulze, Anderson Daniel Ramos, Anna Berggren, Yihai cao, Johan Hartman, Wytske van Weerden, Jonas Bergh, Pär nordlund & Sara Lööf

[1]These authors contributed equally

Sci Rep. 2019 Dec 18;9(1):19384.

Abstract

The use of taxanes has for decades been crucial for treatment of several cancers. A major limitation of these therapies is inherent or acquired drug resistance. A key to improved outcome of taxane-based therapies is to develop tools to predict and monitor drug efficacy and resistance in the clinical setting allowing for treatment and dose stratification for individual patients. To assess treatment efficacy up to the level of drug target engagement, we have established several formats of tubulin-specific Cellular Thermal Shift Assays (CETSAs). This technique was evaluated in breast and prostate cancer models and in a cohort of breast cancer patients. Here we show that taxanes induce significant CETSA shifts in cell lines as well as in animal models including patient-derived xenograft (PDX) models. Furthermore, isothermal dose response CETSA measurements allowed for drugs to be rapidly ranked according to their reported potency. Using multidrug resistant cancer cell lines and taxane-resistant PDX models we demonstrate that CETSA can identify taxane resistance up to the level of target engagement.An imaging-based CETSA format was also established, which in principle allows for taxane target engagement to be accessed in specific cell types in complex cell mixtures. Using a highly sensitive implementation of CETSA, we measured target engagement in fine needle aspirates from breast cancer patients, revealing a range of different sensitivities. Together, our data support that CETSA is a robust tool for assessing taxane target engagement in preclinical models and clinical material and therefore should be evaluated as a prognostic tool during taxane-based therapies.

Introduction

The use of taxanes has been a cornerstone in the treatment of cancers for several decades. Today taxanes are used in several cancer types and are a part of first line treatment in breast, non-small-cell lung cancer, castration-resistant prostate cancer, esophageal, head and neck cancers, and Kaposi sarcoma.[1-3]

Taxanes are particularly important in the treatment of both early-stage and metastatic breast cancer patients where robust improvements of overall survival have been shown.[4,5] Both paclitaxel, a substance isolated from the Pacific yew tree (*Taxus brevifolia*), and docetaxel, a more potent semisynthetic derivate of paclitaxel, derived from the European yew tree (*Taxus baccata*), are standard treatment in breast cancer. Taxanes are also used for prostate cancer patients and are currently the only type of chemotherapy used for this type of cancer. Athough the mainstay therapy for metastatic prostate cancer has been hormone depletion, no effective therapy was available for patients who had progressed under androgen deprivation therapy until the introduction of docetaxel in 2004.[6] Currently the treatment landscape for patients with castrate-resistant prostate cancer (CRPC) has vastly expanded, including cabazitaxel. This novel taxane has been shown to remain effective in docetaxel-resistant CRPC patients.[7] Of note, the addition of docetaxel in parallel to androgen deprivation therapy was recently shown to increase overall survival, suggesting that an earlier switch to taxane regime might be favorable in these cases.[8] The taxanes exert their effect by binding to β-tubulin on the luminal side of microtubules leading to the stablization of microtubules via inhibition of depolymerization.[9] Therefore taxanes suppress microtubule dynamics, with the major mechanism for cell toxicity being the effect on the mitotic spindle, which leads to cell cycle arrest typically in G2- and M-phase, followed by cell death in rapidly dividing cells.[10] Vinca alkaloids is another family of tubulin modulators, including vinorelbine and vincristine, which act by inhibiting microtubule polymerization, also arresting cells in G2- and M-phase.

Taxanes are widely used for both early- and late-stage disease, but as for other cytotoxic cancer drugs, inherent or acquired resistance is often seen, leading to lack of efficacy or time-limited responses, and eventually progressive disease and mortality. There have been multiple mechanisms attributed to taxane resistance where a specific focus has been on the overexpression of efflux pumps, for example P-glycoprotein 1 (*MDR1*) or down-regulation of influx transporters.[11] The activation of efflux pumps leads to depletion of the intracellular pool of the taxane, which affects the extent of binding to β-tubulin, i.e. decrease the target engagement (TE). Attenuated TE has also been suggested to occur due to point mutations or post translational modifications of β-tubulin, modified expression levels of microtubule-associated proteins (MAPs) or altered levels of tubulin isoforms such as up-regulation of *TUBB3*.[12-14] However, the mechanisms for how *TUBB3* overexpression overcomes cell cycle arrest remains only partially defined. Other general

mechanisms for resistance to cytotoxic drugs have also been suggested to affect taxane sensitivity such as altered expression of anti-apoptotic proteins (e.g. Bcl-2 and Bcl-xL)[15,16] and NFkB modulation.[17]

However, although several potential mechanisms and biomarkers for cellular drug efficacy and resistance have been proposed, none of these have been proven predictive for efficacy in the clinical setting. This is unfortunate since different taxanes appear to have different efficacy profiles, as well as different adverse effects, and thus biomarkers and predictive assays could potentially help in stratifying drug or drug combinations at different stages of taxane-based combination therapy.

A basic requirement for taxane efficacy is sufficient TE of β-tubulin. After the drug has reached the tumor environment, TE is mainly determined by cellular influx, efflux, and drug catabolism, yielding the effective intra- cellular drug concentration. During therapy the pharmacokinetic (PK) profile in the individual patient will also affect TE by determining the amount of taxanes reaching the tumor environment. To optimize PK, drug monitoring is sometimes used during taxane therapy to demonstrate appropriate serum concentrations of the drug.[18]

Considering the critical role of TE for drug efficacy, information on absolute and relative TE for different drugs in patient-derived samples could potentially help in stratification of cancer therapies with taxanes. However, direct measurements of TE in cells and tissues have previously been very challenging when no general technique for such measurements has been available. To meet this challenge, our lab has introduced the Cellular Thermal Shift Assay (CETSA), a biophysical assay which allows for TE to be measured in intact cells and tissues.[19] CETSA can directly assess drug binding at the target protein level (the protein reports) by applying the critical heating step while cells are still intact and the target protein is in its proper cellular environment. After determining overall melting behavior of a target protein, isothermal dose response (ITDR) curves can be determined with CETSA to assess relative doses needed to obtain TE. Combined with mass spectrometry (MS-CETSA) the method has allowed for comprehensive characterization of both direct drug binding, and protein interaction state changes induced by downstream and stress effects introduced by drugs.

Although CETSA is most often explored to study TE in cell cultures, single protein CETSA experiments on tissue samples have previously been done for drug treated mice, for example, in the initial CETSA study for METAP2[19] and in several mice tissues for RIPK1.[20] Proteome wide MS-CETSA experiments have also recently been performed in multiple tissues of drug treated mice (ref. https://www.biorxiv.org/content/10.1101/500306v1). In the present work we implemented different formats of tubulin-specific CETSA and used these to study taxane TE in cell lines of breast and prostate cancer as well as mouse xenografts. Using cognate pairs of sensitive and resistant cell lines we show that CETSA can efficiently reveal the presence of drug resistance mechanisms. Finally, using miniaturized

CETSA we demonstrate that TE responses can be measured in fine needle aspirates from breast cancer patients and therefore can be used to validate tubulin CETSA as a potential prognostic biomarker for taxane sensitivity in clinical trials.

Results

Tubulin melting behavior and drug stabilization in western blot-based CETSA.

To validate the applicability of CETSA to assess TE for tubulin-targeted drugs we implemented several CETSA formats as shown in Fig. 1A. We first developed a western blot-based assay to investigate the feasibility of tubulin-based CETSA. Initially melt curves for a- and ß-tubulin were generated in K562-cells, a suspension cell line originating from myelogenous leukemia. Both α- and β-tubulins had relatively high melting temperatures, around 61-63 °C, compared to 52 °C as the average melting temperature of proteins of the human proteome.[21] The high melting temper- atures of tubulins might be due to stabilizing effects of the extensive protein-protein interactions made within the microtubule polymer. This is consistent with the finding that the non-polymerized subunits of tubulin, in lysates, melt more than 10 °C earlier (Fig. S1A, B).

In addition to paclitaxel, which preferentially binds to a site on β-tubulin localized in the lumen of microtubules leading to stabilization of microtubules, we used vinorelbine, that binds to the vinca-binding domain, a site on β-tubulin distinct from the taxane-binding domain and which inhibits tubulin polymerization.[22-24] Treatment of K562-cells for 1 h with both drugs produced a significant stabilization of β-tubulin with the largest difference between vehicle and treated seen around 63 °C (Fig. 1B and Table 1). A significant shift was also observed for α-tubulin following treatment with paclitaxel (Fig. 1C and Table 1). However, no shifts were observed in cell lysates (Fig. S1A, B), consistent with the fact that drug binding is considered to occur only with intact microtubules.[12] In lysate, microtubules are depolymerized and tubulin is only present as soluble dimers. Although the drugs used bind specifically to the β-tubulin subunit, both the α- and β-subunits show shifts in CETSA melt curves (Fig. 1B-E and Table 1). We recently described the correlation of CETSA melt curves of interacting proteins and named this phenomena thermal proximity co-aggregation (TPCA)[25,26], which is the likely explanation for the correlated shifts of the tubulin subunits. CETSA melt curves were also generated in MCF-7 cells, a commonly used model system for hormone-positive breast cancer.

Paclitaxel generated clear shifts in both α- and β-tubulin in these cells, while docetaxel produced even larger shifts (Fig. 1D, E and Table 1). As negative controls we have generated melt curves for MCF-7 cells treated with the anthracycline daunorubicin, or with the pyrimidine analogue cytarabine which, as expected, produced no shifts in neither α- nor β-tubulin (Fig. 1F, G). Since the temperatures needed to generate tubulin melting are high, there might be a risk of losing cell membrane integrity during heating. We therefore tested the temperature and time dependent effects on the cell membranes in K562 and MCF-7 cells using a trypan blue assay (Fig. S1C-F).

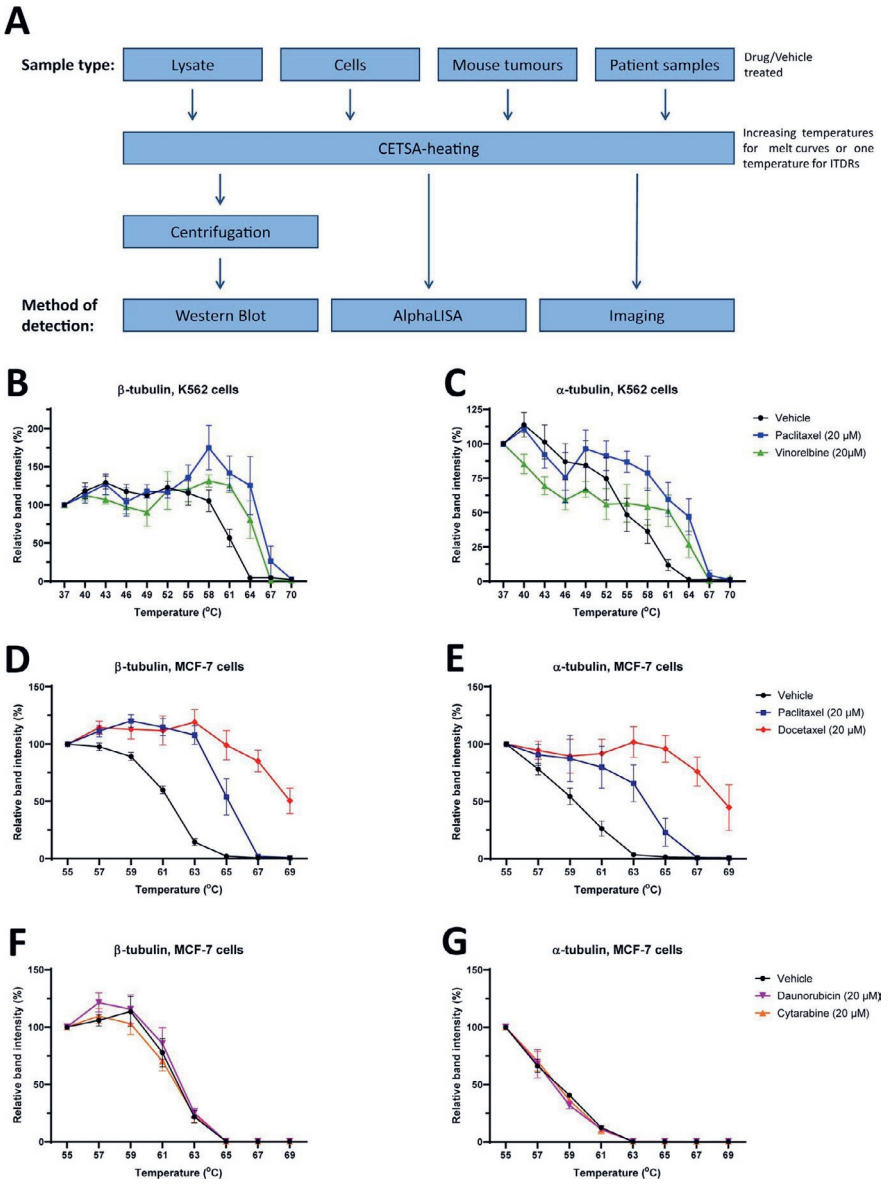

Figure 1. CETSA shows distinct melt curves for α- and β-tubulin that shift upon drug binding in cancer cells. Schematic overview of the CETSA method (A). Western blot-CETSA shows that the tubulin-binding drugs paclitaxel and vinorelbine (20 μM) produce clear shifts for β-tubulin in K562-cells (B and C). In MCF-7 cells, the two taxanes, paclitaxel and docetaxel (20 μM), produce significant CETSA shifts for both β-tubulin and α-tubulin (D and E). Daunorubicin and cytarabine (negative controls) produced no shift in both β-tubulin and a-tubulin (F and G). All data represent the mean ± S.E.M from independent experiments (n = 5-6 in D and E, and n = 3 in B, C, F and G) and are presented as a percentage of the signal detected at the lowest temperature in each melt curve.

Although some cell lysis was induced above 60 °C, the majority of cells remained intact up to 63 °C. In a time dependent experiment, the cell lysis occurred mainly after 1 minute of the total 3 minutes heating time (Fig. S1E,F), which is beyond the time point when the most prominent effects on protein stability are expected (the remaining heating time is expected to mainly drive the efficient precipitation of unfolded protein).
Importantly, when the melting temperature of tubulin in lysates is much lower than in cells, proteins from lysed cells will not be seen above 60 °C. Furthermore, no stabilizing effect by taxanes can be observed on tubulin in lysed cells when tubulin is then present only as soluble dimers, as discussed above. Therefore, the heat-induced lysis of a fraction of the cells is not likely to quantitatively affect the TE measurements with tubulin CETSA.

Table 1. Overview of melting temperatures (Tm), CETSA shifts (ΔTm), with associated standard errors and statistical significance of the measured CETSA shift for the data presented in Fig. 1B-G. *The significance of the CETSA shifts was calculated using one-way ANOVA for Tm values from independent experiments. Adjusted P-values ns P > 0.05, *P < 0.05, **P < 0.01, ***P < 0,001, ****P < 0,0001 compared to vehicle.

	β-tubulin			**α-tubulin**		
K562 cells	**Tm (°C)**	**ΔTm (°C)**	**Significance***	**Tm (°C)**	**ΔTm (°C)**	**Significance***
Vehicle	61,0 ± 0,6	—	—	54,0 ± 2,1	—	—
Paclitaxel (20 μM)	66,1 ± 0,8	5,1 ± 1,0	***	63,0 ± 1,0	9,0 ± 3,1	*
Vinorelbine (20 μM)	64,7 ± 0,8	3,7 ± 1,1	*	62,5 ± 0,5	8,5 ± 3,8	ns
MCF-7 cells	**Tm (°C)**	**ΔTm (°C)**	**Significance***	**Tm (°C)**	**ΔTm (°C)**	**Significance***
Vehicle	61,2 ± 0,2	—	—	58,9 ± 0,3	—	—
Paclitaxel (20 μM)	64,9 ± 0,2	3,7 ± 0,3	****	63,8 ± 0,7	4,9 ± 0,6	***
Docetaxel (20 μM)	68,9 ± 0,4	7,7 ± 0,4	****	68,5 ± 0,6	9,6 ± 0,6	****
Daunorubicin (20 μM)	61,9 ± 0,3	0,7 ± 0,4	ns	57,7 ± 0,3	−1,2 ± 0,6	ns
Cytarabine (20 μM)	61,7 ± 0,3	−0,5 ± 0,4	ns	58,1 ± 0,3	−0,7 ± 0,6	ns

Miniaturization of CETSA for β-tubulin using AlphaLISA.

Since measurements on clinical samples typically are limited by the amount of available cells, and screening studies using cell lines can require high sample throughput, we established a miniaturized tubulin CETSA based on AlphaLISA (overview of method in Fig. 2A). Antibody pairs can be chosen to only detect native protein in these assays with the advantage that, after heating, centrifugation of the lysate is not needed to remove aggregated protein (Figs. 2C, D and S2B, C). Several combinations of antibodies were tested and two pairs were found to give a robust signal: pair 2 consisting of ab6046 (Abcam) in combination with sc-398937 (Santa Cruz) and pair 8 consisting of ab6046 (Abcam) and T5201 (Sigma). Both pairs could detect CETSA melt curves and target stabilization in response to docetaxel and vinorel- bine with very similar shape as detected with western blot (Fig. 2C, D, Table 2, and Fig. S2B, C). Also CETSA ITDR experiments performed at 64 °C showed very similar curves with both detection methods (Fig. S2A).

In order to optimize the cell numbers required for these assays different amounts of lysate were analyzed with both antibody pairs (Figs. 2E and S2D). The two pairs showed similar curves with pair 8 being somewhat more sensitive and having slightly shorter linear range. To increase the sensitivity even further, the pair 8 antibodies were directly conjugated to the AlphaLISA beads (Figs. 2B and S2E). Also a polyclonal SOD-1 antibody (R&D systems AF3418) was used in a conjugated AlphaLISA assay to function as loading control since SOD-1 is stable also at higher temperatures (Fig. S2G).[27] The SOD1 assay had a linear range up to 500 cells (Fig. S2H). Interestingly, a time course experiment showed the stabilization of tubulin by docetaxel in K562 cells to be fully saturated already after 5 min drug treatment (Fig. S2F).

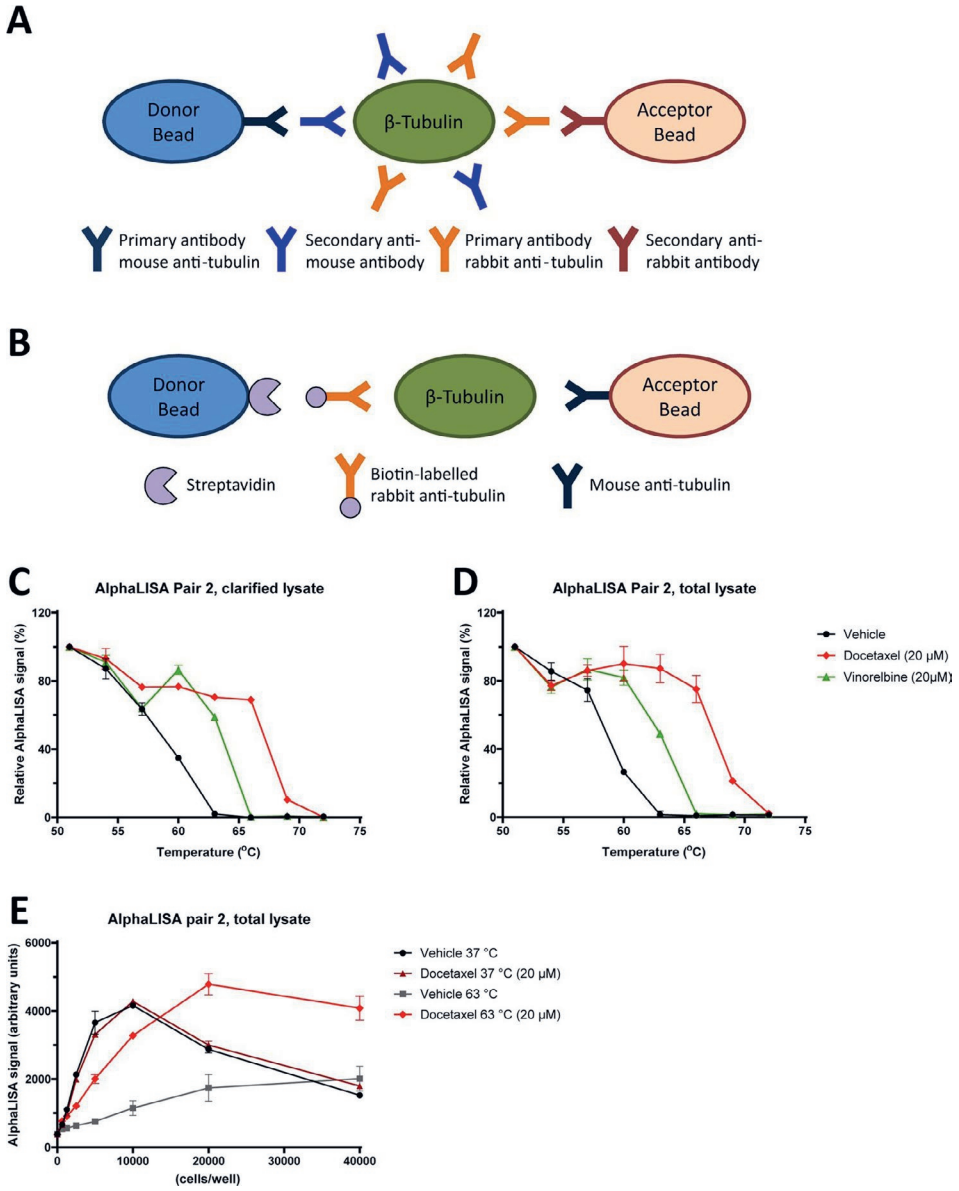

Figure 2. Miniaturization of the β-tubulin CETSA assay. Schematic drawing of the principle of standard and conjugated AlphaLISA (A and B). CETSA melt curves in K562 cells treated with docetaxel or vinorelbine (20 μM). β-tubulin was detected in total and clarified cell lysate with AlphaLISA pair 2 (C and D). Cell density titration for AlphaLISA pair 2 in lysate from K562 cells treated with docetaxel (20 μM) or vehicle and heated to 37 or 63 °C (E). The data represent the mean ± S.E.M from technical replicates and are presented as a percentage of the signal detected at the lowest temperature in each melt curve.

Detection of acquired drug resistance at the TE level using CETSA.

To investigate the feasibility of using CETSA for assessing acquired drug resistance, multidrug-resistant K562-R cells were studied. The K562-R cells are previously described as vincristine-resistant due to overexpression of P-gp.[28] We used AlphaLISA as readout method for ITDR-CETSA in order to compare the dose dependence of different taxanes in K562-R and the parental counterpart K562-P after a 1 h 45 min exposure to drugs. The ITDR-CETSA data showed that K562-R cells required in the range of 5,3x higher paclitaxel or docetaxel concentrations to establish the same TE response as in the parental cells (Fig. 3A, E, and Table 2) despite no difference in the total amount of tubulin (Fig. 3K). Measurements of cell viability after 72 h using the resazurin viability assay confirmed resistance in the K562-R cells compared to K562-P (Fig. 3B, F, and Table 2). Interestingly, the differences in both cell survival and CETSA shifts were abolished by the potent P-gp-inhibitor tariquidar (Fig. 3C, D, G, H, and Table 2), directly supporting that the resistance mechanism is indeed due to up-regulation of P-glycoprotein. Furthermore, these cells were exposed to epothilone B, a tubulin targeting drug which is not a P-glycoprotein substrate.

Table 2. Overview of EC50 values with associated standard errors and 95% confidence intervals (CI), and statistical significance calculated for the ITDR-CETSA curves in Fig. 3A-J. *The significance was determined for K562-R vs. K562-P using a two-tailed T-test for EC50 values from independent experiments. P-values ns P > 0.05, *P < 0.05, **P < 0.01, ***P < 0,001, ****P < 0,0001 compared to K562-P.

	K562-P		**K562-R**		
CETSA	**EC50 and St. Error (μM)**	**95% CI**	**EC50 and St. Error (μM)**	**95% CI**	**Significance***
Docetaxel	0,30 ± 0,08	0,18-0,5	1,54 ± 0,25	1,10-2,20	***
Docetaxel + 0,5 μM Tariquidar	0,37 ± 0,09	0,23-0,58	0,26 ± 0,07	0,16-0,42	ns
Paclitaxel	1,55 ± 0,3	0,96-2,51	8,34 ± 1,63	5,90-11,81	***
Paclitaxel + 0,5 μM Tariquidar	1,06 ± 0,21	0,66-1,72	1,2 ± 0,27	0,80-1,78	ns
Epothilone B	0,08 ± 0,02	0,06-0,13	0,1 ± 0,01	0,08-0,14	ns
Viab. Assay	**(nM)**	**(nM)**			
Docetaxel	0,64 ± 0,08	0,50-0,85	150 ± 30	106-213	****
Docetaxel + 0,5 μM Tariquidar	1,64 ± 0,32	1,16-2,32	1,65 ± 0,35	1,13-2,43	ns
Paclitaxel	0,58 ± 0,14	0,37-1,02	457 ± 106	306-680	**
Paclitaxel + 0,5 μM Tariquidar	3,18 ± 0,76	2,14-4,72	3,29 ± 0,69	2,30-4,72	ns
Epothilone B	1,1 ± 0,17	0,83-1,44	1,2 ± 0,16	0,92-1,53	ns

Epothilone B induced almost identical CETSA curves in K562-R as in K562-P and did not show any difference in the resazurin assay, further supporting that the observed difference between the two cells lines is mainly P-gp-dependent. Consistent with these findings, the protein levels of P-gp were found to be high in K562-R and barely detectable in K562-P as examined by western blot (Fig. 3L). Together these data illustrate that CETSA can be used to detect development of acquired drug resistance, as well as report on the mechanism of resistance in specific cases.

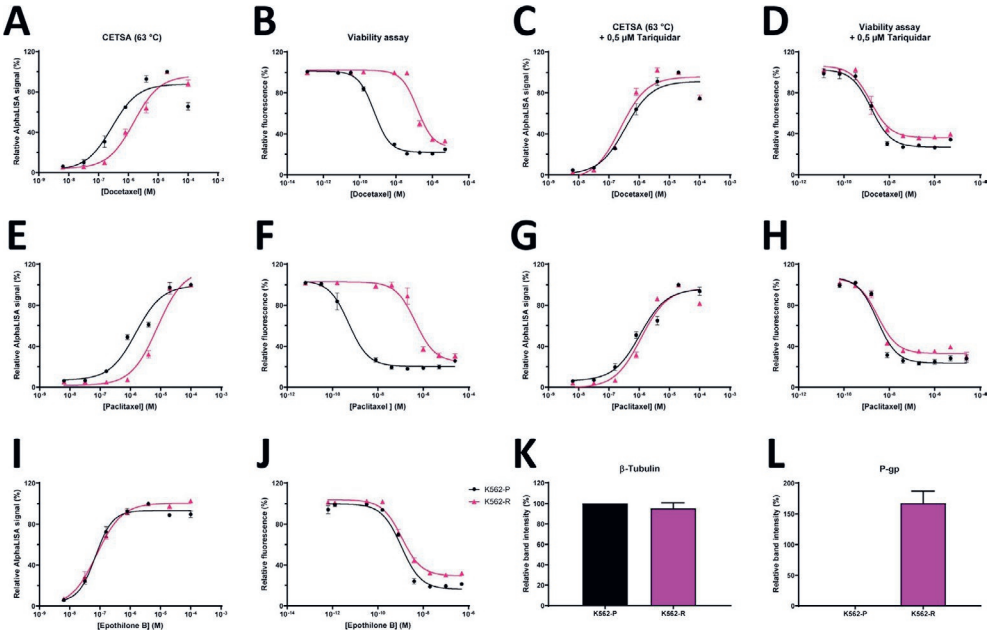

Figure 3. CETSA TE measurements correlate to sensitivity to taxanes and report on the mechanism of resistance. ITDR-CETSA for β-tubulin at 63 °C and viability assays in multidrug-resistant (K562-R) and the corresponding parental cells (K562-P) in response to increasing concentrations of docetaxel (A-D) or paclitaxel (E-H) and in the absence or presence of the Pgp-inhibitor tariquidar (C,D,G,H). ITDRs at 63 °C and viability assays performed in response to the non-Pgp-substrate epothilone B (I and J). β-tubulin was detected with AlphaLISA in the ITDR-CETSA experiments. Pgp- and β-tubulin-expression in the two cell lines was detected with western blot (K,L). ITDR-CETSA data are presented as relative to the compound concertation where maximum stabilization is achieved. Cell viability data is relative to the untreated samples. All data represent the mean ± S.E.M from independent experiments (n = 3-4).

Image-CETSA to monitor TE in specific cell types in heterogeneous samples.

For clinical applications, the analysis of TE in individual cells is of high interest since it would facilitate assessment of TE in specific cell types within a heterogeneous cell population existing in one tumor sample. One potential way to accomplish single cell resolution in CETSA is to quantify stabilization by antibody-based cell imaging, using an antibody that specifically recognizes the folded form of the protein. We developed an imaging CETSA format where we investigated several tubulin-directed antibodies and optimized the protocols, resulting in the experimental scheme as shown in Fig. S4A. Starting from cells in suspension, after drug treatment and subsequent CETSA heating in PCR-tubes, cells were washed and collected by centrifugation before being transferred to clear bottom plates where they were fixed and stained (anti-tubulin and Hoechst). After we had developed this CETSA imaging format, two articles describing related methods were published on CETSA drug screening on adherent cells, demonstrating the feasibility of the image-based detection of target engagement.[29,30] Our method is, however, more versatile and allows for studies of clinical samples of cell suspensions such as fine needle aspirates. Moreover, our protocol allows the use of different temperatures to generate melt curves.

To test our tubulin Image-CETSA implementation for assessing drug efficacy, we first generated melt curves by exposing K562 cells to different temperatures after incubation with and without docetaxel or paclitaxel (Fig. 4A and Table 3). The Image-CETSA melt curves were similar to melt curves produced by western blot CETSA from the same samples and both drugs have apparent stabilization (Figs. S4B and 4A). We then performed ITDR-CETSA experiments, showing that the imaging protocol was able to generate dose response curves (Figs. S4C and 4B). ITDRs with docetaxel were also performed in the resistant K562-R cells comparing them with their parental counterparts K562-P. A shift towards a higher EC50 value was observed in the ITDR-CETSA curve corresponding to K562-R cells for both paclitaxel and docetaxel, supporting that Image-CETSA can indeed be used to monitor drug sensitivity (Fig. 4B,C and Table 3). In Fig. 4D, representative images show that Image-CETSA in principle can reveal TE information in individual cells and should be applicable to monitor TE in individual cell types in heterogeneous samples.

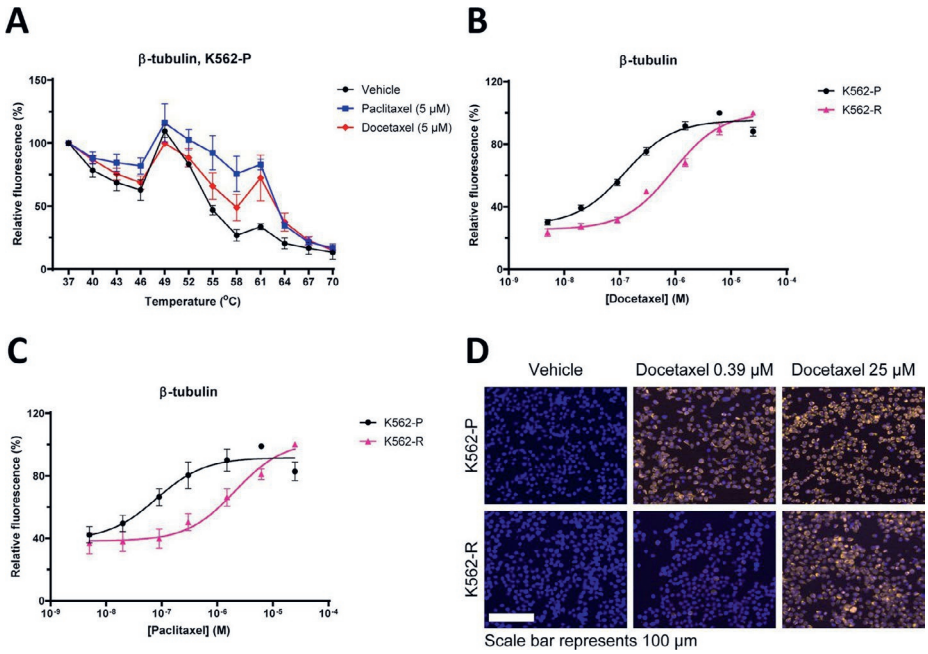

Figure 4. Imaging-CETSA has the potential of quantifying TE in individual cells and report on cellular resistance. Imaging-CETSA melt curves for β-tubulin in response to docetaxel and paclitaxel (5 μM) (A). ITDR- CETSA in multidrug-resistant (K562-R) and parental (K562-P) cells after exposure to different concentrations of docetaxel (B) or paclitaxel (C) and heating at 56 °C. Representative images of K562-P and K562-R cells treated with docetaxel or vehicle (D). Hoechst staining of the nuclei is shown in blue while β-tubulin staining is shown in yellow. All data represent the mean ±S.E.M from independent experiments (n = 3-4) and are presented as a percentage of the signal detected at the lowest temperature in each melt curve (A) or maximum stabilization detected in each series (B and C).

Table 3. Overview of EC50 values with associated standard errors and 95% confidence intervals (CI), and statistical significance calculated for the ITDR-CETSA curves in Fig. 4B,C. *The significance was determined for K562-R vs. K562-P using a two-tailed T-test for EC50 values from independent experiments. P-values ns P > 0.05, *P < 0.05, **P < 0.01, ***P < 0,001, ****P < 0,0001 compared to K562-P.

	Imaging-CETSA		
Docetaxel	**EC50 and St. Error (μM)**	**95% CI**	**Significance***
K562-P	0,12 ± 0,02	0,09-0,16	—
K562-R	0,83 ± 0,12	0,60-1,17	**
Paclitaxel	**EC50 and St. Error (μM)**	**95% CI**	**Significance***
K562-P	0,08 ± 0,04	0,03-0,20	—
K562-R	2,00 ± 0,83	0,73-5,41	**

Taxane TE in mouse xenografts in ex vivo and in vivo settings.

An advantage of CETSA is that the same measurement principle for target engagement can be used in both cell lines and tissues samples. To explore the use of tubulin CETSA in animal models, we used xenografts in mice for *ex vivo* and *in vivo* treatment. First, mice with MCF-7 derived xenografts were injected i.v. with drug or vehicle 30 min before euthanasia, directly followed by tumor sampling and preparation for CETSA analysis. In this first experiment a dose of 50 mg/kg was used, which is equivalent to 150 mg/m^2 for humans,[31] a dose that is somewhat higher than routinely used in the clinic. A significant stabilization of β-tubulin was observed for β-tubulin at 60 °C (Fig. 5A and Table 4).
In a second experiment we therefore repeated the treatment with 50 mg/kg docetaxel in mice bearing MCF-7 xenografts and included two additional docetaxel doses (33 mg/kg and 16,5 mg/kg) and two additional temperatures for the melt curves. This is equivalent to human doses of 100 mg/m^2 and 50 mg/m^2, which are commonly used in monotherapy and combination treatment respectively. A significant stabilization of tubulin was observed also with lower doses of docetaxel, demonstrating that CETSA-based TE can potentially be detected at clinically relevant doses (Fig. 5B and Table 4).

For comparing local tumor cell effects of different drugs, an *ex vivo* setting experiment is preferred, since this format would allow to evaluate target binding of multiple drugs in e.g. the same patient biopsy. To test this setting and an additional xenograft model, *ex vivo* experiments were performed in MDA-MB-231 (triple negative breast cancer cell line) derived xenograft tumors. *Ex vivo* exposure to 50 μM docetaxel also showed a very prominent shift, albeit with larger standard deviations than in the *in vivo* treated MCF-7 samples (Fig. 5C and Table 4). Possibly, the larger standard deviations could be due to poorer drug penetration in the solid tumor MDA-MB-231 pieces in the *ex vivo* setting and indicate that analysis of tissue samples with *ex vivo* drug treatment should be done using cell suspensions obtained by digesting solid biopsies, rather than by treating pieces. Alternatively, to avoid digestion of tumor tissue, a process that could potentially affect cell characteristics, the tissue could be freshly sliced using a vibratome before incubating with drug.

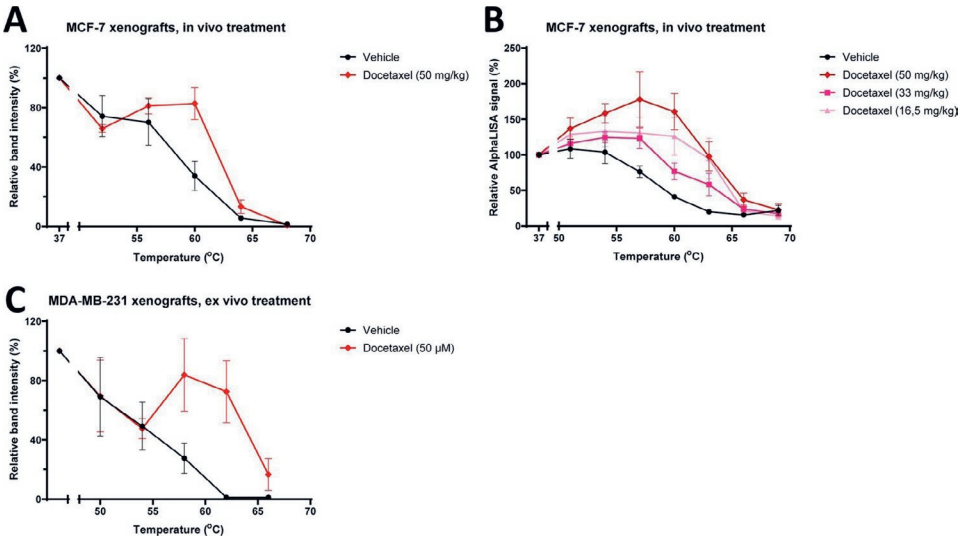

Figure 5. Docetaxel produces CETSA shifts for β-tubulin in both *in vivo* and *ex vivo* mice models. SCID-mice bearing MCF-7 xenograft tumors were treated *in vivo* for 30 min with docetaxel at a dose of 50 mg/kg before being sacrificed and the tumors taken for β-tubulin analysis with western blot-CETSA (A). SCID-mice bearing MCF-7 xenograft tumors were treated *in vivo* with different doses of docetaxel and samples were analyzed with AlphaLISA (B). Pieces of MDA-MB-231 xenografts were treated *ex vivo* with Docetaxel (50 µM) before β-tubulin analysis with western blot-CETSA (C). All data represent the mean ±S.E.M from different tumors in each condition (n = 2-3 in A, and n = 4 in B and C) and are presented as a percentage of the signal detected at the lowest temperature in each melt curve.

Table 4. Overview of the statistical significance of the measured CETSA shift for the data presented in Fig. 5A-C. *The significance of the CETSA shifts was calculated using one-way ANOVA. Adjusted P-values ns P > 0.05, *P < 0.05, **P < 0.01, ***P < 0,001, ****P < 0,0001 compared to vehicle.

MCF-7 Xenografts	**β-tubulin**
in vivo (60 °C)	Significance*
Vehicle	—
Docetaxel (50 mg/kg)	*
in vivo (60 °C)	Significance*
Vehicle	
Docetaxel (16,5 mg/kg)	*
Docetaxel (33 mg/kg)	ns
Docetaxel (50 mg/kg)	**
ex vivo (62 °C)	Significance*
Vehicle	—
Docetaxel (50 µM)	*

Characterization of resistance in prostate cancer PDX models.

As previously mentioned, an attractive setting to predict clinical outcome of drug treatment is to examine drug response *ex vivo* in biopsy samples. To investigate if drug TE measured with CETSA in *ex vivo* experiments could predict *in vivo* biology of the same drug, we performed experiments using patient-derived xenograft (PDX) based models of tumors drug resistance in castration-resistant prostate cancer. To study taxane sensitivity in resistant models we used two PDX models, PC346C and PC339, and their docetaxel-resistant counterparts PC346C-DOC and PC339-DOC, previously described by de Morrée et al.[32] Relevant details regarding the abovementioned PDX models are summarized in Table S1A. We first compared the effect of docetaxel, cabazitaxel, paclitaxel, and vinorelbine in cell lines corresponding to the PDX models PC346C and PC339. We found a pronounced difference in potency between the drugs in both cell lines with cabazitaxel as the most potent drug, followed by docetaxel, paclitaxel, and vinorelbine as the least potent drug (Figs. 6A, S5A and Table S1B). The observed ranking correlates with previous studies showing cabazitaxel is more efficient than docetaxel in inhibiting cell proliferation and suppression of microtubule dynamics.[33]

Studies of the PC346C and PC346C-DOC cell lines support that the taxane-resistant cells have attenuated TE in response to docetaxel, cabazitaxel, and paclitaxel (Fig. 6B-D and Table S1D) when both EC50s and maximum response levels are affected, reiterating the published *in vivo* results showing that taxane uptake is strongly impaired in the PC346C-DOC model.

PC346C-DOC express less of the influx transporter *SLCO1B3*, as compared to the parental counterpart PC346C, which is shown to result in almost fully depleted intratumoral taxane levels.[34] The effect of cabazitaxel on TE was more pronounced than that of docetaxel in both PC364C and PC346C-DOC tumor slices, which is in line with its reported higher efficacy.[35]

Similar studies of PC339C and PC339C-DOC do not show any significant difference between the cell lines, consistent with that processes effecting residual target engagement are not altered in this model.

Subsequently, *ex vivo* treatments of PC346C and PC339 PDX tumors (freshly sliced using a vibratome) with increasing concentrations of docetaxel and cabazitaxel were performed. Standard deviations were high for these experiments for technical reasons, as discussed below, but the results support that maximum β-tubulin TE in PC346C-DOC compared to the parental counterpart PC346C after both docetaxel and cabazitaxel treatment (Fig. 6E) is changed in a similar manner as in the cell lines. In contrast, PC339 and the docetaxel resistant variant PC339-DOC did not show effects on TE (Fig. S5E). Previous data show PC339-DOC to remain sensitive to cabazitaxel and that the docetaxel resistance in this model is possible to overcome by increased dosing of docetaxel.[32] These results support

that the mechanism of resistance in PC339-DOC is to be downstream of, or alternatively bypassing, target engagement. Taken together, our data support that CETSA TE studies can differentiate between sensitive and resistant tumors in the cases where taxane resistance occurs up to the level of TE, for example in the case of altered expression of membrane transporters.

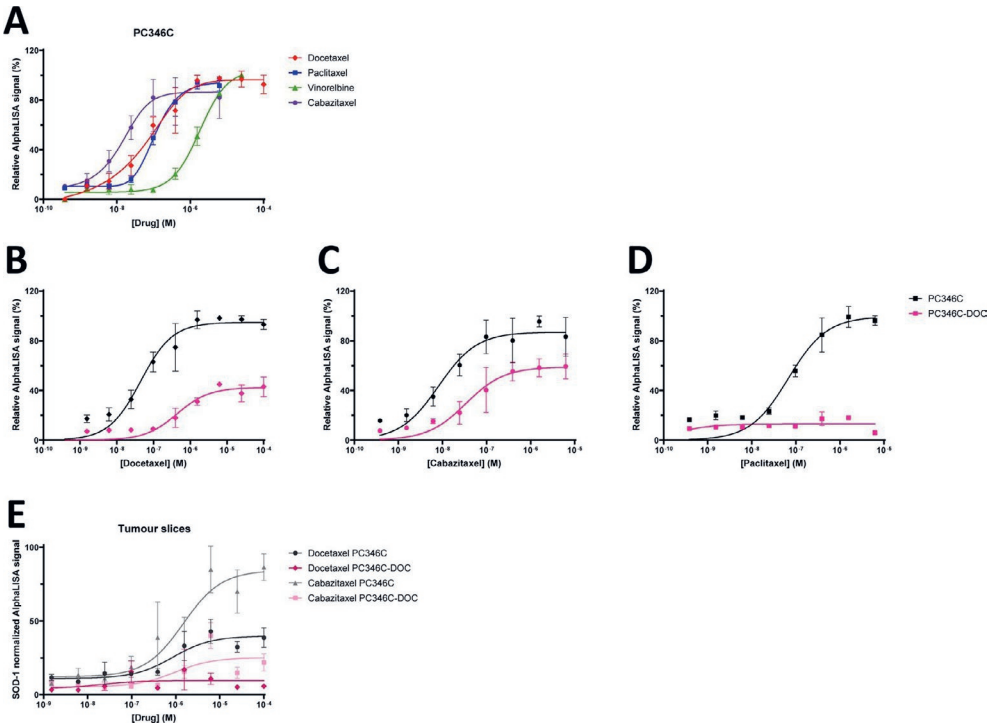

Figure 6. CETSA TE levels correlate with sensitivity to taxanes and reported resistance mechanisms in mouse PDX models of prostate cancer. PDX-derived cell line PC346C was treated with different concentrations of tubulin-binding drugs and ß-tubulin TE was analyzed with AlphaLISA (A) PC346C cells and the corresponding resistant cell line PC346C-DOC were treated with different concentrations of taxanes (B-D). Tumors from the PDX model PC346C and the resistant counterpart PC346C-DOC were treated *ex vivo* with increasing doses of docetaxel and cabazitaxel (E). Data from tumors slices were normalized to SOD-1 levels. All data represent the mean ±S.E.M from either different tumors in each condition (E) or from independent experiments (n = 3 in A-D).

Drug TE measurements in fine needle aspirates from breast cancer patients.

As shown above in several model systems, tubulin CETSA for taxanes generally correlates with drug sensitivity. To establish and evaluate the method for clinical samples we used fine needle aspirates (FNAs), since previous data indicates that measurements in cell suspensions tend to have lower variation than tissue pieces and that tumor cells are highly enriched in FNA samples.[36] We first tested the amenability of using FNAs by taking such samples from mouse xenografts. CETSA stabilization upon *ex vivo* treatment with 25 μM docetaxel of FNAs from MCF-7 xenografts was detected by AlphaLISA and shown to be linear for several cell concentrations (Fig. 7A). Next, the applicability of CETSA for patient material was assessed by performing experiments on FNAs collected from surgically resected primary tumors from breast cancer patients that have not received any previous treatment. All FNAs were exposed to docetaxel for 15 min, an incubation time that was shown to be sufficient to give full stabilization (Fig. S2F) and yet short enough to have minimal impact on cell viability as well as minimizing potential effect of transcription or other alterations that might occur in cells after being removed from their original environment. A major challenge with this approach was however the low cell number and viability typically obtained from the FNAs, although this varied very significantly between samples (Fig. S6). FNAs containing enough material (at least 10 000 live cells per experiment for detection with conjugated beads, and 100 000 per experiment for detection with standard AlphaLISA) were subjected to docetaxel treatment and subsequent CETSA analysis. Clear stabilization of β-tubulin could be detected in most samples analyzed and variability was acceptable between technical replicates. In cases where a sufficient number of viable cells were obtained, FNA samples were incubated with several doses of docetaxel. Surprisingly, these experiments revealed large differences at TE level between patients, up to 100 times (Fig. 7B and Table S2).

FNAs were also collected by cytological aspiration directly from the untreated primary tumors of breast cancer patients. In this case, the viability of the cells was somewhat higher with a mean of 43% cell viability compared to 16% in the FNAs from surgically removed tumors (Fig. S6). This improvement in cell viability may have been the result of the shorter time between FNA collection and performing the CETSA analysis. When FNAs were collected from surgically removed tumors this was typically done at least 1 hour after time of ischemia, which could have contributed to the differences in viability. The assay quality was, however, similar when analyzing samples taken directly from patients and from surgically removed tumors. Again, samples showed a dose dependent response to docetaxel but the efficacy varied between patients (Fig. 7C). K562 cells were treated and analyzed in parallel in each experiment as a technical control of the experiment and for confirming the reproducibility of the AlphaLISA assay. The K562 control experiments resulted in ITDR-CETSA curves for docetaxel with very similar EC50 values for all tested

samples (data not shown).

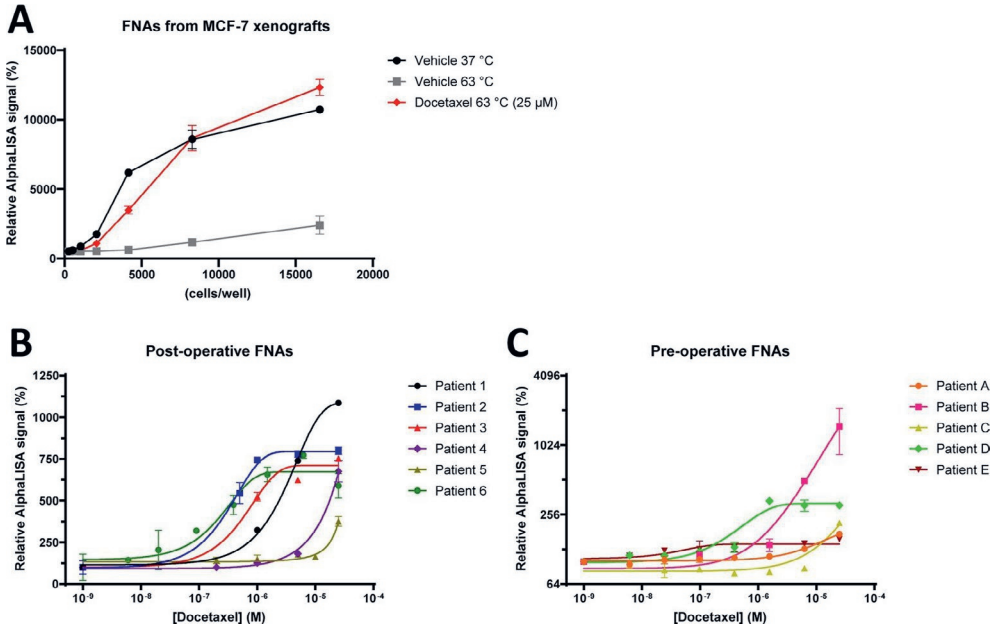

Figure 7. CETSA for assessing TE for taxanes in *ex vivo*-treated breast cancer patient FNAs. Fine needle aspirates (FNAs) were taken from freshly removed MCF-7 xenografts and treated with docetaxel (25 µM) for 15 min before CETSA-heating at 37 or 63 °C. β-tubulin for different lysate concentrations was analyzed with AlphaLISA (A). Fine needle biopsies from surgically removed tumors (B) or directly from patients (C) were treated with different concentrations of docetaxel for 15 min before CETSA-heating at 63 °C and β-tubulin analysis with AlphaLISA. The data represent the mean ± S.E.M from technical replicates and are presented as a percentage of the signal detected in the vehicle-treated samples.

Discussion

In the present work we establish different formats of CETSA to assess target engagement of taxanes, and other tubulin directed drugs, to microtubules in cells and tissues, including breast cancer patient FNAs. The different CETSA formats give consistent measurements of melting behavior and ITDRs, although some quantitative differences are seen in melting curve shapes. We show that melt curves are stabilized by several tubulin modulators binding at both the vinca and the taxane site on β-tubulin. The very stabilization by vinorelbine is surprising and indicates that this family of drugs, in addition to inhibiting tubulin polymerization, also have a dramatic effect in intrinsic microtubule stability, which might add significantly to their cytotoxic mechanism. The optimized AlphaLISA assays provide a miniaturized and sensitive format allowing for measurements using relatively small number of cells (1000 cells per measurement point). Miniaturized and sensitive CETSA measurements are particularly valuable when many measurements points (replicates, doses, time points, etc.) are assessed in model studies, and sensitivity is essential for measurements on biopsy material where low cell number is often the limiting factor. The imaging CETSA implementation provides an interesting alternative, when different cell types can be selected from images, and TE can in principle be assessed in each cell type (although this was not directly tested in this study).

A specific challenge of the tubulin specific assay is the unusually high melting temperature of tubulin in intact cells, being in the range where some cells are prone to heat induced lysis. Fortunately, tubulins are depolymerized when cells lyse and do not bind taxanes. Furthermore, tubulin in lysed cells melt some 10 °C earlier than in intact cells, so no protein from lysed cells is detected at the temperature used for most of the ITDRs (63 °C).

Most studies of cancer drug sensitivity is done using cell viability assays with durations of 48-72 h, but such assays are typically hard to establish in reproducible formats for material from solid tumors. Also, different cell programs and distribution of different cancer cell clones in the sample can change very significantly during extended culturing, as compared to the situation in the tumor. An advantage with the *ex vivo* CETSA assay is that it allows for rapid measurement of TE, where fresh tumor samples are incubated with different drugs for short time periods (15-120 minutes), during which cell programs and cell clone distributions are less affected. On the other hand, CETSA only assesses cellular responses up to the target engagement level. For tubulin-directed drugs, however, several mechanisms proposed so far for drug resistance include the level of effective intracellular drug concentrations (through changes in influx, efflux, or catabolism) as well as modulation of tubulin structure (e.g. tubulin mutations or overexpression of beta-III-tubulin),[12-14] which should be directly accessible with CETSA measurements.

In support that CETSA-derived measurement of tubulin binding correlates well with cell toxicity we show that CETSA ITDRs reflect known ranking of toxicities of different tubulin

binding drugs in cell lines. When toxicity of tubulin inhibition is primarily expected in M-phase, this suggests that drug binding and buildup of effective drug concentration in other cell cycle phases, that dominate our samples, correlates well with the situation in M-phase. Importantly, CETSA directly reflects the difference between parental and resistant cells as shown for the multidrug resistant K562 cells as well as for PC346C-DOC taxane-resistant prostate cancer.

In the PC339-DOC PDX model TE was retained, consistent with the known increased drug accumulation of cabazitaxel in the resistant cells. This supports a bypass, or downstream mechanism of acquired resistance for this PDX model which remains to be characterized. This illustrates that even in cases were CETSA reveals TE not to be affected, such information will be valuable for dissecting resistance mechanisms for cancer drugs, since CETSA captures both effective intracellular drug concentrations and target modifications. In cases where TE is not changed in resistant cells, focus can instead be put on discovering downstream mechanisms for resistance. The mass-spectrometry implementation of CETSA (MS-CETSA) now provides a novel mean to dissect down- stream/bypass mechanisms for drug resistance involving modulations of protein interaction states.[26]

Clinical evaluation of tubulin CETSA is outside the scope of this work and remains to be done for the validation of the usefulness of the assay to predict clinical outcome and to stratify drug selection. The present work does, to the best of our knowledge, for the first time present CETSA data for patient samples revealing variations in dose response. When tubulin CETSA data show correlation with drug toxicity in models it has the potential to be useful as an early prognostic biomarker to detect the emergence of resistance for different drugs up to the TE level in patient biopsies, where the cross resistance to alternative tubulin directed therapies can also be accessed. It is likely that drug targets for many other clinical drugs are similarly applicable for CETSA and that the resistance of other classes of drugs in combination therapies can be accessed in parallel with tubulin-specific acquired resistance. In the clinical situation, it has previously been difficult to pin down acquired resistance for individual drugs in combination regimes, except in cases where information on specific mutational patterns leading to target protein modifications has been available.

In conclusion, we have established and validated several protocols for measuring tubulin-specific CETSA of taxanes in cell lines and mouse models, demonstrating that drug effects up to the level of TE can be rapidly assessed in cells and tissues. Correlation of CETSA-based detection of TE with cell toxicity in several of the tested models support that CETSA measurements can provide a novel and valuable alternative in the clinical setting to rapidly generate actionable information for therapeutic decisions. Experiments on FNAs from breast cancer patients demonstrate that CETSA TE can indeed be measured in some patient samples with sufficient accuracy in the *ex vivo* setting. The relatively broad range of responses on the TE level seen in these non-treated patients, suggest varying drug sensitivity and potentially that initial resistance can be detected in patients.

To rapidly assess the relative efficacy of several tubulin directed drugs could therefore help in stratification of next line therapies. However, in spite of the high sensitivity of the miniaturized assays, for many patients the number of viable cells were not sufficient from a single FNA (Fig. S6) suggesting that e.g. core biopsies, and more sensitive detection methods are needed for CETSA measurements in a majority of patients.

Materials and Methods

Drugs.

Docetaxel (S1148), paclitaxel (S1150), vinorelbine (S4269), epothilone B (S1364), daunorubicin (S3035), and cytarabine (S1648) were obtained from Selleckchem. All drugs were solubilized in DMSO at a con- centration of 50 mM and stored frozen until use. Drugs were generally diluted 4 times in DMSO before further dilution in HBSS or media.

Cell culture.

All cell lines were cultured in 5% CO2 and 37 °C. K562 (ATCC-CCL-243) was grown in RPMI (Sigma R8768), SK-BR-3 (ATTCC-HTB-30) in McCoy's 5a media (Sigma), and MCF-7 (ATCC-HTB-22) and MDA-MB-231 (ATCC-HTB-26) were grown in DMEM high glucose (Sigma D6429). All media were supplemented with 10% heat inactivated fetal bovine serum (FBS) (Gibco 10500-064) and antibiotic-antimycotic (Life technologies 15240-062). Multidrug-resistant and parental K562 cells were kindly provided by Sören Lehmann and Christer Paul at the Karolinska Institute. Cells were passaged every second to third day. For adherent cells passaging included washing the cells in HBSS (Life technologies 14175-053 -CaCl2, -MgCl2) and detaching in TrypLE (Life Technologies 12563-029). The PC346C and PC339C cell lines were cultured in prostate growth media (PGM) as described[37] and the docetaxel-resistant counterparts were cultured in the presence of 0.1 nM docetaxel. The multidrug-resistant K562-cells were incubated for 72-96 hours with 150 nM vincristine (or DMSO for the parental cells) once a week.

CETSA melt curves and ITDR-CETSA with intact cells.

Cells were harvested, washed, and diluted in HBSS (Life technologies 14025100 + CaCl2, + MgCl2) to 4 million cells/ml for western blot and 3,33 million cells/ml for AlphaLISA. The cell suspension was mixed with drug or vehicle before aliquoting into PCR-tubes and kept at 37 °C for 1 h unless otherwise indicated. During longer incubations, tubes were rotated every 20 min. CETSA heating for 3 min, unless otherwise stated, was performed in a Veriti Thermal cycler (Applied Biosystems), either at a range of temperatures for melt curves or at 63 °C for ITDRs unless otherwise specified. Cells were subsequently lysed by three rounds of freeze-thawing by alternating exposure of the samples to liquid nitrogen and 20 °C in a PCR-machine. For western blot experiments the aggregated proteins were removed by centrifugation at 20 000 g for 20 min at 4 °C and the supernatant was collected. Samples were either analyzed directly or stored at -80°.

CETSA melt curves with cell lysate.

Cells were harvested, washed, and diluted in HBSS (Life technologies 14025100 + CaCl2, + MgCl2) to 40 million cells/ml and freeze-thawed three times, as described above, with vortexing in between for proper cell lysis. The high cell density was used in order to obtain a protein concentration more similar to that inside intact cells. The lysates were centrifuged at 20 000 g for 20 min at 4 °C, the supernatant collected, and the clarified lysate was stored at -80° until use. For the experiments, the lysate was mixed with drug or vehicle and incubated in PCR-tubes for 10 min at RT. CETSA heating and centrifugation were performed as described above. Before western blot analysis the samples were diluted to 5x in HBSS before mixing with the western blot loading buffer in order to get the same protein concentration in the samples as used for the intact-cell experiments.

Western blot.

Samples were mixed with NuPage loading buffer consisting of NuPage LDS sample buffer (Life technologies NP008) and reducing agent (Life technologies NP009) and vortexed. Proteins were separated on a Bis-Tris 4-12% polyacrylamide midi gel (Invitrogen WG1403BX10) for 45-50 min at 200 mV. Directly after the run the gels were washed in deionized water and transferred to nitrocellulose membranes using the iBlot 2 system (Invitrogen) and iBlot 2 NC Regular stacks (Invitrogen IB23001). Membranes were washed for 10 min in TBS with 0,05% Tween 20 (Medicago 09-7510-100) (TBS-T) and blocked in 5% (w/v) non-fat milk (Semper AB) in TBS-T for 1 h before incubation with primary antibody over night at 4 °C with gentle shaking. After washing in TBS-T for 5 × 5 min, membranes were exposed to secondary antibodies for 1 h, washed again 5 × 5 min in TBS-T and developed using Clarity Western ECL Substrate (BioRad #170-5061). The chemiluminescent signal was detected using the ChemiDocTM XRS + imaging system from BioRad and band intensities were quantified using ImageLabTM software (BioRad).

Primary antibodies used were T5201 from Sigma for ß-tubulin, sc-32293 from Santa Cruz for a-tubulin, and HPA001401 from Sigma or sc-11407 from Santa Cruz for SOD-1. When comparing western blot with Image-CETSA the ß-tubulin antibody #2128 from Cell Signalling was used since that is the same clone (9F3) as the Alexa Fluor 488 conjugated antibody #3623 that was used for Image-CETSA.

Secondary antibodies used were either sc-2055 from Santa Cruz or W402B from Promega for mouse and sc-2374 from Santa Cruz or W401B from Promega for rabbit. All antibodies were diluted in 5% (w/v) non-fat milk in TBS-T.

Trypan blue exclusion.

In order to monitor membrane integrity after heating, cells were harvested according to the same protocol as for the CETSA experiments (see above) and heated in the Veriti Thermal cycler according to the indicated temperatures and time points. After heating, a 10 µl aliquot was immediately taken and mixed with 10 µl 0.4% Trypan Blue stain (Gibco/ Life Technologies 15250-061). 10 µl of this mix was directly loaded on a counting slide (BioRad #145-011) and read in an automated cell counter (BioRad TC20).

Standard AlphaLISA assay.

For detection with AlphaLISA, 3 µl of each sample was loaded in duplicates in an AlphaPlate (Perkin Elmer 6008350) followed by addition of 2 µl antibody mix. Two different combinations of antibodies were used: either the mouse-anti-tubulin antibody sc-398937 (raised against amino-acids 209- 305 within an internal region of human β4-tubulin, Santa Cruz) in combination with the rabbit-anti-tubulin antibody ab6046 (raised against a synthetic peptice corresponding to human beta tubulin amino-acids 1-100, Abcam) referred to pair 2, or pair 8 where the mouse antibody was changed to T5201 (recognizes all five isoforms of beta-tubulin and binds to the carboxy-terminal part, Sigma). Sc-389837 was diluted to 45 nM in order to get the final concentration of 1 nM, T5201 to 135 nM to get final concentration of 3 nM, and ab6046 was diluted to 450 nM to get 10 nM in the final mix. All dilution was made in AlphaLISA Immunoassay Buffer (Perkin Elmer AL000F). Anti-rabbit acceptor beads (Perkin Elmer AL104M) and anti-mouse donor beads (Perkin Elmer AS104D) were diluted in the same AlphaLISA buffer to 22.5 µg/ml and 90 µg/ml respectively to get 10 µg/ml and 40 µg/ml as final concentration when adding 4 µl of the mix to each well. All handling of the beads was done in a room with green light. Plates were sealed with sticky film, covered in foil, and spun at 177 rcf for 1-3 min. After overnight incubation in the dark, plates were spun briefly at 300 rcf and read in an Enspire 2300 (Perkin Elmer).

Conjugation of AlphaLISA beads.

Two antibody pairs were conjugated: ab6046 (abcam) and T5201 (Sigma) for tubulin (pair 8) and the polyclonal AF3418 for SOD-1. The SOD-1 antibody AF3418 (R&D Systems) was divided in two aliquots of which one was biotinylated and one was conjugated to the Acceptor beads (Perkin Elmer 6772001). For β-tubulin ab6046 (abcam) was biotinylated and T5201 (Sigma) was used for conjugation to Acceptor beads. Biotinylation of respective antibody were performed using an antibody biotinylation kit (Pierce/ Thermo scientific 90407).

Before performing biotinylation, the buffer of ab6046 needed to be exchanged to PBS which was done using Zeba spin column (Thermo Scientific 89882) according to the manufacturer's instructions. Then 100 µl PBS was added to one tube of NHS-PEG4-Biotin and mixed by pipetting. A 40-fold excess of biotin was added to the anti- bodies, mixed, and incubated for 30 min at RT. After incubation, the buffer was exchanged using the Zeba spin column (Thermo Scientific 89882) according to manufacturer's protocol. Biotinylated antibodies were aliquoted and stored at -20 °C before use.

The antibodies T5201 and AF3418 were conjugated to Acceptor beads (Perkin Elmer 6772001). 0.033 mg beads were used for 0.333 mg antibody. First, the Acceptor beads were washed by adding 17 µl PBS (Life technologies 10010), centrifuged at 16 000 rpm for 15 min, supernatant discarded, and the pellet dissolved in at mix with 0.033 mg antibody and 130 mM sodium phosphate puffer (pH 8.0) in a final volume of 67 µl. In later conjugations, this volume was reduced to half in order to increase the yield. To this mix 0.43 µl of 10% Tween-20 (P1379) and 3.33 µl of 400 mM NaHB3CN (Sigma Aldrich 296945) was added, mixed gently by pipetting and incubated for 18-24 h at 37 °C with mild agitation (~60 rpm).

The next day 3.33 µl of 65 mg/ml Carboxymethoxylamine (Sigma C13408) in 800 mM NaOH was added and incubated for 1 h at 37 °C with mild agitation to stop the reaction. After incubation the tubes were centrifuged for 15 min at 16 000 rpm at 4 °C and the supernatant discarded. The pellet was resuspended in 67 µl 100 mM Tris-HCl (pH 8.0), centrifuged again and was resuspended in 200 µl PBS with 0.05% Proclin-300 (Sigma Aldrich 48912). The antibodies were vortexed briefly, spun down, and sonicated with 10 pulses before stored at + 4 °C until use.

AlphaLISA assay with conjugated beads.

Samples were diluted in HBSS for optimal linearity for each antibody pair. For human samples, 300 cells/well were used for SOD-1 and 3000 cells/well for ß-tubulin. The PDX-samples were diluted 10 x for tubulin and 500 times for SOD1. 3 µl of each sample was loaded in AlphaPlate (Perkin Elmer 6008350), in duplicate when possible. 2 µl biotinylated antibody was added to each well and the plate were then briefly spun down before addition of Acceptor beads. For both β-tubulin and SOD-1 the biotinylated antibody (biotin-AF3418 and biotin-ab6046 respectively) were used at a final concentration of 3 nM.

Acceptor breads (2 µl) were added and the plate was spun briefly and incubated on a shaker for 1 h at 60 rpm. For SOD-1, Acceptor beads were diluted to 45 µg/ml for a final concentration of 10 µg/ml and for β-tubulin T5201-conjugated Acceptor beads were used at a concentration of 180 µg to get at final concentration of 40 µg/ml. Then 2 µl Donor beads (Perkin Elmer 6760002S) was added at a concentration of 180 µg/ml for get at final

con- centration of 40 µg/ml. Handling of beads was only done in a room with green light. Plates were sealed with sticky film, covered in foil, briefly spun down, and incubated in the dark over night before being read in an EnSpire 2300 (Perkin Elmer).

ITDR-CETSA in multidrug-resistant K562 cells.

For the intact cell ITDR-CETSA experiments, studied compounds (docetaxel, paclitaxel, or epothilone B) were prepared in RPMI supplemented with 5% FBS at double the final compound concentration and with or without the addition of tariquidar (also at double the final concentration). Multidrug-resistant and parental K562 cells were harvested, washed in + 5% FBS, and resuspended at 6,66 million cells/ml in RPMI + 5% FBS. Cells were then mixed 1:1 in PCR tubes with the previously prepared compound dilutions so that the final cell density was 3,33 million cells/ml in 50 µl total volume. The final tariquidar concentration in the allocated samples was 0,5 µM. Vehicle-treated samples were also included at a final concentration of 0,4% DMSO. The treated cells were incubated at 37 °C for 1 h 45 min followed by heating for 3 minutes at 63 °C in a Veriti thermal cycler (Applied Biosystems). Unheated samples were also included. Immediately after the heating, all samples were freeze-thawed three times using liquid nitrogen. The samples were vortexed after every freeze-thaw cycle. The remaining soluble β-tubulin was analyzed in the total lysate using AlphaLISA pair.[8]

Resazurin cytotoxicity assay.

For assessment of drug toxicity, multidrug-resistant and parental K562 cells in duplicates of 10 000 cells/well, were seeded in black 96-well clear bottom polystyrene microplates (Sigma) containing various drug concentrations diluted in RPMI supplemented with 5% heat inactivated FBS. Following, 72 h incubation at 37 °C, 10 µg/ml resazurin sodium salt (Sigma) was added to each well and further incubated for 2 h at 37 °C. Resorufin fluorescence was measured at a wavelength of 590 nm using an Enspire plate reader (Perkin Elmer).

Image-CETSA.

Multidrug-resistant and parental K562 cells were propagated in RPMI-1640 medium supplemented with 10% heat inactivated FBS and continuously maintained at a cell density of 2 × 105 cells/ml. Drug resistance was preserved with 150 nM vincristine or vehicle DMSO, in the resistant and parental K562 cells respectively, by selection for 72-96 h. Prior to each experiment, cells were washed once in HBSS before transfer to PCR tubes with RPMI-1640 medium containing 5% heat inactivated FBS and various drug

concentrations at a density of 4 million cells/ml. After 2 h incubation at 37 °C, CETSA heating was performed at 56 °C in a Veriti Thermal Cycler (Applied Biosystems) for 3 min. After heating, cells were collected by centrifugation at 200 rcf for 3 min at 4 °C and washed twice in HBSS before transfer to black 96-well clear bottom polystyrene microplates (Sigma) pre-coated with 1% aqueous Alcian Blue solution (Electron Microscopy Sciences) for 15 min for cell adherence. Supernatant was aspirated after centrifugation at 200 rcf for 5 min at 4 °C, after which cells were fixed in 4% w/v formaldehyde (Thermo Scientific) for 15 min at room temperature. Next, the cells were washed twice in DPBS/Modified (GE Healthcare) and permeabilized by incubation with 5% v/v Triton X-100 (Sigma) for 15 min at room temperature with gentle agitation. After an additional three washes, blocking was performed in 2% w/v bovine serum albumin (Sigma) for 1 h at room temperature with gentle agitation. β-tubulin conjugated Alexa Fluor 555 (#3623, Cell Signaling) was diluted 1:200 in blocking buffer and added for overnight incubation protected from light at 4 °C with gentle agitation. Next, the cells were washed twice with 0.1% v/v Tween 20 (Sigma) and counterstained with 1 mg/ml v/v Hoechst (Chemometec) diluted in DPBS/Modified for 5 min at room temperature with gentle agitation. After an additional two washes, the Tween 20 wash buffer was replaced with DPBS/ Modified for subsequent image analysis.

Images and analysis were acquired with the CytellTM Cell Imaging system (GE Healthcare) using a 2-colour BioApp specific for cytoplasmic image analysis. A blue (390/430) and a yellow (544/588) channel were applied for nuclear and cytoplasmic imaging respectively. Fifty-one fields covering the entire well were captured with a 10x Plan Apo 0.45 NA objective. Raw data based on average cellular cytoplasmic intensity for each individual well was further analyzed and plotted using GraphPad Prism version 6.

CETSA on in vivo treated xenografts.

Female NOD-SCID mice were obtained from the breeding unit at the Department of Microbiology, Tumor and Cell Biology, Karolinska Institute. All mouse studies were approved by the Northern Stockholm Experimental Animal Ethical Committee (Dnr N 192/13 and Dnr N 2/17) and were performed in accordance with the relevant guidelines and regulations. Tumor volumes were measured with a caliper and calculated according to the standard formula (length × width2 × 0.52).

For the *in vivo* experiments, NOD-SCID mice were injected with approximately 5×10^6 MCF-7 cells into a mammary gland. When the tumor sizes reached 0.2-0.3 cm^3, the mice were injected with either vehicle (EtOH 1:1 in polysorbate 80 and then diluted in 5% dextrose) or docetaxel 30 min before they were euthanized by inhalation of a lethal dose of CO2 followed by cervical dislocation. Tumors were removed and cut into pieces using a scalpel and put in PCR-strips (Applied Biosystems N8010580). 30 µl HBSS (Life technologies 14025100 + CaCl2, + MgCl2) was added and the samples heated to different temperatures

in a Veriti Thermal cycler (Applied Biosystems). After heating samples were frozen in liquid nitrogen and then thawed at 20 °C. High salt lysis buffer (50 mM tris-HCl, 300 mM NaCl, 0.5% NP40, 1 mM EDTA, pH 7.2) and Halt Protease Inhibitor (Thermo Scientific 1861279) was added and the freeze-thawing repeated two additional times. The tumor pieces were further homogenized by crushing them with bent plastic pipette tips.

Soluble proteins were isolated by centrifugation at 20000 x g for 20 minutes at 4 °C and the tubulin detected with western blot or AlphaLISA pair 2. SOD-1 was used as loading control in order to minimize the potential effect of differences in size of tumor pieces, this did however only give minimal change to the graph appearance, why we chose not to use this in the analysis of xenografts. Total five animals were used for the first pilot experiment and 16 mice were used for the second.

CETSA on ex vivo treated xenografts.

NOD-SCID mice were injected with approximately 5 million MDA-MD-231 cells into a mammary gland. At the day of the experiment, four mice were euthanized by inhalation of a lethal dose of CO2 followed by cervical dislocation and tumors removed directly. Each tumor was divided into 12 pieces, which were incubated in vehicle (DMSO, 0.5%) or 50 µM docetaxel in HBSS (Life technologies 14025100 + CaCl2, + MgCl2) supplemented with Halt Protease Inhibitor (Thermo Scientific 1861279) for 1 h at 37 °C. After incubation samples were heated to different temperatures in a Veriti Thermal cycler (Applied Biosystems). After heating samples were frozen in liquid nitrogen and then thawed at 20 °C. High salt lysis buffer (50 mM tris-HCl, 300 mM NaCl, 0.5% NP40, 1 mM EDTA, pH 7.2) was added and the freeze-thawing repeated two additional times. The tumour pieces were further homogenized by crushing them with bent plastic pipette tips. Soluble proteins were isolated by centrifugation at 20000 rcf for 20 minutes at 4 °C and tubulin was detected with western blot.

CETSA on ex vivo treated PDX-tumors.

These animal experiments were performed at the Erasmus University Medical Centre in Rotterdam and all experiments were approved by the Animal Experiment Committee under the Dutch Experiment on Animals Act and adhered to the European Convention for Protection of Vertebrate Animals used for Experimental Purposes (Directive 2010/63/EU).

Sixteen mice were inoculated with one of four prostate cancer cell lines bilaterally at 5 million cells on each side. The following prostate cancer cell lines were used: PC346C and PC339, and the docetaxel resistant lines PC346C-Doc and PC339-Doc. Cells were maintained as described previously.[37]

Tumor volume was monitored twice weekly by digital calipers, and tumors were excised

28-37 days after inoculation (tumor volumes ranged between 125 and 1500 mm^3).

At the day of the experiment, mice were sacrificed (cervical dislocation), the tumors removed and fixed on a layer of low melting agarose using cyanoacrylate glue. The tumors were sliced using the Leica VT1200S Vibratome at a thickness of 300 µm and the slices were transferred to PCR strips containing HBSS (Life technologies 14025100 + CaCl2, + MgCl2) and treated with a range of drug concentrations as indicated for 1 h at 37 °C and 5% CO2. After incubation, samples were heated in a PCR-machine (Biometra T1 thermocycler) at 63 °C for 3 min and then snap frozen in liquid nitrogen. All samples were stored at -80 °C until detection.

For detection, all samples were frozen and thawed three times in liquid nitrogen and a 20 °C program on a PCR-machine. High salt lysis buffer (50 mM tris-HCl, 300 mM NaCl, 0.5% NP40, 1 mM EDTA, pH 7.2) was added and samples were vortexed vigorously before slices and debris were removed by centrifugation for 20 min at 1000 rpm. Supernatant was isolated and analyzed for β-tubulin and SOD-1 content using AlphaLISA. For β-tubulin detection antibody pair 2 was used and the samples were diluted 10 times prior to AlphaLISA detection, while for SOD-1 samples were diluted 500 times.

Patient fine needle aspirates (FNAs).

All experiments performed on human material were approved by the Regional Ethical Board in Stockholm. Samples were either anonymized (Dnr 2016 957-31) or taken from patients who signed informed consent (Dnr 2015/1694-31/1 with approved amendments 2016/2599-32, 2017/1353-32 and 2017/1267-32). All methods were performed in accordance with the relevant guidelines and regulations. FNAs were taken by pathologists or cytologists from tumors after surgery or directly from patients and placed in tubes with L15 media (Gibco L-15 21083-027). Cells were counted, spun down, and resuspended in HBSS (Life technologies 14025100 + CaCl2, + MgCl2) and treated with docetaxel for 15 min. When 100 000 cells or more were obtained, cells were resuspended to a final concentration of 3 million cells/ml and detected with AlphaLISA pair 8. When 20 000 to 100 00 cells were obtained cells were suspended to 1 million/ml and detected with conjugated AlphaLISA pair 8.

Data analysis.

The presented data were generated in independent experiments n = 3 except Figs. 2C-E, S2D-F and Fig. 7, where data correspond to technical duplicates. All graphs were generated using GraphPad Prism (versions 6-8). All data are presented as mean with error bars representing the standard error of the mean (S.E.M). Error bars that are smaller than the displayed data points are not shown by the software e.g. in Fig. 2C.

ITDR-CETSA and cell viability data are presented as a percentage of the signal corresponding to the com- pound concentration where maximum stabilization was achieved in each series, with the exception of Figs. 6E and S5E where data are presented as normalized to SOD-1, Fig. 6B-D where data are presented as a percentage of the signal obtained for the drug-sensitive cells at maximum stabilization, and Fig. 7B,C where data are presented as a percentage of the signal detected for the untreated samples in each series. Sigmoidal curves were fit in GraphPad Prism using non-linear regression of the type [Inhibitor] vs. Response (three parameters) with the function Y = Bottom + (Top-Bottom)/ (1 + (X/IC50)). ITDR-CETSA curves in Fig. 7 were fit using non-linear regression of the type [Inhibitor] vs. Response (four parameters) with the function Y = Bottom + (Top-Bottom)/ (1 + (IC50/X)^HillSlope). The EC50 values with associated standard errors and 95% confidence intervals calcu- lated for the curves are presented in corresponding tables. The statistical significance of the difference observed between the dose-response curves in each graph was calculated using a T-test for the EC50 values obtained in each individual experiment.

For CETSA melt curves (Figs. 1B-G, 2C,D, 4A and 5A-C), data are presented as a percentage of the signal detected at the lowest temperature in each melt curve and a line connecting the data points was automatically generated by the abovementioned software. Melting temperatures (Tm) and the size of the CETSA shifts (ΔTm) were also determined in GraphPad Prism. One-way ANOVA was used for analyzing the CETSA melt curve data in Figs. 1B-G and 5A-C. The significance levels for these statistical analyses are presented in corresponding tables.

Data availability

The datasets generated and analyzed during the current study are available from the corresponding author on reasonable request.

Acknowledgements

We would like to acknowledge Sören Lehmann and Christer Paul at the Karolinska Institute for kindly providing us with the multidrug-resistant K562 cells, Eva Darai Ramkvist, Edneia Tani and the puncture reception at Radiumhemmet for collecting the pre-operative biopsies, and Johanna Klinge, Helen Eriksson, Lisa Viberg, Susanne Agartz, Ran Ma, and Xinsong Chen for help with administration and logistics of clinical samples. PN acknowledges grants from the Swedish Research Council (VR-MH and VR-NT), the Swedish Cancer Society, Radiumhemmet's funds, the Swedish Childhood Cancer Fund, and the Knut and Alice Wallenberg Foundation. JB acknowledges grants from PCM/ Radiumhemmet's funds, and the Knut and Alice Wallenberg Foundation. Open access funding provided by Karolinska Institute.

Supplementary information is available for this paper at https://doi.org/10.1038/s41598-019-55526-8.

References

1. Dumontet, C. & Jordan, M. A. Microtubule-binding agents: a dynamic field of cancer therapeutics. Nat Rev Drug Discov 9, 790-803, https://doi.org/10.1038/nrd3253 (2010).
2. Ercolak, V., Sahin, B., Gunaldi, M., Duman, B. B. & Afsar, C. U. Efficacy of paclitaxel in the treatment of Kaposi sarcoma. Eur Rev Med Pharmacol Sci 19, 4095-4100 (2015).
3. Prithviraj, G. K. et al. Carboplatin and paclitaxel as first-line treatment of unresectable or metastatic esophageal or gastric cancer. Dis Esophagus 28, 782-787, https://doi.org/10.1111/dote.12279 (2015).
4. Perez, E. A. Paclitaxel in Breast Cancer. Oncologist 3, 373-389 (1998).
5. King, K. M. et al. Optimal use of taxanes in metastatic breast cancer. Curr Oncol 16, 8-20 (2009).
6. Tannock, I. F. et al. Docetaxel plus prednisone or mitoxantrone plus prednisone for advanced prostate cancer. N Engl J Med 351, 1502-1512, https://doi.org/10.1056/NEJMoa040720 (2004).
7. de Bono, J. S. et al. Prednisone plus cabazitaxel or mitoxantrone for metastatic castration-resistant prostate cancer progressing after docetaxel treatment: a randomised open-label trial. Lancet 376, 1147-1154, https://doi.org/10.1016/S0140-6736(10)61389-X (2010).
8. Sathianathen, N. J. et al. Taxane-based chemohormonal therapy for metastatic hormone-sensitive prostate cancer. Cochrane Database Syst Rev 10, CD012816, https://doi.org/10.1002/14651858.CD012816.pub2 (2018).
9. Field, J. J., Díaz, J. F. & Miller, J. H. The binding sites of microtubule-stabilizing agents. Chem Biol 20, 301-315, https://doi. org/10.1016/j.chembiol.2013.01.014 (2013).
10. Dorr, R. T. Pharmacology of the taxanes. Pharmacotherapy 17, 96S-104S (1997).
11. Trock, B. J., Leonessa, F. & Clarke, R. Multidrug resistance in breast cancer: a meta-analysis of MDR1/gp170 expression and its possible functional significance. J Natl Cancer Inst 89, 917-931 (1997).
12. Orr, G. A., Verdier-Pinard, P., McDaid, H. & Horwitz, S. B. Mechanisms of Taxol resistance related to microtubules. Oncogene 22, 7280-7295, https://doi.org/10.1038/sj.onc.1206934 (2003).
13. Murray, S., Briasoulis, E., Linardou, H., Bafaloukos, D. & Papadimitriou, C. Taxane resistance in breast cancer: mechanisms, predictive biomarkers and circumvention strategies. Cancer Treat Rev 38, 890-903, https://doi.org/10.1016/j.ctrv.2012.02.011 (2012).
14. Parker, A. L., Teo, W. S., McCarroll, J. A. & Kavallaris, M. An Emerging Role for Tubulin Isotypes in Modulating Cancer Biology and Chemotherapy Resistance. Int J Mol Sci 18, https://doi.org/10.3390/ijms18071434 (2017).
15. Ferlini, C. et al. Bcl-2 down-regulation is a novel mechanism of paclitaxel resistance. Mol Pharmacol 64, 51-58, https://doi. org/10.1124/mol.64.1.51 (2003).
16. Wang, Z., Goulet, R., Stanton, K. J., Sadaria, M. & Nakshatri, H. Differential effect of anti-apoptotic genes Bcl-xL and c-FLIP on sensitivity of MCF-7 breast cancer cells to paclitaxel and docetaxel. Anticancer Res 25, 2367-2379 (2005).
17. Mabuchi, S. et al. Inhibition of inhibitor of nuclear factor-kappaB phosphorylation increases the efficacy of paclitaxel in in vitro and in vivo ovarian cancer models. Clin Cancer Res 10, 7645-7654, https://doi.org/10.1158/1078-0432.CCR-04-0958 (2004).
18. Gerritsen-van Schieveen, P., Royer, B. & Therapeutics, T. d. m. g. o. t. F. S. o. P.a. Level of evidence for therapeutic drug monitoring of taxanes. Fundam Clin Pharmacol 25, 414-424, https://doi.org/10.1111/j.1472-8206.2010.00874.x (2011).
19. Martinez Molina, D. et al. Monitoring drug target engagement in cells and tissues using the cellular thermal shift assay. Science 341, 84-87, https://doi.org/10.1126/science.1233606

(2013).
20. Ishii, T. et al. CETSA quantitatively verifies in vivo target engagement of novel RIPK1 inhibitors in various biospecimens. Sci Rep 7, 13000, https://doi.org/10.1038/s41598-017-12513-1 (2017).
21. Savitski, M. M. et al. Tracking cancer drugs in living cells by thermal profiling of the proteome. Science 346, 1255784, https://doi. org/10.1126/science.1255784 (2014).
22. Jordan, M. A. & Wilson, L. Microtubules as a target for anticancer drugs. Nat Rev Cancer 4, 253-265, https://doi.org/10.1038/ nrc1317 (2004).
23. Downing, K. H. Structural basis for the interaction of tubulin with proteins and drugs that affect microtubule dynamics. Annu Rev Cell Dev Biol 16, 89-111, https://doi.org/10.1146/annurev.cellbio.16.1.89 (2000).
24. Vindya, N. G., Sharma, N., Yadav, M. & Ethiraj, K. R. Tubulins - the target for anticancer therapy. Curr Top Med Chem 15, 73-82 (2015).
25. Tan, C. S. H. et al. Thermal proximity coaggregation for system-wide profiling of protein complex dynamics in cells. Science 359, 1170-1177, https://doi.org/10.1126/science.aan0346 (2018).
26. Dai, L. et al. Horizontal Cell Biology: Monitoring Global Changes of Protein Interaction States with the Proteome-Wide Cellular Thermal Shift Assay (CETSA). Annu Rev Biochem. https://doi.org/10.1146/annurev-biochem-062917-012837 (2019).
27. Miettinen, T. P. & Björklund, M. NQO2 is a reactive oxygen species generating off-target for acetaminophen. Mol Pharm 11, 4395-4404, https://doi.org/10.1021/mp5004866 (2014).
28. Löfgren, C. et al. Mechanisms of cross-resistance between nucleoside analogues and vincristine or daunorubicin in leukemic cells. Biochem Biophys Res Commun 320, 825-832, https://doi.org/10.1016/j.bbrc.2004.06.016 (2004).
29. Axelsson, H. et al. In Situ Target Engagement Studies in Adherent Cells. ACS Chem Biol 13, 942-950, https://doi.org/10.1021/ acschembio.7b01079 (2018).
30. Massey, A. J. A high content, high throughput cellular thermal stability assay for measuring drug-target engagement in living cells. PLoS One 13, e0195050, https://doi.org/10.1371/journal.pone.0195050 (2018).
31. Nair, A. B. & Jacob, S. A simple practice guide for dose conversion between animals and human. J Basic Clin Pharm 7, 27-31, https:// doi.org/10.4103/0976-0105.177703 (2016).
32. de Morrée, E. et al. Understanding taxanes in prostate cancer; importance of intratumoral drug accumulation. Prostate 76, 927-936, https://doi.org/10.1002/pros.23182 (2016).
33. Azarenko, O., Smiyun, G., Mah, J., Wilson, L. & Jordan, M. A. Antiproliferative mechanism of action of the novel taxane cabazitaxel as compared with the parent compound docetaxel in MCF7 breast cancer cells. Mol Cancer Ther 13, 2092-2103, https://doi. org/10.1158/1535-7163.MCT-14-0265 (2014).
34. de Morrée, E. S. et al. Loss of SLCO1B3 drives taxane resistance in prostate cancer. Br J Cancer 115, 674-681, https://doi.org/10.1038/ bjc.2016.251 (2016).
35. Jarvis, C., Nelius, T., Martinez-Marin, D., Sennoune, S. R. & Filleur, S. Cabazitaxel regimens inhibit the growth of prostate cancer cells and enhances the anti-tumor properties of PEDF with various efficacy and toxicity. Prostate 78, 905-914, https://doi. org/10.1002/pros.23647 (2018).
36. Ernst, L. M. & Rimm, D. L. Quantitative examination of mechanophysical tumor cell enrichment in fine-needle aspiration specimens. Cancer 96, 275-279, https://doi.org/10.1002/cncr.10746 (2002).
37. Marques, R. B. et al. The human PC346 xenograft and cell line panel: a model system for prostate cancer progression. Eur Urol 49, 245-257, https://doi.org/10.1016/j.eururo.2005.12.035 (2006).

Chapter V

Continued Androgen Signaling Inhibition Improves Cabazitaxel Efficacy in Prostate Cancer

Lisanne Mout, Martin E. van Royen, Corrina de Ridder, Debra Stuurman, Wesley S. van de Geer, Rute Marques, Pim J. French, Harmen J.G. van de Werken, Ron H.J. Mathijssen, Ronald de Wit, Martijn P. Lolkema, Wytske M. van Weerden

manuscript submitted

Abstract

Purpose

The androgen receptor (AR) signaling pathway is a key driver of neoplastic behavior in the different stages of metastatic prostate cancer (mPCa). Inhibiting AR signaling therefore remains the cornerstone for mPCa treatment. We have previously reported that activation of AR signaling affects taxane chemo-sensitivity in preclinical models of castration resistant PCa (CRPC). Here, we explored the anti-tumor efficacy of the AR signaling targeted inhibitor enzalutamide combined with cabazitaxel.

Methods

We used the AR positive CRPC model PC346C-DCC-K to assess the *in vitro* and *in vivo* activity of combining enzalutamide with cabazitaxel. Subsequent validation studies were performed using an enzalutamide resistant VCaP model. To investigate the impact of AR signaling on cabazitaxel activity we used RNA-sequencing, quantitative live-cell imaging of tubulin stabilization and apoptosis related nuclear fragmentation.

Findings

Enzalutamide strongly amplified cabazitaxel anti-tumor activity in both the PC346C-DCC-K (median time to humane endpoint 77 versus 48 days, $P<0.0001$) and VCaP-Enza-B tumor model (median time to humane endpoint 80 versus 53 days, $P<0.001$). Importantly, enzalutamide treatment still effectively suppressed AR signaling in PC346C-DCC-K tumors as shown by differential gene expression (normalized enrichment score -1.74, false discovery rate 0.09). AR inhibition enhanced cabazitaxel induced apoptosis as shown by live-cell imaging ($P<0.001$).

Interpretation

Our study demonstrates that cabazitaxel efficacy can be improved by simultaneous blocking of AR signaling by enzalutamide, even if AR targeted treatment no longer affects tumor cell proliferation. These findings support clinical studies that combine AR signaling targeted inhibitors with cabazitaxel in CRPC.

Introduction

The androgen receptor (AR) signaling pathway is a major driver of neoplastic behavior in the different stages of metastatic prostate cancer (mPCa). Hence, androgen deprivation therapy (ADT), which blocks the production of the AR ligands testosterone and dihydrotestosterone levels, is the cornerstone of mPCa treatment. Although ADT effectively infers disease regression in the vast majority of patients, disease recurrence is inevitable and is classified as castration resistant prostate cancer (CRPC). Multiple studies have shown that the AR continues to play a major role in ADT resistance and progression to CRPC, as AR amplifications and mutations conferring androgen hypersensitivity and ligand promiscuity are frequently identified in samples from CRPC patients.[1,2] Large scale whole genome sequencing studies showed that AR alterations occur in 80-85% of CRPC patients, which are rare in castration naïve patients.[3,4] This underlines the importance of continued suppression of AR signaling by ADT or targeted inhibitors such as enzalutamide in CRPC patients. We have previously reported on the impact of androgens and AR pathway signaling on taxane treatment efficacy in CRPC. Taxanes represent a vital therapeutic option for CRPC, however, treatment efficacy is limited by intrinsic and acquired resistance. We showed that testosterone supplementation impairs the activity of both docetaxel and cabazitaxel.[5,6] Moreover, stimulating AR signaling by testosterone was able to counteract docetaxel induced long-term tumor regression, demonstrating that AR signaling directly contributed to taxane resistance. We therefore hypothesized that taxane treatment efficacy is enhanced by simultaneous blockade of AR signaling, through targeted inhibitors such as enzalutamide. Here, we show that indeed combining enzalutamide with cabazitaxel, significantly improved activity in enzalutamide resistant patient-derived xenograft models. We demonstrate that targeting of AR signaling enhances the rate of cabazitaxel induced apoptosis. Our results support new combination treatments for CRPC patients that potentially remains effective after resistance to AR signaling targeted agents occurs.

Material and Methods

Cell culture and treatment sensitivity in vitro

The AR expressing CRPC model PC346C-DCC-K was obtained by long-term exposure to steroid stripped cell culture conditions as described previously.[5,7] VCaP-Enza-B was obtained through long-term propagation of the parental VCaP cell line (RRID:CVCL_2235, a kind gift from Dr. Pienta, Baltimore, Maryland, USA) in RPMI (cat. no. BE12-167F, Lonza, Basel, Switzerland) supplemented with 10% FCS and 10 µM enzalutamide (cat. no 1613, Axon Medchem, Groningen, the Netherlands). Cell line authentication was performed by short tandem repeat analysis using the Promega PowerPlex 16 kit and compared to the parental cell lines. Absence of mycoplasma contamination was assessed regularly (MycoAlert kit, cat. no. LT07-318, Lonza). For cell viability assays, PC346C-DCC-K and VCaP-Enza-B cells were plated at a cell density of $5*10^3$ cells per well in 100 µl medium. VCaP-Enza-B cells were maintained in RPMI containing 10% steroid stripped (DCC) serum, while PC346C-DCC-K cells were maintained in PGM-DCC medium.[7,8] The following day, cells were exposed to a dose-range of cabazitaxel (0-10 nM, Sanofi-Aventis, Paris, France), enzalutamide or the combination of cabazitaxel with 1 µM enzalutamide in the presence of 0·1 nM R1881 (cat. no. D5027, Sigma-Aldrich, Saint-Louis, MO). After 7 (VCaP-Enza-B) or 10 days (PC346C-DCC-K), cell viability was measured by the MTT assay (cat. no. M2128, Sigma-Aldrich) as described previously, and normalized to vehicle control.[8] Characterization of the newly acquired VCaP-Enza-B cell line was performed by examining the RNA and protein expression of the AR, AR-V7 and several AR target genes. In short, RNA was isolated using the RNeasy mini kit (#74104, Qiagen) and qRT-PCR was performed as described previously.[5] Gene-expression of the following targets was assessed using TaqMan assays; *AR*, *AR-V7*, *KLK3* (PSA) (using custom assays), *FKBP5* and *TMPRSS2* (using commercial kits Hs01561006 and Hs01120965 respectively, ThermoFisher Scientific). PBGD and HPRT1 were measured by SYBER Green assay (SensiMix Syber Lo-ROX). The custom TaqMan assays and primer sequences used for SYBER Green have been described previously.[5,9] For protein expression, 20 µg protein lysate was used for immunoblotting and blots incubated with the following primary antibodies; rabbit-anti-AR binding targeting the N-terminal domain (Sp107, #200R-14, Cell Marque at 1:2000), anti-PSA (#A0562, Dako Agilent at 1:1000) and anti-β-actin used as loading control (#A1978, Sigma-Aldrich, RRID:AB_476692 at 1:10000).

Combining enzalutamide with cabazitaxel in vivo

Fifty-two, six weeks old, NMRI nu/nu male mice (Janvier, Le Genest Saint Isle, France) were subcutaneously inoculated with $5*10^6$ PC346C-DCC-K cells. Tumor growth was observed after 2-5 weeks in ~80% of the mice. Once tumor size surpassed a volume of 150 mm^3, mice were stratified based on tumor size to receive daily oral enzalutamide treatment at 60 mg/kg or vehicle control (1% carboxymethylcellulosesodium salt, cat. no. C4888, Sigma-Aldrich with 0.1% Tween 80, cat. no. P1754, Sigma-Aldrich). Once tumors surpassed 300 mm^3 in size, mice were again stratified based on tumor volume to receive a single intraperitoneal administration of 33 mg/kg cabazitaxel or placebo control (NaCl). Overall we had four treatment groups with 9-12 mice each, cabazitaxel and enzalutamide mono-treatment, the combination treatment and placebo control. Tumor volume was monitored every 3-4 days by calipers and mice were followed until tumors exceeded a volume of 1500 mm^3, or a maximum follow up of 60 days after cabazitaxel treatment. Blood samples for PSA analysis were obtained at first tumor measurement, when mice were stratified to receive treatment and at the end of the experiment. For VCaP-Enza-B we performed a pilot study to assess tumorigenicity, response to enzalutamide and cabazitaxel treatment. Sixteen mice were inoculated with $5*10^6$ VCaP-Enza-B cells mixed with 100 µl Matrigel (cat. no 356231, Corning, NY), tumor take was observed in all mice. Once tumors surpassed 150 mm^3, mice were stratified based on tumor volume to receive daily enzalutamide treatment (60 mg/kg) or vehicle control for a period of 14 days. Impact of enzalutamide treatment on tumor growth during treatment was assessed using the log-cell kill method.[10] After completing treatment with enzalutamide or placebo control, we exposed nine mice to cabazitaxel for dose optimization. Four mice received an intravenous administration of 33 mg/kg cabazitaxel, three mice received 16 mg/kg and two mice received 10 mg/kg. All mice were followed for at least two weeks to monitor tumor response. Subsequently we examined the enzalutamide with cabazitaxel treatment combination versus cabazitaxel alone. Twenty mice were inoculated with $3*10^6$ VCaP-Enza-B cells mixed with Matrigel, tumor take was observed in 19 out of 20 mice. Once tumors surpassed 150 mm^3, mice were stratified to receive daily enzalutamide (60 mg/kg) treatment or vehicle control, then all mice received a single intravenous administration of cabazitaxel at tumor volume 750 mm^3 at 10 mg/kg. Histology of the VCaP-Enza-B tumors and expression of the AR and cell cycle marker Ki67 were subsequently investigated by immunohistochemistry as described previously.[6] Details regarding humane endpoints, general maintenance of the mice and statistical analysis have been described elsewhere.[6]

Animal Welfare

All animal experiments were approved by the Animal experiment committee under the Dutch experiments on Animal Act, with the reference number AVD101002017867. The current study is in compliance with the Arrive guidelines. Group size and experimental set-up were based on pilot experiments. All operations (tumor inoculation, blood sampling) were conducted under adequate anesthesia to minimize animal discomfort as described previously.[5] Subcutaneously growing tumors only cause mild discomfort.

RNA-sequencing of enzalutamide treated PC346C-DCC-K tumors

Twenty-one, six week old, NMRI nu/nu male mice were subcutaneously inoculated with PC346C-DCC-K cells. The experimental set-up was similar as described above with the following adaptations; mice were stratified to a 2:1 ratio to receive daily enzalutamide treatment or placebo control for seven days and were subsequently sacrificed and tumor xenografts snap-frozen. Total RNA was isolated from tumor xenografts as described previously.[6] Library Prep was performed using the NEBNext Ultra Directional RNA Kit for Illumina according to the protocol "NEBNext Ultra Directional RNA Library Prep Kit for Illumina" (NEB #E7420S/L). Briefly, mRNA was isolated from total RNA using the oligo-dT magnetic beads. After mRNA fragmentation, cDNA synthesis was performed and used for ligation with adapters and PCR amplification of the resulting product. The quality and yield after sample preparation was measured with the Fragment Analyser. One sample was re-sequenced due high frequency of multi-mapped reads implicating inadequate depletion of ribosomal RNA. Paired-end RNA-Seq data of enzalutamide PDX samples (N = 15) was analyzed using UCSC human genome build hg38 and GENCODE annotation release v26 (GRCh38.p10) and mouse genome build mm10 (reference strain C57BL/6J) with GENCODE annotation release M15 (GRCm38.p5) for downstream disambiguation of human/mouse data. FASTQC (v0.11.5)[11] was applied on the paired-end FASTQ files for quality control, both before and after running trimmomatic (v0.36),[12] which removed TrueSeq adapter sequences. STAR (v2.5.3a) was used as aligner, with 2-pass mapping for each sample separately. AstraZeneca's disambiguation algorithm (Python variant, 2013)[13] for reads aligned to two species has been used to assess the best alignments and disambiguate the BAM files. Mapping quality plot was generated and checked based on sambamba Flagstat (v0.6.7)[14] statistics. Count files, with the number of reads for each gene were created with subread FeatureCounts (v1.5.2)[15] on the disambiguated BAM files. R (version 3.4.3) was used for further statistical analyses and data visualization. Differential expression analysis was performed with condition 'enzalutamide treated' (N = 10) versus 'untreated' (N = 5) using the DESeq2 package (v1.18.1)[16] and the Wald-test. P values were adjusted using the Benjamini-Hochberg procedure.[17] Settings of different tools can be

seen in the supplementary data file. Gene set enrichment analysis (GSEA, v4.1.0) was performed using normalized gene expression values (count per million) of the individual tumor samples, with condition 'enzalutamide treated' versus 'untreated' and applied to the Molecular Signatures Database (MSigDB) hallmark gene set collection.[18]

Live cell imaging of cabazitaxel induced microtubule stabilization and apoptosis in PC346C-DCC-K cells

To study the impact of AR pathway inhibition on cellular response to cabazitaxel treatment, PC346C-DCC-K cells were engineered to overexpress enhanced yellow fluorescent protein (EYFP) labelled beta-tubulin (EYFP-β-Tubulin) and the human histone H2B gene fused to red fluorescent protein (H2B-RFP). The EYFP-β-Tubulin expression was used to monitor taxane target engagement and the histone marker for visualizing treatment induced perturbations of mitosis, proliferation and apoptosis. PC346C-DCC-K cells were first transduced to stably express H2B-RFP, selected based on RFP expression, transfected with EYFP-tubulin and again selected based on fluorescent expression of both markers. Large scale lentiviral production was performed by calcium phosphate transfection of Hek293T (RRID:CVCL_1926) cells with the LV-RFP construct expressing H2B-RFP, pMD2.G plasmid for the viral envelope and psPAX2 for packaging.[19] Viral supernatant was collected 24 and 48h after transfection and centrifuged at 3000g to remove cellular debris. The LV-RFP construct expressing H2B-RFP was kindly gifted by Elaine Fuchs (RRID:Addgene_26001, Addgene, Watertown, MA).[20] Viral supernatant was added to the PC346C-DCC-K cells, incubated overnight and the medium was refreshed the following day. Cells were passaged three times before selection and transfection with the second marker to ensure the viral particles were washed away. For transfection with the expressing EYFP-α-Tubulin plasmid (kindly provided by Dr. Galjart, Erasmus MC) we used Lipofectamin 2000 (cat. no. 11668030, Thermo Fisher Scientific, Waltham, Massachusetts, USA). Selection PC346C-DCC-K cells was performed by fluorescent activated cell sorting (FACS) using a BD FACS Aria III (BD Biosciences, Franklin Lakes, New Jersey, USA) equipped with 4 lasers and a 85 µm nozzle. mRFP1 fluorescence was detected using a 561 nm yellow-green laser and a 600 LP + 610/20 BP emission filters, similar to mCherry RFP. EYFP fluorescence was detected using a 488 nm blue laser and 502LP + 530/30 BP emission filters, similar to GFP. Dead cells were gated out by means of Hoechst 33258 fluorescence (Hoechst 33258, Sigma Aldrich). Doublets and multicellular clusters were gated out using forward and side scattering according to standard protocols: FSC-W/FSC-A gate, followed by SSC-W/SSC-A gate, verified on FSC-A vs FSC-H gate. Sorting purity, viability, and absence of doublets was verified after sorting, by re-analysis of sorted cells. Cell viability and response to taxane treatment was compared to the parental PC346C-DCC-K, using the MTT assays as described above. No significant impact of the expression of H2B-RFP and EYFP-β-Tubulin

on taxane sensitivity was found. For live cell imaging, $1*10^4$ PC346C-DCC-K cells co-expressing H2B-RFP and EYFP-β-tubulin were plated with 100 µl PGM-DCC medium in a 96-wells Cell Carrier Ultra plates suited for live cell imaging (cat. no. 6055302, PerkinElmer, Hamburg, Germany). Cells were incubated for 72 hours to ensure optimal attachment and cell spreading. One hour before imaging cells were pre-treated with 1 µM enzalutamide and/or 0.1 nM R1881. After imaging an initial pre-treatment time point (t-1), cells were exposed to 3 nM cabazitaxel and image acquisition was continued for 100 hours with an interval of 150 minutes. During intervals, the cells were stored in an integrated cell culture incubator to optimize cell viability. Sixteen images covering 103714 μm^2 (containing minimally 1000 cells at the start of the experiment) were acquired using an Opera Phenix spinning-disk confocal high-content screening system (PerkinElmer), equipped with a 40x water immersion object and a 16 bit sCMOS 4 Megapixel camera. EYFP-β-tubulin and H2B-RFP were sequentially excited with 488 nm and 561 nm solid state laser lines, detected at 500-550 nm and 570-630 nm wavelength ranges, respectively. Both analyses, apoptosis induction and microtubule stabilization, were performed using custom image analysis protocols in the Harmony analysis software (version 4.9, Perkin Elmer). First, total area covered by cells was selected using the EYFP-β-tubulin signal. The level of microtubule stabilization was determined in the total area covered by EYFP-β-tubulin expressing cells, using the Haralick Contrast parameter.[21,22] To quantify apoptosis, fragmented nuclei of cells expressing RFP-H2B were detected as spots and clustered by a maximum distance of 5 µm to be assigned to individual apoptotic cells and expressed as percentage to total nuclei.

Role of the funding source

This study was financially supported by an unrestricted grant by Sanofi, however Sanofi was not involved in the design and interpretation of this study.

Results

Enzalutamide improves cabazitaxel activity in a model of CRPC

The impact of enzalutamide on cabazitaxel activity was first evaluated in an *in vitro* setting. We used the AR expressing CRPC cell line PC346C-DCC-K, for which we previously reported an interaction between AR signaling and taxane resistance.[6] PC346C-DCC-K harbors intrinsic taxane resistance, as the maximum response to cabazitaxel plateaued at <50% reduction in cell viability (Figure 1a). The addition of 1 μM enzalutamide to the cabazitaxel dose range consistently reduced cell viability by ~25% compared to cabazitaxel monotherapy (P<0.0001; IC50 0.32 nM cabazitaxel). In line with the *in vitro* results, cabazitaxel was found to be only temporarily effective *in vivo* with 11 out of 12 mice showing initial regression of PC346C-DCC-K tumors followed by rapid outgrowth (Figure 1b, blue data points). The combination treatment of enzalutamide and cabazitaxel was able to induce a complete tumor regression in 4/12 mice and substantially delayed the onset of progression in the remaining mice (Figure 1b, orange data points). Of note, the addition of enzalutamide did not result in greater toxicity, as bodyweight loss following cabazitaxel administration was comparable in mice receiving the combination or mono-treatment (Supplementary figure 1a). Overall, combining enzalutamide with cabazitaxel significantly improved tumor response compared to cabazitaxel monotherapy, with median time to humane endpoint 77 days and 48 days respectively (P<0.0001, Supplementary figure 1b). Although the combination treatment greatly impacted tumor response, enzalutamide monotherapy was found to be ineffective (Figure 1c, supplementary figure 1b log-rank test P=0.17). However, enzalutamide treatment in PC346C-DCC-K tumor bearing mice did reduce PSA plasma levels, suggesting effective inhibition of the AR pathway (Figure 1d, P<0.001).

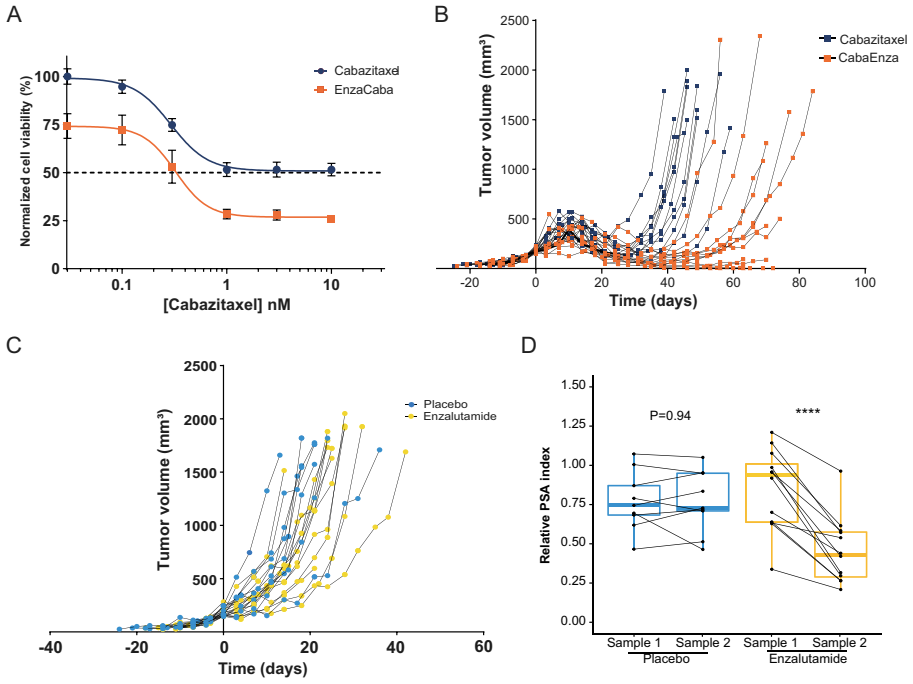

Figure 1: Combined treatment efficacy of enzalutamide and cabazitaxel towards a model of AR positive castrate resistant prostate cancer. A) Efficacy of cabazitaxel mono-therapy or combined with enzalutamide, towards an AR positive CRPC cell line. Cell viability was assessed by exposing PC346C-DCC-K cells to a dose range of cabazitaxel (blue) alone or with the addition of 1 µM enzalutamide (orange) for 10 days. Shown is the median cell viability of three individual experiments normalized to vehicle controls, error bars display standard error of the mean (SEM) and non-linear regression analysis was used to compare and calculate IC50 values (cabazitaxel IC50 not reached, enzalutamide with cabazitaxel IC50 0.33 nM, P<0.0001). **B-C)** Antitumor efficacy of cabazitaxel, enzalutamide and the treatment combination *in vivo*. Shown are individual tumor growth curves of the PC346C-DCC-K model. On day 0 tumors surpassed a volume of 150 mm^3 and mice were stratified based on tumor volume to receive either daily enzalutamide treatment or placebo control. Once tumors doubled in size, mice were again stratified to either receive a single dose of cabazitaxel treatment (b) or placebo control (c). Mice were followed until tumors surpassed 1500 mm^3 in size or a maximum follow-up of 60 days after cabazitaxel treatment. One mouse in the cabazitaxel mono-treatment group was excluded due to bodyweight loss and abnormal behavior which, was unrelated to treatment. **D)** Impact of enzalutamide treatment (n=12) on PSA plasma levels as compared to placebo controls (n=9). Plasma was sampled when mice were stratified to receive daily enzalutamide treatment or vehicle control (Sample 1) and when mice were stratified to receive cabazitaxel or placebo control (Sample 2). Relative PSA index was calculated by dividing PSA levels by tumor volumes at time of sampling. Matched samples are connected by a line, boxplots represent the median values with 25th and 75th percentile and hinges span the 1.5 interquartile range.

Adding enzalutamide to cabazitaxel improves overall activity even in an enzalutamide resistant model

Given the impact of the treatment combination, even in anti-androgen resistant setting, we selected an enzalutamide resistant VCaP sub line for validation studies. VCaP-Enza-B maintains AR signaling activity under high dose enzalutamide treatment (Figure 2A, supplementary figure 2). In contrast to PC346C-DCC-K, VCaP-Enza-B displayed high taxane sensitivity, as 1 nM of cabazitaxel reduced cell viability by 90% (Figure 2B). Nevertheless, adding enzalutamide to cabazitaxel further reduced cell viability as we identified a significant IC50 shift from 0.24 nM for cabazitaxel to 0.11 nM for the combination ($P<0.0001$). For subsequent *in vivo* studies, we first confirmed enzalutamide resistance of VCaP-Enza-B and optimized cabazitaxel dosing (Supplementary figure 3A-C). Low dose cabazitaxel treatment was found to induce a partial tumor response, thus creating a therapeutic window to study the addition of enzalutamide. Combining enzalutamide with cabazitaxel treatment improved overall activity compared to cabazitaxel monotherapy with median time to humane endpoint 80 and 53 days respectively ($P<0.001$, Figure 2C and supplementary figure 3D). Similar to PC346C-DCC-K, enzalutamide treatment reduced plasma PSA levels in VCaP-Enza-B tumor bearing mice while having no impact on tumor growth (Figure 2D). Overall, we conclude that combining enzalutamide and cabazitaxel treatment showed superior anti-tumor efficacy compared to cabazitaxel without targeting AR signaling.

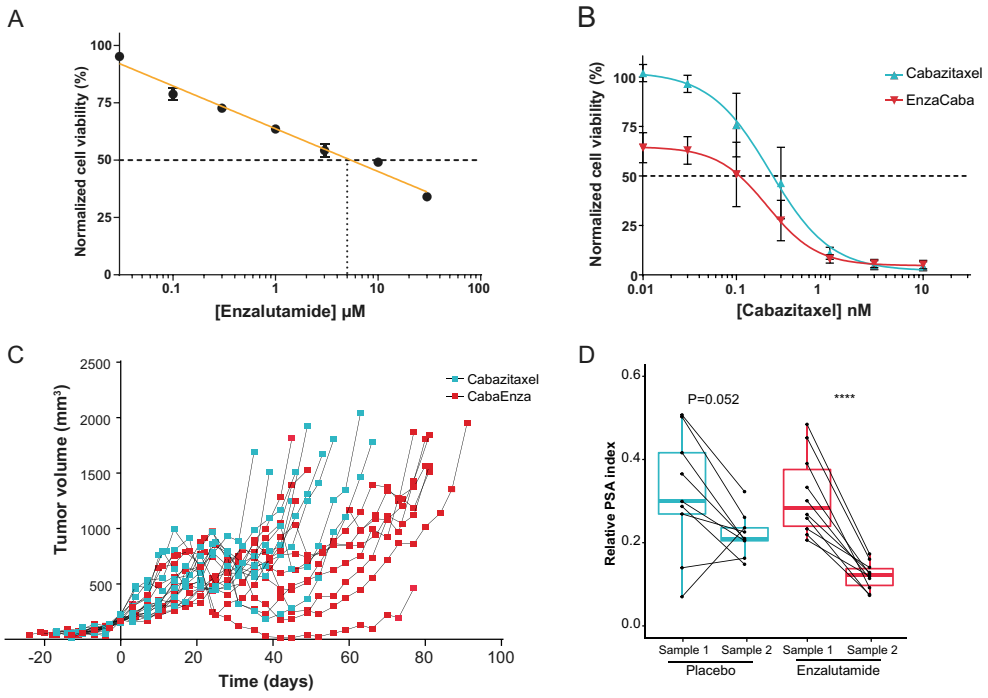

Figure 2: Combined treatment efficacy of enzalutamide and cabazitaxel towards an enzalutamide resistant prostate cancer model. A-B) Efficacy of enzalutamide, cabazitaxel and the combination with enzalutamide *in vitro* using an AR positive enzalutamide resistant cell line. Cell viability was assessed by exposing VCaP-Enza-B cells to a dose range of enzalutamide (A), cabazitaxel (turquoise, B) alone or with the addition of 1 µM enzalutamide (red, B) for 7 days. Shown is the median cell viability of three individual experiments normalized to vehicle controls, error bars display standard error of the mean (SEM) and non-linear regression analysis was used to compare and calculate IC50 values (cabazitaxel IC50 0.24, enzalutamide with cabazitaxel IC50 0.11 nM, P<0.0001). Efficacy of enzalutamide was calculated using linear regression analysis (IC50 5.4 µM). **C)** Antitumor efficacy of cabazitaxel and the treatment combination *in vivo*. Shown are individual tumor growth curves of the VCaP-Enza-B model. On day 0 tumors surpassed a volume of 150 mm^3 and mice were stratified based on tumor volume to receive either daily enzalutamide treatment or placebo control. Once tumors surpassed a volume of 750 mm^3 mice were received a single dose of cabazitaxel treatment. Mice were followed until tumors surpassed 1500 mm^3 in size or a maximum follow-up of 60 days after cabazitaxel treatment. **D)** Impact of enzalutamide treatment (n=10) on PSA plasma levels as compared to placebo controls (n=9). Plasma was sampled when mice were stratified to receive daily enzalutamide treatment or vehicle control (Sample 1) and when mice received cabazitaxel (Sample 2). Relative PSA index was calculated by dividing PSA levels by tumor volumes at time of sampling. Matched samples are connected by a line, boxplots represent the median values with 25th and 75th percentile and hinges span the 1.5 interquartile range.

Enzalutamide effectively suppresses AR signaling even in a treatment resistant model

To confirm active inhibition of AR signaling by enzalutamide treatment and to identify potential compensatory growth mechanisms, we investigated differential gene expression in short-term enzalutamide treated PC346C-DCC-K tumors. Although tumor growth of PC346C-DCC-K was unaffected, enzalutamide treatment significantly altered the expression of over 1,900 genes (supplementary data file). Principle component analysis of gene expression data clearly separated tumors obtained from enzalutamide treated from placebo control mice (Figure 3A). Subsequent gene set enrichment analysis (GSEA) identified 'Androgen response' as the most significantly altered gene-set with a normalized enrichment score of -1.74 and a false discovery rate of 0.09 (Figure 3B). Interestingly several metabolic pathways, including fatty acid metabolism, were significantly repressed by enzalutamide treatment (Figure 3C). GSEA did not identify any significantly upregulated gene-sets that could reflect compensatory growth mechanisms as a result of enzalutamide treatment (Supplementary figure 4). Overall, RNA-sequencing confirmed that enzalutamide treatment repressed AR signaling in PC346C-DCC-K tumors.

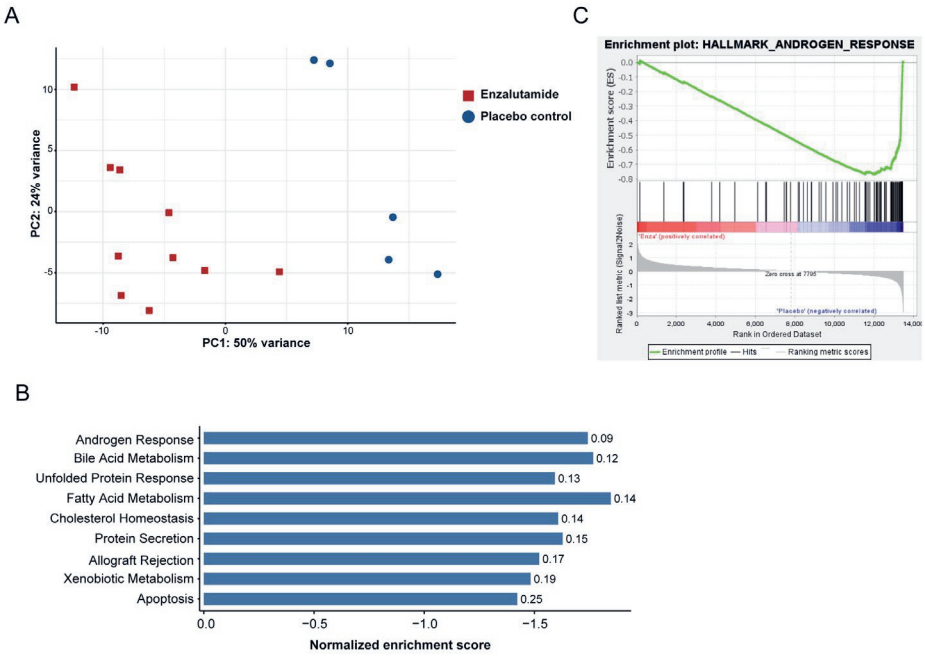

Figure 3: Differential gene expression inferred by enzalutamide treatment in PC346C-DCC-K. A) Principle component analysis of mRNA expression in PC346C-DCC-K tumors obtained from enzalutamide treated (n=10) and placebo control mice (n=5). Mice were treated for seven days by daily administration of enzalutamide or vehicle control upon which tumors were isolated and used for RNA-sequencing. **B-C)** Gene set enrichment analysis (GSEA) of differential gene expression caused by enzalutamide treatment in PC36C-DCC-K tumors using the 'hallmark collection'. **B)** Overview of significantly enriched gene-sets caused by enzalutamide treatment. Significantly enriched gene-sets were selected based on P value (<0.05) and false discovery rate (FDR <0.25). Y-axis displays the normalized enrichment scores for the individual gene-sets, negative values infer pathway inhibition. Gene-sets are ranked based on lowest FDR, thus highest confidence level. **C)** GSEA plot for the hallmark gene-set 'Androgen signaling'.

Targeting AR signaling enhances cabazitaxel induces apoptosis

To further unravel the impact of either inhibiting or stimulating AR signaling on cabazitaxel activity we used live-cell imaging. PC346C-DCC-K cells were transfected to dually express fluorescently labelled H2B and β-tubulin, a histone marker used to track mitosis and to monitor taxane induced tubulin stabilization, respectively. After cabazitaxel exposure (3 nM) we observed rapid formation of tubulin bundles with high fluorescent intensity, indicative of taxane induced tubulin stabilization (Figure 4A, second column). As expected, tubulin stabilization induced abnormal and prolonged mitosis, which led to mitotic slippage and multinucleated cells (Figure 4A, third column). In androgen supplemented conditions (R1881), apoptosis was rarely observed during the treatment span of 100h. Within the first 48h, we did not observe a substantial impact of either castrate (minus R1881) or enzalutamide treated conditions on cabazitaxel activity. However, subsequent cell divisions more frequently resulted in apoptosis in androgen suppressed conditions. To validate these observations we used image-based quantification of proliferation, apoptosis and tubulin stabilization. Indeed, cabazitaxel treatment induced rapid tubulin stabilization as identified by Haralick contrast (Figure 4B). Proliferation was effectively suppressed by cabazitaxel treatment, although androgen stimulation induced a small but significant increase (Figure 4C, $P<0{\cdot}0001$). The low percentage of fragmented nuclei as a consequence of apoptosis confirmed our observation of cabazitaxel resistance in androgen supplemented conditions (Figure 4D). Either castrate culture conditions or the addition of enzalutamide increased the percentage of cabazitaxel induced apoptotic cells by 1.5-2% ($P<0{\cdot}001$).

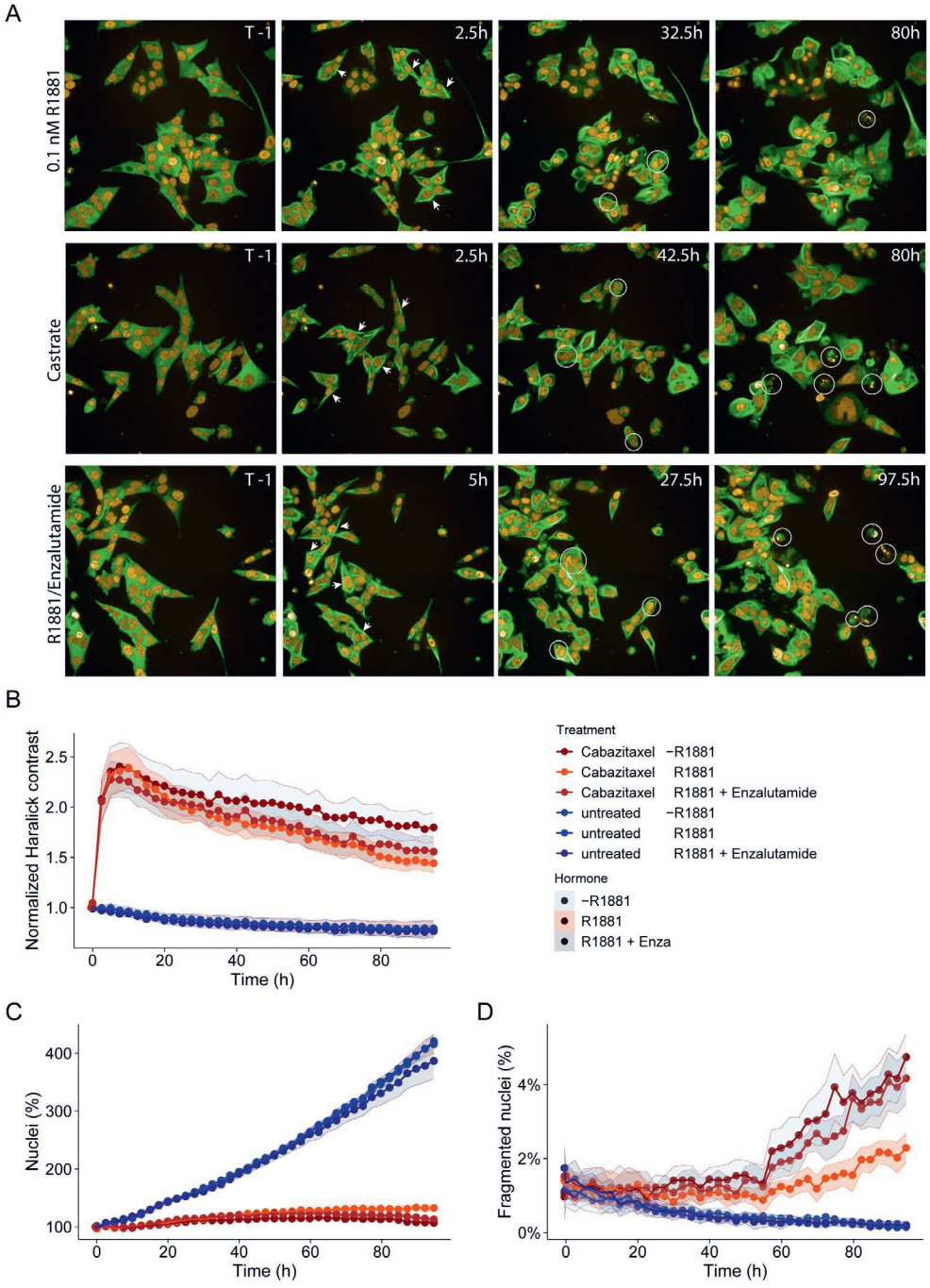

Legend on the next page

Figure 4: Impact of AR pathway manipulation on cabazitaxel treatment efficacy as studied by live-cell imaging. a) Representative images of PC346C-DCC-K cells expressing EYFP-β-tubulin (green) and H2B-RFP (orange) treated with 3 nM cabazitaxel. The rows represent the different androgen conditions, in the top row culture media was supplemented with 0.1 nM of the synthetic androgen R1881, panels in the middle show cells in castrate culture conditions and lowest show enzalutamide treatment(1 μM) in the presence of R1881. The first column depicts images obtained before addition of cabazitaxel while the second column shows images obtained during the first or second interval after taxane treatment. The arrows highlight tubulin structures as a result of cabazitaxel treatment. The third column shows cells treated with cabazitaxel for 24-48h, in which multinucleated cells are circled. The fourth column displays images obtained four days after initiating treatment and highlights fragmented cells, which point to treatment induced apoptosis. Scale bars represent 50 μm in size. **B-D)** Results of image based quantification of normalized Haralick contrast **(B)**, nuclear count **(C)** and percentage fragmented cells **(D)**. Shown are the results of four individual experiments performed in triplicate, data points represent median values with SEM displayed as a band. Haralick contrast measures pixel to pixel differences in fluorescent intensities and was applied to inspect tubulin structures. Normalization to Haralick contrast levels in pre-treatment images was performed. The slow reduction in Haralick contrast over time is most likely a result of monitor bleaching. Nuclear count was used to monitor proliferation and normalized to numbers in pre-treatment images. Fragmented cells were quantified and normalized to nuclear count for each individual time point to calculate the percentage apoptotic cells.

Discussion

The present study explored whether cabazitaxel treatment efficacy could be enhanced by targeting AR signaling. We showed that adding enzalutamide to cabazitaxel inferred greater anti-tumor activity, compared to both single treatments. Importantly, the combination treatment was found to remain active in patient-derived xenograft models of enzalutamide resistant CRPC where AR signaling could still be effectively blocked by enzalutamide treatment. Moreover, targeting AR signaling increased the rate of cabazitaxel induced apoptosis. Overall, our study shows that cabazitaxel efficacy is directly affected by AR signaling which paves the way for promising combination treatments in CRPC.

Taxane chemotherapeutics exert their function by targeting the β-tubulin subunit of the tubulin polymer, which forms the microtubule network, and induces stabilization. During mitosis, taxane treatment interferes with chromatid separation and eventually leads to cell cycle stalling in the G2/M phase. Arrest in mitosis can directly induce cell death by mitotic catastrophe, although cancer cell lines have shown to display variable response to taxane treatment.[23] Live-cell imaging revealed that in taxane resistant cells, cabazitaxel treatment effectively induces cell cycle stalling, mitotic slippage and multinucleation although this rarely triggers mitotic cell death. Adding enzalutamide did further suppress proliferation and increased the percentage of fragmented cells, but only after 48h of taxane treatment. Blocking the AR pathway therefore likely decreases cell viability after the first abnormal cell cycle. Of note, the impact of enzalutamide co-administration increased the percentage of apoptotic cells by only 1.5-2%. However, we expect that over time, the accumulation of apoptotic cells would significantly contribute to therapeutic efficacy.

Sustained AR signaling plays a major role in CRPC, as exemplified by the frequency of genetic aberrations and splice-variant expression driving resistance to AR signaling targeted treatment.[3,24] The current study, together with our previous reports, implicates a major role for AR signaling in taxane treatment efficacy.[5,6] The underlying mechanisms resulting in greater cabazitaxel sensitivity in enzalutamide treated PCa cell remains to be clarified, although several metabolic pathways were significantly impacted by enzalutamide treatment. Potentially, multinucleated cells may become sensitive to enzalutamide induced suppression of metabolic activity and are more likely to trigger apoptosis. Clearly further investigation is warranted.

A preclinical study by Martin et al., also reported an added benefit of combining cabazitaxel with AR signaling targeted treatment in AR positive PCa models.[25] The authors concluded that adding enzalutamide to cabazitaxel was effective in hormone sensitive PCa but not in CRPC cell lines. Moreover, the addition of enzalutamide to cabazitaxel did not significantly

decrease the tumor mass of 22Rv1 xenografts. However, activity of the combination treatment was assessed using a different dosing schedule and based on a single tumor measurement obtained four days after completing the cabazitaxel treatment. In our *in vivo* experiments, the greatest impact of the combination treatment was on long-term suppression of tumor-growth after cabazitaxel treatment. Martin et al. did identify an impact of the combination treatment on the frequency of proliferating and apoptotic cells upon inspection of the 22Rv1 tumors. Overall, we argue that a premature endpoint potentially compromised the assessment of the combination treatment.

The addition of enzalutamide to cabazitaxel has been investigated in a phase I clinical trial performed at our institute.[26] Enzalutamide is a known CYP3A4 inducer and could impact on cabazitaxel exposure through increased clearance. Indeed, concomitant enzalutamide treatment was found to reduce cabazitaxel plasma levels by 22%. We have previously shown that adequate taxane exposure is key for optimal anti-tumor activity.[27] However, in the clinical study two cycles of the combination treatment was still found to induce a >50% PSA reduction in 8/13 CRPC patients.[26] This suggests that combining enzalutamide with cabazitaxel is an effective treatment, despite the moderately decreased systemic cabazitaxel exposure. Moreover, our current preclinical data suggest that patients who are no longer responsive to enzalutamide treatment, could benefit from combining enzalutamide with cabazitaxel. Several ongoing phase II/III clinical trials investigate the feasibility of combining AR signaling targeted agents with taxane chemotherapeutics for advanced PCa.[28] With the treatment landscape of mPCa moving towards effective combination strategies, adding AR signaling targeted inhibitors to taxane chemotherapeutics provides a promising strategy for CRPC patients.

Acknowledgements

The authors would like to thank Andrea Sachetti for providing support in flow cytometry and Wendy Wisse-van Dam for providing support in the acquisition and analysis of the VCaP-Enza-B cell line.

Funding

This study was financially supported by an unrestricted grant by Sanofi, however Sanofi was not involved in the design and interpretation of this study.

References

1. Visakorpi T, Hyytinen E, Koivisto P, Tanner M, Keinanen R, Palmberg C, et al. In vivo amplification of the androgen receptor gene and progression of human prostate cancer. Nat Genet. 1995;9(4):401-6.
2. Tilley WD, Buchanan G, Hickey TE, Bentel JM. Mutations in the androgen receptor gene are associated with progression of human prostate cancer to androgen independence. Clin Cancer Res. 1996;2(2):277-85.
3. van Dessel LF, van Riet J, Smits M, Zhu Y, Hamberg P, van der Heijden MS, et al. The genomic landscape of metastatic castration-resistant prostate cancers reveals multiple distinct genotypes with potential clinical impact. Nature Communications. 2019;10(1):5251.
4. Quigley DA, Dang HX, Zhao SG, Lloyd P, Aggarwal R, Alumkal JJ, et al. Genomic Hallmarks and Structural Variation in Metastatic Prostate Cancer. Cell. 2018;174(3):758-69 e9.
5. Mout L, de Wit R, Stuurman D, Verhoef E, Mathijssen R, de Ridder C, et al. Testosterone Diminishes Cabazitaxel Efficacy and Intratumoral Accumulation in a Prostate Cancer Xenograft Model. EBioMedicine. 2018;27:182-6.
6. Mout L, Moll JM, Chen M, de Morree ES, de Ridder CMA, Gibson A, et al. Androgen receptor signalling impairs docetaxel efficacy in castration-resistant prostate cancer. Br J Cancer. 2020.
7. Marques RB, van Weerden WM, Erkens-Schulze S, de Ridder CM, Bangma CH, Trapman J, et al. The human PC346 xenograft and cell line panel: a model system for prostate cancer progression. Eur Urol. 2006;49(2):245-57.
8. Marques RB, Erkens-Schulze S, de Ridder CM, Hermans KG, Waltering K, Visakorpi T, et al. Androgen receptor modifications in prostate cancer cells upon long-termandrogen ablation and antiandrogen treatment. Int J Cancer. 2005;117(2):221-9.
9. Marques RB, Aghai A, de Ridder CMA, Stuurman D, Hoeben S, Boer A, et al. High Efficacy of Combination Therapy Using PI3K/AKT Inhibitors with Androgen Deprivation in Prostate Cancer Preclinical Models. Eur Urol. 2015;67(6):1177-85.
10. Corbett TH, White K, Polin L, Kushner J, Paluch J, Shih C, et al. Discovery and Preclinical Antitumor Efficacy Evaluations of LY32262 and LY33169. Investigational New Drugs. 2003;21(1):33-45.
11. Schmieder R, Edwards R. Quality control and preprocessing of metagenomic datasets. Bioinformatics. 2011;27(6):863-4.
12. Bolger AM, Lohse M, Usadel B. Trimmomatic: a flexible trimmer for Illumina sequence data. Bioinformatics. 2014;30(15):2114-20.
13. Ahdesmaki MJ, Gray SR, Johnson JH, Lai Z. Disambiguate: An open-source application for disambiguating two species in next generation sequencing data from grafted samples. F1000Res. 2016;5:2741.
14. Tarasov A, Vilella AJ, Cuppen E, Nijman IJ, Prins P. Sambamba: fast processing of NGS alignment formats. Bioinformatics. 2015;31(12):2032-4.
15. Liao Y, Smyth GK, Shi W. featureCounts: an efficient general purpose program for assigning sequence reads to genomic features. Bioinformatics. 2014;30(7):923-30.
16. Love MI, Huber W, Anders S. Moderated estimation of fold change and dispersion for RNA-seq data with DESeq2. Genome Biol. 2014;15(12):550.
17. Benjamini Y, Hochberg Y. Controlling the False Discovery Rate - a Practical and Powerful Approach to Multiple Testing. J R Stat Soc B. 1995;57(1):289-300.
18. Liberzon A, Birger C, Thorvaldsdóttir H, Ghandi M, Mesirov JP, Tamayo P. The Molecular Signatures Database (MSigDB) hallmark gene set collection. Cell Syst. 2015;1(6):417-25.

19. Hermans KG, van der Korput HA, van Marion R, van de Wijngaart DJ, Ziel-van der Made A, Dits NF, et al. Truncated ETV1, Fused to Novel Tissue-Specific Genes, and Full-Length ETV1 in Prostate Cancer. Cancer Research. 2008;68(18):7541-9.
20. 20. Beronja S, Livshits G, Williams S, Fuchs E. Rapid functional dissection of genetic networks via tissue-specific transduction and RNAi in mouse embryos. Nat Med. 2010;16(7):821-7.
21. Berges N, Arens K, Kreusch V, Fischer R, Di Fiore S. Toward Discovery of Novel Microtubule Targeting Agents: A SNAP-tag-Based High-Content Screening Assay for the Analysis of Microtubule Dynamics and Cell Cycle Progression. SLAS Discov. 2017;22(4):387-98.
22. Haralick RM, Shanmugam K, Dinstein I. Textural Features for Image Classification. IEEE Transactions on Systems, Man, and Cybernetics. 1973;SMC-3(6):610-21.
23. Gascoigne KE, Taylor SS. Cancer cells display profound intra- and interline variation following prolonged exposure to antimitotic drugs. Cancer Cell. 2008;14(2):111-22.
24. Fraser M, Sabelnykova VY, Yamaguchi TN, Heisler LE, Livingstone J, Huang V, et al. Genomic hallmarks of localized, non-indolent prostate cancer. Nature. 2017;541(7637):359-64.
25. Martin SK, Pu H, Penticuff JC, Cao Z, Horbinski C, Kyprianou N. Multinucleation and Mesenchymal-to-Epithelial Transition Alleviate Resistance to Combined Cabazitaxel and Antiandrogen Therapy in Advanced Prostate Cancer. Cancer Res. 2016;76(4):912-26.
26. Belderbos BPS, Bins S, van Leeuwen RWF, Oomen-de Hoop E, van der Meer N, de Bruijn P, et al. Influence of Enzalutamide on Cabazitaxel Pharmacokinetics: a Drug-Drug Interaction Study in Metastatic Castration-resistant Prostate Cancer (mCRPC) Patients. Clin Cancer Res. 2018;24(3):541-6.
27. de Morree E, van Soest R, Aghai A, de Ridder C, de Bruijn P, Ghobadi Moghaddam-Helmantel I, et al. Understanding taxanes in prostate cancer; importance of intratumoral drug accumulation. Prostate. 2016;76(10):927-36.
28. Corn PG, Agarwal N, Araujo JC, Sonpavde G. Taxane-based Combination Therapies for Metastatic Prostate Cancer. Eur Urol Focus. 2019;5(3):369-80.

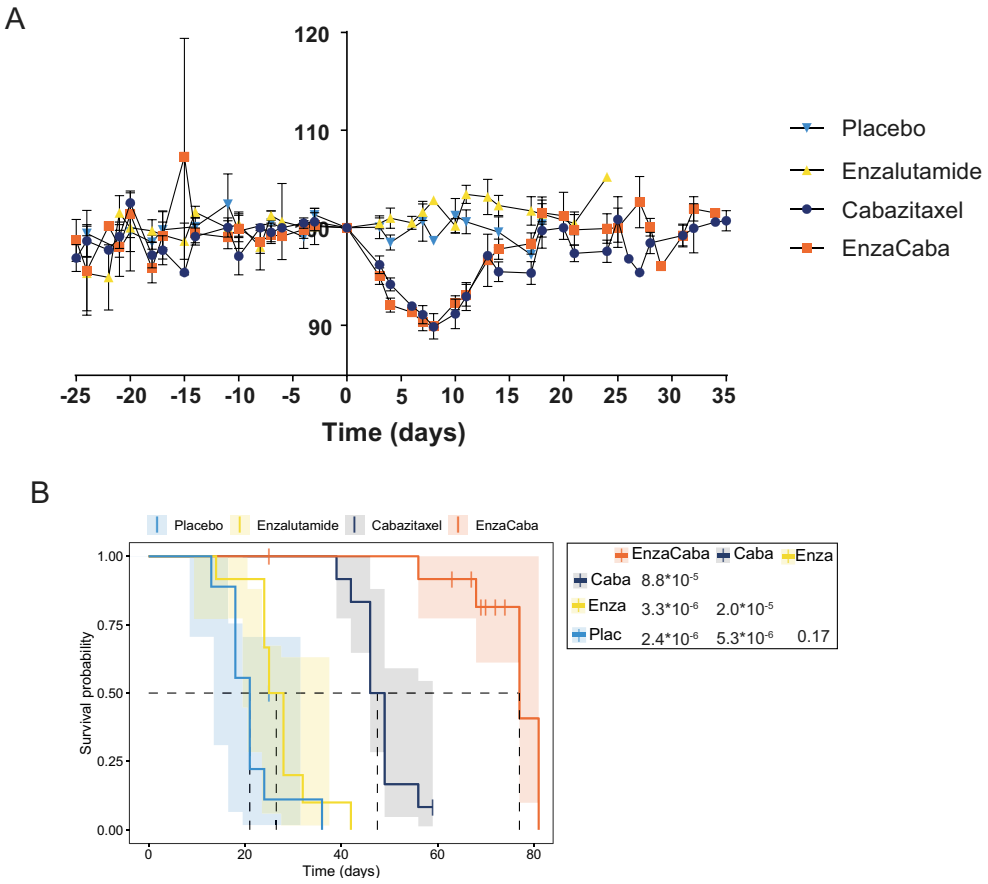

Supplementary figure 1: *In vivo* anti-tumor efficacy of the enzalutamide and cabazitaxel combination treatment towards the PC346C-DCC-K patient derived xenograft. A) Normalized bodyweights of tumor bearing mice receiving cabazitaxel (dark blue), enzalutamide (yellow) or combination treatment (orange) compared to placebo controls (light blue). Bodyweights of individual mice were normalized to weight on day 0, when mice were stratified to receive cabazitaxel treatment or placebo control. Displayed are the median normalized bodyweights (%) per treatment group with error bars showing standard error of the mean (SEM). Loss of bodyweight induced by cabazitaxel treatment did not surpass 20% which is used as a humane endpoint. **B)** Kaplan Meier curve displaying the cumulative survival for the four treatment groups placebo control (light blue), enzalutamide (yellow), cabazitaxel (dark blue) and the treatment combination (EnzaCaba, orange). Survival was calculated from the day mice were stratified to start enzalutamide treatment until tumors exceeded a volume of 1500 mm^3. Mice were censored when tumors did not reach 1500 mm^3 in size during the maximum follow-up of 60 days after cabazitaxel treatment. One mouse in the EnzaCaba treatment group was found dead two weeks after cabazitaxel treatment. Results from the pair-wise comparison, using the log-rank test with Bonferroni correction are shown in the table.

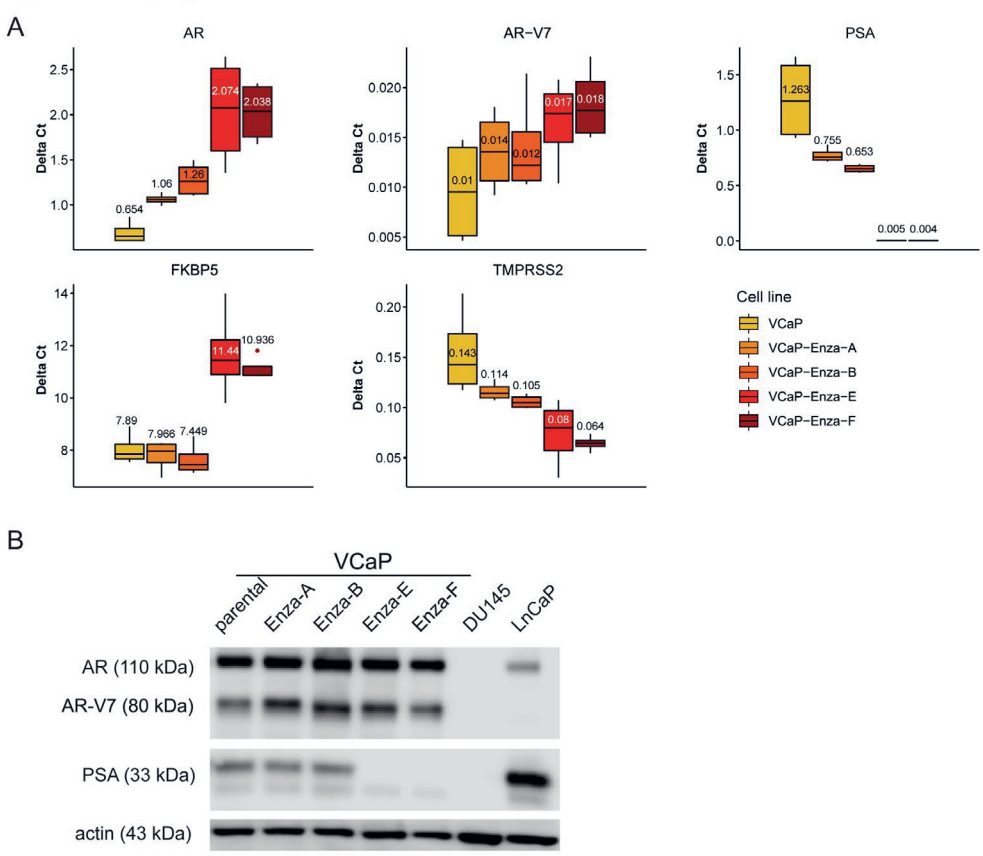

Supplementary figure 2: characterization of enzalutamide resistant VCaP cell lines. A) RNA expression of the androgen receptor (*AR*), AR-variant 7 (*AR-V7*) and the target genes *FKBP5*, *KLK3* and *TMPRSS2* in VCaP and its enzalutamide resistant cell lines as assessed by qRT-PCR. The hinges of the boxplots represent the 25th and 75th percentile with median expression and the whiskers represent 1.5x the interquartile range (IQR). For each gene two technical replicates were included and expression was normalized to two household genes using the $2^{-\Delta Ct}$ method. **B)** Protein expression of AR, AR-V7 and PSA in VCaP and its enzalutamide resistant cell lines as assessed by western blot. Protein lysate from the DU145 cell line was used as a negative control for AR, AR-V7 and PSA expression while LnCaP was used as a positive control for AR and PSA expression. Actin was used as a loading control.

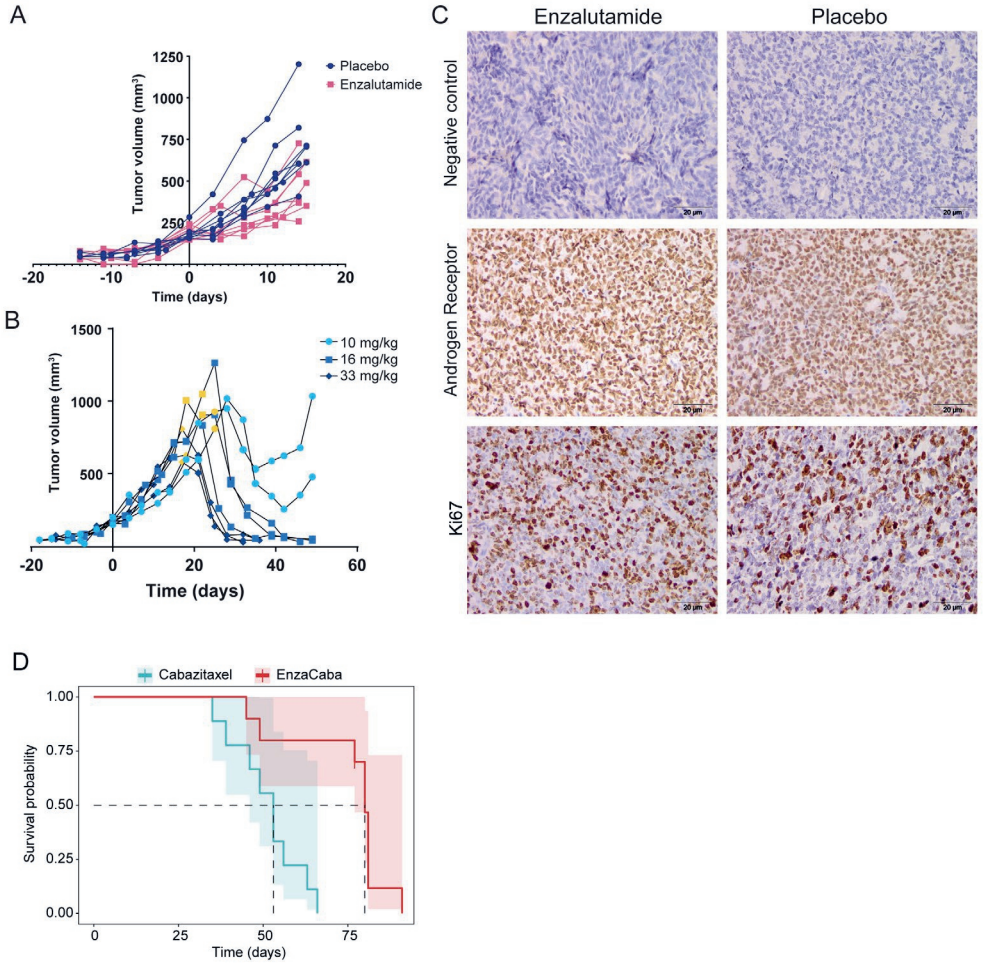

Supplementary figure 3: *In vivo* characterization and treatment sensitivity of VCaP-Enza-B. A) Enzalutamide resistance of the VCaP-Enza-B tumor model. Shown are individual tumor growth curves of mice receiving either daily enzalutamide treatment or placebo control for two weeks. Impact of enzalutamide treatment was assessed using the log-cell kill calculation (0.087), VCaP-Enza-B was confirmed as enzalutamide resistant (log-cell kill <0.7). **B)** Response of the VCaP-Enza-B tumor model to different cabazitaxel dosages. Subset of VCaP-Enza-B tumor bearing mice as displayed in A were subjected to either 10 mg/kg (N=2 light blue), 16 mg/kg (N=3, blue) or 33 mg/kg (N=4, dark blue) cabazitaxel treatment. Timing of cabazitaxel administration is highlighted in yellow. **C)** Histological assessment and immunohistochemical staining of the androgen receptor and Ki67 in VCaP-Enza-B tumors.

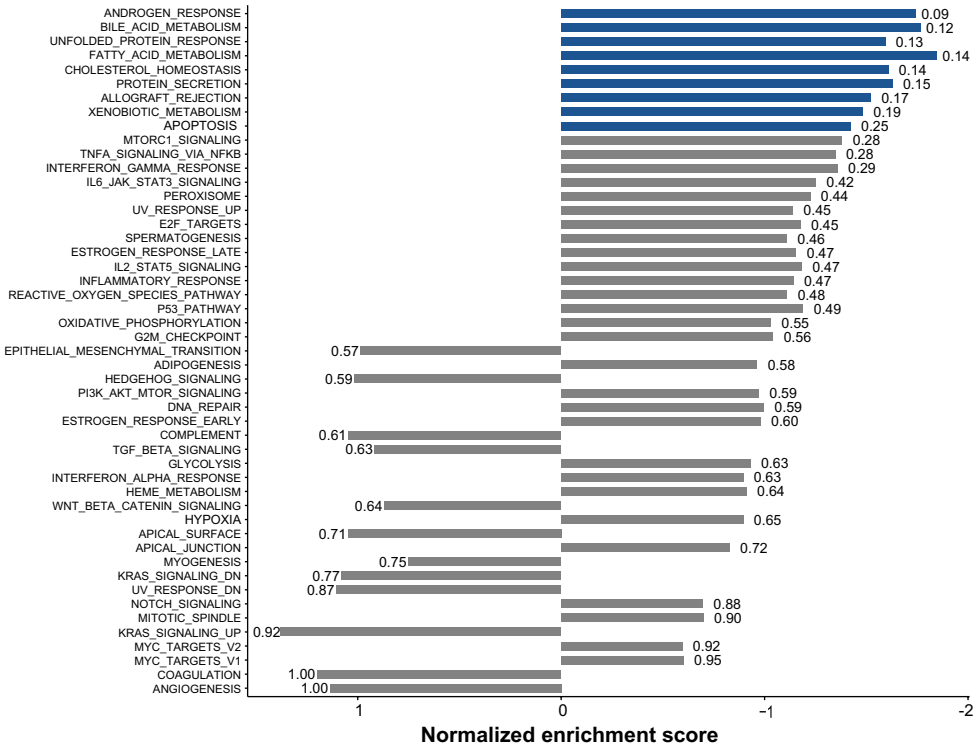

Supplementary figure 4: Gene set enrichment analysis of differential gene expression induced by enzalutamide treatment in PC346C-DCC-K tumors. Gene set enrichment analysis (GSEA) using the Hallmarks gene sets applied to differential gene expression induced by enzalutamide treatment in PC346C-DCC-K tumors. Shown is an overview of normalized enrichment scores (Y-axis) of the individual gene sets and the matching false discovery rate (FDR). Gene sets that meet the significance, with a FDR ≤0.25, are highlighted in blue.

Part II

CTC-Derived Organoids for Personalized Cancer Therapy

Chapter VI

Generating Human Prostate Cancer Organoids from Leukapheresis Enriched Circulating Tumor Cells

Lisanne Mout[1], Lisanne F. van Dessel[1], Jaco Kraan, Anouk C. de Jong, Rui P.L. Neves, Sigrun Erkens-Schulze, Corine M. Beaufort, Anieta M. Sieuwerts[†], Job van Riet, Thomas L.C. Woo, Ronald de Wit, Stefan Sleijfer, Paul Hamberg, Yorick Sandberg, Peter A.W. te Boekhorst, Harmen J.G. van de Werken, John W.M. Martens, Nikolas H. Stoecklein, Wytske M. van Weerden, Martijn P. Lolkema

manuscript accepted for publication,
European Journal of Cancer

Abstract

Background

Circulating tumor cell (CTC) derived organoids have the potential to provide a powerful tool for personalized cancer therapy, but are restrained by low CTC numbers provided by blood samples. Here, we used diagnostic leukapheresis (DLA) to enrich CTCs from metastatic prostate cancer (mPCa) patients and explored whether organoids provide a platform for *ex vivo* treatment modelling.

Methods

We prospectively screened 102 mPCa patients and performed DLA in 40 patients with ≥5 CTCs/7.5 mL blood. We enriched CTCs from DLA using white blood cell (WBC) depletion alone or combined with EpCAM selection. The enriched CTC samples were cultured in 3D to obtain organoids and used for downstream analyses.

Results

The DLA procedure resulted in a median yield of 5312 CTCs as compared to 22 CTCs in 7.5 mL of blood. Using WBC depletion, we recovered 46% of the CTCs, which reduced to 12% with subsequent EpCAM selection. From the isolated and enriched CTC samples, organoid expansion succeeded in 35%. Successful organoid cultures contained significantly higher CTC numbers at initiation. Moreover, we performed treatment modelling in one organoid cell line and identified substantial tumor heterogeneity in CTCs using single cell DNA sequencing.

Conclusions

DLA is an efficient method to enrich CTCs, although the modest success rate of culturing CTCs precludes large scale clinical application. Our data do suggest that DLA and subsequent processing provides a rich source of viable tumor cells. Therefore, DLA offers a promising alternative to biopsy procedures to obtain sufficient number of tumor cells to study sequential samples in mPCa patients.

Introduction

Translational studies on advanced prostate cancer (PCa) have often been limited to static sources, such as resection of the primary tumor or biopsies.[1-4] However, cancer is an ever moving target, as dynamic evolution drives spatial and temporal heterogeneity allowing tumors to adapt and escape therapeutic interventions. We therefore require new methods that provide real-time insights into evolving cancer biology for treatment tailoring. Circulating tumor cells (CTCs) could serve as a dynamic tumor source which captures the genetic and phenotypic heterogeneity of cancer and can be obtained at multiple time-points during the disease course to assess clinical progression.[5] Additionally, CTCs can be obtained from peripheral blood in a relatively non-invasive manner, thus providing an easily accessible source of metastatic cells as an alternative to tumor biopsies. This is particularly beneficial for patients with primarily bone metastasis such as in metastatic PCa (mPCa). In mPCa, CTC numbers have already been shown to harbor significant prognostic and predictive value.[6-10] The possibility to obtain viable CTCs also provides the opportunity to propagate CTCs *ex vivo*. The development of cancer organoids has allowed us to better capture the tumor-specific characteristics than standard 2D culture methods.[11] Together, this provides the opportunity to use CTC derived organoids as a representative model of the current disease status and use for drug discovery and sensitivity-screening.[12] PCa CTCs can be cultured as organoids, although the reports thus far suggest a very low efficiency rate for success.[13,14] Previous reports suggest that one important obstacle is the high number of CTCs needed to initiate organoid propagation.[13,15] Since the median CTC count in mPCa patients is 2-20 CTCs per 7.5 mL of blood[10], *ex vivo* expansion of CTCs is unlikely to be successful in most patients. Diagnostic leukapheresis (DLA) is a standardized procedure to enrich for mononuclear cells by continuous centrifugation of blood. Since CTCs have a similar density to mononuclear cells, they are enriched as well.[16] Importantly, DLA is a minimally-invasive and generally safe procedure, that is well tolerated by patients.[17] Within this prospective study we set out to isolate CTCs from mPCa patients by DLA. We hypothesized that the increased number of CTCs obtained by DLA, will allow us to culture CTC derived organoids and potentially provide a platform for individualized disease modelling. Using optimized methods we validated DLA as a feasible and safe method to enrich for CTCs in mPCa patients. CTCs could be propagated as short-term organoid cultures in 35% of the samples, from which we could obtain one stable organoid cell line. These short-term organoid cultures expressed the classical markers of PCa and maintained genomic variants previously identified in metastatic samples. Overall, our study provides an important step forward in implementing CTCs in individualized disease modelling, nevertheless identifies several challenges that require further optimization.

Material and methods

Patients with mPCa were included and selected based on the presence of ≥5 per 7.5 mL of blood. The study was conducted in accordance with the Declaration of Helsinki and was approved by the medical ethical committee of the Erasmus Medical Center Rotterdam (EMC16-449), full exclusion and inclusion criteria are described in the supplementary material and methods. DLA was performed using the standard settings, only the plasma pump rate was adjusted. CTCs from DLA were enriched by negative depletion of white blood cells using RosetteSep(tm) CTC Human CD45 Depletion Cocktail (STEMCELL Technologies, Vancouver, British Colombia, Canada), with or without subsequent manual positive immunomagnetic enrichment using CellSearch EpCAM ferrofluids. The enriched DLA samples were cultured under optimized conditions to obtain PCa organoids.

Patient and tumor characteristics	N = 37*
Age, years (median, range)	70 (49-83)
WHO status at registration	
0	12
1	23
2	2
Hormone status at time of inclusion	
HSPC	12
CRPC	25
Gleason score at diagnosis	
≤ 6	2
7	8
8	9
9-10	13
Missing	5
M-stage at diagnosis	
M0	5
M1	21
Mx	9
Missing	2
Type of prior therapy	
Local therapy (i.e. radical prostatectomy or RT on prostate)	16
ADT (i.e. chemical or surgical)	25
Chemotherapy	17
Hormonal therapy (other than ADT)	16
Radionucleotide therapy	8
Other	5
Diagnostic leukapheresis characteristics	
Total duration of DLA (minutes; median, range)	104 (25-925)
Total processed blood volume (mL; median, range)	5112 (1153-10001)
Volume of collected DLA product (mL; median, range)	96 (18-178)
Missing	3

Table 1: Patient characteristics. Baseline characteristics are shown for patients who were eligible for the diagnostic leukapheresis (DLA) procedure. Prior systemic treatments are only applicable to castration-resistant prostate cancer (CRPC) patients as concomitant androgen deprivation therapy (ADT) was an exclusion criteria for hormone-sensitive prostate cancer (HSPC) patients. In addition we show the duration, processed blood volume and collected volume of the DLA procedure. *Four patients underwent DLA twice.

Results

Patient characteristics and CTC screening

We screened 102 mPCa patients for eligibility and selected 45 patients who had ≥5 CTC in 7.5 mL of peripheral blood (PB) for CTC collection by DLA (Figure 1A). Metastatic castration resistant PCa (mCRPC) patients screened for study participation tended to have a higher CTC burden compared to the metastatic hormone sensitive PCa (mHSPC) patients (median of 5 CTC/7.5 mL vs 1 resp. P=0.07, supplementary figure 1A). Moreover, 50% of the mCRPC patients had 5 or more CTCs while 39% of the mHSPC patients were included. The overall median CTC count of the included patient population was 22 CTCs per 7.5 mL PB prior to DLA, with 10 CTCs/7.5 mL and 26 CTCs/7.5 mL for mHSPC and mCRPC patients resp. (Figure 1B). The CTC burden was monitored in 24 patients and was found to remain stable in between screening, prior to the DLA and after completion of the DLA procedure (P=0.37, supplementary figure 1B).

Diagnostic leukapheresis

After initial screening, a total of 40 patients successfully underwent DLA, as four patients withdrew and the DLA procedure was terminated in one patient because of an adverse event (grade 3 vasovagal reaction directly after start of the procedure). No other grade ≥3 adverse events were observed. The baseline characteristics of the patient population and DLA procedure are described in Table 1. Four patients were included twice at separate time points during their treatment course, resulting in serial samples for subjects 9, 11, 24 and 22 (annotated as e.g. 9-I/II). We examined the impact of DLA density settings on CTC enrichment in four patients, by performing the DLA procedure in two fractions of both 5L blood at 2% and 5% hematocrit respectively. As there was a trend towards higher CTC yield when DLA was performed at 5% hematocrit (Supplementary figure 1C, P=0.125), we continued the DLA procedure using high DLA density settings and processed 5L of total blood volume, which limited the procedure time to approximately 2 hours. The median CTC concentration of the DLA product was 64/mL compared to 2.5/mL in PB samples pre-DLA (P<0.001), with an estimated median yield of 5312 CTCs in 96 mL of DLA product (Figure 1C). Using these DLA settings, we were able to retrieve a median of 36% of the estimated CTCs available given the processed blood volume and the CTC count in PB (Supplementary figure 1D).

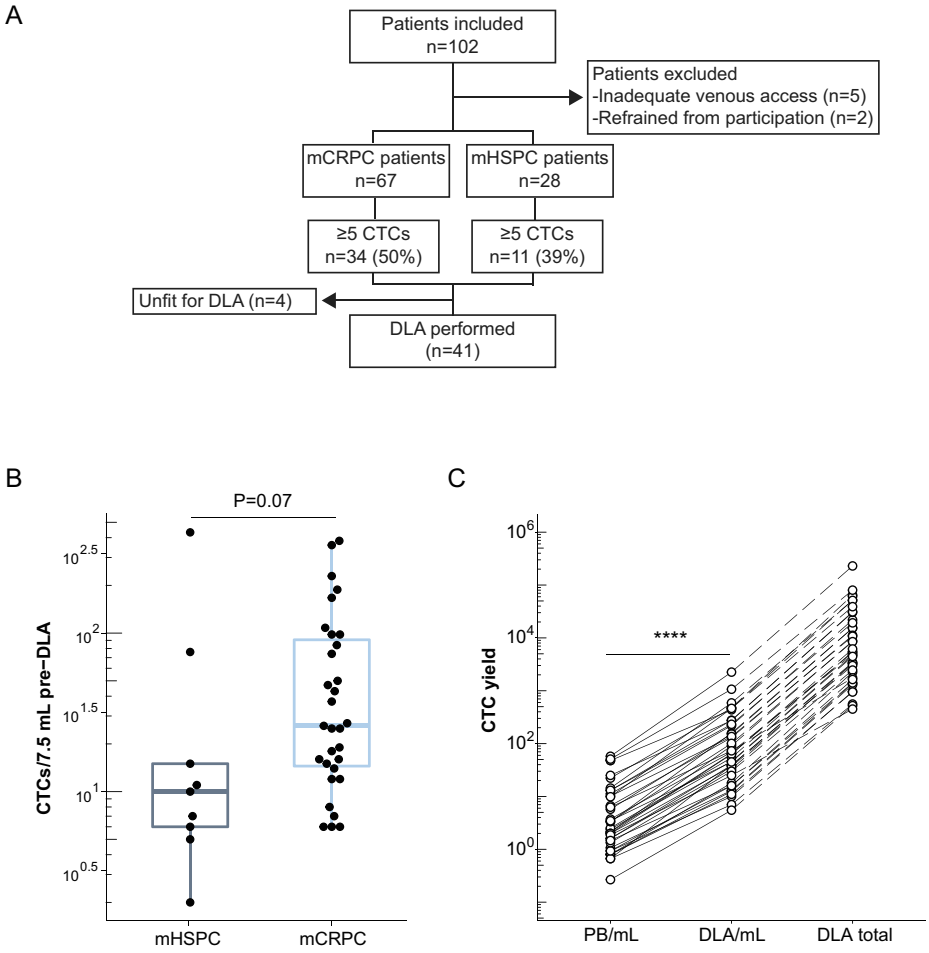

Figure 1: Overview of patient inclusion, diagnostic leukapheresis procedure and subsequent circulating tumor cell enrichment methods. A) Patients were eligible for diagnostic leukapheresis (DLA) if they had adequate venous access and ≥5 circulating tumor cells (CTCs). Two patients refrained from participation because of urge-incontinence and because of pain. Five patients were not screened for the presence of CTCs in peripheral blood due to inadequate venous access. After screening and inclusion four patients refrained from DLA because of progressive disease. **B)** CTC count in metastatic castration resistant (mCRPC, n=31) and hormone sensitive prostate cancer (mHSPC, n= 9) patients who succesfully underwent DLA. CTC burden was determined in 7.5 mL peripheral blood (PB) sampled before the start of DLA. Statistical comparison was performed using an unpaired two-sided Wilcoxon rank test P=0.07. **C)** Absolute CTC count in PB and DLA product. The X-axis shows CTC count per mL PB, per mL DLA product and extrapolated to total DLA volume. Each dot represents an individual subject (n=40) and for all subjects we show the results of the 5% RBC density setting in 5L processed blood volume. Samples from the same subject are connected by a (dashed) line. Y-axis is a logarithmic scale. Statistical comparison of CTC yield per mL DLA versus PB was performed by a paired two-sided Wilcoxon rank test P<0.0001.

CTC enrichment from DLA material

We compared two methods to enrich and isolate CTCs from the DLA product: depletion of WBCs using the RosetteSep™ method, with or without subsequent positive selection using EpCAM directed antibodies. For the RosetteSep(tm) method to function, WBCs are cross-linked with RBCs leading to erythrocyte rosetting of WBC allowing for gradient separation. Since the DLA product contains a high WBC and relative low RBC concentration, we needed to add RBCs to achieve an optimal WBC:RBC ratio for depletion of WBCs. Using the autologous RBCs from 40 mL of PB, we were able to effectively process a median of 25.5 mL out of the 96 mL DLA obtained. We compared the impact of WBC depletion alone and subsequent EpCAM enrichment using twelve paired samples (Supplementary figure 2). WBC depletion alone was found to reduce the WBC concentration from $93.6*10^6$/mL to $0.12*10^6$/mL, resulting in a WBC depletion factor of 3.1 $\log_{10}$-fold. With subsequent EpCAM enrichment of CTCs, we further reduced the WBC concentration to 4.1 $\log_{10}$-fold. However, this was at expense of a substantial CTCs loss, as the median CTC recovery reduced from 54% with WBC depletion alone to 11.5% with additional EpCAM selection ($P<0.001$). We therefore chose to use WBC depletion alone for the majority of the remaining samples and only applied additional EpCAM selection if WBC depletion insufficiently enriched the sample. In the overall population, we reduced the WBC concentration by 3.21 $\log_{10}$-fold and recovered 46% from the CTCs with WBC depletion alone (Figure 2).

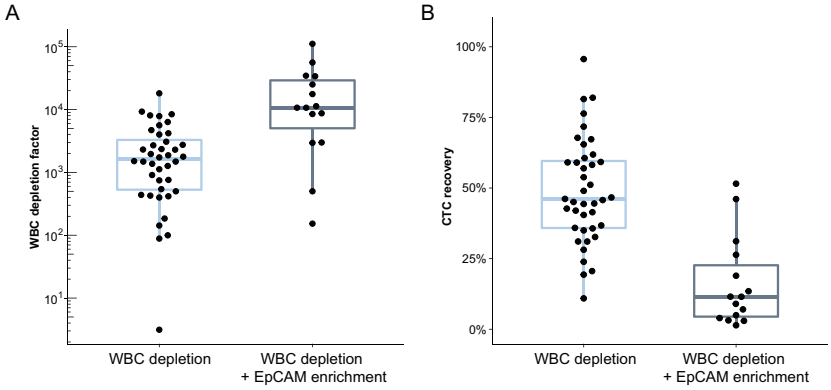

Figure 2: Efficiency of CTC enrichment and isolation techniques for diagnostic leukapheresis. A-B) Two CTC enrichment methods were compared (depicted on the X-axis): (1) white blood cell (WBC) depletion (n=40) and (2) WBC depletion followed by EpCAM enrichment (n=15). The boxplot depicts the median, upper and lower quartiles, whiskers indicate 1.5 times the interquartile range (IQR). Individual data points are shown. **A)** WBC depletion factor after CTC enrichment. To calculate the WBC depletion factor, the number of WBCs before enrichment was divided by the number of WBCs after enrichment. WBC concentration was measured by a hematology analyzer. Y-axis is a logarithmic scale. **B)** Relative CTC recovery (%) after CTC enrichment. To calculate CTC recovery, the absolute CTC count after the enrichment was divided by the absolute CTC count before the enrichment. Absolute CTC counts were extrapolated from 1 mL samples.

CTC derived organoids

After 18 DLA samples we performed an interim analysis to assess the success rate of organoid cultures from isolated and enriched CTC samples. In nine out of eighteen samples we obtained organoid samples of which seven could be maintained for at least six weeks and thus we continued with the second stage of our prospective study. In total, we established CTC derived organoids in 14 out of 40 DLA samples (35% success rate, Supplementary figure 3). At this point we terminated recruitment as the primary endpoint of 50% success rate was no longer a feasible goal. Both the absolute CTC yield after enrichment and the tumor cell percentage in culture was found to be higher in samples that resulted in organoid propagation *ex vivo* ($P<0.001$ and $P<0.01$ resp, Figure 3A and B). Moreover, only one out of nine mHSPC samples, with the highest CTC yield within the population (subject 38; 64,155), could be propagated as organoid. The majority of the organoid cultures could be maintained for six to eight weeks until proliferation stalled, thus providing limited number of organoids for downstream applications (Figure 3C). Two organoid cultures (EMC-PCa-25 and EMC-PCa-41) could be expanded and maintained for over six months, the latter yielding a stable cell line. Validation of the PCa origin of the organoids was shown by quantitative real-time PCR (qRT-PCR) analysis of prostate (cancer) specific transcripts (Table 2, Supplementary figure 4). The vast majority of the isolated samples were positive for *AR* and/or *KLK3* (PSA) while expression of *AR-V7* was identified in only one sample. Three out of 14 organoid cultures (Subject 16, 41 and 93) expressed the *TMPRSS2-ERG* fusion transcript. We performed additional validation of PCa origin using patient specific somatic SNVs previously identified in metastatic biopsies (Table 2, Supplementary table 2 and 3)4. We validated PCa origin in the matched organoid cultures from subject 9-I/II, 79 and 24-I/II by detection of the TP53 and PTEN SNVs resp. Subject 79 was a patient with neuro-endocrine PCa (NEPC), of whom the CTC derived organoids maintained their NEPC features as they lacked AR and KLK3 expression.

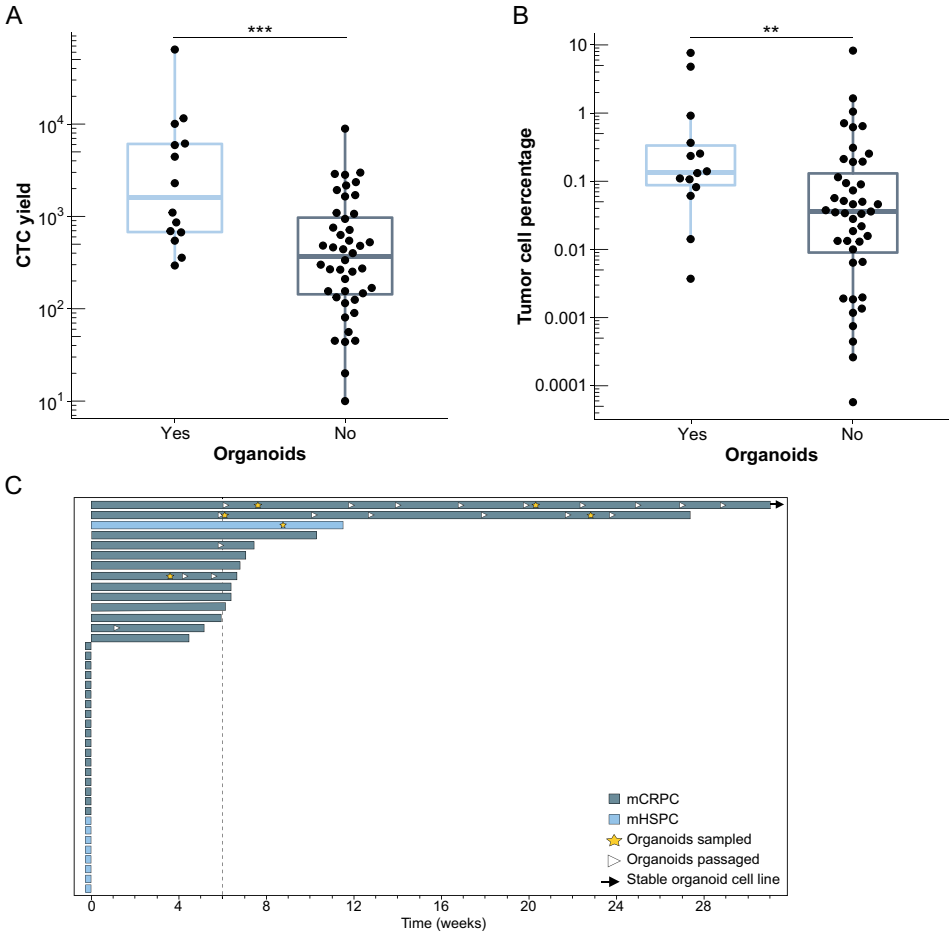

Figure 3: Overview of successful CTC derived organoid cultures. A-B) Results of CTC enrichment and isolation of samples that generated organoids (n=14) and those that did not (n=44). From eleven DLA products we cultured two samples, as white blood cell (WBC) depletion alone and subsequent EpCAM enrichment was performed. A) Estimated CTC yield after CTC enrichment and isolation as determined by CTC count from 1 mL sample and extrapolated to the entire product after processing. Y-axis is a logarithmic scale. Statistical comparison was performed by a paired two-sided Wilcoxon rank test, P<0.001 and P<0.01 resp. **B)** Tumor cell percentage in sample after CTC enrichment and isolation. Percentage of tumor cells was calculated by dividing CTC count by WBC count in sample after enrichment and isolation. Y-axis is a logarithmic scale. **C)** Swimmersplot of all patient samples used to generated CTC derived organoids (marked by ticks), for confirmed organoid samples the time in culture is shown. Most organoid cultures could be maintained as short-term cultures and were subsequently isolated for genetic and/or transcriptional analysis. Organoid sampling is marked by a star and passaging of organoids is marked by arrow heads. Light blue bars represent CTC samples from metastatic hormone sensitive prostate cancer (mHSPC) patients while dark grey is used for metastatic castrate resistant prostate cancer (mCRPC). Subject 41 was deemed a stable organoid cell line (EMC-PCa-41) after 10 passages. X-axis depicts the time in weeks since initiating organoid culture.

Table 2: Validation of prostate (cancer) transcripts and patient specific somatic variants in CTC derived organoids. Overview of genomic and transcriptomic characteristics of the isolated organoids. Expression of prostate (cancer) transcripts in the organoid samples was acquired by qRT-PCR. Positive expression was determined by a ΔΔCq above -8.5 (normalized to EPCAM/KRT19 and VCaP RNA used as calibrator). Patient specific somatic single nucleotide variants (SNVs) were selected using WGS data from metastatic biopsies (CPCT-02 study) and validated using dPCR. Shown are the SNVs and variant allele frequency as defined by dPCR in the organoid samples. NT, not tested.

Subject ID	Expression prostate (cancer) transcripts	Somatic variant (variant allele frequency)
9-I	AR and AR-V9	TP53 c.407A>T (99.7%)
9-II	NT	TP53 c.407A>T (83.9-99.9%)
16	AR, KLK3 and TMPRSS2-ERG	NT
21	AR and KLK3	NT
24-I	PSA	PIK3CA c.3140A>G (1.9%)
24-II	AR and KLK3	PIK3CA c.3140A>G (45%)
25	AR, KLK3 and AR-V9	PLCG2 c.655G>A (27.5%)
38	AR and KLK3	NT
41	AR, KLK3 and TMPRSS2-ERG	NT
79	-	TP53 c.733G>A (97%)
91	AR and KLK3	NT
93	AR, KLK3 and TMPRSS2-ERG	NT
94	AR and KLK3	NT
97	AR and KLK3	NT

Characterization of CTC derived organoid cell line

From the organoid culture samples we were able to generate one stable organoid cell line, which enabled us to perform in-depth genomic and phenotypical characterization. WGS of EMC-PCa-41 revealed a triploid genome with an estimated tumor cell purity of 99%, an overall tumor mutational burden of 2.13 somatic mutations per mega base pairs and no predominant mutational signature (Figure 4A). We identified multiple CNAs including a focal amplification on chromosome Xq, encompassing the *AR* locus and a focal deep deletion on 10q causing loss of *PTEN*. Furthermore, EMC-PCa-41 was characterized by multiple inter- and intra-chromosomal rearrangements, including the interstitial deletion leading to the *TMPRSS2-ERG* fusion as was identified by qRT-PCR (Table 2, Supplementary figure 4). Moreover, ERG expression in the organoids was validated by immunohistochemistry (Figure 3B). Overall, EMC-PCa-41 harbors genomic features which are frequently identified in mCRPC tumors, such as alteractions encompassing the *AR*, *PTEN* and *ERG* gene.[4] Next, we determined the sensitivity of EMC-PCa-41 to commonly used treatments for mCRPC; enzalutamide and taxane chemotherapeutics (Figure 4C and D). Both androgen depleted culture conditions (-R1881) and enzalutamide treatment could only partially inhibit cell proliferation of EMC-PCa-41, suggesting resistance. Interestingly, subject 41 started with enzalutamide after the DLA procedure and switched treatment after only two months due to rising PSA levels (Supplementary figure 5).

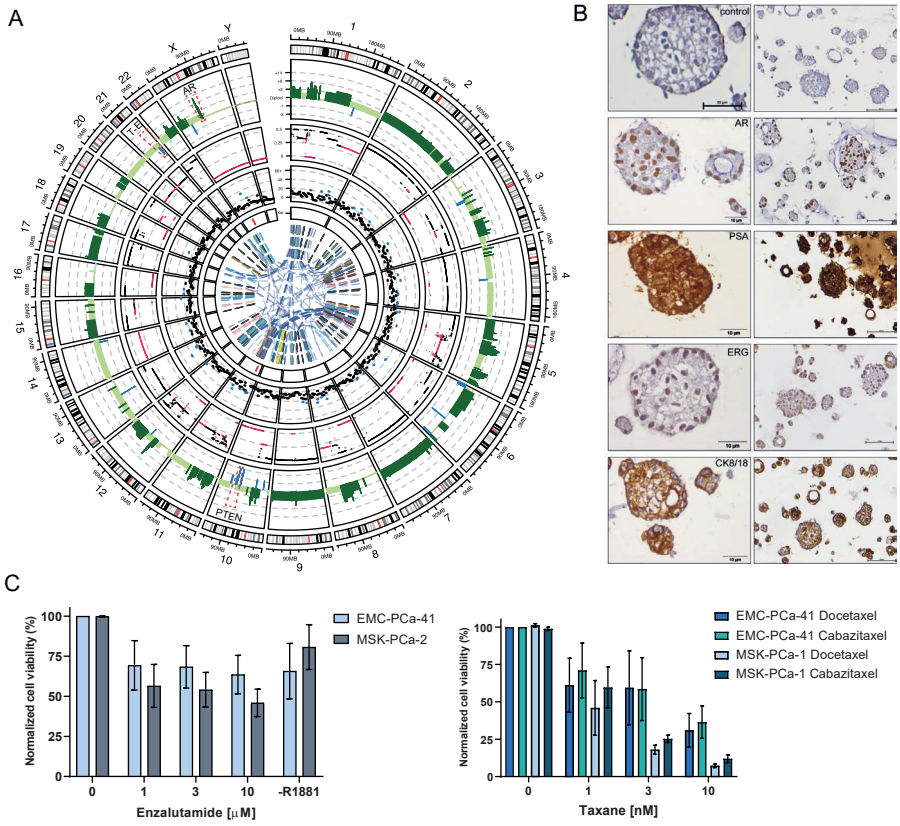

Figure 4: Genetic and phenotypic characterization of the CTC derived stable organoid cell line, EMC-PCa-41. A) CIRCOS plot representing the whole genome characterization of EMC-PCa-41 as obtained by whole genome sequencing. The first outer track depicts the genomic ideogram. The second track displays the copy number profile with amplifications marked in light-green, deep amplification in dark-green, deletions in blue and deep deletions in dark-blue. The third track depicts the lower-allele frequency (LAF) values of individual copy-number segments (LAF values =0.33 in pink and LAF values >0.33 in black). The fourth track displays the number of mutations per 5 megabase pairs (Mb), with regions of mutational frequency above 20 Mb marked in blue. The fifth track highlight regions marked by regional hypermutation (kataegis). Inner circle displays structural variants, with deletions in black, translocations in dark blue, insertions in yellow, inversions in light-blue and tandem duplication in red. **B)** Representative overview and detailed images of immunohistochemical staining on EMC-PCa-41 organoids of AR, PSA, cytokeratin 8/18 (CK8/18) and ERG, and counterstained with hematoxylin. Top row depicts negative control in which the primary antibody was omitted. Scale bar represents 10 μm in size in the detailed images and 100 μm in the overviews. **C)** Drug sensitivity of the organoid cell line EMC-PCa-41 towards the anti-androgen treatment enzalutamide and taxane chemotherapeutics, as compared to the established PCa organoid cell lines. Data shown is the average of 3 individual cell viability experiments with three technical replicates, scale bars represent SEM. Hormone sensitivity of EMC-PCa-41 was determined by cell viability in androgen depleted conditions (-R1881) and compared to the AR positive cell organoid cell line MSK-PCa-2. Chemosensitivity was compared to the AR negative cell line MSK-PCa-1.

CTC and organoid heterogeneity by single cell copy number alterations

To investigate the heterogeneity within CTCs and early-stage organoid cultures, we performed low-pass WGS on multiple single cells obtained from the two long-term mCRPC organoid samples with matched CTCs and WBCs that served as normal controls (subject 25 and 41). The genomic profiles revealed several single cells without any distinct CNA that clustered together with WBC controls. Additional validation excluded these single cells, as they lacked tumor-specific SNVs and were likely non-malignant (supplementary figure 6). We then performed a t-SNE analysis to identify clusters of tumor cells bearing similar copy-number profiles to assess heterogeneity and extract consensus copy number profiles. The CTCs and organoid cells isolated from subject 25 separated into five distinct clusters (Figure 5A). The organoid cells isolated from early cultures clustered separately (cluster 1) from the CTCs and displayed unique focal amplifications on chromosome 11p, 14 and 15 (supplementary figure 7). Tumor cells obtained from subject 41 clustered into three distinct groups (Figure 5B) and showed distinct heterogeneity and ploidy between clusters. Moreover, the consensus plot from cluster 1 revealed a baseline copy number of 6 with focal amplifications on chromosome 4, 13 and 20. Cluster 3, encompassing 8 of 18 CTCs, harbored a triploid genome and closely resembled the focal amplifications previously identified in the matched organoid cell line EMC-PCa-41.

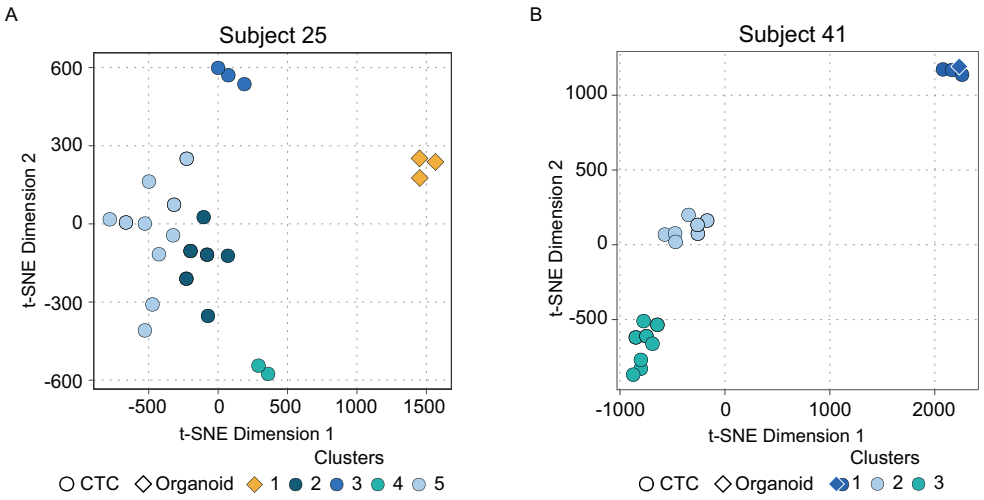

Figure 5: Clustering of individual circulating tumor cells and organoid cells based on low-pass whole genome sequencing data. t-SNE plot (k-nearest neighbor algorithm; Louvain method) of tumor cells, clustering by absolute copy-number values (0.01 Mb). Copy-number values were obtained by low-pass whole genome sequencing of single tumor cells after whole genome amplification, white blood cells were taken along as negative controls (not displayed in t-SNE).

Discussion

This study confirms that DLA is a safe and efficient method to harvest large amounts of CTCs from mPCa patients. Furthermore, we have optimized WBC depletion methods to efficiently recover CTCs and remove WBCs from DLA samples. From the isolated and enriched CTC fractions we were able to establish organoid cultures in 35% of the samples which were mostly of short-term nature, although one sample led to a stable organoid line. Our study shows that DLA is a promising method to obtain viable tumor cells from mPCa patients for subsequent downstream analyses such as single cell sequencing. Unfortunately, the modest success rate to expand organoid cultures precluded us from using CTC derived organoid cultures as a platform to select personalized treatment options for now.

The use of living cells, directly obtained from patients as "real-life" drug screening models, is an appealing prospect in our quest to improve personalized cancer treatment. Indeed, phenotyping living tumor cells has the advantage to directly measure the response to treatment compared to "phenotyping after fixation" based stratification.[18] Previous reports on CTC cultures indicated that one of the main factor for success is the number of cells to initiate expansion.[13,15] Indeed, we found that samples that were successfully propagated as organoids contained significantly higher number and percentage of CTCs after enrichment and isolation. While DLA allows us to obtain vast numbers of CTCs, processing of the DLA material provides new challenges due to the excess of WBCs present in the sample. The currently available methods for WBC depletion or CTC enrichment require an excess of magnetic beads or RBCs to achieve the appropriate ratio to capture all cells by antibodies. This limited the DLA volume that can be (cost)effectively processed. In our study, we were limited to one-fourth of the DLA sample from 5L blood and thus the number of CTCs obtained for culture. Further optimization of DLA sample processing could therefore tremendously impact the amount of viable tumor cells obtained and benefit downstream applications.

In our study we obtained DLA samples from 40% of the screened patients and were able to generate organoids in 35% of the obtained DLA samples including two long-term cultures. This is a substantial improvement compared to previous reports that used CTCs for *ex vivo* organoid cultures.[19] The paper of Gao et al. described the formation of one (long-term) organoid culture out of 17 patient samples (success-rate of 6%).[13] Noteworthy, patients were preselected based on >100 CTCs per 10 mL of PB, although the number of patients screened were not reported. Lambros et al. described the formation of one neuro-endocrine organoid culture out of 14 patient samples (success-rate of 7%) which was used for genetic profiling.[14] Whether these organoids could be maintained as long- or

short-term cultures is unclear. Unfortunately, most of the organoids obtained in our study could be maintained as short-term cultures with limited proliferative capacity, implicating that the current culture techniques do not provide an optimal environment for sustained viability. We were able to maintain two samples for ≥6 passages (subject 25 and 41), eventually leading to one stable organoid line (EMC-PCa-41). Obtaining preclinical models of PCa has been notoriously difficult, presumably due to the low proliferative capacity of PCa as well as overgrowth of benign epithelial and stromal cells. Therefore, establishing PCa cell lines from liquid biopsy samples provides several advantages, including lack of normal epithelial cells and the possibility to obtain metastatic samples from patients with bone only disease in a minimally-invasive manner. The CTC derived organoid cell line EMC-PCa-41 provides an unique novel model for mCRPC with enzalutamide resistance similarly to the patient. Moreover, EMC-PCa-41 harbors genomic alterations similar to a large subset of mCRPC patients as well as the TMPRSS2-ERG gene fusion, which is underrepresented in the currently available models of PCa.[4,20]

Treatment modalities for mPCa have profoundly changed and expanded during the last decade. Understanding how PCa cells adapt to the selective pressure of treatment is becoming increasingly important to further improve treatment outcome. Therefore, we need patient derived materials that reflect the current status of the patient's cancer, including the spatial and temporal tumor heterogeneity. Here we show that DLA enables in-depth studies into intra-tumor heterogeneity in mPCa by performing single cell whole genome DNA sequencing on CTCs. The single cell analysis distinguished clusters of cells with unique copy number alteration which is in line with a previous study.[14] Within our study we were also able to obtain matched samples in four patients, which shows that longitudinal CTC sampling by DLA is feasible, providing a platform to study clonal evolution and adaptation to treatment. Overall, our study provides an important step forward in implementing CTCs in individualized disease modelling, nevertheless identifies several challenges that require further optimization to enable the development of a personalized drug screening platform.

References

1. Armenia J, Wankowicz SAM, Liu D, et al. The long tail of oncogenic drivers in prostate cancer. Nat Genet. 2018;50(5):645-651.
2. Wedge DC, Gundem G, Mitchell T, et al. Sequencing of prostate cancers identifies new cancer genes, routes of progression and drug targets. Nat Genet. 2018;50(5):682-692.
3. Carreira S, Romanel A, Goodall J, et al. Tumor clone dynamics in lethal prostate cancer. Sci Transl Med. 2014;6(254):254ra125.
4. van Dessel LF, van Riet J, Smits M, et al. The genomic landscape of metastatic castration-resistant prostate cancers reveals multiple distinct genotypes with potential clinical impact. Nature Communications. 2019;10(1):5251.
5. Miyamoto DT, Zheng Y, Wittner BS, et al. RNA-Seq of single prostate CTCs implicates noncanonical Wnt signaling in antiandrogen resistance. Science. 2015;349(6254):1351-1356.
6. de Bono JS, Scher HI, Montgomery RB, et al. Circulating tumor cells predict survival benefit from treatment in metastatic castration-resistant prostate cancer. Clin Cancer Res. 2008;14(19):6302-6309.
7. Scher HI, Lu D, Schreiber NA, et al. Association of AR-V7 on Circulating Tumor Cells as a Treatment-Specific Biomarker With Outcomes and Survival in Castration-Resistant Prostate Cancer. JAMA Oncol. 2016;2(11):1441-1449.
8. Antonarakis ES, Lu C, Wang H, et al. AR-V7 and resistance to enzalutamide and abiraterone in prostate cancer. N Engl J Med. 2014;371(11):1028-1038.
9. Onstenk W, Sieuwerts AM, Kraan J, et al. Efficacy of Cabazitaxel in Castration-resistant Prostate Cancer Is Independent of the Presence of AR-V7 in Circulating Tumor Cells. Eur Urol. 2015;68(6):939-945.
10. Heller G, McCormack R, Kheoh T, et al. Circulating tumor cell number as a response measure of prolonged survival for metastatic castration-resistant prostate cancer: A comparison with prostate-specific antigen across five randomized phase III clinical trials. J Clin Oncol. 2018;36(6):572-580.
11. Drost J, Clevers H. Organoids in cancer research. Nat Rev Cancer. 2018;18(7):407-418.
12. Yu M, Bardia A, Aceto N, et al. Cancer therapy. Ex vivo culture of circulating breast tumor cells for individualized testing of drug susceptibility. Science. 2014;345(6193):216-220.
13. Gao D, Vela I, Sboner A, et al. Organoid cultures derived from patients with advanced prostate cancer. Cell. 2014;159(1):176-187.
14. Lambros MB, Seed G, Sumanasuriya S, et al. Single-Cell Analyses of Prostate Cancer Liquid Biopsies Acquired by Apheresis. Clin Cancer Res. 2018;24(22):5635-5644.
15. Cayrefourcq L, Mazard T, Joosse S, et al. Establishment and characterization of a cell line from human circulating colon cancer cells. Cancer Res. 2015;75(5):892-901.
16. Stoecklein NH, Fischer JC, Niederacher D, Terstappen LW. Challenges for CTC-based liquid biopsies: low CTC frequency and diagnostic leukapheresis as a potential solution. Expert Rev Mol Diagn. 2016;16(2):147-164.
17. Stenzinger M, Bonig H. Risks of leukapheresis and how to manage them-A non-systematic review. Transfus Apher Sci. 2018;57(5):628-634.
18. Ooft SN, Weeber F, Dijkstra KK, et al. Patient-derived organoids can predict response to chemotherapy in metastatic colorectal cancer patients. Sci Transl Med. 2019;11(513).
19. Van Hemelryk A, van Weerden WM. Novel patient-derived 3D culture models to guide clinical decision-making in prostate cancer. Current Opinion in Endocrine and Metabolic Research.

2020;10:7-15.
20. Navone NM, van Weerden WM, Vessella RL, et al. Movember GAP1 PDX project: An international collection of serially transplantable prostate cancer patient-derived xenograft (PDX) models. Prostate. 2018;78(16):1262-1282.

Funding

This work was supported by KWF-Alpe d'HuZes project [EMCR 2015-8037] and in parts by a grant from the Dutch Association of Medical Oncology (NVMO).

Role of the funding agency

KWF (Dutch Cancer Society) had no role in the design of the study; the collection, analysis or interpretation of the data; preparing and submitting the manuscript for publication. The content of this manuscript is solely the responsibility of the authors. KWF was informed about the progress and results of the presented study.

Acknowledgements

We thank Fred Guurink for his philanthropic support of our study, Katharina Raba and Jean Helmijr for her technical support with the single cell selection. We thank Elena Martens-Uzunova for carefully reading the manuscript. We thank Cancer Genomics Netherlands for financial support of coauthor A.S. We thank Wouter Karthaus and Jack Schalkes for providing us with the MSK-PCa1 and MSK-PCa2 organoid cell lines. We also thank the Hartwig Medical Foundation (www.hartwigmedicalfoundation.nl) and the Center of Personalized Cancer Treatment (www.CPCT.nl) for their help with generating and analyzing the WGS data.

Supplementary table 1: Description of adjusted prostate cancer organoid media (APCOM) and prostate growth media (PGM) used to culture circulating tumor cell derived organoids.

Media	Reagent	Concentration in media	Stock concentration	Supplier (info supplier, catologue number)
APCOM	Advanced DMEM/F12[1] (AdMEM/F12)	NA	NA	ThermoFisher Scientific (Waltham, MA, USA, 12634028)
APCOM	Hepes[1]	10 mM	1 M	ThermoFisher Scientific (15630056)
APCOM	L-Glutamine[1]	2 mM	200 mM	Lonza (Basel, Swizerland, 17-605E)
APCOM	Noggin[2]	-	-	Conditioned media from Hek293T-Noggin-Fc (Heijmans et al.)
APCOM	R-spondin[2]	-	-	Conditioned media from Hek293T-hRSpo1 (Kim et al.)
APCOM	A-83-01	500 nM	25 mM	Tocris Bioscience (Bristol, UK, 2939)
APCOM	Prostaglandin E2 (PGE2)	1 µM	10 mM	Tocris Bioscience (2296)
PGM	DMEM/F12	NA	NA	ThermoFischer Scientific (11330032)
PGM	Insulin-Transferrin-Selenium (ITS)	10 µg/mL, 5.5 µg/mL and 6.7 ng/mL	1 mg/mL, 0.55 mg/mL and 0.67 µg/mL	ThermoFischer Scientific (41400045)
PGM	Bovine serum albumin Fraction V (BSA)	0.01% (w/v)	10 % (w/v)	Sigma-Aldrich (Saint Louis, MO, 10735094001)
PGM	Fetuin	20 µg/mL	8 mg/mL	Sigma-Aldrich (F3385)
PGM	Fibronectin	100 ng/mL	100 µg/mL	Alfa Aesar (Haverhill, MA, USA, J65460)
PGM	Triiodo-L-thyronine (T3)	0.6 ng/mL	600 ng/mL	Sigma-Aldrich (T6397)
PGM	Phosphoethanolamine (PEA)	100 µM	100 mM	Sigma-Aldrich (P0503)
PGM	Choleratoxin	50 ng/mL	50 µg/mL	Sigma-Aldrich (C8052)
PGM	Fetal Bovine serum (FBS)	2% (v/v)		ThermoFischer Scientific (10270106)
PGM	Hydrocortisone	0.5 µg/mL	0.5 mg/mL	Sigma-Aldrich (H0888)
Both	Epithelial growth factor (EGF)	20 ng/mL or 10 ng/mL	10 µg/mL	Sigma-Aldrich (USA, F29644)
Both	Fibroblast growth factor 2 (FGF-2)	5 ng/mL	50 µg/mL	R&D Systems (Minneapolis, MN, USA, 233-FB-025)
Both	Fibroblast growth factor 10 (FGF-10)	10 ng/mL	100 µg/mL	PeproTech (Rocky Hill, NJ, USA, 100-26)
Both	Y-27632 dihydrochloride	10 µM	10 mM	Abmole Bioscience (Houston, TX, USA,M1817)
Both	R1881	0.1 nM	0.1 µM	Sigma-Aldrich (D5027)
Both	Penicilline/streptomycine[1]	100 U and 100 µg/mL	10.000 U and 10.000 µg/mL	Lonza (17-602E)

[1] Components for AdMEM/F12+++. APCOM additives are diluted in AdMEM/F12+++, and top up till desired volume. [2] Desired supplement concentration is determined by an ELISA assay (Kim et al.)

Supplementary table 2: Primer and probe design for digital PCR. Custom and commercial digital polymerase chain reaction (dPCR)assays used for validation of liquid biopsy derived organoids from subject 9-I/II (TP53), subject 24-I/II (PIK3CA) and subject 25 (PLCG2).

Gene	Cosmic ID	Amino acid variant	Somatic variant	Forward primer	Reverse primer	Probe*
TP53	COSV53122800	p.Q136L	c.407A>T	5′-ACT CCC CTG CCC TCA ACA A-3′	5′- AAG ACC TGC CCT GTG CAG C-3′	5′ –TGT TTT GCC [A/T]AC TGG C-3′
TP53	COSV52661877	p.G245S	c.733G>A	5′-TGT TAT CTC CTA GGT TGG CTC TGA-3′	5′-AGG ATG GGC CTC CGG TT-3′	5′-CTG CAT GGG C[G/A]A GCA-3′
PIK3CA	COSV55873195	p.H1047R	c.3140A>G	Assay ID**: AHPAVCD		
PLCG2	COSV63869132	p.D219N	c.655G>A	5′-TGC ATT AAG TGA CTT GTC TAA GGT TCT TT-3′	5′-CCA GGA TGA ACA CGG ACG AAT C-3′	5′-TTT CAG ATT CTC [G/A]AT GAA TT-3′
*Reporter dye/quencher: wildtype, VIC; mutant, FAM / NFQ **Validated TaqMan® SNP genotyping assay (ThermoFisher Scientific)						

Supplementary table 3: Genomic characteristics of metastatic prostate cancer patients who underwent diagnostic leukapheresis. Actionable and cancer associated genomic alteration detected in metastatic biopsies from included patients whose whole genome sequencing (WGS) data was used to validate organoid cultures. WGS data was generated as part of the CPCT-02 study. Shown are the somatic variants, gain/losses, gene-fusions and gene-disruptions in cancer associated genes (as described in Priestley et al.). Threshold for high tumor mutational load was 140 and MSI samples were defined by a MSiSeq score above 4, - indicated that this aberration was not detected and ? if not reported.

Subject ID	Somatic variants	Somatic gains and losses	Somatic gene fusions	Somatic gene disruption	Microsatal-ite status	Tumor mutational load
9-I/II	TP53 c.407A>T; CDK12 c.2350C>T; CDK12 c.3002T>A	Copy-gain: MYC, CCND1, MDM2, PTPN11 and CDK4	-	?	?	Low
16	TP53 c.243_249delACCGGCG; AR c.2623C>T; CTNNB1 c.133T>C	Copy-loss: PTEN	CDC27-ETV4; TMPRSS2-ERG	PMS2:INV intron 12	Stable	Low
24-I/II	MYCN c.1226C>T; MSH2 c.1699delA; MSH6 c.2554_2556delAAG; PIK3CB c.2056G>A ; PIK3CA c.3140A>G; APC c.1660C>T; APC c.4385_4386delAG; EZH2 c.1730C>T; PTEN c.734A>C; ATM c.7927+5_7927+6insT; MDM2 c.1181C>A; HNF1A c.521C>T; FLT3 c.1419- 4dupT; TSC2 c.348delG; AR c.2105T>A; AR c.2623C>T			MSH2: INV intron 7	Unstable	High
25				BRAF: INV intron 1 (2x) FANCG: INV promotor region	Stable	Low
79	TP53 c.733G>A; ERBB2 c.1796G>A; ESR1 c.1514C>T; RASA1 c.1211C>T; ASXL c.1264A>T	Copy-loss: PTEN, RB1	FASN-ETV4	CUX1: DEL intron 1-> intron 22; BRCA: INV intron 20; CBFB: BND intron 3	Stable	Low

Supplementary table 4: Single nucleotide variants and primer design for validation of single cell sequencing. Single nucleotide variants of subject 25 and 41 previously identified in whole genome sequencing of metastatic biopsy or matched organoid cell line resp. A nested polymerase chain reaction was used for amplification and subsequent Sanger sequencing.

Subject ID	Gene	Somatic variant	Cosmic ID	Outer primers		Inner primers	
				Forward	Reverse	Forward	Reverse
25	CUX1	c.1381G>C	-	AGCTCCT-TCTCCTACCCAGG	GCTCCAGGTCCTTTAGCT-GG	ATAGCCAGCACTCTCA-CAGC	TGTCACCAGCTGCCT-GATAC
41	TP53	c.927dup	COSM6951762	AGGACCTGATTTCCT-TACTGCC	TTAGTTAGCTACAACCAG-GAGCC	AGTGGTAATCTACTGG-GACGG	CCCCAATTGCAGGTAAAA-CAGTC
41	NKX3-1	c.406G>A	COSM5733098	CGATGACAGTGGGCT-GTTTG	TAGAGACACCCTGGG-GAAGG	CCTTCCCCACTCTCCT-TTCC	CCCACGCAGTACAGG-TATGG
41	MYO10	c.4798C>T	COSM4874050	GCATTGCATC-CGTCCTCCTC	TAAGCTTGCTCAGG-CAACCC	GCCCTATTCTGAACCCCT-CAG	CAGTGCCCCACCTGTG-TAAG
41	CLDN12	c.109C>T	COSM1248386	TCTGAGGTCACACA-CACCTG	GCCAGGAAAAATAG-CAGCCC	GTGTGT-CACCCCCTAGTCTG	GTTTGATGTTGGGCAC-CGAG

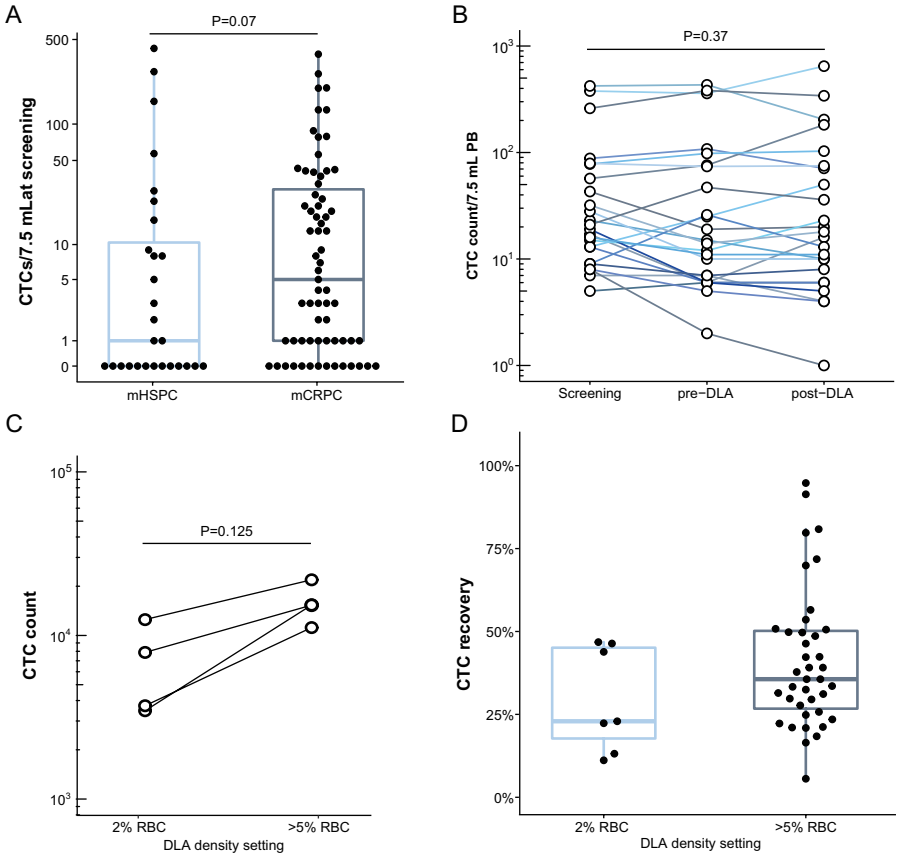

Supplementary figure 1: Circulating tumor cell burden in metastatic prostate cancer patients and optimization of diagnostic leukapheresis. A) Circulating tumor cell (CTC) count at screening of all metastatic prostate cancer patients (mPCa) included in this study (n=98). The boxplots depict the upper and lower quartiles, with the median shown as a solid line; whiskers indicate 1.5 times the IQR. Y-axis is a pseudo log scale. CTC count per 7.5 mL peripheral blood is shown for mPCa patients with hormone sensitive (n=28) and castrate resistant (n=67) disease and compared using an unpaired two-sided Wilcoxon sign rank test (P=0.07). **B)** CTC count per 7.5 mL peripheral blood (PB) as obtained during different stages of study participation. For 24 patients we assessed the CTC burden in samples acquired at screening, just prior to diagnostic leukapheresis (pre-DLA) and post-DLA. Y-axis is a log-scale, matched samples are connected with a line. CTC burden in the different samples was compared by a Friedman test, no statistical significant impact was observed (P=0.37). **C)** Estimated CTC yield in the DLA product obtained at different densities. X-axis displays the two tested density conditions: 2% red blood cells (RBC) and >5% RBC. Each dot represents an individual subject (n=4), and samples from the same subject are connected. Y-axis is a logarithmic scale. Statistical comparison was performed by a paired two-sided Wilcoxon rank test (P=0.125). **D)** Relative CTC recovery (%) in DLA product processed at different densities. The X-axis displays the two tested density conditions: 2% and >5% RBC (n=7 and n=46 fractions resp.). In six patients two DLA fractions were collected. The boxplots depict the upper and lower quartiles, with the median shown as a solid line; whiskers indicate 1.5 times the IQR.

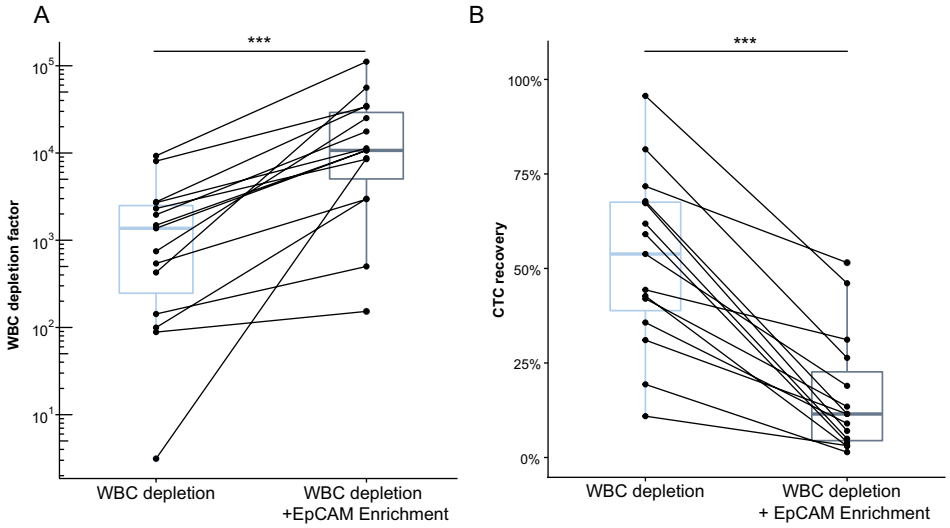

Supplementary figure 2: Comparison of white blood cell depletion with or without EpCAM enrichment for the efficacy to enrich for circulating tumor cells. A-B) Two CTC enrichment methods were compared in twelve paired samples (depicted on the X-axis): (1) white blood cell (WBC) depletion and (2) WBC depletion followed by EpCAM enrichment. The boxplots depict the upper and lower quartiles, with the median shown as a solid line; whiskers indicate 1.5 times the IQR. Paired samples are connected with a line. Statistical comparison was performed by a paired two-sided Wilcoxon rank test, P<0.001 for both datasets. **A)** Displays the WBC depletion factor after CTC enrichment. To calculate the WBC depletion factor, the number of WBCs before enrichment was divided by the number of WBCs after enrichment. Y-axis is a logarithmic scale. **B)** Displays the relative CTC recovery (%) after CTC enrichment. To calculate relative CTC recovery, the estimate CTC count after the enrichment was divided by the estimate CTC count before the enrichment. Estimate CTC counts were extrapolated from 1 mL samples.

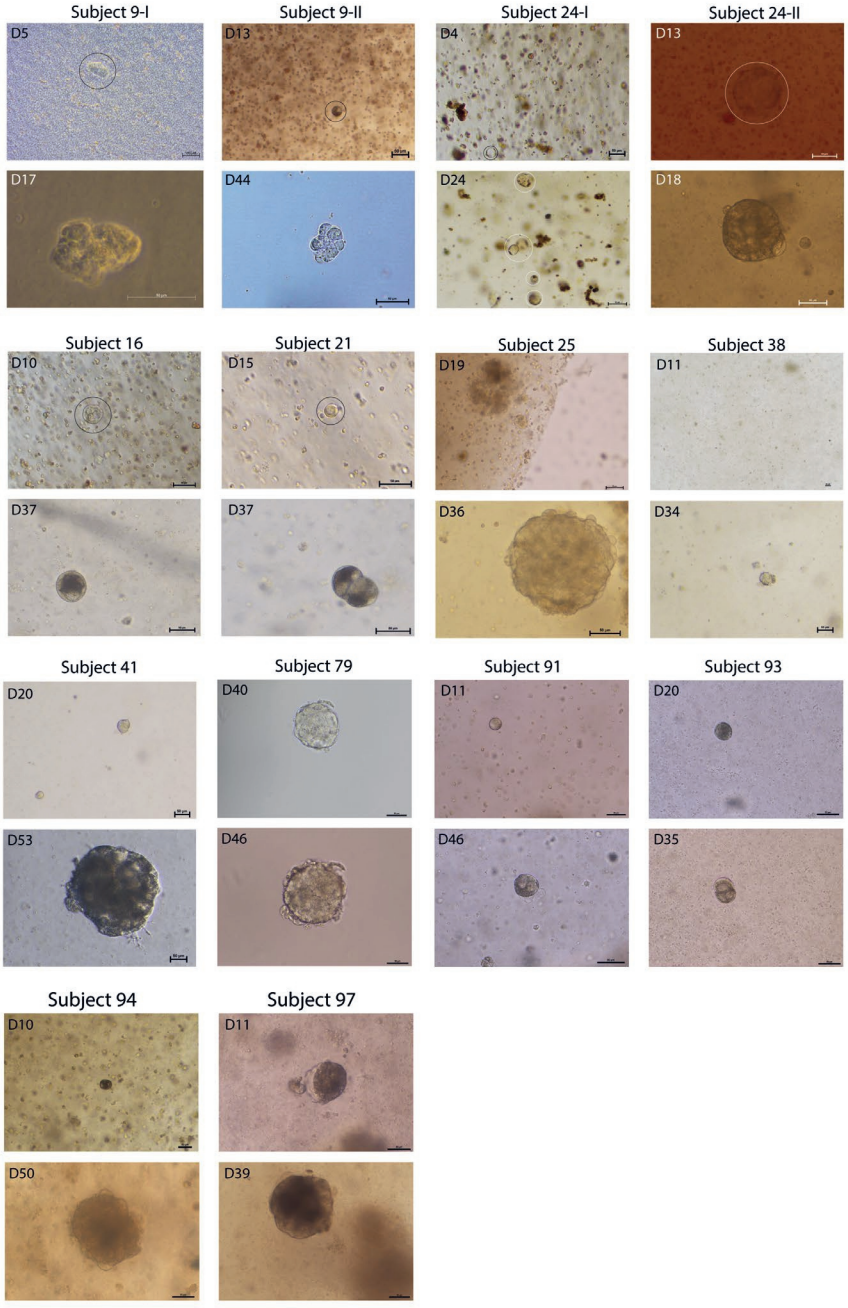

Supplementary figure 3: Overview of successful CTC derived organoid cultures.
Overview of all successful circulating tumor cells (CTC) derived organoid cultures obtained (n=14), and organoid expansion observed over time. Timespan (in days) of organoid cultures are indicated in the top left corners, scale bars depicted are 50 µm in size with the exception of the day 5 image of subject 9 (100 µm).

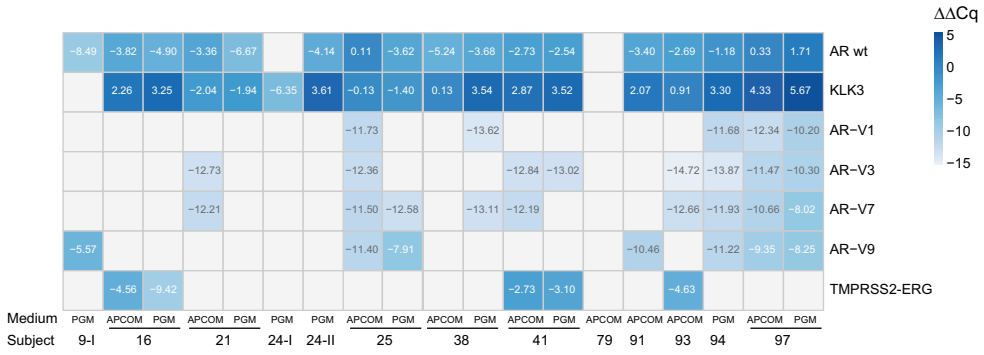

Supplementary figure 4: Results of qPCR validation of prostate (cancer) associated genes of circulating tumor cell derived organoids. Heatmap of androgen receptor full length (AR fl), AR splice variant 7 (AR-V7), KLK3 (PSA) and TMPRSS2-ERG expression as determined by qPCR in circulating tumor cell (CTC) derived organoid cultures. Expression is depicted by ΔΔCq which is defined by target Ct values normalized to EPCAM/KRT19 expression and VCaP RNA used as calibrator. If several organoid samples were obtained, median expression per culture media (PGM or APCOM) was calculated and depicted in the heatmap. Organoids were deemed positive for expression of prostate (cancer) associated genes if ΔΔCq were above -8.5.

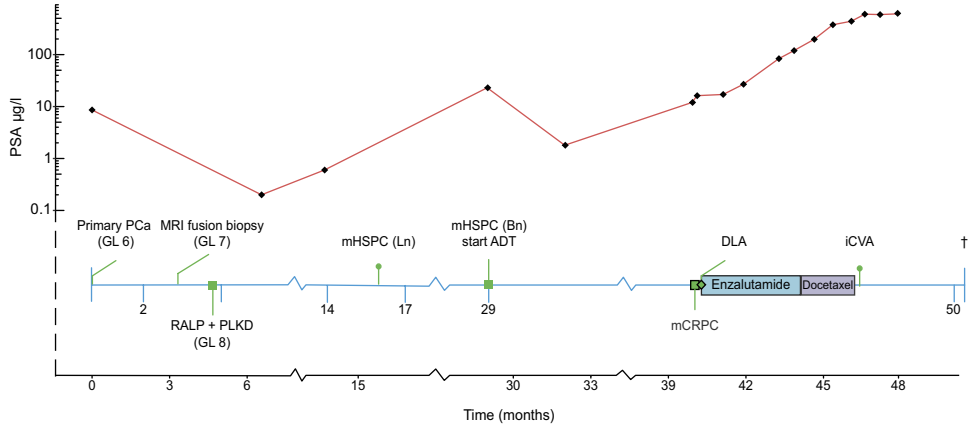

Supplementary figure 5: Clinical overview of subject 41. Clinical overview of subject 41, including PSA levels during the disease course (top part). Initially, a Gleason (GL) 6 adenocarcinoma of the prostate was diagnosed by systematic biopsies at an initial PSA of 8.6 µg/L (while the patient was using dutasteride). MRI showed a PIRADS 5 lesion which was target biopsied and revealed a Gleason 7 adenocarcinoma of the prostate. After robot-assisted laparoscopic prostatectomy (RALP) with pelvic lymph node dissection (PLND), PSA remained detectable at 0.2 µg/L. Upon PSA progression metastases in lymph node (Ln) and bone (Bn) were detected and androgen deprivation therapy (ADT) was started. Before start of enzalutamide, the patient underwent diagnostic leukapheresis (DLA). The patient received four cycles of docetaxel which was discontinued because of an ischemic cerebrovascular accident (iCVA).

Subject 25

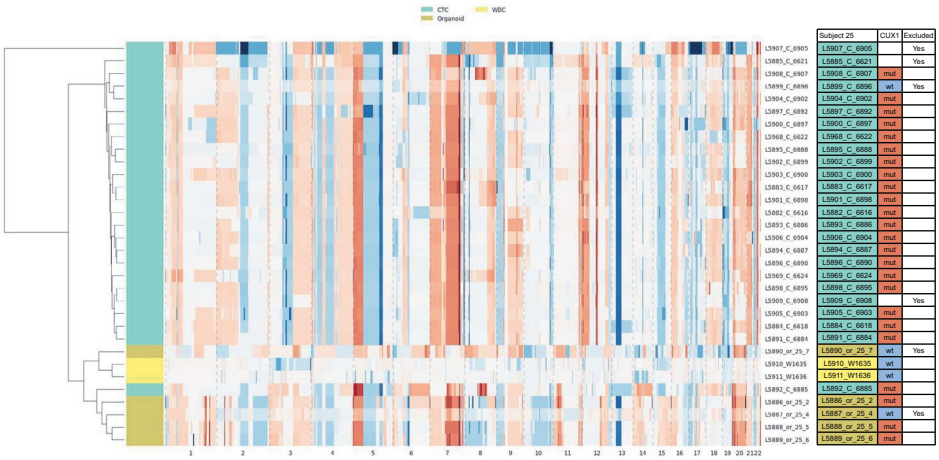

Subject 41

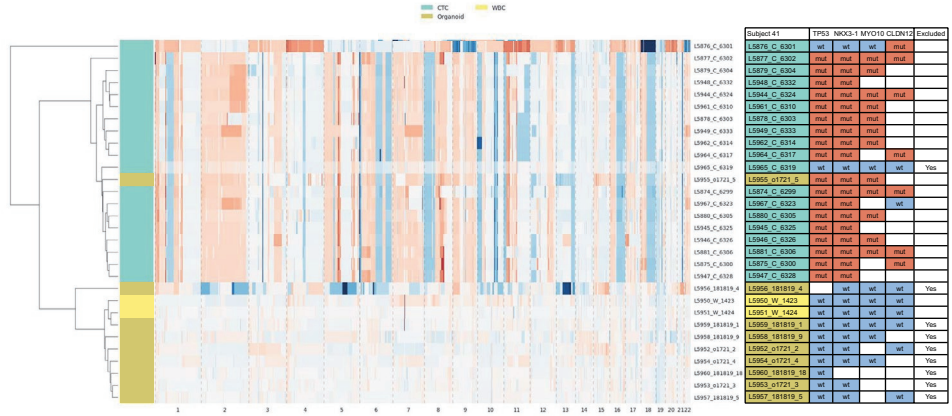

Supplementary figure 6: Initial clustering of copy number alterations in circulating tumor cells and early organoids from two metastatic castration resistant prostate cancer samples and subsequent validation. Unsupervised hierarchical clustering with dendogram (Euclidean distance; ward method) using $\log_2$ ratio of normalized counts per 0.25 megabase, depicting CNA of individual circulating tumor cells (CTCs, aqua), organoid cells (beige) and white blood cells (WBCs, yellow) for subject 25 (top panel) and 41 (bottom panel). CNA segments for each individual cell (column) are shown from left to right and ordered on chromosome (indicated below). The color gradient represents copy number deletions in dark blue (-2 to 0) and amplification in dark red (0 to 2).The tables alongside the hierarchical clustering represent the results from the validation experiments. Sanger sequencing was performed to identify somatic variants in whole genome amplified DNA from the CTCs, organoids and WBCs from subject 25 and 41. Empty wells represent missing data, shown are the organoid and CTC samples excluded based on validation.

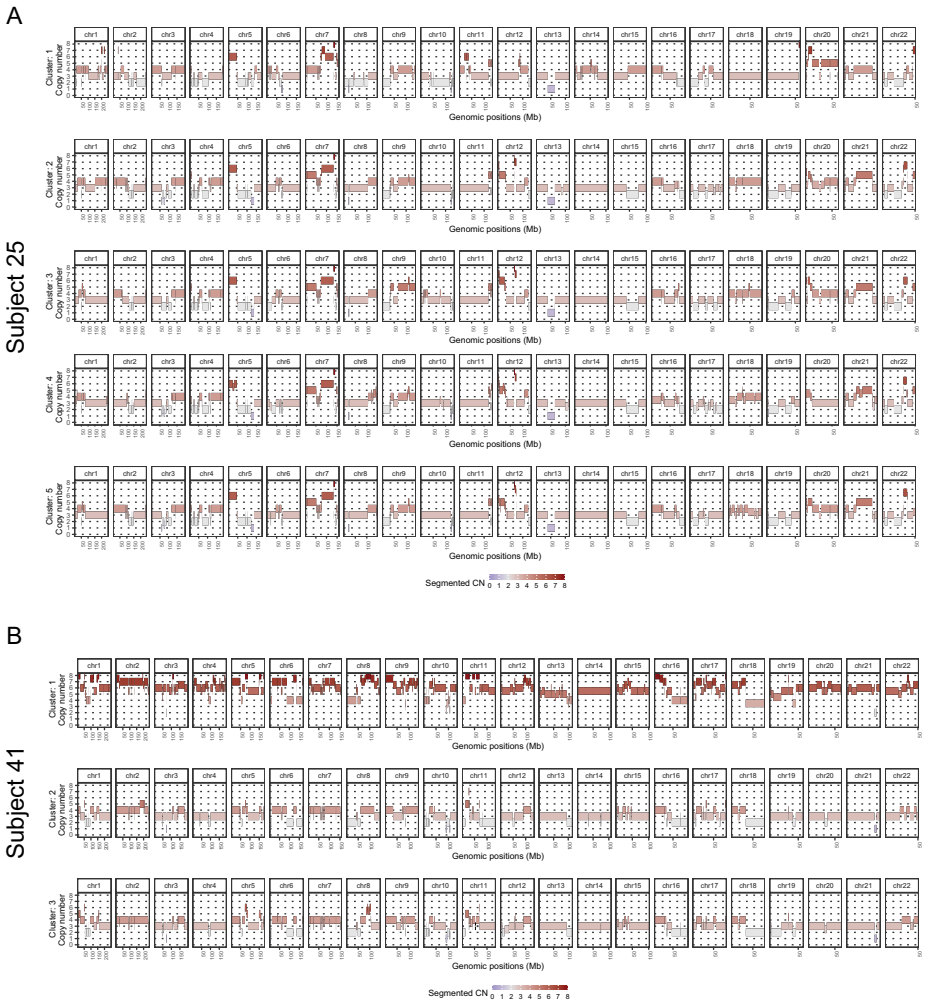

Supplementary figure 7: Copy number heterogeneity in circulating tumor cells and organoids. A-B) Consensus profiles per t-SNE cluster, depicting median absolute copy numbers in **A)** subject 25 and (n=24) B) subject 41 (n=19). The Y-axis displays the absolute copy number ranging from 0 to (≥) 8 copies. X-axis displays the genomic position of the copy-number segments, ticks indicate 50 megabase (Mb). The color gradient represents absolute copy number, with deletions in blue (0 to <2) and amplification in red (>2 to (≥)8).

Supplementary material and methods

Study design

This prospective study was conducted in accordance with the Declaration of Helsinki and was approved by the medical ethical committee of the Erasmus Medical Center Rotterdam (EMC16-449). The study was performed using a Simon's two-stage design[1], with an interim analysis after 18 DLAs were performed. Continuation to the second stage could only continue if seven out of 18 samples yielded successful organoid cultures meaning that organoids could be propagated for six weeks or longer and PCa origin could be validated. The study protocol, including sample size calculations, has been added as supplemental information.

Patients

From November 2016 till July 2020, patients with mPCa were prospectively included (NL6019; https://www.trialregister.nl/trial/6019). All patients provided written informed consent before any study procedure took place. Patients ≥18 years in age were eligible if they had histologically or cytologically confirmed PCa, with measurable metastatic lesion(s) (according to PCWG2 and/or RECIST 1.1 criteria)[2,3] and intended to start a new line of systemic treatment. Patients should have at least two adequate peripheral veins as access point for DLA. Additionally, patients should be in good physical condition (WHO performance status ≤ 2), have an adequate hematology, coagulation status and liver/renal function as assessed by routine laboratory tests (see study protocol for details). Exclusion criteria were, CTC count of <5 per 7.5 mL of blood at screening, known hypersensitivity to anticoagulant used during DLA, hemorrhage disease or coagulation disorders and chronic viral infections. We excluded hormone sensitive PCa patients currently undergoing ADT, to prevent possible interference of ADT on the number of CTCs and CTC characteristics. After completing the DLA procedure hormone sensitive patients started with ADT. Patients were allowed to enter the study multiple times during their treatment course. All patients provided written informed consent before any study procedure. The study procedures included a blood draw at baseline to screen for eligibility criteria, a blood draw before start of the DLA procedure and the DLA procedure itself. Clinical data on disease characteristics, previous therapies and response on the subsequent systemic therapy were collected in an electronic case report form (ALEA Clinical).

Primary and secondary endpoints

The primary endpoint of this study was the rate of successfully cultured organoids from CTCs obtained by DLA with successfully being defined as i) propagation for at least 6 weeks in culture and ii) proven PCa characteristics. PCa characteristics include epithelial origin CK8/18, lack of p63 (not basal cells), and (combined) expression of TMPRSS2-ERG fusion, AR (splice variants) expression, PTEN loss, MYC amplification (together indicative of PCa) or the detection of patient-specific somatic variants (known from previously characterized tumor material).

Study procedures

The study procedures included a blood draw at baseline to screen for eligibility criteria, including CTC count, a blood draw before start of the DLA procedure and the DLA procedure itself. All study procedures were performed before start of a new line of treatment.

Circulating tumor cell enumeration using CellSearch

For CTC enumeration, 7.5 mL of blood; 1 mL of DLA product diluted in 6.5 mL of PBS (Thermo Fisher Scientific, Waltham, MA); or a proportion of the enriched fraction was collected in a CellSave Preservative tube (Menarini Sillicon Biosystems, Castel Maggiore, BO, Italy). All samples were processed within 96 hours and CTC enumeration was performed using the Circulating Epithelial Cell Kit on the CellSearch® system (Menarini Sillicon Biosystems) by certified personnel. Briefly, samples were subjected to immunomagnetic capture using ferrofluids coupled to anti-EpCAM antibodies and enriched cells were stained with antibodies specific for cytokeratin (CK) 8, 18, and 19, CD45 and nucleic acid dye (DAPI). Images were captured using the CellTracks Analyzer II (Menarini Silicon Biosystems) and manually examined to determine the presence of CTCs. Cells were defined as CTCs when positive for CK and DAPI and negative for CD45 according to the manufacturer's instructions. CellSearch cartridges were stored in the dark at 4°C before further analyses.

Diagnostic leukapheresis

DLA was performed at the department of Hematology at the Erasmus Medical Center using the Spectra Optia Cell Separator machine (Terumo BCT, Lakewood, CO). Only peripheral venous access was used to process a maximum volume of 10 L of circulating blood. Citrate dextrose solution A was used as anticoagulant. For CTC isolation the standard settings for white blood cell (WBC) isolation were applied, only the plasma pump rate was increased to collect a slightly higher cell density with an approximate hematocrit of 5% instead of 2%. In addition, extra blood was drawn for the collection of red blood cells (40 ml in EDTA tubes), CTC count of peripheral blood (20 ml in CellSave tubes) and routine hematological tests. Fresh DLA product was immediately processed for CTC enrichment. Excess DLA product was stored in liquid nitrogen at 2 mL aliquots containing 50% autologous plasma and 10% DMSO (Sigma-Aldrich, Saint Louis, MO) for biobank purposes. All grade ≥3 (serious) adverse events during and within 48 hours after DLA were registered.

Circulating tumor cell enrichment

CTCs from DLA were enriched by negative depletion of WBC using RosetteSep™ CTC Human CD45 Depletion Cocktail (STEMCELL Technologies, Vancouver, BC, Canada) with the following modifications. WBC concentration of the DLA product was measured using a hematology analyzer (Beckman Coulter, Brea, CA) and diluted with phosphate buffered saline (PBS) to a final concentration of $50x10^6$ WBC/mL. Red blood cells (RBCs) were collected in K2EDTA vacutainer® tubes (BD, Franklin Lakes, NJ) before start of the DLA procedure and concentrated by centrifugation at 800g for 8 minutes. These autologous RBCs were added to the DLA product to achieve a 1:50 WBC:RBC ratio before incubation with the RosetteSep™ Cocktail to induce crosslinking of RBCs with WBCs. RBC/WBC rosettes were depleted using Sepmate™-50 tubes and Lymphoprep™ as density gradient medium (both STEMCELL Technologies), by centrifugation at 1200g for 12 minutes at room temperature with the brake off. Enriched CTCs were washed using PBS. For 15 DLA samples additional manual positive immunomagnetic enrichment was performed. Ten mL of CD45 depleted fraction was incubated with 150 µL CellSearch EpCAM ferrofluids and 150 µL capture enhancement reagent for 10 min, at room temperature on a roller mixer. To separate the magnetic labeled CTCs, the tube was placed next to a MagCellect magnet (R&D systems, Minneapolis, MN) and the supernatant aspirated. A second magnetic separation was performed for optimized enrichment. Finally, the enriched CTCs were collected in culture medium and used for organoid culture.

Organoid culture from circulating tumor cells

The enriched CTC suspension was collected by centrifugation at 1200g for 8 minutes. The cell pellet was cooled on ice and mixed with Matrigel (MG; Corning, cat. no. 356231, Corning, New York). The cell suspension-MG mix was dispensed in a pre-warmed 24-wells plate (Corning, cat. no. 3527), in 30-40 µl droplets. Subsequently, the plate was placed upside-down at 37°C and incubated for 15 minutes to let the MG solidify. Next, 500 µl of medium was added; CTCs were cultured in prostate growth medium (PGM) and adjusted prostate cancer organoid medium (APCOM) in parallel (overview in supplementary table 1).[4] APCOM was based on the previously published organoid culture media described by Gao et al. and Beshiri et al.[5,6] Weekly images were obtained to monitor organoid growth using the Zeiss Axiovert 25 equipped with 10x and 20x Plan-Neofluar objectives, a AxioCam ICc1 camera and AxioVision imaging software (version 4.8.2.0, Oberkochen, Germany) and Nikon Eclipse TS2 equipped with 4x, 10x CFI Achro brightfield objectives and a 20x Fluor ELWD objective, a DS-Fi3 camera and NIS-Elements imaging software (Minato, Tokyo, Japan). Cell culture media was either replaced or supplemented every 3-4 days.

DNA/RNA isolation and PCR analyses of CTC derived organoids

For DNA and RNA isolation, organoids were collected, lysed with RLT buffer (Qiagen, cat. no. 79216, Hilden, NRW, Germany) and stored at -80°C until further processing. DNA and RNA isolation using the QIAcube system (Qiagen, cat. no. 9001293) in combination with the AllPrep DNA/RNA Micro Kit (Qiagen, cat. no. 80284,) was performed as described previously.[7] cDNA was generated from RNA using the RevertAid H Minus First Strand cDNA Synthesis Kit according to the manufacturer's protocol (Thermo Fisher Scientific, cat. no. K1632). Subsequently, cDNA (0.1 to 1 ng/µL) was pre-amplified for patient-specific targets and/or a multiplex prostate gene expression panel 7 with a Taqman assay covering wildtype and mutant molecules during 15 cycles using TaqMan PreAmp Master Mix (Thermo Fisher Scientific) as recommended by the manufacturer. Prior to downstream processing, the pre-amplified product was diluted 15-fold in LoTE buffer (3 mM Tris-HCl/0.2 mM EDTA, pH 8.0). Gene expression levels were measured in real-time in the pre-amplified samples by qRT-PCR and subsequently analyzed as described previously.[7] For validation of single nucleotide variants (SNVs) in organoids (Supplementary table 2), digital PCR (dPCR) reactions were performed with either the QuantStudio 3D Digital PCR System (Thermo Fisher Scientific) or the Naica™ Crystal Digital PCR System (Stilla Technologies, Villejuif, France) according to the manufacturer's protocol. For the former, each pre-amplified cDNA sample or DNA sample was partitioned into 20,000 wells of a QuantStudio 3D Digital PCR v2 Chip and run on a ProFlex 2x Flat PCR System (Thermo Fisher Scientific). The target-specific optimized PCR program was: 10 min at 96°C, followed

by 40 cycles of 30 sec incubation at 98°C and 2 min at 55°C and a final pause for up to 16 hours at 10°C. Chips were read in a QuantStudio 3D Digital PCR Instrument and analyzed with the web-based Quantstudio 3D dPCR Analysis Software version 3.01 (Thermo Fisher Scientific). For the latter, each pre-amplified cDNA sample or DNA sample was partitioned into 30,000 crystal droplets and amplified by the following program: 45 cycles of 30 sec at 95°C and 15 sec at 58°C. Chips were read in a Naica Prism3 instrument and analyzed with the Crystal Miner software (Stilla Technologies). For both, at least one positive and one negative control sample was included in every run.

Single cell isolation

Single cells were isolated and after whole genome amplification (WGA) sequencing was performed as described in the supplementary material and methods. CellSearch enriched CTCs were sorted by flow cytometry using MoFlo XDP sorter (Beckman Coulter, Germany) and Single cell isolation of organoids was performed using the VyCAP Puncher System (VyCAP, Enschede, The Netherlands) as previously described.[8,9]

Passaging and isolating organoids for phenotyping

For passaging and isolation of early stage organoids, MG droplets were mechanically disrupted and dispensed in a pre-cooled 96-wells plate (Corning, cat. no. 3595). TryplE (Thermo Fisher Scientific, cat. no. 12605010) was added to the wells and incubated at 37°C and organoids were resuspended regularly until the organoids were fractioned. Organoids were collected in cold medium (AdMEM/F12+++), centrifuged at 1200g for 5 min at 4°C and plated as described previously. For cell viability assays, enzymatic disruption was prolonged to acquire mostly single cells and plated at a density of 2500 cells per well in 8 µl of MG in a 96-wells plate. To allow for organoid formation, cells were incubated for seven days with 100 µl media. We used APCOM without Y-27632 and R1881, as this would interfere with treatment induced cell-death and anti-androgen response. Subsequently medium was replaced to contain the appropriate drug/androgen concentration and incubated for another seven days (Enzalutamide Axon Medchem, Groningen, the Netherlands, cat. no 1613; R1881 details in Supplementary table 1 and Taxanes were provided by Sanofi, Paris, France). Cell viability was measured using the CellTiter-Glo® 3D (Promega, cat. no. G9681, Madison, WI), and normalized to untreated controls. MSK-PCa1 and MSK-PCa2 were maintained in the organoid culture media described by Gao et al.[5] and cell viability assays were performed as described above. For cryopreservation, isolated organoids were mixed with 1 mL cooled Recovery™ Cell Culture Freezing Medium (Thermo Fisher Scientific, cat. no. 12648010), stored in a Styrofoam container (Westburg CoolCell LX, cat. no. BCS-405, Leusden, The Netherlands) overnight at -80°C and subsequently transferred to liquid

nitrogen storage. For immunohistochemistry, organoids in MG were formalin fixed for four hours, and subsequently embedded in 4% agarose and paraffin. Four µm section were stained for the expression of the androgen receptor (AR; 1:200, SP107, Cell Marque, Rocklin, CA), prostate specific antigen (PSA ;1:500, N1517, Dako, Santa Clara, CA), CK8/18 (1:150, Ma5-14088, Thermo Fisher Scientific) and ERG (1:100, EPR3864, Abcam, Cambridge, UK) and visualized with DAB/H2O2 (EnVision kit, Dako). Images were obtained using the Olympus BX41 microscope equipped with 2x, 10x, 20x and 40x UPlanFL N objectives, a ColorView III camera and CellB imaging software (version 3.4, Olympus Shinjuku, Tokyo, Japan).

Whole genome sequencing and variant calling of EMC-PCa-41

From six patients, whole genome sequencing (WGS) data from metastatic tissue was present as part of the CPCT-02 study (NCT01855477) and used to identify somatic SNVs for validation studies (Supplementary table 3).[10] EMC-PCa-41 organoids were collected for WGS (passage no 5) in a similar fashion as passaging, washed with cold PBS and dry cell pellets were stored at -80°C. WBCs isolated from DLA were used as matched normal cells for sequencing. DNA isolation and WGS was performed by the Hartwig Medical foundation as previously described.[10] In short, Illumina technology was used for WGS of DNA libraries on the HiSeq X Ten system using paired-end (2x150bp) sequencing (Illumina, San Diego, CA) to a minimum sequencing depth of 30x and 60x for the matched normal and tumor sample respectively. The human reference genome (GRCh37) was used for alignment and post-processing and subsequent somatic analysis for variants (SNVs, small insertion/deletions and multi-nucleotide variants), copy number alterations (CNA), structural variants was performed as previously described.[10,11]

Single cell isolation, whole genome amplification and sequencing of CTCs and single cells from organoids

For single cell isolation we used fresh DLA product diluted in CellSearch dilution buffer, collected in a CellSave tube and processed within 96 hours, or stored DLA product which was thawed before processing. Samples were processed on the CellSearch system as described above. CellSearch cartridges were stored in the dark at 4°C before further analyses. Isolation of single CTCs, defined as DAPIpos/CKpos/CD45neg cells, and single white blood cells WBCs, defined as DAPIpos/CKneg/CD45pos, was performed by flow cytometry using MoFlo XDP sorter (Beckman Coulter, Germany) as previously described.[8] Single cells were sorted into individual empty PCR tubes and stored at -20 °C until analysis. Single cell isolation of organoids was performed using the VyCAP Puncher System (VyCAP, Enschede, The Netherlands), combining a silicon chip with microwells, fluorescence

imaging, and a punching method to isolate and transfer the single cells to standard reaction tubes as previously described.[9] Subsequent whole genome amplification (WGA) for all picked/sorted single cells was performed using adapter-linker PCR as previously described,[12,13] and commercialized as Ampli1™ WGA Kit by Menarini Sillicon Biosystems. Ampli1™ LowPass kit for Illumina (Menarini Silicon Biosystems, Bologna, Italy) was used for preparing low-pass WGS libraries at Menarini Silicon Biosystem facilities. For high-throughput processing, the manufacturer procedure was implemented in a fully automated workflow on a STARlet Liquid Handling Robot (Hamilton, Reno, NV, USA). Resulting libraries were sequenced on HiSeq instrument (Illumina, Hayward, CA, USA) and the obtained FASTQ files were aligned to the human reference genome (GRCH37) sequence using Burrows-Wheeler Aligner version 0.7.12 (BWA).[14] Quality control (QC) included read count distribution and derivative log ratio spread as described previously,[15] two CTCs from subject 41 failed to pass QC. CNA in the data were identified using Control-FREEC software (version 11.0) and ploidy level was analyzed using the MSBiosuite pipeline based on best fitting of profiles to underlying copy number levels.[16]

Validation of single cell sequencing

Validation of single cell sequencing was performed by Sanger sequencing of known SNVs from subject 25 and 41, identified in WGS of the patient's tumor or patient derived organoid cell line resp. In short, a nested PCR strategy was used to amplify genomic regions with known SNVs from the single cell WGA product (supplementary table 4). PCRs were performed using Phusion High-Fidelity DNA polymerase (Thermo Fisher Scientific, cat. no. F530) and the final product was purified (QIAquick PCR purification kit, Qiagen, cat. no. 28104). The amplicons were Sanger sequenced (Macrogen Europe, Amsterdam, The Netherlands) and results were analyzed using pairwise alignment with the reference gene (BLAST, NCBI). CTCs and organoids samples that did not harbor any tumor specific SNVs were excluded, WBC served as negative controls.

Bioinformatics analysis of single cell copy number alterations

For the clustering of the complete dataset (Supplementary figure 6) we used the median ratio obtained by the Control-FREEC software, normalized each profile on fixed bins length (weighted mean on 0.25 Megabase (Mb) bins) and calculate the $\log_2$ values. Subsequently, after setting the minimum value to -2 and maximum value to 2, hierarchical clustering of profiles was performed, using "Euclidean" distance metric and "ward" clustering method. For clustering the validated tumor cell profiles, absolute copy-numbers were binned into 0.01 Mb bins which were subsequently annotated by the mean copy-number of overlapping copy-number segments and rounded to the nearest integer. These bins (0.01

Mb) were used as input for t-SNE (θ = 0.5 with a perplexity of 2) using the Rtsne package (v0.15).[17] Subsequent clustering of the t-SNE results, outputted as two dimensions, was performed using the k-nearest neighbor algorithm (k = 15) and the Louvain method for community detection, as implemented by the igraph package (v1.2.5) from the statistical platform R (v3.6.1).[18,19] Per cluster, a consensus copy-number profile was generated by adopting the median copy-number value per bin (0.01 Mb) over all samples captured within the respective cluster. Within the consensus copy-number profiles, the maximum absolute copy-number was capped to 8.

Statistical analysis

Sample size calculation for the patient inclusion is described in the attached clinical protocol. For comparison of CTC count in PB samples obtained at screening versus before the DLA procedure, CTC yield in low versus high density fraction enrichment by DLA, CTC yield and WBC depletion after WBC depletion with or without EpCAM enrichment we used a paired, two-sided Wilcoxon-rank test due to the non-normality of the data. Data visualization and statistical testing were performed using the statistical platform R (version 3.6.1)[19] or Graphpad Prism (version 5.01, GraphPad Software, San Diego, CA), we considered statistical significance with $P<0.05$.

Code availability

For the tools and scripts used for analyzing the organoid cell line WGS data, we refer to the previous report of L. van Dessel and J. van Riet et al., other tools and scripts will be made available upon request.[11]

Data availability

The CTC derived organoid cell line EMC-PCa-41 will be made available to academic institutions under the Erasmus MC Biological Uniform Material Transfer Agreement. The WGS data from metastatic biopsies were part of the CPCT-02 study, which has been made available by the Hartwig Medical Foundation. Both WGS and clinical data are freely available for academic use from the Hartwig Medical Foundation through standardized procedures and request forms can be found at
https://www.hartwigmedicalfoundation.nl. The WGS data from the organoid cell line as analyzed in this manuscript will be made available at publication.

References

1. Simon R. Optimal two-stage designs for phase II clinical trials. Controlled Clinical Trials. 1989;10(1):1-10.
2. Eisenhauer EA, Therasse P, Bogaerts J, et al. New response evaluation criteria in solid tumours: revised RECIST guideline (version 1.1). Eur J Cancer. 2009;45(2):228-247.
3. Scher HI, Morris MJ, Basch E, Heller G. End points and outcomes in castration-resistant prostate cancer: from clinical trials to clinical practice. J Clin Oncol. 2011;29(27):3695-3704.
4. Marques RB, Erkens-Schulze S, de Ridder CM, et al. Androgen receptor modifications in prostate cancer cells upon long-termandrogen ablation and antiandrogen treatment. Int J Cancer. 2005;117(2):221-229.
5. Gao D, Vela I, Sboner A, et al. Organoid cultures derived from patients with advanced prostate cancer. Cell. 2014;159(1):176-187.
6. Beshiri ML, Tice CM, Tran C, et al. A PDX/organoid biobank of advanced prostate cancers captures genomic and phenotypic heterogeneity for disease modeling and therapeutic screening. Clin Cancer Res. 2018.
7. Sieuwerts AM, Mostert B, van der Vlugt-Daane M, et al. An In-Depth Evaluation of the Validity and Logistics Surrounding the Testing of AR-V7 mRNA Expression in Circulating Tumor Cells. Journal of Molecular Diagnostics. 2018;20(3):316-325.
8. Neves RP, Raba K, Schmidt O, et al. Genomic high-resolution profiling of single CKpos/CD45neg flow-sorting purified circulating tumor cells from patients with metastatic breast cancer. Clin Chem. 2014;60(10):1290-1297.
9. Andree KC, Abali F, Oomens L, et al. Self-Seeding Microwells to Isolate and Assess the Viability of Single Circulating Tumor Cells. Int J Mol Sci. 2019;20(3).
10. Priestley P, Baber J, Lolkema MP, et al. Pan-cancer whole-genome analyses of metastatic solid tumours. Nature. 2019;575(7781):210-216.
11. van Dessel LF, van Riet J, Smits M, et al. The genomic landscape of metastatic castration-resistant prostate cancers reveals multiple distinct genotypes with potential clinical impact. Nature Communications. 2019;10(1):5251.
12. Klein CA, Schmidt-Kittler O, Schardt JA, Pantel K, Speicher MR, Riethmuller G. Comparative genomic hybridization, loss of heterozygosity, and DNA sequence analysis of single cells. Proceedings of the National Academy of Sciences of the United States of America. 1999;96(8):4494-4499.
13. Stoecklein NH, Erbersdobler A, Schmidt-Kittler O, et al. SCOMP is superior to degenerated oligonucleotide primed-polymerase chain reaction for global amplification of minute amounts of DNA from microdissected archival tissue samples. Am J Pathol. 2002;161(1):43-51.
14. Li H, Durbin R. Fast and accurate short read alignment with Burrows-Wheeler transform. Bioinformatics. 2009;25(14):1754-1760.
15. Ferrarini A, Forcato C, Buson G, et al. A streamlined workflow for single-cells genome-wide copy-number profiling by low-pass sequencing of LM-PCR whole-genome amplification products. PLoS One. 2018;13(3):e0193689.
16. Boeva V, Popova T, Bleakley K, et al. Control-FREEC: a tool for assessing copy number and allelic content using next-generation sequencing data. Bioinformatics. 2012;28(3):423-425.
17. van der Maaten L. Accelerating t-SNE using Tree-Based Algorithms. J Mach Learn Res. 2014;15:3221-3245.
18. Csardi G, Nepusz T. The Igraph Software Package for Complex Network Research. InterJournal.

2005;Complex Systems:1695.
19. R: A Language and Environment for Statistical Computing [computer program]. Version Version 1.1.463. Vienna, Austria: R Foundation for Statistical Computing; 2019.

Part III

General Dicussion and Summary

Chapter VII

General Discussion and Summary

Part I Impact of androgens and AR signaling on taxane treatment efficacy

The therapeutic landscape of metastatic prostate cancer (mPCa) has been transformed in the past two decades. Until 2004 androgen deprivation therapy (ADT) was the only effective treatment for patients with mPCa. Since then, taxane chemotherapeutics, androgen receptor signaling targeted inhibitors and combination strategies have been introduced. This has substantially improved the outlook of mPCa patients, as illustrated by a recent report by the Dutch Cancer registry (IKNL). The median overall survival after diagnosis of metastatic disease, increased from 26.5 to 37.2 months between 2004-2008 and 2014-2018, respectively.[1] The landmark CHAARTED and STAMPEDE studies have paved the way for combination treatments in hormone sensitive PCa (HSPC) patients when they showed that adding docetaxel to ADT induces a strong survival benefit.[2,3] These findings have been implemented into the daily clinical practice of mPCa, although an underlying mechanisms for greater efficacy of the combination treatment remains unresolved. Preclinical research into clinical findings has previously been able to reveal drivers of PCa which subsequently provided opportunity for targeted approaches. The greater impact of docetaxel in a setting where ADT effectively suppresses androgen receptor (AR) signaling led us to hypothesize that the AR pathway and AR signaling directly interacts with taxane anti-tumor activity. In part I of this thesis we showed that AR signaling and AR targeted agents determine taxane treatment efficacy.

Testosterone interferes with taxane tumor accumulation

Using an AR positive model of castration resistant PCa (CRPC) we showed that testosterone interferes with cabazitaxel and docetaxel activity (**Chapter II and III**). Under castrate conditions, both docetaxel and cabazitaxel treatment induced long-term regression in the PC346C-DCC-K tumor model. In contrast, the activity of the taxane chemotherapeutics was negated in the presence of testosterone. To dissect the underlying mechanisms, we first examined taxane pharmacokinetics and tumor accumulation, which are key steps in achieving optimal treatment exposure (Figure 1, top panels). Testosterone supplementation did not impact taxane plasma levels but strongly reduced tumor accumulation levels (Chapter II). The impact of impaired taxane tumor accumulation on activity has been exemplified by a previous publication from our lab.[4] Here, we showed that docetaxel resistant xenografts had strongly diminished taxane tumor accumulation in comparison to their docetaxel-sensitive counterparts. Subsequent transcriptomics analyses identified numerous differentially expressed genes in the docetaxel resistant xenograft, including loss of *SLCO1B3*.[5]

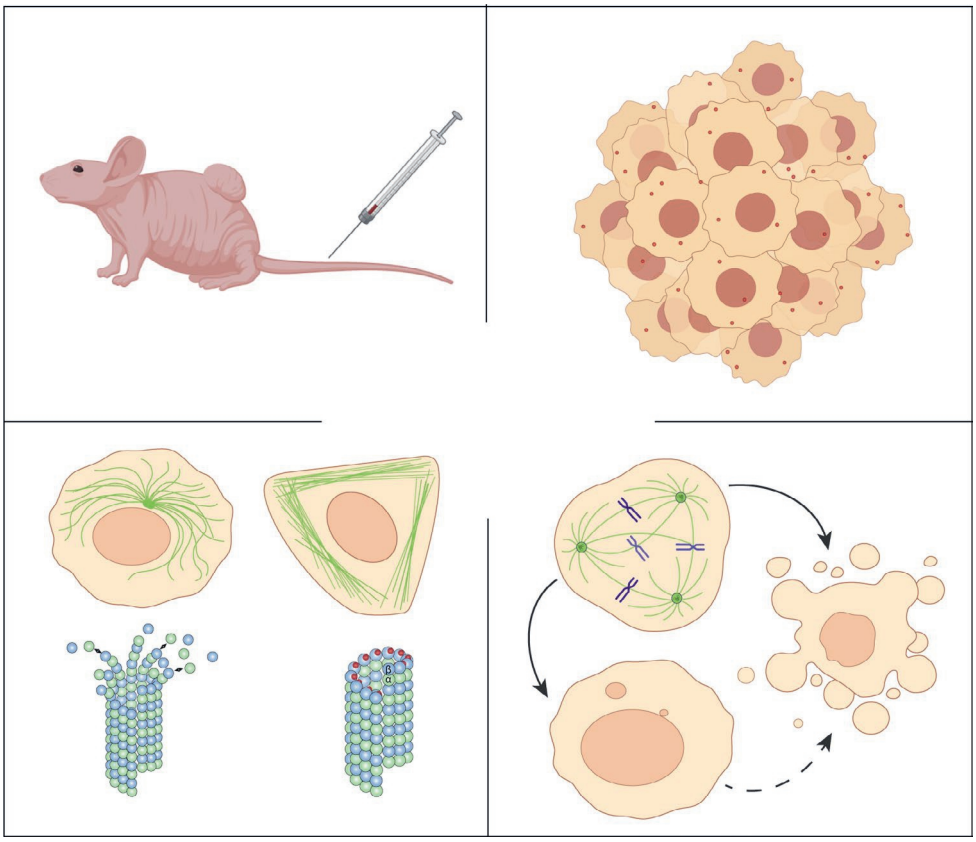

Figure 1: A representation of taxane pharmacodynamics. After administration of the chemotherapeutic (top left), taxanes accumulate into the tumor tissue and cells (top right). Taxanes bind to the beta subunit of tubulins, which leads to stabilization of microtubule filaments (bottom left). Microtubule stabilization impedes accurate chromosome segregation in mitosis leading to cell cycle stalling (bottom right). This may directly result in apoptosis or (cancer) cells can slip out of mitosis without completing cell division. Our results suggest that these cells could die during secondary mitosis which can be enhanced by AR directed treatment. Figure made using Biorender.

This transporter is of high interest as substrates for OATP1B3 (encoded by *SLCO1B3*) uptake include taxane chemotherapeutics and testosterone. We therefore hypothesized that testosterone might interfere with docetaxel uptake by OATP1B3 leading to impaired tumor accumulation. Using drug-uptake assays we demonstrated that testosterone competes with docetaxel for OATP1B3 mediated uptake, which reduced docetaxel accumulation (Chapter III). We thereby provided a possible mechanism of impaired docetaxel tumor accumulation in the presence of testosterone.

Given the combined use of docetaxel with ADT, even in CRPC patients, the impact of testosterone on OATP1B3 mediated docetaxel uptake might be limited due to low levels of circulating testosterone. In castration resistant disease, AR signaling is frequently reinstated to promote proliferation This can be achieved by AR alterations and alternative androgen production through upregulation of adrenal enzymes such as 17β-HSD.[6] As a result, testosterone levels are elevated in metastatic tissue samples and sufficient to promote AR signaling.[6,7] This suggests that testosterone could interfere with docetaxel tumor accumulation in CRPC. This mechanism could then be counteracted by abiraterone, which inhibits the CYP17A enzyme and further suppresses androgen levels.[6,8] Interestingly, abiraterone has also been described as substrate for OATP1B3 uptake and potentially competes with docetaxel uptake.[8] Taken together, these observations suggest that uptake competition mechanisms play a role in treatment efficacy and could disturb taxane tumor accumulation, although clinical validation is warranted.

Taxane target engagement as biomarker for treatment efficacy

The impact of testosterone levels on taxane exposure and tumor accumulation likely impairs taxane target engagement (Figure 1, bottom left panel). Taxanes function by blocking tubulin depolymerization, which leads to stabilization of microtubule filaments. Target engagement can be assessed by immunoblotting of acetylated-α-tubulin, a post-translation modification following microtubule stabilization. We found that acetylated-α-tubulin levels were somewhat reduced in tumor samples obtained from docetaxel treated and testosterone supplemented mice, which correlated with impaired docetaxel accumulation (Chapter III). To accurately assess the relationship between taxane tumor accumulation, target engagement and activity we require more sensitive assays. One such detection method is CETSA (cellular thermal shift assay). CETSA examines taxane target binding with high specificity and sensitivity *in vitro*, as well as in tissue samples.[9] We applied CETSA to PCa docetaxel resistant xenograft models with underlying impaired drug accumulation and identified decreased target binding as compared to docetaxel-naïve counterparts (**Chapter IV**). The clinical feasibility of CETSA was explored using fine needle aspirations obtained from breast cancer patients, where it revealed high inter-

patient heterogeneity in paclitaxel target engagement.

The application of CETSA on clinical samples offers an opportunity to investigate the relationship between taxane pharmacokinetics, tumor accumulation, target engagement and treatment outcome in cancer patients. Although variation in taxane pharmacokinetics have been well-described, little is known about the factors that define tumor accumulation and microtubule stabilization.[10] CETSA may provide insight into the limited efficacy of docetaxel rechallenge in mCRPC patients that previously received chemohormonal treatment for HSPC. A retrospective analysis of the GETUG-AFU 15 trial showed that docetaxel treatment induced a PSA response in 14% of the CRPC patient who progressed on chemohormonal treatment as compared to 45% of the patients who received ADT alone.[11] Investigating taxane tubulin binding may help identify whether docetaxel rechallenges fails because of reduced tumor accumulation and/or target engagement. A subsequent effective treatment for these patients could be to switch to cabazitaxel. Preclinical cell line studies have shown that cabazitaxel more effectively accumulates into tumor cells and stabilizes microtubules compared to docetaxel, which could explain the treatment efficacy of cabazitaxel in docetaxel refractory patients.[12] Concluding, CETSA provides a method to accurately quantify taxane target binding and offers further insight into treatment dynamics and outcome in cancer patients.

AR signaling determines taxane treatment efficacy

In addition to impaired taxane tumor accumulation, testosterone may deminish taxane activity through the AR pathway. Supplementing mice with testosterone strongly promoted androgen signaling in the AR positive PC346C-DCC-K xenograft model, as shown by increased PSA release and transcriptional activity (Chapter III). Using two *in vitro* AR positive CRPC models, we confirmed that AR stimulation increased viability in docetaxel exposed cells. Subsequently, we re-supplemented castrate mice with testosterone after docetaxel induced long-term tumor regression, leading to rapid outgrowth of the vast majority of these small and dormant tumors. We concluded that AR signaling impairs taxane activity, therefore continued blockade of androgen signaling is vital to sustained taxane treatment efficacy.

Based on the results described in Chapter II and III, we hypothesized that taxane anti-tumor activity can be improved by an AR signaling targeted agent. We therefore investigated the combined anti-tumor efficacy of enzalutamide with cabazitaxel as compared to both mono-treatments (**Chapter V**). The AR positive CRPC model PC346C-DCC-K is responsive to cabazitaxel treatment, although rapid tumor progression was invariably observed in non-castrate mice. Enzalutamide as a mono-treatment did not inhibit or delay tumor

growth, although a clear reduction in PSA plasma levels implied adequate AR inhibition by enzalutamide. Combining enzalutamide with cabazitaxel inferred greater anti-tumor activity than cabazitaxel alone. The efficacy of this combination was validated in a second enzalutamide resistant VCaP xenograft model. To dissect the underlying mechanism of enhanced cabazitaxel activity, we examined differential gene expression inferred by enzalutamide in PC346C-DCC-K tumors. Transcriptomic analysis confirmed that AR signaling was suppressed in enzalutamide treated tumors despite sustained proliferation. Unfortunately, no significant compensatory mechanism was identified that could sustain proliferation in the presence of AR pathway suppression. Blocking AR signaling lead to downregulation of metabolic enzymes that could compromise the overall fitness of cancer cells. Hypothetically, taxane induced mitotic disruptions and subsequent multinucleation combined with disruption of energy homeostasis could enhance anti-tumor efficacy (Figure 1, bottom right). Live cell imaging analysis confirmed that cabazitaxel treatment resulted in abnormal mitosis and improper segregation of the genetic material, which initially did not trigger apoptosis. The addition of enzalutamide, did enhance the activation of apoptosis in cells that survived the primary abnormal cell division. Overall, targeting AR signaling was shown to increase cabazitaxel efficacy even in models where enzalutamide treatment could not effectively block proliferation.

PSA plasma levels are widely used as a biomarker in PCa, especially in patients with metastatic disease where PSA dynamics inform on tumor burden and treatment response.[13] In patients receiving AR signaling directed treatment, PSA response can be a direct effect of repressed AR transcriptional activity. Indeed, PSA decline strongly correlates with progression free survival in enzalutamide treated patients.[14] In almost 90% of the CRPC patients, first-line enzalutamide treatment induced at least a 30% decline in PSA levels. This suggests that at least some level of AR signaling suppression is achieved in the vast majority of patients and could potentiate cabazitaxel efficacy. Interestingly, in 10-30% of enzalutamide treated patients PSA dynamics did not predict radiographic response, as disease progression was observed within 6 to 12 months.[14,15] These observations hint that the AR pathway is still effectively suppressed in a subset of patients that develop enzalutamide resistance. A similar phenomenon was observed in the enzalutamide resistant xenograft models where PSA levels declined after treatment initiation (Chapter V).

The potential greater efficacy of combining taxanes with AR signaling directed treatments for advanced PCa is currently investigated in several phase II/III clinical trials.[16] Previously, docetaxel-based combinations with anti-angiogenic, immunotherapy and microenvironment targeted agents have been evaluated in clinical trials.[16] Unfortunately, the addition of these novel compounds failed to show a significant survival benefit for CRPC

patients in large phase III clinical studies. The underlying reason for the negative outcome has been ascribed to overall lack of efficacy, increased toxicity leading to treatment discontinuation and absence of biomarkers to select the right patient population.[17-19] For example, the use of a dual inhibitor of SRC family kinases and the pro-apoptotic protein ABL appeared a promising strategy for PCa. Preclinical studies showed encouraging results but failed to provide a mechanistic interaction for combining with docetaxel.[20,21] This might have contributed to the negative outcome of the large multi-center phase III clinical study.[17] Future clinical trials should focus on combination strategies that are based on a mechanistic interaction to enhance taxane activity or vice versa. To support this, we should focus on dissecting the mechanism of action that taxanes invoke in patients. The impact of taxane chemotherapeutics on tubulin dynamics, cell cycle progression and mitotic cell death has been extensively described in cultured cells, but validation using patient tumor tissue is rare. A breast cancer study suggested that the therapeutic efficacy of taxane is independent of cell cycle stalling and subsequent mitotic catastrophe. The intra-tumor paclitaxel concentrations reached in breast cancer patients did not induce mitotic arrest in cultured cells, although viability was effectively compromised through long-term exposure.[22] Gaining mechanistic insight into taxane efficacy in a clinically relevant setting could provide a framework to select treatment combinations. Our results showed that androgens and AR signaling determine the outcome of taxane treatment, which provided a substantial basis for combining a taxane with AR signaling directed agent. The improved anti-tumor efficacy of adding enzalutamide to cabazitaxel confirmed that AR signaling impacts taxane activity both *in vitro* and *in vivo*. Our results also suggest that targeting AR signaling could enhance cabazitaxel efficacy in enzalutamide refractory patients. Overall, Part I of this thesis provides mechanistic insight and subsequent validation for targeting AR signaling in taxane treated patients that fits within the current treatment landscape of CRPC.

Part II Optimizing personalized cancer treatment using CTC derived organoids

With the addition of ADT based combination treatments for HSPC and potential expansion of the CRPC treatment repertoire, defining the optimal treatment for the individual patient at the right moment has become increasingly complex. Predictive and prognostic biomarkers can be used to guide treatment selection and asses response in the individual patient. The use of liquid biopsies, such circulating tumor cells (CTC) and circulating tumor DNA (ctDNA) represent opportunities in the biomarker field.[23] In addition to the prognostic value of CTC numbers to indicate tumor burden, presence of the AR splice variant 7 (AR-V7) in CTCs has shown to correlate with response to AR signaling targeted treatments. A prospective clinical trial in high-risk CRPC patients treated with abiraterone or enzalutamide confirmed that AR-V7 status at baseline was a strong predictor of poor response.[24] At disease progression the percentage of AR-V7 positive patients had increased, suggestive of selection or adaptation of resistant tumor cells, although the majority of the patients remained negative. Moreover, other treatment resistance mechanisms contribute to disease progression in patients receiving AR signaling directed treatments, which are currently not evaluated. In addition there are currently no predictive biomarkers for response to taxane treatment ready for daily clinical practice. An interesting alternative to biomarker based treatment selection that incorporates both genotypic and phenotypic tumor characteristics is the use of patient derived tumor cells for *ex vivo* expansion and treatment screening. In addition, the cultivation of tumor cells as organoids provides a model that more accurately represents the complexity of cancer. Organoids maintain a 3D organization which reflects the tumor morphology more closely and stem cell factors promote phenotypical heterogeneity, which offers an improved models from classical 2D cell lines.[25] This concept has been applied to other cancer types, such as gastro-intestinal where patient-derived organoids reflected the response to chemotherapy.[26] For PCa this has been more challenging due to the low-proliferative capacity, contamination of normal cells and limited availability of tissue samples from metastatic patients.

Alternatively, CTCs can be expanded as patient-derived organoids as sampling provides a less invasive alternative for metastatic patients.[27,28] The major limitation of using CTCs for *ex vivo* expansion lies in the number of tumor cells obtained from a single sample, as the median CTC count in metastatic cancer patients typically ranges between 0-20 cells per 7.5 mL of peripheral blood (PB). Studies thus far have suggested that successful *ex vivo* organoid expansion is limited to samples containing several hundred CTCs.[27,28] Diagnostic leukapheresis (DLA) may be used as a method to enrich mononuclear cells from the peripheral blood stream, which include CTCs in metastatic cancer patients.[29] A platform that incorporates CTC sampling and *ex vivo* organoid expansion could provide treatment screening that reflects the current disease state of the patient. We performed a prospective clinical study (CIRCLE) to assess the feasibility of DLA to enrich CTCs, provide biomaterial for organoid culture and perform subsequent treatment screening in mPCa (**Chapter VI**).

In the CIRCLE study 102 mPCa patients were screened for study participation. After selecting patients with ≥5 CTC per 7.5 mL peripheral blood and fit to undergo the DLA procedure, we obtained enriched CTC samples from 40 patients. DLA was generally safe, and provided a 240-fold enrichment of CTCs compared to PB samples. We obtained pre- and post-treatment samples from four patients, which opens up the possibility to study cancer evolution and adaptation to treatment. As DLA enriches for mononuclear cells, stringent methods are needed to effectively deplete white blood cells while retaining the majority of the viable CTCs. Using an antibody cocktail based method, we depleted the white blood cell concentration by 3.1 $\log_{10}$-fold while maintaining 46% of the CTCs. This is an improvement in comparison to a previous report, where a similar method yielded a CTC enrichment efficacy of 37%.[30] Unfortunately, this method limited the DLA volume that can be cost-effectively processed to about one fourth of the original product, reducing the yield for subsequent organoid cultures. From the isolated and enriched CTC samples we were able to obtain organoids in 35% of the cultured samples, including one stable organoid line, EMC-PCa-41. Samples that could be propagated as organoids contained significantly higher number of CTCs, implicating that maximizing the number of viable cells obtained contributes to success. Most organoid samples could be maintained for 6-8 weeks before proliferation ceased which provided insufficient biomaterial to perform treatment screening.

Organoids as disease models for cancer

The stable organoid line EMC-PCa-41 enabled us to perform treatment screening, phenotypic and genotypic characterization. Cell viability assays revealed that EMC-PCa-41 displayed enzalutamide resistance, which reflected the patients response to the same treatment. The genetic composition of EMC-PCa-41 showed alterations frequently observed in CRPC, such as whole genome duplication, *AR* amplification and *TMPRSS2-ERG* fusion. *In vitro* models should reflect recurrent driver alterations in the different stages of cancer. However, the currently available PCa cell lines and organoid models that were propagated directly from patient samples, have been obtained from metastatic tissue. We therefore examined whether the somatic alterations frequently identified in mCRPC are reflected in EMC-PCa-41, the MSK organoid panel and the four classical PCa cell lines (Table 1).[27,31,32] The most common alterations identified in mCRPC patients, inactivation of TP53 and PTEN, amplification of AR, MYC and the fusion of TMPRSS2-ERG are relatively well represented in the PCa models. Although some alterations are underrepresented, such as *AR* amplifications and *TMPRSS2-ERG* fusions, while alterations in *TP53* and *PTEN* are seemingly overrepresented. Inactivation of TP53 interferes with apoptosis, senescence and cell cycle stalling in response to different stress signals such as cell DNA damage, which likely benefit cancerous cells exposed to a foreign environment.[33] Amplifications and mutations in the *AR* are less frequently observed *in vitro* compared to the mCRPC patient population. Moreover, lack of AR/KLK3 RNA expression was observed in five of the seven organoid cell lines acquired by Gao et al.[27] EMC-PCa-41 contains a focal amplification of the AR enhancer as the gene itself, a combination of alterations that was identified in almost 60% of the mCRPC patients.[31] The amplification of the AR enhancer and gene body has previously been identified in LNCaP.[31,34] Overall, *in vitro* PCa models that express the AR and model androgen-driven castrate disease are limited. This gap has been expanded by PDX-derived cell lines and CRPC models obtained through *in vitro* exposure to castrate conditions, although this does frequently result in AR negative clones. Therefore, our addition to the current *in vitro* model repertoire of AR positive CRPC is evident.

Table 1: Representation of recurrent somatic variants in PCa cell lines and organoid models. Publicly available data (Cancer Cell line Encyclopedia (CCLE), cBioPortal) obtained from either whole genome, exome sequencing or array-CGH (MSK organoid panel). Somatic alterations include missense mutations, gene amplifications, deletions and fusions (TMPRSS2-ERG). X indicates that an oncogenic alteration is present.

recurrent somatic alterations		MSK organoid panel (Gao et al. 2014, Cell)							Classical cell lines (CCLE)					
	EMC-PCa-41	PCa1	PCa2	PCa3	PCa4	PCa5	PCa6	PCa7	DU145	LNCAP	PC3	VCaP	mCRPC %	*in vitro* %
TP53	X	X	X		X	X			X		X	X	53,3	66,7
AR	X		X							X		X	64,5	33,3
PTEN	X	X	X	X	X	X	X			X	X		46,2	75,0
TMPRSS2-ERG	X	X		X								X	42,6	33,3
MYC (incl. amp 8q)		X	X		X	X	X	X		X	X	X	72,1	75,0
8p del			X	X	X	X	X	X					19,3	50,0
RB1 (incl. del 13q)									X				18,8	8,3
APC										X			17,8	8,3
FOXA1					X			X-	X*	X-			17,3	33,3
PIK3CA													15,7	0,0
SPOP								X					10,7	8,3
CDK12					X								8,1	8,3

*DU145 frameshift deletion in FOXA1 oncogene.

-The biologic significance of the mutation is unknown.

In-depth analysis of the genomic alterations identified in EMC-PCa-41 suggested a lack of clonal heterogeneity, as the lower allele frequency was relatively stable. The presence of multiple clones with unique somatic variant would result in a more even distribution of the lower allele frequency. We therefore investigated genetic heterogeneity using matched single cell sequencing of CTCs and organoids obtained from two CRPC patients. Unfortunately, organoid cells obtained from early stage cultures were misidentified, most likely contaminated white blood cells and thus excluded. Within the CTC pool of both patients, several distinct clones with unique copy-number alterations were identified. These results suggest that the CTCs obtained by DLA capture inter and intra-patient heterogeneity. Whether the intra-patient heterogeneity was maintained upon organoid culture, or lost during extensive propagation should be further explored.

We generated patient derived organoid cultures from 35% of the CTC samples which limited our capacity to perform comprehensive treatment screening PCa organoids. The primary obstacle was the limited proliferative capacity of PCa cells cultured *ex vivo*, which hampers initial organoid expansion, the number of organoids obtained and long-term viability. Recent studies in pancreatic, colorectal and gastro-intestinal cancer have reported ~60-75% success-rate in patient derived organoid expansion.[26,35,36] In contrast, the limited number of studies that reported on patient derived organoids obtained from mPCa showed a success-rate between 7 and 18%.[27,29,37] We obtained sufficient number of organoids to perform treatment sensitivity assays at ~4 months of culture, while a recent colorectal cancer study reported a turn-over for treatment sensitivity screening of 2 weeks.[36] Taken together, for mPCa patients CTC derived organoids do not yet provide an platform for treatment evaluation in the context of personalized medicine.

Single tumor cell based disease modelling

Alternatively, viable CTCs may be directly used to assess response to treatment without *ex vivo* expansion. A direct readout of treatment activity could be based on general markers of cell viability or tailored to the individual drug. For example, treatment activity could be assessed using functional assays for microtubule stabilization, AR nuclear localization or DNA damage repair proficiency.[38,39] If functional assays determine treatment response on a single cell level, this could provide insight into intra-tumor heterogeneity and detect underlying resistance mechanisms. Self-seeding microwells have been used to capture single breast and prostate CTCs, which remain viable for several days and can be used to quantify protein secretion.[40] The seeding procedure ensures single cell capture using punctured microwells and a flow-through, where each cell that enters a well blocks the flow through. In a follow-up project of CIRCLE, DLA will be used to enrich CTCs from HSPC patients and investigate the impact of AR directed treatments on PSA secretion by CTCs, using self-seeding microwells. Potentially single cell PSA secretion can be combined with transcriptomic analysis to examine how CRPC cells cope with blocked AR signaling and how this translates to enzalutamide treatment efficacy. In conclusion, using short-term assays to investigate treatment response in viable CTCs might provide a solution for the limited success rate of *ex vivo* PCa organoid expansion.

One of the main challenges in oncology is the emergence of (pre-existing) treatment resistant sub-clones through Darwinian selection. Applying single cell sequencing on CTCs obtained through serial sampling could help to identify emerging treatment resistant clones. In addition single cell based techniques will provide a more comprehensive insight into intra-tumor heterogeneity than deconvolution of bulk tumor tissue samples.[41] We performed single cell low-coverage DNA sequencing on two enriched CTC pools obtained from CRPC patients. Copy number status was used to define clusters within the 18-21 CTCs obtained in each sample and to assess heterogeneity. Single cell sequencing and whole genome amplification of CTCs had a ~70% success-rate with 85% of the sequenced cells passing quality control and validation. This shows that a substantial CTCs pool has to be isolated to generate significant insight into intra-tumor heterogeneity, which can be more easily obtained from enriched samples obtained by DLA. Previous studies using multiregional biopsy sampling at autopsy, have shown that mPCa harbors substantial intra-patient heterogeneity and revealed complex seeding routes.[42,43] Such genetic heterogeneity will likely contribute to disease progression. Indeed, phylogenetic reconstruction of localized PCa revealed multi-clonality correlated with disease recurrence.[44] In addition, single cell RNA-sequencing identified upregulation of Wnt signaling in mPCa patients receiving enzalutamide treatment which impaired enzalutamide activity *in vitro*.[45] Our study showed that DLA resulted in a 240-fold

enrichment of CTCs in mPCa patients thus providing sufficient number of tumor cells to accurately determine intra-patient heterogeneity. Previous studies have also shown that CTCs can be identified in DLA samples obtained from patients with no tumor cells in peripheral blood samples. This provides the opportunity to trace back emerging treatment resistant subclones. Taken together, Part II of this thesis offers optimized CTC enrichment techniques which facilitate their use in single cell based characterization and describes the establishment of one stable CTC-based organoid line.

The research presented in this thesis provides a step forward in bench-to-bedside and bedside-to-bench solutions for mPCa.

References

1. H. F, M. A, L B, et al. uitgezaaide kanker in beeld. Integraal Kankercentrum Nederland;2020.
2. Sweeney CJ, Chen YH, Carducci M, et al. Chemohormonal Therapy in Metastatic Hormone-Sensitive Prostate Cancer. N Engl J Med. 2015;373(8):737-746.
3. James ND, Sydes MR, Clarke NW, et al. Addition of docetaxel, zoledronic acid, or both to first-line long-term hormone therapy in prostate cancer (STAMPEDE): survival results from an adaptive, multiarm, multistage, platform randomised controlled trial. Lancet. 2016;387(10024):1163-1177.
4. de Morree E, van Soest R, Aghai A, et al. Understanding taxanes in prostate cancer; importance of intratumoral drug accumulation. Prostate. 2016;76(10):927-936.
5. de Morree ES, Bottcher R, van Soest RJ, et al. Loss of SLCO1B3 drives taxane resistance in prostate cancer. Br J Cancer. 2016;115(6):674-681.
6. Snaterse G, Visser JA, Arlt W, Hofland J. Circulating steroid hormone variations throughout different stages of prostate cancer. Endocr Relat Cancer. 2017;24(11):R403-R420.
7. Montgomery RB, Mostaghel EA, Vessella R, et al. Maintenance of intratumoral androgens in metastatic prostate cancer: a mechanism for castration-resistant tumor growth. Cancer Res. 2008;68(11):4447-4454.
8. Mostaghel EA, Cho E, Zhang A, et al. Association of Tissue Abiraterone Levels and SLCO Genotype with Intraprostatic Steroids and Pathologic Response in Men with High-Risk Localized Prostate Cancer. Clinical Cancer Research. 2017.
9. Prabhu N, Dai L, Nordlund P. CETSA in integrated proteomics studies of cellular processes. Current Opinion in Chemical Biology. 2020;54:54-62.
10. Nieuweboer AJ, de Morree ES, de Graan AJ, Sparreboom A, de Wit R, Mathijssen RH. Inter-patient variability in docetaxel pharmacokinetics: A review. Cancer Treat Rev. 2015;41(7):605-613.
11. Lavaud P, Gravis G, Foulon S, et al. Anticancer Activity and Tolerance of Treatments Received Beyond Progression in Men Treated Upfront with Androgen Deprivation Therapy With or Without Docetaxel for Metastatic Castration-naïve Prostate Cancer in the GETUG-AFU 15 Phase 3 Trial. European Urology. 2018;73(5):696-703.
12. Azarenko O, Smiyun G, Mah J, Wilson L, Jordan MA. Antiproliferative mechanism of action of the novel taxane cabazitaxel as compared with the parent compound docetaxel in MCF7 breast cancer cells. Mol Cancer Ther. 2014;13(8):2092-2103.
13. Armstrong AJ, Garrett-Mayer E, Ou Yang Y-C, et al. Prostate-Specific Antigen and Pain Surrogacy Analysis in Metastatic Hormone-Refractory Prostate Cancer. Journal of Clinical Oncology. 2007;25(25):3965-3970.
14. Armstrong AJ, Lin P, Higano CS, et al. Prognostic Association of Prostate-specific Antigen Decline with Clinical Outcomes in Men with Metastatic Castration-resistant Prostate Cancer Treated with Enzalutamide in a Randomized Clinical Trial. European Urology Oncology. 2019;2(6):677-684.
15. Bryce AH, Alumkal JJ, Armstrong A, et al. Radiographic progression with nonrising PSA in metastatic castration-resistant prostate cancer: post hoc analysis of PREVAIL. Prostate Cancer and Prostatic Diseases. 2017;20(2):221-227.
16. Corn PG, Agarwal N, Araujo JC, Sonpavde G. Taxane-based Combination Therapies for Metastatic Prostate Cancer. Eur Urol Focus. 2019;5(3):369-380.
17. Araujo JC, Trudel GC, Saad F, et al. Docetaxel and dasatinib or placebo in men with metastatic

castration-resistant prostate cancer (READY): a randomised, double-blind phase 3 trial. The Lancet Oncology. 2013;14(13):1307-1316.
18. Tannock IF, Fizazi K, Ivanov S, et al. Aflibercept versus placebo in combination with docetaxel and prednisone for treatment of men with metastatic castration-resistant prostate cancer (VENICE): a phase 3, double-blind randomised trial. Lancet Oncol. 2013;14(8):760-768.
19. Chi KN, Higano CS, Blumenstein B, et al. Custirsen in combination with docetaxel and prednisone for patients with metastatic castration-resistant prostate cancer (SYNERGY trial): a phase 3, multicentre, open-label, randomised trial. Lancet Oncol. 2017;18(4):473-485.
20. Koreckij T, Nguyen H, Brown LG, Yu EY, Vessella RL, Corey E. Dasatinib inhibits the growth of prostate cancer in bone and provides additional protection from osteolysis. Brit J Cancer. 2009;101(2):263-268.
21. Lara PN, Evans CP. Dasatinib and docetaxel in advanced prostate cancer. The Lancet Oncology. 2013;14(13):1248-1249.
22. Zasadil LM, Andersen KA, Yeum D, et al. Cytotoxicity of Paclitaxel in Breast Cancer Is due to Chromosome Missegregation on Multipolar Spindles. Science Translational Medicine. 2014;6(229):229ra243-229ra243.
23. van Dessel LF, Martens JWM, Lolkema MP. Fundamentals of liquid biopsies in metastatic prostate cancer: from characterization to stratification. Current Opinion in Oncology. 2020;32(5):527-534.
24. Armstrong AJ, Halabi S, Luo J, et al. Prospective Multicenter Validation of Androgen Receptor Splice Variant 7 and Hormone Therapy Resistance in High-Risk Castration-Resistant Prostate Cancer: The PROPHECY Study. Journal of Clinical Oncology. 2019;37(13):1120-1129.
25. Bleijs M, van de Wetering M, Clevers H, Drost J. Xenograft and organoid model systems in cancer research. EMBO J. 2019;38(15):e101654.
26. Vlachogiannis G, Hedayat S, Vatsiou A, et al. Patient-derived organoids model treatment response of metastatic gastrointestinal cancers. Science. 2018;359(6378):920-926.
27. Gao D, Vela I, Sboner A, et al. Organoid cultures derived from patients with advanced prostate cancer. Cell. 2014;159(1):176-187.
28. Cayrefourcq L, Mazard T, Joosse S, et al. Establishment and characterization of a cell line from human circulating colon cancer cells. Cancer Res. 2015;75(5):892-901.
29. Lambros MB, Seed G, Sumanasuriya S, et al. Single-Cell Analyses of Prostate Cancer Liquid Biopsies Acquired by Apheresis. Clin Cancer Res. 2018;24(22):5635-5644.
30. Andree KC, Mentink A, Zeune LL, et al. Toward a real liquid biopsy in metastatic breast and prostate cancer: Diagnostic LeukApheresis increases CTC yields in a European prospective multicenter study (CTCTrap). Int J Cancer. 2018;143(10):2584-2591.
31. van Dessel LF, van Riet J, Smits M, et al. The genomic landscape of metastatic castration-resistant prostate cancers reveals multiple distinct genotypes with potential clinical impact. Nature Communications. 2019;10(1):5251.
32. Ghandi M, Huang FW, Jané-Valbuena J, et al. Next-generation characterization of the Cancer Cell Line Encyclopedia. Nature. 2019;569(7757):503-508.
33. Aubrey BJ, Kelly GL, Janic A, Herold MJ, Strasser A. How does p53 induce apoptosis and how does this relate to p53-mediated tumour suppression? Cell Death Differ. 2018;25(1):104-113.
34. Takeda DY, Spisák S, Seo JH, et al. A Somatically Acquired Enhancer of the Androgen Receptor Is a Noncoding Driver in Advanced Prostate Cancer. Cell. 2018;174(2):422-432 e413.
35. Tiriac H, Belleau P, Engle DD, et al. Organoid Profiling Identifies Common Responders to Chemotherapy in Pancreatic Cancer. Cancer Discov. 2018;8(9):1112-1129.

36. Ooft SN, Weeber F, Dijkstra KK, et al. Patient-derived organoids can predict response to chemotherapy in metastatic colorectal cancer patients. Sci Transl Med. 2019;11(513).
37. Puca L, Bareja R, Prandi D, et al. Patient derived organoids to model rare prostate cancer phenotypes. Nat Commun. 2018;9(1):2404.
38. Mukhtar E, Worroll D, Galletti G, Schuster S, Piha-Paul SA, Giannakakou P. Quantitative analysis of taxane drug target engagement of microtubules in circulating tumor cells from metastatic castration resistant prostate cancer patients treated with CRXL301, a nanoparticle of docetaxel. Cancer Drug Resist. 2020;3:636-646.
39. Meijer TG, Verkaik NS, Sieuwerts AM, et al. Functional Ex Vivo Assay Reveals Homologous Recombination Deficiency in Breast Cancer Beyond BRCA Gene Defects. Clin Cancer Res. 2018;24(24):6277-6287.
40. Andree KC, Abali F, Oomens L, et al. Self-Seeding Microwells to Isolate and Assess the Viability of Single Circulating Tumor Cells. Int J Mol Sci. 2019;20(3).
41. Baslan T, Hicks J. Unravelling biology and shifting paradigms in cancer with single-cell sequencing. Nat Rev Cancer. 2017;17(9):557-569.
42. Gundem G, Van Loo P, Kremeyer B, et al. The evolutionary history of lethal metastatic prostate cancer. Nature. 2015;520(7547):353-357.
43. Woodcock DJ, Riabchenko E, Taavitsainen S, et al. Prostate cancer evolution from multilineage primary to single lineage metastases with implications for liquid biopsy. Nat Commun. 2020;11(1):5070.
44. Espiritu SMG, Liu LY, Rubanova Y, et al. The Evolutionary Landscape of Localized Prostate Cancers Drives Clinical Aggression. Cell. 2018;173(4):1003-1013 e1015.
45. Miyamoto DT, Zheng Y, Wittner BS, et al. RNA-Seq of single prostate CTCs implicates noncanonical Wnt signaling in antiandrogen resistance. Science. 2015;349(6254):1351-1356.

Chapter VIII

Nederlandse samenvatting

Het vooruitzicht voor patiënten met uitgezaaide prostaatkanker is in de laatste twee decennia sterk verbeterd, dit komt voornamelijk door de introductie van nieuwe behandelingen. Een van de recente ontwikkelingen is de combinatie van hormonale therapie, ook wel androgeen deprivatie therapie genoemd, met het chemotherapeuticum docetaxel. Bij androgeen-deprivatie therapie wordt testosteronproductie met medicatie onderdrukt, wat de androgeenreceptor inactiveert en proliferatie van de prostaatkankercellen een halt toeroept. De combinatie van androgeen deprivatie therapie met docetaxel is in staat om ziekte progressie naar het castratie-resistente stadium, waarbij androgeen deprivatie therapie niet meer effectief is, sterk uit te stellen. Deze klinische resultaten suggereren dat de behandeling met docetaxel effectiever is door het wegnemen van testosteron en blokkeren van de androgeenreceptor activiteit. Deze interactie hebben wij in het laboratorium onderzocht om zo inzicht te genereren in de factoren die de effectiviteit van taxaan behandeling beïnvloeden.

In **hoofdstuk II en III** van dit proefschrift hebben wij de interactie tussen testosteron en de effectiviteit van taxaan chemotherapeutica behandeling onderzocht in preklinische modellen van castratie-resistente prostaatkanker. Door tumordragende muizen te behandelen met testosteron, als zowel taxanen, toonden wij aan dat dit androgeen een sterk negatieve impact had op de behandeling. Terwijl in de afwezigheid van testosteron, taxaan behandeling de tumorgroei effectief onderdrukte, was er geen substantiële impact bij gelijktijdige toediening. Verder onderzoek onthulde een verlaagde concentratie van taxanen in de prostaattumoren van muizen met hoge testosteronspiegels, wat correleert met verminderde effectiviteit van de chemotherapie. Vervolgens hebben we in hoofdstuk III aangetoond dat testosteron kan interfereren met de opname van docetaxel via een transport eiwit, dit mechanisme kan de verlaagde taxaan concentraties in tumorcellen verklaren. Taxanen zoals docetaxel functioneren door tubuline eiwitten te binden en stabiliseren, wat de celdeling verstoord. In **hoofdstuk IV** hebben we tubuline-binding als marker voor taxaan-effectiviteit onderzocht. Gebruik makend van een nieuwe methode, genaamd CETSA, konden wij taxaan-resistente tumormodellen onderscheiden van de taxaan-gevoelige. Daarnaast kon CETSA ook worden toegepast op biopten van borstkankerpatiënten, wat het mogelijk maakt om het effect van chemotherapie en de uitkomst van behandeling in patiënten te onderzoeken.

In **hoofdstuk V** hebben we interactie tussen androgeenreceptor activiteit en taxaan behandeling bestudeerd door de taxaan cabazitaxel te combineren met de androgeen gerichte remmer enzalutamide. Opvallend genoeg was de toevoeging van enzalutamide op de antitumor effectiviteit van cabazitaxel groter dan de impact van enzalutamide alleen. Om de interactie tussen enzalutamide en cabazitaxel beter te begrijpen, hebben wij m.b.v. microscopie levende tumorcellen bestudeerd tijdens behandeling. Blootstelling

aan cabazitaxel resulteerde in tubuline stabilisatie en verstoorde celdelingen, maar leidde opvallend genoeg zelden tot celdood van de prostaatkankercellen. De toevoeging van enzalutamide zorgde ervoor dat deze resistente prostaatkankercellen wel vaker doodgingen aan de cabazitaxel behandeling, wat de effectiviteit van de combinatie behandeling onderstreept. Samengevat impliceren onze resultaten dat deze combinatie strategie, van een taxaan chemotherapeuticum met een androgeen gerichte remmer, een veelbelovende optie is voor castratie-resistente prostaatkankerpatiënten. Deze strategie wordt momenteel onderzocht in verschillende klinische studies.

Selectie van de optimale behandeling voor de individuele prostaatkankerpatiënt wordt steeds complexer door de toevoegingen van nieuwe (combinatie)behandelingen. In **hoofdstuk VI** bespreken we de resultaten van een klinische studie die een nieuwe methode voor geïndividualiseerde therapieselectie onderzocht. Hierbij werden levende tumorcellen uit het bloed, ook wel circulerende tumorcellen genoemd, van uitgezaaide prostaatkanker patiënten geïsoleerd. Het doel was om deze tumorcellen te kweken in het laboratorium, als 3D celstructuren genaamd organoïden, om vervolgens therapie gevoeligheid te bepalen. Daarmee zouden deze organoïden fungeren als representatieve modellen voor de individuele patiënt en therapieselectie kunnen ondersteunen.
Om zoveel mogelijk circulerende tumorcellen te isoleren, hebben we prostaatkankerpatiënten een leukaferese procedure laten ondergaan. Deze methode bleek zeer effectief de tumorcellen te verrijken en is over het algemeen weinig invasief. Het product wordt vervolgens verwerkt om de concentratie van ongewenste bloedcomponenten te verlagen, voornamelijk witte bloedcellen, terwijl de tumorcellen worden behouden.

Na het kweken van deze samples groeiden bij 14 van de 40 (35%) de tumorcellen uit als organoïden, die meestal 6-8 weken in leven konden worden gehouden. Helaas leverde dit niet genoeg organoïden op om de therapiegevoeligheid voor verschillende medicijnen te kunnen testen. Bij twee samples waren we in staat de organoïden langdurig in kweek te houden wat uiteindelijk leidde tot één nieuwe stabiele organoïde lijn. Deze organoïde lijn bleek enzalutamide-resistent te zijn, wat een reflectie was van de kortdurende therapie response bij de patiënt waarvan we de circulerende tumorcellen hadden verkregen. Uit deze studie moeten we concluderen dat het kweken van prostaatkanker organoïden uit circulerende tumorcellen zeer beperkt mogelijk is en momenteel onvoldoende garantie biedt voor het testen van therapieresponse. Deze resultaten laten wel zien dat het mogelijk is om grote hoeveelheden tumorcellen te verzamelen met behulp van leukaferese. Dit biedt bijvoorbeeld de mogelijkheid om circulerende tumorcellen genetisch en fenotypisch te karakteriseren. Wanneer verschillende samples gedurende de ziekteverloop worden verzameld kan dit mogelijk inzicht bieden in de progressie van de ziekte en de response op behandeling. Samengevat bieden deze resultaten interessante

mogelijkheden voor vervolgstudies.

De resultaten besproken in dit proefschrift bieden nieuwe aangrijpingspunten in de voortdurende ontwikkeling om behandelingen van patiënten met uitgezaaide prostaatkanker te verbeteren.

Appendices

Erasmus MC PhD Portfolio

Name PhD student	Lisanne Mout
Erasmus MC department	Medical Oncology
Research School	Molecular Medicine (MolMed)
PhD period	2014-2020
Promotor	Prof. Dr. Ronald de Wit
Co-promotoren	Dr. Wytske M. van Weerden and Dr. Martijn P. Lolkema

Course	Year	ECTS
Basic and Translational Oncology	2015	1.8
Introduction in GraphPad Prism Version 7	2015	0.3
Basic Introduction Course on SPSS	2015	1
Presenting Skills for junior researchers	2016	1
Scientific Integrity	2016	0.3
CC02 Biostatistical Methods I: Basic Principles	2016	5.7
Biomedical English Writing	2017	2
Basic Course on 'R'	2019	2
(Inter)national conferences		
ESUR-SBUR15, Nijmegen	2015	1
AACR annual meeting, Washington	2017	1
ESUR, Porto	2019	1
AACR annual meeting virtual meeting II	2020	1
Dutch Uro-Oncology Studygroup (DUOS) yearly symposium, Utrecht	2018	0.3
Tour d'Europe, Rotterdam	2018	0.3
Presentations and meetings		
JNI meeting	2015-2020	1
Urology labmeeting	2015-2020	1
Urology Journal Club	2015-2020	1
Medical Oncology PhD progress meeting	2015-2020	1
MolMed day	2017	0.3
Medical Oncology Research meeting	2017	0.3
Urologie Refereeravond	2017	0.3
Interlab meeting (with Technical University Twente)	2017-2020	1
Medical Oncology Research day	2018	0.3

Erasmus MC Cancer institute Research day	2018	0.3
Transpot Kick-off meeting	2018	0.3
Urology PhD meeting	2020	0.3
Teaching		
Urology skills lab for medical students	2015-2018	1
Supervising bachelor student (Aron Bakker)	2016	2
Supervising master student (Anouk de Jong)	2017	2
Total		**30.8**

A

List of Publications

Mout L, van Royen ME, de Ridder C, Stuurman D, van de Geer WS, Marques R, French PJ, van de Werken HJG, Mathijssen RHJ, de Wit R, Lolkema MP, van Weerden WM. Continued Androgen Signaling Inhibition improves Cabazitaxel Efficacy in Prostate Cancer. *Submitted*

Mout L, van Dessel, Kraan J, de Jong AC, Neves RPL, Erkens-Schulze S, Beaufort CM, Sieuwerts AM†, van Riet J, Woo TLC, de Wit R, Sleijfer S, Hamberg P, Sandberg Y, te Boekhorst PAW, van de Werken HJG, Martens JWM, Stoecklein NH, van Weerden WM, Lolkema MP. Generating Human Prostate Cancer Organoids From Leukapheresis Enriched Circulating Tumor Cells. *Manuscript accepted for publication.*

Mout L, Moll JM, Chen M, de Morrée ES, de Ridder CMA, Gibson A, Stuurman D, Aghai A, Erkens-Schulze S, Mathijssen RHJ, Sparreboom A, de Wit R, Lolkema MP, van Weerden WM. Androgen receptor signalling impairs docetaxel efficacy in castration-resistant prostate cancer. *Br J Cancer.* 2020 Dec;123(12):1715-1719.

Langebäck A, Bacanu S, Laursen H, **Mout L,** Seki T, Erkens-Schulze S, Ramos AD, Berggren A, Cao Y, Hartman J, van Weerden W, Bergh J, Nordlund P, Lööf S. CETSA-based target engagement of taxanes as biomarkers for efficacy and resistance.
Sci Rep. 2019 Dec 18;9(1):19384.

Verhagen CVM, Vossen DM, Borgmann K, Hageman F, Grénman R, Verwijs-Janssen M, **Mout L**, Kluin RJC, Nieuwland M, Severson TM, Velds A, Kerkhoven R, O'Connor MJ, van der Heijden M, van Velthuysen ML, Verheij M, Wreesmann VB, Wessels LFA, van den Brekel MWM, Vens C. Fanconi anemia and homologous recombination gene variants are associated with functional DNA repair defects in vitro and poor outcome in patients with advanced head and neck squamous cell carcinoma.
Oncotarget. 2018 Apr 6;9(26):18198-18213.

Mout L, de Wit R, Stuurman D, Verhoef E, Mathijssen R, de Ridder C, Lolkema M, van Weerden W. Testosterone Diminishes Cabazitaxel Efficacy and Intratumoral Accumulation in a Prostate Cancer Xenograft Model. *EBioMedicine.* 2018 Jan;27:182-186.

Srebniak MI, **Mout L,** Van Opstal D, Galjaard RJ. 0.5 Mb array as a first-line prenatal cytogenetic test in cases without ultrasound abnormalities and its implementation in clinical practice. *Hum Mutat.* 2013 Sep;34(9):1298-303.

About the author

Lisanne Mout was born on May 3rd 1991 in Rotterdam, the Netherlands and grew up in the nearby town Poortugaal. After graduating from secondary school (Angelus Merula, Spijkenisse) in 2008, she studied Biomedical Laboratory Sciences at the Rotterdam University of Applied Sciences. Her interest in scientific research drove her to continue her studies at the University of Amsterdam were she enrolled into the Biomedical Sciences master program in 2012. During her studies she became interested in oncology research and focused on DNA damage repair signaling. Driven to do translational oncology research she started her PhD research at the end of 2014, under the supervision of Prof. Dr. R. de Wit, Dr. W.M. van Weerden and Dr. M.P. Lolkema. Her PhD thesis focusses on the interaction between androgen signaling with taxane treatment efficacy and the use of circulating tumor cell derived organoids in metastatic prostate cancer. She will continue her research with a postdoctoral research fellowship at the Princess Margaret Cancer, Toronto, Canada under supervision of Dr. M. Lupien. Here she will focus on the epigenetic landscape of advanced prostate cancer.

Dankwoord

Eind 2014 begon ik met veel enthousiasme aan dit avontuur dat promotieonderzoek heet, terugkijkend had ik geen flauw benul wat me te wachten stond. De afgelopen zes jaar zijn gepaard gegaan met flink wat vallen en weer opstaan. Daarentegen heeft het mij enorm veel leuke ervaringen en interacties opgeleverd, die ik zeker niet had willen missen. Dit proefschrift, de publicaties en projecten hadden natuurlijk niet mogelijk geweest zonder de support van fantastische begeleiders, collega's, vrienden en familie.

Allereerst wil ik mijn promotor en copromotoren bedanken voor hun begeleiding en support in de afgelopen jaren. Prof. Dr. De Wit, beste Ronald, jouw klinische visie en expertise zijn een cruciale factor geweest in de translatie van het preklinisch werk. In het begin moest ik vaak even puzzelen wanneer je me naar de relevantie van een nieuw experiment vroeg, maar het heeft mij geleerd altijd zich te houden op de patiënt. Dr. Lolkema, beste Martijn, jouw enthousiasme en inspiratie waren vaak dat zetje wat ik nodig had om over teleurstellingen en twijfel heen te stappen. Ik kijk vooral met plezier terug op de meetings waarbij je al discussiërend en priegelend op een white-board mij uitdaagde om met nieuwe verklaringen en hypotheses te komen. Dr. van Weerden, beste Wytske, ik kon altijd bij je terecht met mijn overpeinzingen en je reageerde vol enthousiasme wanneer ik weer eens een mooie plaatje of filmpje had, wat altijd enorm motiveerde. Als wetenschapper weet je altijd nieuwe samenwerkingen te vinden in projecten, die onder andere tot onze CETSA publicatie hebben geleidt.

Daarnaast wil ik de leescommissie bedanken voor het bestuderen van de verschillende manuscripten en de bereidheid om met mij van gedachte te wisselen.

Uiteraard wil ik iedereen van de Experimentele Urologie bedanken, ik heb mij in de afgelopen jaren altijd enorm thuis gevoeld. Beste Corrina en Debra, het eerste gedeelte van dit proefschrift had natuurlijk niet zonder jullie tot stand kunnen komen. Terwijl ik in zes jaar geen enkele muis heb aangeraakt, hebben jullie eigenhandig een enorme hoeveelheid experimenten volbracht. Ik heb daarnaast jullie recht-door-zee communicatie altijd enorm kunnen waarderen. Beste Sigrun, we hebben in het begin van CIRCLE helaas veel organoid kweken zien verschrompelen onder de microscoop. Maar ik denk dat we, mede door de succesvolle en plezierige samenwerking, toch enorm veel stappen hebben gezet en successen weten te boeken. Beste Wilma, als veelzijdige labexpert kwam ik vaak even bij je langs voor input. Je was altijd geïnteresseerd, enthousiast en kon me ook vaak op weg helpen. Beste Joke, vaak begonnen onze gesprekken over wat de beste films/series op je favoriete streamingsdienst waren en eindigden bij politieke discussies. Maar het was altijd gezellig. Daarnaast wil ook zeker Ashraf, Mirella, Natasja en Diana bedanken

voor jullie betrokkenheid en enthousiasme.

Ook wil ik mijn collega's van de Medisch Oncologie bedanken, want vooral bij het CIRCLE project was een goede samenwerking cruciaal. Beste Lisanne en Anouk, jullie hebben beide enorm veel energie in de klinische kant van dit project gestopt, iets wat voor mij vaak onzichtbaar bleef. Het was vaak een enorme puzzel om de enorme hoeveelheid data die uit dit project kwam op een duidelijke manier weer te geven en te beschrijven, maar ik denk dat we samen tot de beste versie zijn gekomen. Beste Jaco, jouw expertise was een belangrijke sleutel in dit geheel en heeft er voor gezorgd dat we grote stappen hebben gezet in het verwerken van de leukaferese samples. Ook John wil ik bedanken voor zijn input en ideeën die dit project hebben gevormd. En Khrystany, je hebt het gehoord, PICTURES gaat het grote succes worden en ik heb er alle vertrouwen in dat dit gaat lukken.

Daarnaast wil ook het translationele farmacologie lab bedanken, beste Ron in de afgelopen jaren ben je nauw betrokken geweest bij het taxaan onderzoek wat ik heb verricht en had je vaak een scherp oog op de uitvoering en interpretatie. Peter, Mei en Inge, jullie wil ik bedanken voor de technische expertise, hulp en gezelligheid. Beste Bodine, samen met Ron heb jij de preklinische studies weten te vertalen naar een succesvolle fase I studie, het gebeurt niet vaak dat de kliniek op het lab vooruit loopt. Zo zie je dat een hechte samenwerking van biomedische onderzoekers en artsen het beste resultaat oplevert. Beste Stefan, ik weet zeker dat het vervolg dat deze studies in goede handen ligt bij jou en ik kijk uit naar het resultaat.

Naast mijn (co)promotoren, heb ik de afgelopen jaren ook regelmatig advies gevraagd aan de wetenschappers die de promotie traject al hadden overwonnen. Dear Elena, you were often the person who provided me with a sufficient doses of tough love. You often advised me to stop doubting myself and confront my problems head-first, which changed the way I viewed and handled challenges. Beste Martin, ik ben heel erg blij dat de hoeveelheid tijd en energie die we in het live-cell imaging hebben gestoken zich heeft vertaald naar de prachtige resultaten in dit proefschrift. Je wist mijn ingewikkelde ideeën voor experimenten te vertalen naar daadwerkelijke resultaten en stopte niet tot de beste uitkomst was behaald. Daarnaast was je altijd bereid om te luisteren en advies te geven over de verschillende uitdagingen van promotieonderzoek. Beste Harmen, je kritische blik op de bioinformatica ging gelukkig gepaard met een uitgebreide uitleg over de opzet en interpretatie van de experimenten. Dit heeft samen met mijn korte deelname aan de CCBC journal club zeker mijn interesse in bioinformatica aangewakkerd. Daarnaast gaf je vaak een optimistisch perspectief aan alles wat gaande was. Rute, ook jou wil ik enorm bedanken voor alle goede adviezen in de afgelopen jaren. Ten slotte, beste Guido, ik heb met enige regelmaat jouw zondagse rust op het lab verstoordt, maar vol enthousiasme

gaf je antwoord op mijn overpeinzingen. Ik hoop dat ik ooit ook zo enthousiast en helder over mijn onderzoek kan praten.

One of the great aspects of being a PhD student is that you have the chance to meet a lot of people who deal with the same challenges. While having a cup of coffee, or a beer, you often find yourself sharing struggles but also victories. I fondly look back at the conversations I had with Ellen, Annelies, Merle, Job, Wesley, Youri, Eline, Daniela, Ardelan and all the student that passed through our lab in the last six years. The funny thing is that sometimes you find yourself discussing the same issues you had in the beginning.

As a PhD student you sometimes find yourself in the lucky position to spend some time in a lab abroad. Alex, I want to thank you and your lab members for the opportunity you provided, that short period of time had a tremendous positive impact on my personal and scientific development.

Ten slotte wil ik mijn vrienden en familie bedanken voor hun support. Elaisha, onze hechte vriendschap is van onschatbare waarde geweest in de afgelopen zes jaar. Of het nou een typische vrijdagavond met comfortfood, een blockbuster movie-night, een semi-emergency phone call, je was altijd een luisterend oor met de emotionele support of afleiding die ik nodig had. Steef, weet dat ik enorm trots op je ben, ondanks alle tegenslagen heb je altijd de ene voet voor de andere weten te zetten. Jij bent zo'n zorgheld die tijdens deze crisis er altijd stond. Ik ben enorm blij dat jullie m'n paranimfen zijn. Lieve Mam en Pap, het advies was altijd, doe wat je leuk vindt en probeer het gewoon. Het was de steun die ik nodig had om dit pad te kiezen. Ik kan me voorstellen dat promotie onderzoek altijd een beetje vaag is geweest, maar ik hoop dat jullie trots zijn op het resultaat. Ik ben ook enorm blij dat jullie de stap naar het buitenland supporten.